Optical Limiting Effect of New Synthesized Phthalocyanines in Solution and in Solid State

DISSERTATION

Zur Erlangung des Doktorgrades der Naturwissenschaften
-Dr. rer. Nat.-

vorgelegt dem Promotionsausschuß
des Fachbereichs 2 (Biologie/Chemie)
der Universität Bremen

von

Aneta Słodek

Bremen, Dezember 2010

1. Gutachter: Prof. Dr. D. Wöhrle
2. Gutachter: Prof. Dr. P. Swiderek
Vorgelegt: Im Oktober 2010

To my Sister and my Parents

Dla Katarzyny Kołodziej
- wspaniałej siostry i przyjaciółki
i moich rodziców

Acknowledgements

I would like to express my special acknowledgements to Professor Dieter Wöhrle for giving me the opportunity to work in his group as a PhD student. I am grateful for the numerous scientific meetings and his helpful suggestions and advices, and for his guidance as well as for his encouragement during the scientific work. I am extremely indebted to him for his patience, help, enthusiasm, optimism, and for the creation of great work atmosphere. Thank you very much indeed.

I am especially grateful to Professor Petra Swiderek for her approval to be my co-supervisor.

I am also thankful to Dr. Günter Schnurpfeil and Dr. Andreas Hartwig for being my co-examiners.

I would like to thank all the members of Professor Wöhrle group for pleasant and kind atmosphere, in particular, my special acknowledges to Dr. Łukasz Łapok for the stimulating discussion and useful advices in experimental work, and his help whenever I needed; Sergey Makarow for the scientific discussions and comments, Natasha Baziakina for help in preparation of sealed ampoules and for great time spent together during her staying in Bremen, Angela Wendt for an tremendous technical support. To Dr. Dülcks, I thank for Mass Spectral measurements.

I would like to thank Professor Blau from Department of Physics, Trinity College in Dublin for possibility to carry out the z-scan measurements. I wanted to express my gratitude to James Doyle and Sean O'Flaherty from Professor Werner Blau group who introduced me to the use of z-scan technique in order to perform optical limiting measurements of my samples. I am extremely grateful for your helpful suggestions and principally for all calculations you made.

I would also like to thank the European Union Network under the contract HPRN-00020 for financial support and the opportunity to participle in so fascinating and challenging project.

I am very grateful to my relevant and my friends, in particular to Katarzyna Mikuła for their wonderful support.

Finally, I wish to express my sincere appreciation to my parents, Lucyna and Leopold Słodek, and my sister, Katarzyna Kołodziej for their assistance, great encouragement, motivation and faith in me. Their unreserved love and enormous support gave me strength to complete my work. I cannot tell how much I am grateful to them.

List of Structures

Phthalonitriles and anhydrides

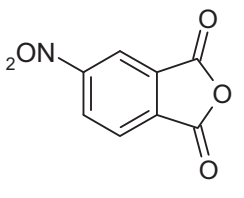

IV

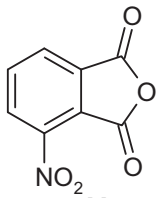

V

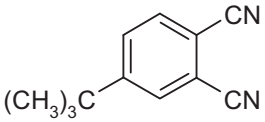

VI

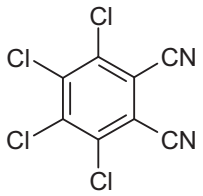

VII

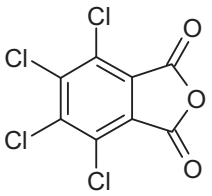

VIII

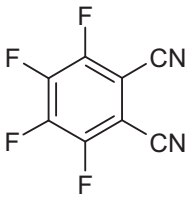

IX

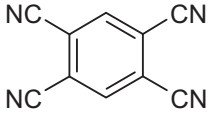

X

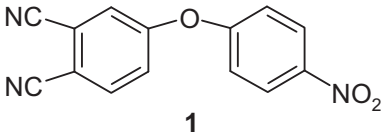

1

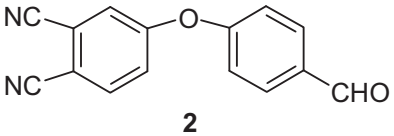

2

Tetra-substituted Phthalocyanines

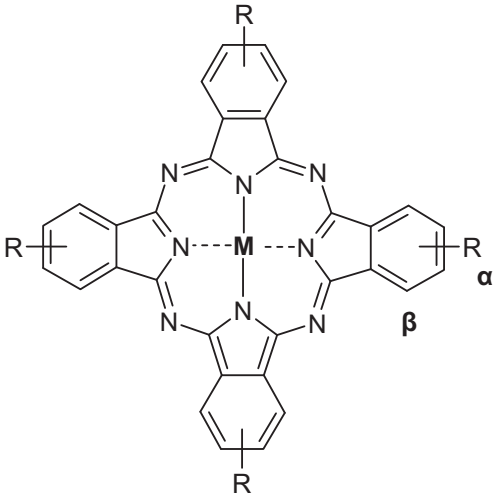

α

β

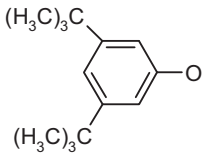

***t*Bu$_2$P**

Phthalocyanine Complexes

α

β

Compound	**M**	R	Abbreviation
3	2H	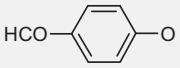	**$(fPhO)_4PcH_2$**
4	2H	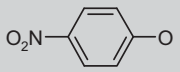	**$(nPhO)_4PcH_2$**
5	$SnCl_2$	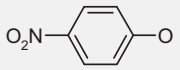	**$(nPhO)_4PcSnCl_2$**
6	$SnCl_2$	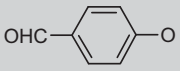	**$(fPhO)_4PcSnCl_2$**
7	$GeCl_2$	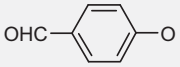	**$(fPhO)_4PcGeCl_2$**
18	$SnCl_2$	NO_2	**$(\beta NO_2)_4PcSnCl_2$**
19	$SnCl_2$	NO_2	**$(\alpha NO_2)_4PcSnCl_2$**
20	$GeCl_2$	NO_2	**$(\beta NO_2)_4PcGeCl_2$**
21	$Ge(OH)_2$	NO_2	**$(\beta NO_2)_4PcGe(OH)_2$**
22	$GeCl_2$	NO_2	**$(\alpha NO_2)_4PcGeCl_2$**
23	$Ge(t Bu_2P)_2$	NO_2	**$(\beta NO_2)_4PcGe(t Bu_2P)_2$**
25	InCl	$C(CH_3)_3$	**(*t*-Bu)$_4$PcInCl**

Octa-substituted Phthalocyanine

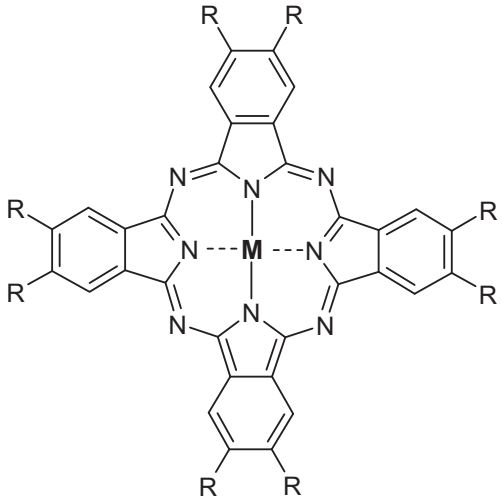

Compound	**M**	R	Abbreviation
24	$SnCl_2$	CN	**$(CN)_8PcSnCl_2$**

Hexadeca-substituted Phthalocyanines

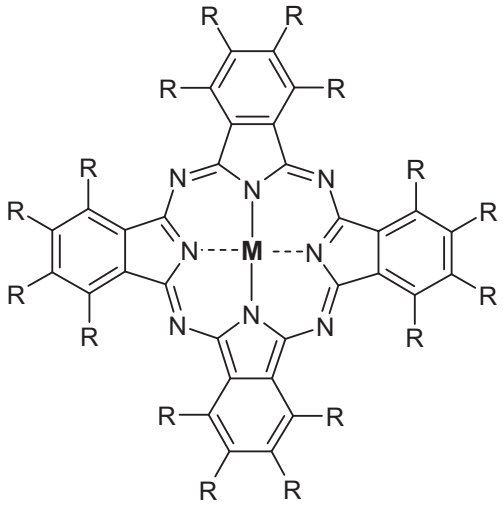

Compound	**M**	**R**	Abbreviation
8	$SnCl_2$	Cl	**$Cl_{16}PcSnCl_2$**
9	$GeCl_2$	Cl	**$Cl_{16}PcGeCl_2$**
10	$Sn(OH)_2$	Cl	**$Cl_{16}PcSn(OH)_2$**
11	$Ge(OH)_2$	Cl	**$Cl_{16}PcGe(OH)_2$**
12	SnF_2	Cl	**$Cl_{16}PcSnF_2$**
13	GeF_2	Cl	**$Cl_{16}PcGeF_2$**
14	$Sn(t Bu_2P)_2$	Cl	**$Cl_{16}PcSn(t Bu_2P)_2$**
15	$Sn(t Bu_2P)_2$	Cl	**$Cl_{16}PcGe(t Bu_2P)_2$**
16	$SnCl_2$	F	**$F_{16}PcSnCl_2$**
17	$GeCl_2$	F	**$F_{16}PcGeCl_2$**

List of Abbreviations

CH_2Cl_2	Dichloromethane
$CHCl_3$	Chloroform
Cln	1-Chloronaphthalene
DBN	1,5-Diazabicyclo[4.3.0]non-5-ene
DBU	1,8-Diazabicyclo[5.4.0]undec-7-ene
DCI	Direct chemical ionisation
DFWM	Degenerate four wave mixing
DMAE	2-N,N-dimethylaminoethanol
DMF	Dimethylformamide
DMSO	Dimethylsulphoxide
e.g.	*exempli gratia* (latin) – for example
EI	Electron ionisation
ESI-MS	Electrospray mass spectrometry
et al.	*et alii* (latin) – and the others
EtOH	Ethanol
FT-IR	Fourier transform infrared
HOMO	Highest occupied molecular orbital
i.e.	*id est* (latin) – that is to say
ISC	Intersystem crossing
LUMO	Lowest unoccupied molecular orbital
M	Metal
$[M^*]$	molecule-ion
MALDI	Matrix Assisted Laser Desorption Ionization
MeOH	Methanol
MPc	Metallophthalocyanine
NLO	Nonlinear optical
OL	Optical limiting
Pc	Phthalocyanine
PEG	Poly(ethylene glycol)
PhTriEOS	Phenyltriethoxysilane
PMMA	Poly(methylmethacrylate)

PS	Poly(styrene)
PVC	Poly(vinylchloride)
RSA	Reverse Saturable Absorption
S_0	Singlet ground state
S_1	Second excited singlet state
SA	Saturable Absorption
T_1	First excited triplet state
TEOS	Tetraethoxysilane
THF	Tetrahydrofuran
THG	Third harmonic generation
TLC	Thin layer chromatography
TPA	Two photon absorption
UV/Vis	Ultra-violet/Visible
X	Axial ligand

List of Symbols and Physical Terms

α_0	linear absorption coefficient [cm^{-1}]
β_I	the intensity-dependent nonlinear absorption coefficient [cm W^{-1}]
c	concentration [g L^{-1}]
d	thickness [µm]
F_{Sat}	the energy density at which the material saturates [J cm^{-2}]
I	light intensity
I_o	the intensity of the light at focus [GW cm^{-2}]
$\mathrm{Im}\{\chi^{(3)}\}$	the effective imaginary third order susceptibility
h	hour
Hz	herz
κ	the ratio between the excited state absorption cross section and that of the ground state (σ_{ex}/σ_0)
λ	wavelength [nm]
λ_{max}	wavelength of maximum absorption (UV/Vis) [nm]
µJ	mikrojoul
M	molecular weight [g mol^{-1}]
σ_0	the ground state absorption section
σ_{ex}	the excited triplet state absorption section
$\chi^{(3)}$	the third order nonlinearity [esu]
T_{min}	the minimum transmission
ns	nanosecond
ps	picosecond
rpm.	rounds per minutes
wt %	weight percentage

Publications and Presentations

Publications

D. Wöhrle, O. Suvorova, R. Gerdes, O. Bartels, Ł. Łapok, N. Baziakina, S. Makarov, A. Słodek, "Efficient oxidation and photooxidation of sulfur compounds and phenols by immobilized phthalocyanines", *Process of Petrochemistry and Oil Refining*, **2002**, 3, 30.

D. Wöhrle, O. Suvorova, R. Gerdes, O. Bartels, Ł. Łapok, N. Baziakina, S. Makarov, A. Słodek, "Efficient Oxidations and Photooxidations with Molecular Oxygen using Metal Phthalocyanines as Catalysts and Photocatalysts", *J. Porphyrins Phthalocyanines*, **2004**, 8, 1020.

A. Slodek, D. Wöhrle, J. J. Doyle, W. Blau, "Metal Complexes of Phthalocyanines in Polymers as Suitable Materials for Optical Limiting", *Macromol. Symp.*, **2006**, 235, 9.

J. J. Doyle, J. Wang, S. M. O'Flaherty, Y. Chen, A. Slodek, T. Hegarty, L. E. Carpenter II, D. Wöhrle, M. Hanack, W. J. Blau, "Nonlinear optical performance of chemically tailored phthalocyanine–polymer films as solid-state optical limiting devices", *J. Opt. A: Pure Appl. Opt*., **2008**, 10, 7.

A. Slodek, D. Wöhrle, "Synthesis and Characterization of New Tin and Germanium Phthalocyanine Complexes", in preparation.

A. Slodek, D. Wöhrle, J. J. Doyle, W. Blau, "Influence of Peripheral and Axial Substitution on Optical Limiting of Tin and Germanium Phthalocyanines in Solution and Polymeric Films", in preparation.

Presentations at the conferences

- Midterm Review Meeting of the European Union Research Program, Katholieke Universiteit Nijmegen, The Netherlands, June 2002.
- Annual Meeting for the 3rd phase of the European Union Research Program, Universität Bremen; Gremany, February 2003.
- Annual Meeting for the 4th phase of the European Union Research Program, University of East Anglia; United Kingdom, October 2003.
- Annual Meeting for the final phase of the European Union Research Program, Universidad Autonoma de Madrid; Spain, September 2004.

1. Aims of the thesis and scientific approach

This work was focused on the investigation of new and beforehand synthesized phthalocyanines in solution and in films as optical limiters. Phthalocyanines (Pcs) and their derivatives possess exceptional physical properties interesting for many applications [1-11] in particular nonlinear optical (NLO) devices [12-15]. Nonlinear optical occurrence deals with changes in the optical properties of materials, which are exposed to light [16]. Practical NLO applications include the use of phthalocyanines with optical limiting (OL) properties. The transmission for light of "ideal" optical limiters is high at normal light intensities and low for intense light intensities. Generally the investigation is based on optical shielding, specifically the protection of human eyes, optical elements and optical sensors from intense laser pulses. The interest for optical limiting properties has led to synthesize a variety of many phthalocyanines. The modification of the macrocycle by peripheral and axial substituents along with a great variety of central metals incorporated into the macrocycle permits control and improvement of NLO properties of Pcs. Phthalocyanines are very promising materials as optical limiters. However for practical application it is essential to investigate the optical limiting of phthalocyanine complexes in solid-state.

As was previously described the NLO properties of phthalocyanines depend on central metal ion [17]. Therefore, in the beginning of this study the preparation of films of series tetra and octasubstituted phthalocyanines with different central metal previously prepared by Wöhrle group [18-20] and further investigation of their OL properties was intended. The solid-state films of the above-mentioned phthalocyanine compounds have been embedded in different polymers on glass or sapphire via spin casting and drop casting techniques.

The major aim of this study was to design the synthesis of phthalocyanines that will be used as good optical limiters. The tin and germanium were chosen as atoms incorporated in the phthalocyanine ring owing to their charge of +4 allowing axial substitution. The possibility of axial substitution enhances largely solubility and prevents aggregation and further alters the packing of the molecule in solid state. Additionally, the axial ligands can introduce a dipole moment perpendicular to the macrocycle and consequently improve the NLO properties for example a magnitude of the third-order nonlinearity $\chi^{(3)}$ [21, 22]. The second reason to choose tin and germanium was to compare the influence of heavier atom as tin on the optical limiting effect. Additionally, syntheses of phthalocyanines were intended to introduce electron-withdrawing groups in annulene rings in order to alteration the electronic properties and transition dipole moment.

Many tetra-, one octa-, and hexadeca-substituted phthalocyanines with different electron-withdrawing groups attached to the phthalocyanine macrocycle (chlorine, fluorine, nitro, *p*-nitrophenoxy, *p*-formylphenoxy, cyano) and with the variation of axial ligands (chlorine, fluorine, hydroxyl, 3,5-di-*tert*-butylphenoxy) have been projected to synthesize.

Further, the tin and germanium phthalocyanine complexes enough soluble were chosen for thin films preparation. For practical application the concentration of phthalocyanine in optical limiting devices should be high in the optical beam in order to reduce the harmful effects associated with the overheating of the sample by irradiation with the intense laser light. On account of this, optically homogenous till seven-layer films possessing deep glassy blue or green appearance has been prepared.

The NLO properties of all synthesized metal-free, germanium and tin phthalocyanines were investigated in solutions. Optical limiting measurements of compounds in this study were conducted using the open-aperture z-scan [23]. The solid-state thin films of various phthalocyanine compounds embedded in different polymers prepared via spin casting method were characterised using the z-scan technique. They were performed using 6 ns Gaussian pulses from a Q switched Nd:YAG laser. Additionally, the polymer solid-state samples were probed by UV/Vis spectra and their thicknesses were measured using a Dektak instrument.

1.1 References

[1] R. A. Collins, K. A. Mohamed, *J. Appl. Phys.*, **1988**, 21, 154.

[2] J. Robertson, A. Smith, J. Duignan, P. Milson, G. Bourhill, *Appl. Phys. Lett.*, **2001**, 78, 1183.

[3] J. Robertson, P. Milsom, J. Duignan, G. Bourhill, *Opt. Lett.*, **2000**, 25, 1258.

[4] M. Kato, Y. Nishioka, K. Kaifu, K. Kawamura, S. Ohno, *Appl. Phys. Lett.*, **1985**, 86, 196.

[5] G. G. Roberts, M. C. Petty, S. Baker, M. T. Fowler, N. J. Thomas, *Thin Solid Films*, **1985**, 132, 113.

[6] M. J. Cook, A. J. Dunn, F. M. Daniel, R. C. O. Hart, R. M. Richardson, S. J. Roser, *Thin Solid Films*, **1988**, 159, 395.

[7] M. A. Mohammad, P. Ottenbreit, W. Prass, G. Schnurpfeil, D. Wöhrle, *Thin Solid Films*, **1992**, 213, 285.

[8] D. Wöhrle, O. Suvorowa, R. Gerdes, O. Bartels, L. Lapok, N. Baziakina, S. Makarov, A. Slodek, *J. Porphyrins Phthalocyanines*, **2004**, 8, 1020.

[9] M. T. Riou, C. Clarisse, *J. Electroanal. Chem.*, **1988**, 249, 181.

[10] D. Schlettwein, D. Wöhrle, N. I. Jäger, *J. Electrochem. Soc.*, **1989**, 136, 2882.

[11] J. F. Van der Pol, E. Neelman, J. W. Zwicker, R. J. M. Nolte, W. Drenth, J. Aerts, R. Visser, S. J. Picken, *Liq. Cryst.*, **1989**, 6, 577.

[12] M. K. Casstevens, M. Samoc, J. Pfleger, P. N. Prasad, *J. Chem. Phys.*, **1990**, 92, 2019.

[13] J. Simon, P. Bassoul, S. Norvez, *New J. Chem.*, **1989**, 13, 13.

[14] A. Slodek, D. Wöhrle, J. J. Doyle, W. Blau, *Macromol. Symp.*, **2006**, 235, 9.

[15] J. J. Doyle, J. Wang, S. M. O'Flaherty, Y. Chen, A. Slodek, T. Hegarty, L. E. Carpenter II, D. Wöhrle, M. Hanack, W. J. Blau, *J. Opt. A: Pure Appl. Opt.*, **2008**, 10, 7.

[16] P. N. Prasad, D. J. Williams, *Introduction to Nonlinear Optical Effects in Molecules and Polymers.* John Wiley & Sons, New York, **1991**.

[17] J. S. Shirk, J. R. Lindle, F. J. Bartoli, Z. H. Kafafi, A. W. Snow, M. E. Boyle, *Intl J. Nonlin Opt. Phys.*, **1992**, 1, 699.

[18] D. Wöhrle, G. Schnurpfeil, G. Knothe, *Dyes and Pigments*, **1992**, 18, 91.

[19] G. Schneider, D. Wöhrle, W.Spiller, J. Stark, G. Schulz-Ekloff, *Photochem. Photobiol.*, **1994**, 60, 333.

[20] D. Wöhrle, V. Schmidt, *J.Chem.Soc., Dalton Trans.,* **1988**, 549.

[21] P. Chen, I. V. Tomov, A. S. Dvornikov, M. Nakashima, J. F. Roach, D. M. Alabran, P. M. Rentzepis, *J. Phys. Chem.*, **1996**, 100, 17507.

[22] G. Rojo, G. Martin, F. Agullo-Lopez, T. Torres, H. Heckmann, M. Hanack, *J. Phys. Chem. B*, **2000**, 104, 7066.

[23] M. Sheik-Bahae, A. A. Said, T. H. Wei, D. J. Hagan, E. W. Van Stryland, *IEEE. J. Quantum Electron.*, **1990**, 26, 760.

2. Phthalocyanines

The synthesis and structure of the metal-free phthalocyanine (Pc) (**Figure 2.1** left) and of some of metallophthalocyanines (MPc) (**Figure 2.1** right) was described by Linstead in 1934 [1-6]. Phthalocyanines also named as tetrabenzotetraazoporphyrins possess an extended π-electron system and show a high thermal and chemical stability.

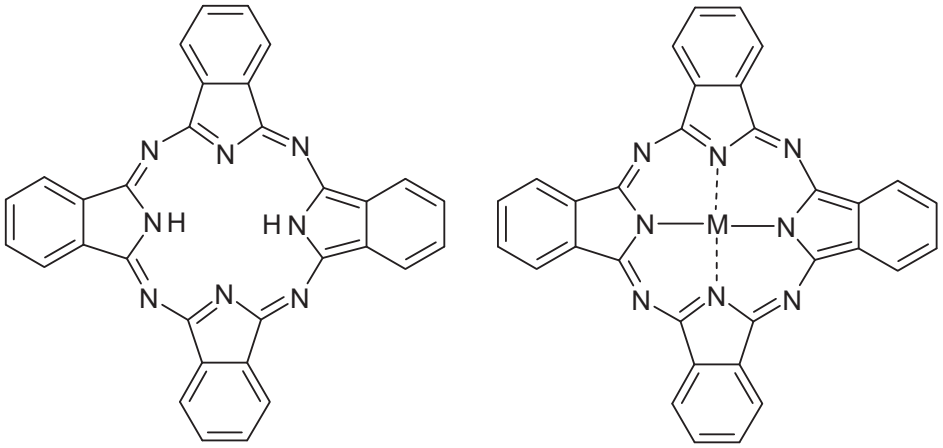

Figure 2.1 Structure of the metal-free (left) and metal-containing phthalocyanine (right).

Phthalocyanines and the related compounds like porphyrins and naphthalocyanines have been investigated in detail for many years especially with regard to their properties as dyes, pigments, paints and colors. Phthalocyanines have attracted attention as a stuffs possessing unconventional physical properties interesting for many applications in material science such as liquid crystals [7, 8], nonlinear optical (NLO) devices [9-12], gas sensors [13-15], photosensitizers [16], Languimar-Blodgett films [17-19], catalysts and photocatalysts [20] and electrochromic devices [21, 22]. Substituted derivatives of phthalocyanines can be also used in the photodynamic therapy of cancer [8, 23].

2.2 General synthesis of phthalocyanines

2.2.1 Synthesis of metal-free phthalocyanines

The blue colored compound that was later known as the metal-free phthalocyanine was obtained accidentally by Braun and Tchermiac in 1934 [24]. The first synthesis of the metal-free phthalocyanine was conducted using *o*-cyanobenzamide in refluxing ethanol (method I, **Figure 2.2**) [24]. The compound was obtained in a very low yield. In 1934, Linstead and co-workers confirmed Braun's result. The same product was found when the reaction mixture was heated at 240 ^{o}C and catalysts like magnesium, antimony metal or magnesium salt were used (method II, **Figure 2.2**) [2]. The structure of phthalocyanine was shown as planar by using the X-ray crystallographic analysis [25-27].

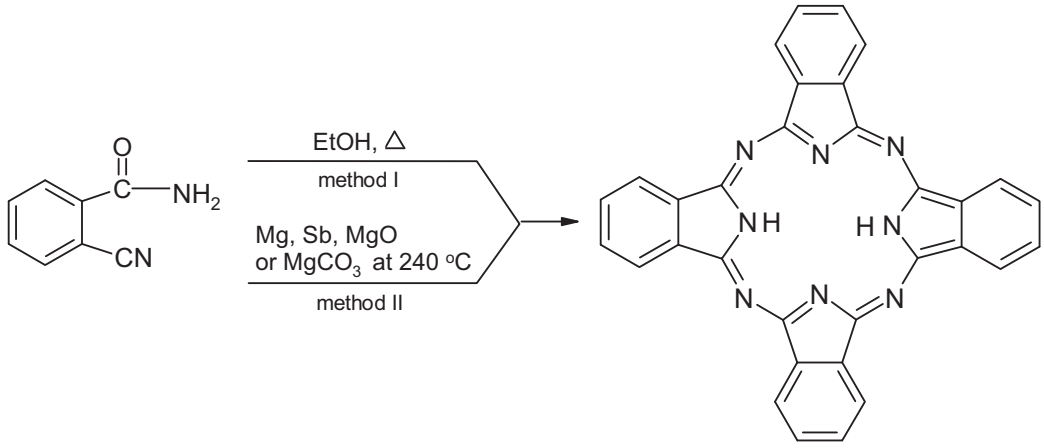

Figure 2.2 Synthesis of metal-free phthalocyanine described by Braun (method I) and Linstead (method II).

The metal-free phthalocyanine can be easily obtained by cyclotetramerization of phthalonitrile or diiminoisoindoline or its substituted derivatives by heating in high boiling alcohols in the presence of alcoholate or in 2-N,N-dimethylaminoethanol (DMAE) (**Figure 2.3**).

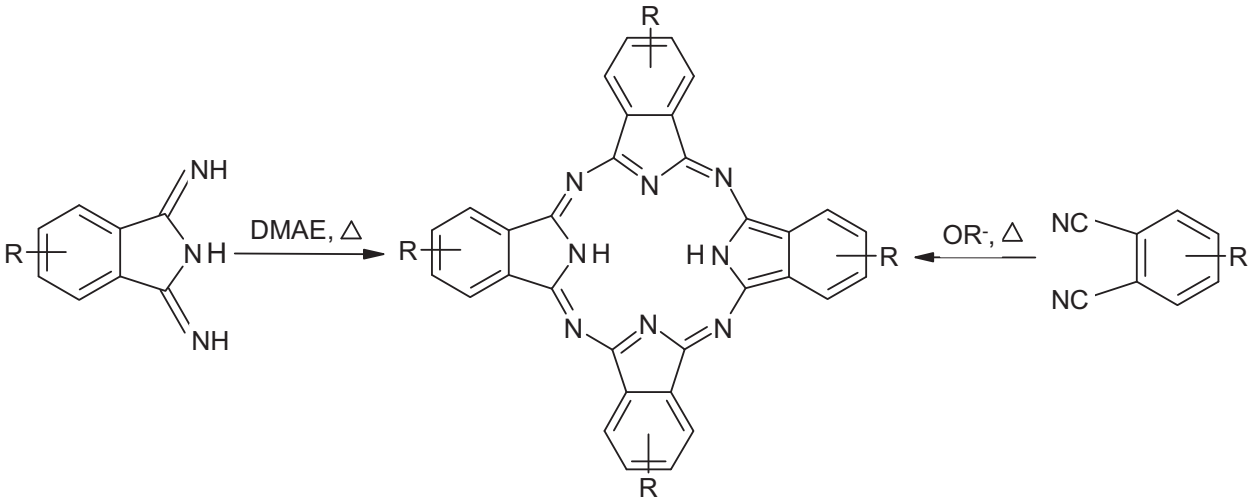

Figure 2.3 Routes to obtain metal-free phthalocyanines.

The formation of the metal-free phthalocyanine from phthalonitrile as a starting material can be carried out by several methods. Heating of phthalonitrile at 130 - 140 ^{o}C in n-pentanol in the presence of 1,8-diazabicyclo[5.4.0]undec-7-ene (DBU) or 1,5-diazabicyclo[4.3.0]non-5-ene (DBN) as strong bases was reported by Tomoda [28]. Cyclotetramerization of phthalonitrile can be conveniently undertaken in the presence of lithium or sodium pentanolate in 1-pentanol solution to give Li_2Pc or Na_2Pc which can be easily demetallated by using glacial acetic acid or concentrated H_2SO_4 [5, 29]. Additionally, cyclotetramerization of phthalonitrile in the melt with an organic reducing agent such as hydroquinone allows the formation of phthalocyanine [30]. 1,3-Diiminoisoindoline can be used as a precursor to form phthalocyanine. Diiminoisoindoline is simply converted to phthalocyanine by refluxing solution of 2-N,N-dimethylaminoethanol (DMAE) [31-33].

2.2.2 Synthesis of metal-containing phthalocyanines

Most metallophthalocyanines can be obtained from phthalonitrile or diiminoisoindoline in addition of a metal, a metal chloride or a metal hydride in high-boiling solvents such as dimethylformamide (DMF), DMAE, quinoline or 1-chloronaphthalene. The cyclotetramerization of phthalonitrile in the melt in the presence of a metal or a metal salt (without solvent) leads macrocycle. In addition, some other precursors such as phthalic acid derivatives or bromobenzenes use in synthesis of metallophthalocyanines are shown in **Figure 2.4**.

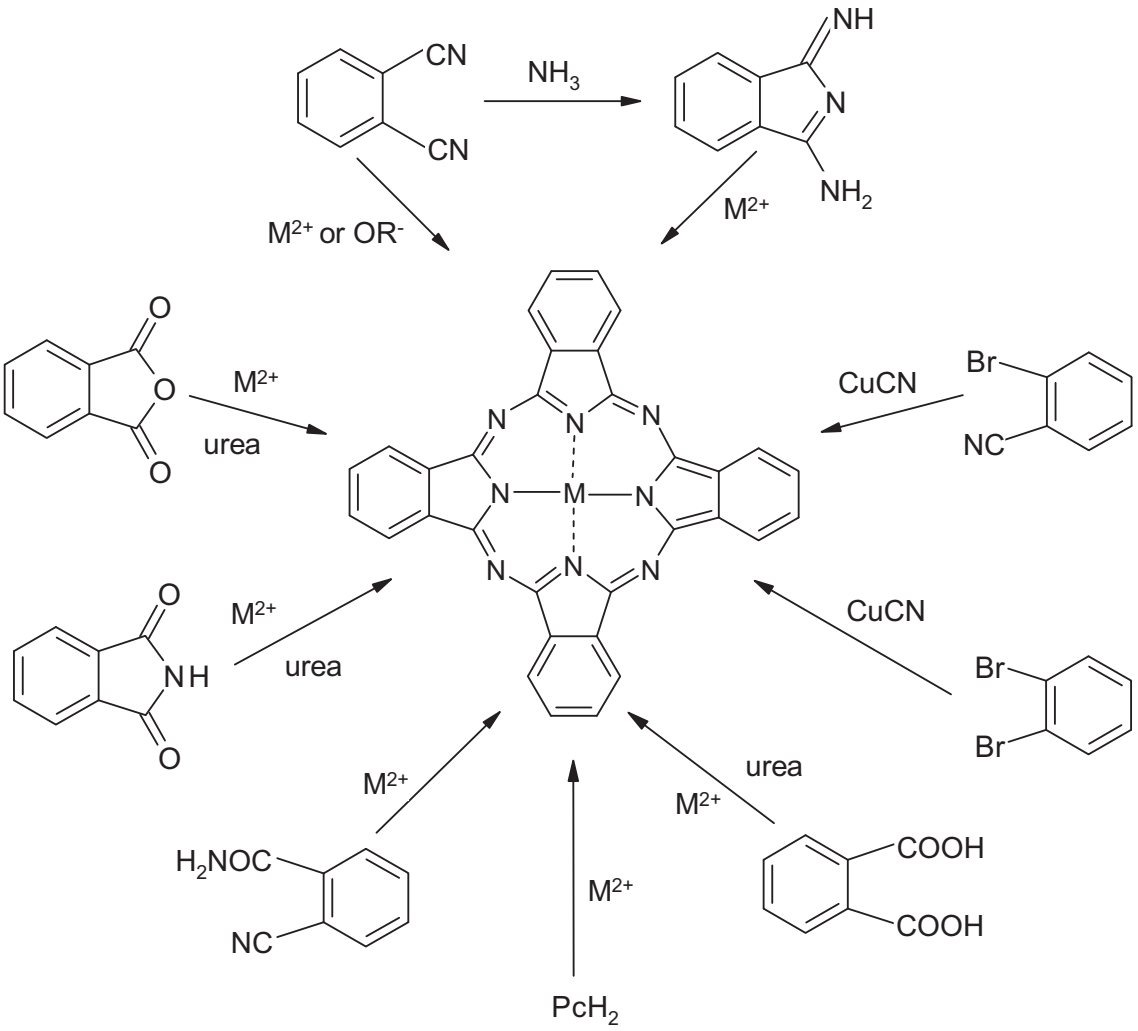

Figure 2.4 Syntheses of metallophthalocyanines.

The reactions of phthalic acid [34], phthalimide [35], or phthalic acid anhydride [36] with a metal salt, urea as a source of nitrogen and a catalyst such as ammonium molybdate can give metal-containing phthalocyanines. The cyclotetramerization of mentioned above precursors is usually conducted in the melt although they are feasible in solvent such as nitrobenzene. Substituted or unsubstituted 1,2-dibromobenzene can be used as a precursor to form substituted or unsubstituted copper(II) phthalocyanine. The reaction is carried out usually in DMF or quinoline by addition of CuCN. Also the cyclotetramerization of 2-cyanobenzamide in DMAE or in bulk with a metal salt or a metal allows the preparation of unsubstituted MPc. Metal-containing phthalocyanine may be successfully prepared by metallation of metal-free phthalocyanines with suitable metal ions in refluxing solvents like DMF, quinoline or 1-chloronaphthalene. The phthalocyanines macrocycle can complex with cations derived from over 70 elements.

2.2.3 Synthesis of axially substituted phthalocyanines

The axial substitution can increase solubility and reduce face-to-face aggregation, which leads to interesting materials with optical and optoelectronic properties. For axial substitution central metal ions in the core of the phthalocyanine in +3 or +4 oxidation state are required. Many examples of axially substituted derivatives of silicon(IV) [37, 38], germanium(IV) [38, 39] and tin(IV) [38, 40] phthalocyanines are known.

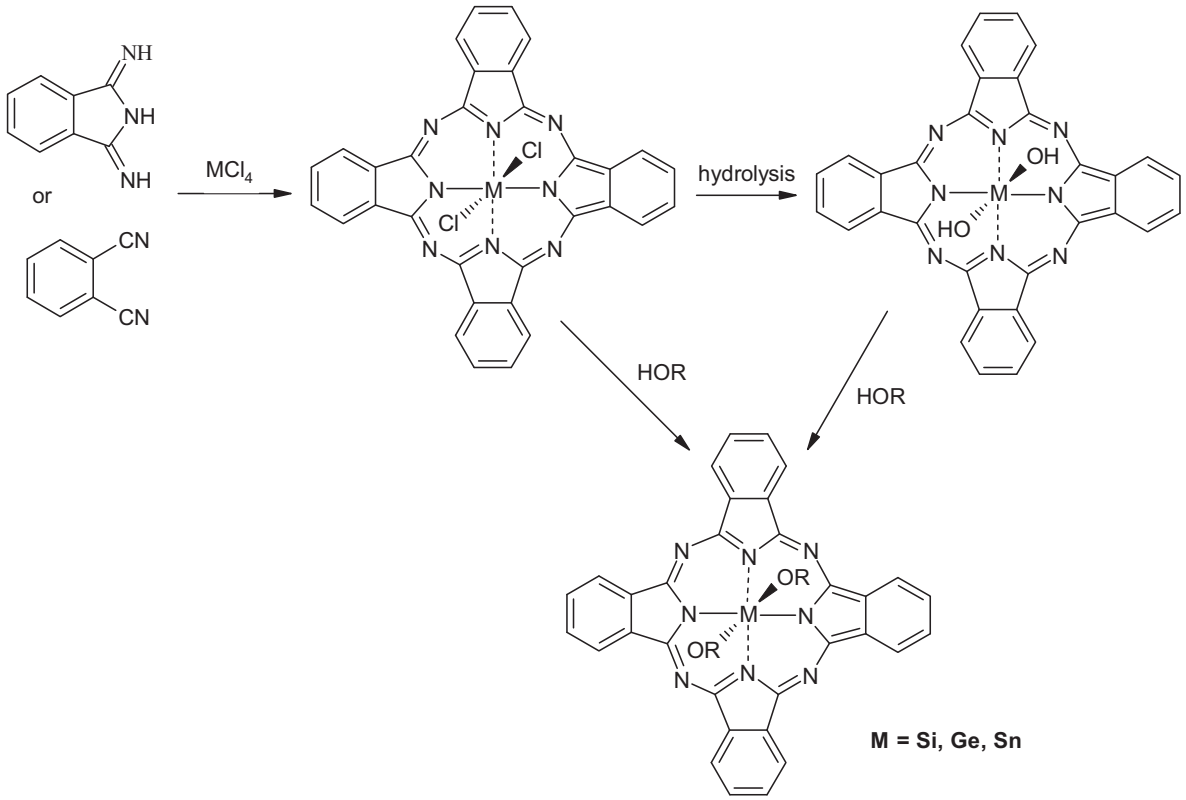

Figure 2.5 Synthesis of axially substituted phthalocyanines.

The cyclotetramerization of phthalonitrile or diiminoisoindoline or its derivatives in the presence of an appropriate metal tetrachloride ($SiCl_4$, $SnCl_4$ and $GeCl_4$) allows the formation dichloro axially substituted metallophthalocyanines (**Figure 2.5**). Hydrolysis using acidic or basic conditions leads to dihydroxy-substituted metallophthalocyanines. For further axial substitution, either dichloro- or dihydroxy-substituted MPcs can be used. $(Cl)_2$MPcs or $(OH)_2$MPcs can react with alcohols, chlorosilanes, and alkyl halides to produce interesting axial substituted materials. Other metal ions such as Al(III), Ga(III), V(IV) and Ti(IV) are also known in the phthalocyanine ring with axially substituted chloride, hydroxyl or oxygen but these complexes suppress less effective the aggregation of the macrocycle than complexes

containing metals of the fourth group. The axially bonded groups at the central metal of Pcs, especially in relatively large size significantly diminish or almost eliminate aggregation of phthalocyanines in solution and in thin films. These axially substituted complexes show considerable solubility in common organic solvents and demonstrate intermolecular edge-to-edge interaction [41, 42] because of the steric effect of the axial substituents that block cofacial interactions.

2.3 Mechanism of phthalocyanine formation

Phthalocyanines can be prepared by many different routes as described in Chapter 2.2. Therefore different mechanisms are possible. Although many cyclotetramerization may proceed via common intermediates, the determined mechanistic steps are often different and in some cases not known.

Some intermediates were isolated (**Figure 2.6**). Borodkin [43] isolated a sodium derivative of methoxyiminoisoindolenine **A** in the preparation of substituted metal-free phthalocyanines using phthalonitrile, sodium or lithium n-pentoxide in pentanol solution. Further Hurley [44] isolated the nickel complexes **C** and **B** as intermediates in the cyclotetramerization of nickel phthalocyanine. During the preparation of tetranitrophthalocyanine the dimeric lithium salt **D** as intermediate was discovered and isolated [45].

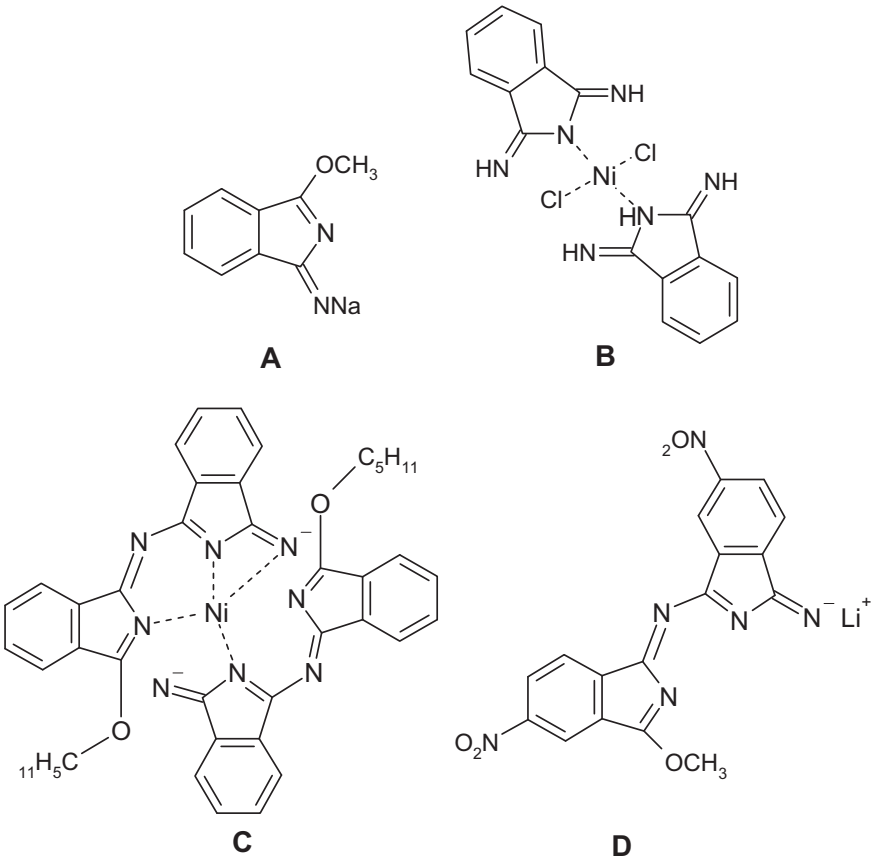

Figure 2.6 The intermediates isolated during phthalocyanines synthesis.

The mechanism presented in **Figure 2.7** gives more detailed information about the cyclotetramerization of phthalonitrile and diiminoisoindoline. All reactions that involve isolated intermediates **E-I** are carried out in alcohol as solvent. The protonated forms of diiminoisoindoline anions **E** and **F** can be isolated [43, 46 and 47]. Both intermediates **E** and **F** most likely appear during phthalocyanine formation in refluxing pentanol. These intermediates are also formed in methanol or ethanol solution. As mentioned above the reaction of the 4-nitrophthalonitrile with lithium methoxide in methanol at 116 ºC gave the isolated intermediates **D** (**Figure 2.6**) and **G** (**Figure 2.7**) in good yield [45]. The compound **C** (**Figure 2.6**) and **H** (**Figure 2.7**) was isolated during the reaction of diiminoisoindoline and MCl_2 (M = Ni) in pentanol in the presence of base. Therefore it was pointed out that the metal ion template effect plays important role in the formation of metallophthalocyanines [44]. Heating of the compound **H** with Ni^{2+} as metal (M) in pentanol led to nickelphthalocyanine and liberated pentanal [44].

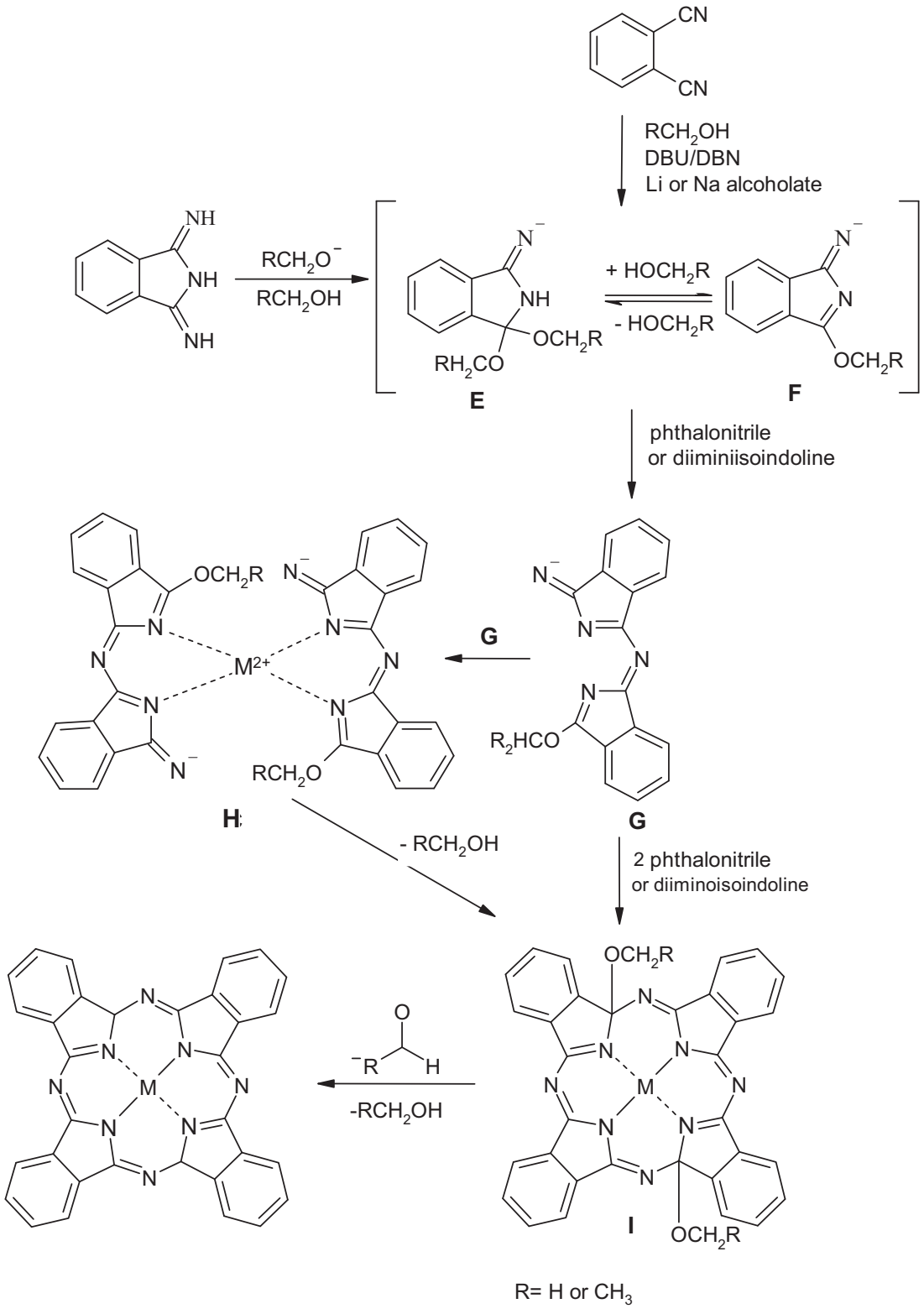

Figure 2.7 Mechanism of phthalocyanine formation.

The ring closure and aromatization to the phthalocyanine occur through the latest known intermediate **I** that was isolated from the solvothermal reaction in methanol [48]. The sequential addition of two molecules of phthalonitrile or diiminoisoindoline to intermediate **G**

produces compound **I**. During the aromatization of **I** to phthalocyanine formation of an aldehyde takes place. The created phthalocyanine possesses a considerable amount of aldehyde. Therefore the alkoxide ion is important as nucleophile and reducing agent [49].

2.4 Optical properties of phthalocyanines

2.4.1 Optical properties of phthalocyanines in solution

Phthalocyanines absorb strongly in the visible region of light giving blue or green colors. The metallated phthalocyanines show in UV/Vis spectra a characteristic absorption band in the visible region at ~ 700 nm termed the Q-band and a weaker one in the ultra-violet region at ~ 360 nm called B-band or Soret band (**Figure 2.8**). The Q-band arises after absorption of light by transition of an electron from the highest occupied molecular orbital (HOMO) (namely the a_{1u}) to the lowest unoccupied molecular orbital (LUMO), (namely the e_g). The transition from a_{2u} to e_g results in the B-band (**Figure 2.9**) [50]. The molar extinction coefficients for the phthalocyanines are rather high in the range of 2×10^5 l mol^{-1} cm^{-1}. The position of the Q-band is particularly influenced by substituents at the anullated benzene rings and by coordinating solvent and by molecules at the central metal.

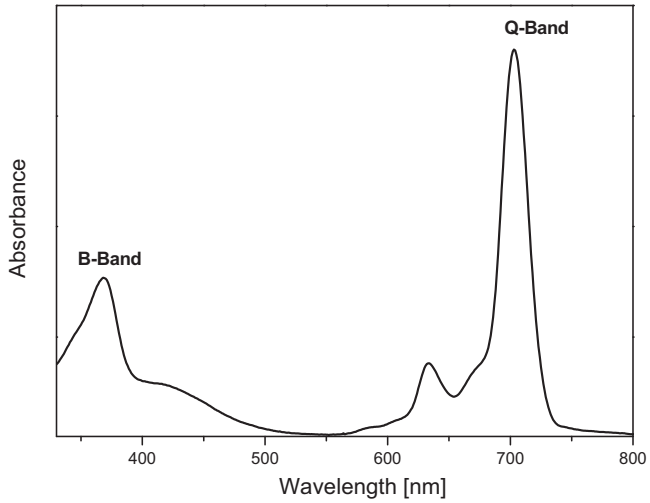

Figure 2.8 Absorption spectrum of a dissolved metallatophthalocyanine.

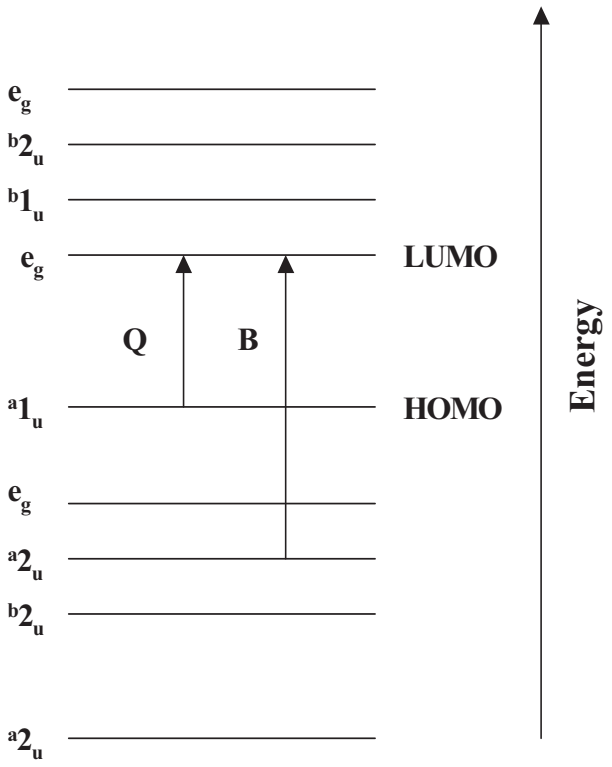

Figure 2.9 Electronic transitions between the HOMO and LUMO inducing the characteristic Q-band and B-band transitions in the UV/Vis spectrum of phthalocyanines.

In the case of metal-free phthalocyanines a split of the Q-band is observed (**Figure 2.10**). This is caused by a difference in symmetry. The metallated phthalocyanines possess D_{h4} symmetry and the metal-free phthalocyanines a lower D_{2h} symmetry.

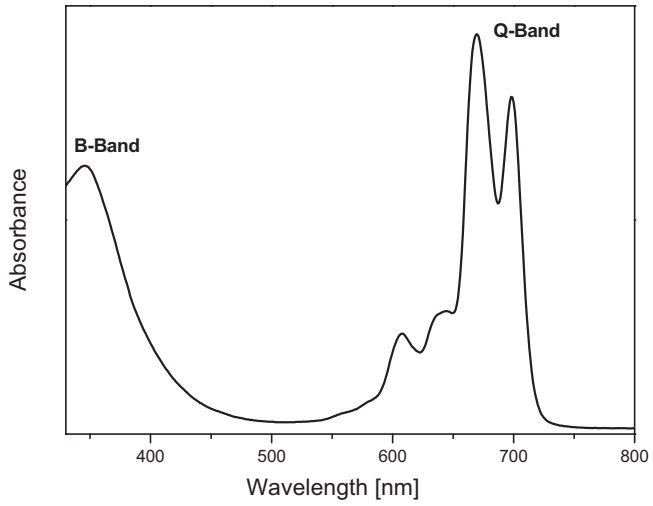

Figure 2.10 Absorption spectrum of a dissolved metal-free phthalocyanine.

2.4.2 Optical properties of phthalocyanines in the solid state

The absorption spectra obtained from solid-state phthalocyanines differ from the absorption spectra in solution. This phenomenon was explained using exciton coupling theory [51]. It is based on the interaction between transition moments of neighbouring molecules (dimer interaction) although it can be extended to include interactions of molecules in boundless stacks [52]. Exciton coupling for two neighbouring metallated phthalocyanines molecules of D_{4h} symmetry gives rise to a splitting of the ^1e_u excited state into two energy levels (**Figure 2.11**). For cofacial dimers, transitions to the higher energy levels are allowed (**Figure 2.11 A**), and the Q-band is blue-shifted in comparison with its position in the solution spectrum. An example in which a blue-shifted Q-band spectrum is obtained is the α-crystal modification of the metal-free phthalocyanines and metallated phthalocyanines (**Figure 2.12 A**), and cofacial siloxane dimers [53] oligomers [54], and polymers of phthalocyanines. In case of phthalocyanines which are parallel but not cofacial oriented, a red-shift to longer wavelength takes place (**Figure 2.11 B**).

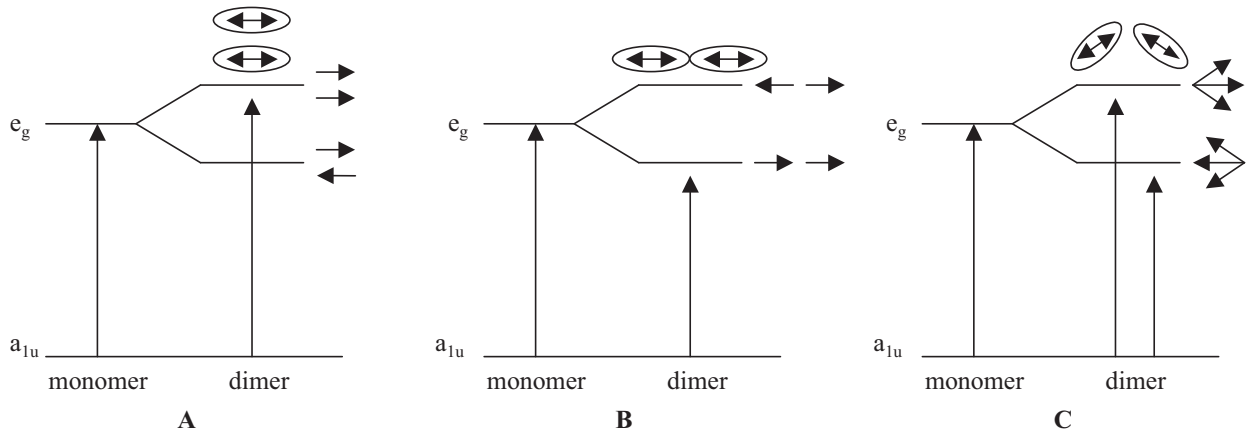

Figure 2.11 Model of exciton splitting of the Q-band between two molecules in cofacial **A**, edge-to-edge **B**, and tilted **C** arrangements.

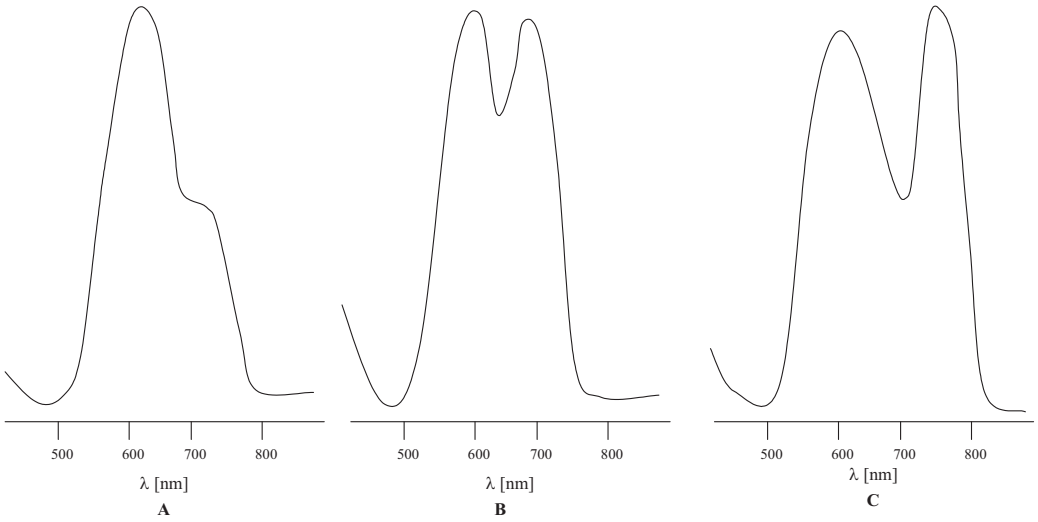

Figure 2.12 UV/Vis spectra of thin films of metal free phthalocyanine **A**, α-form **B**, β-form **C**, X-form.

This phenomenon appears in some axially substituted silicon naphthalocyanines in the solid state [55], and in the χ-form of metal free phthalocyanine (**Figure 2.12 C**) [56]. Phthalocyanines which are in tilted arrangement will display bands both at shorter and at longer wavelengths relative to the Q-band of dissolved phthalocyanines because of the dipoles cancelling each other neither in the higher nor in the lower energy configuration (**Figure 2.11 C**). An example of a tilted structure is the β-form crystal of a metal-free phthalocyanine (**Figure 2.12 B**) [56, 57]. Both red- and blue-shifted absorption bands can appear and they are polarised in an orthogonal sense. This phenomenon is called **Davidov splitting**.

2.5 References

[1] R. P. Linstead, *J. Chem. Soc.*, **1934**, 1016.

[2] G. T. Byrne, R. P. Linstead, A. R. Lowe, *J. Chem. Soc.*, **1934**, 1017.

[3] C. E. Dent, R. P. Linstead, *J. Chem. Soc.*, **1934**, 1027.

[4] C. E. Dent, R. P. Linstead, *J. Chem. Soc.*, **1934**, 1033.

[5] R. P. Linstead, A. R. Lowe, *J. Chem. Soc.*, **1934**, 1022.

[6] R. P. Linstead, A. R. Lowe, *J. Chem. Soc.*, **1934**, 1031.

[7] J. F. Van der Pol, E. Neelman, J. W. Zwikker, R. J. M. Nolte, W. Drenth, J. Aerts, R. Visser, S. J. Picken, *Liq. Cryst.*, **1989**, 6, 577.

[8] J. Simon, C. Sirlin, *Pure Appl. Chem.*, **1989**, 61, 1625.

[9] M. K. Casstevens, M. Samoc, J. Pfleger, P. N. Prasad, *J. Chem. Phys.*, **1990**, 92, 2019.

[10] J. Simon, P. Bassoul, S. Norvez, *New J. Chem.*, **1989**, 13, 13.

[11] A. Slodek, D. Wöhrle, J. J. Doyle, W. Blau, *Macromol. Symp.*, **2006**, 235, 9.

[12] J. J. Doyle, J. Wang, S. M. O'Flaherty, Y. Chen, A. Slodek, T. Hegarty, L. E. Carpenter II, D. Wöhrle, M. Hanack, W. J. Blau, *J. Opt. A: Pure Appl. Opt.*, **2008**, 10, 7.

[13] R. A. Collins, K. A. Mohamed, *J. Appl. Phys.,* **1988**, 21, 154.

[14] J. Robertson, A. Smith, J. Duignan, P. Milson, G. Bourhill, *Appl. Phys. Lett.*, **2001**, 78, 1183.

[15] J. Robertson, P. Milsom, J. Duignan, G. Bourhill, *Opt. Lett.*, **2000**, 25, 1258.

[16] M. Kato, Y. Nishioka, K. Kaifu, K. Kawamura, S. Ohno, *Appl. Phys. Lett.*, **1985**, 86, 196.

[17] G. G. Roberts, M. C. Petty, S. Baker, M. T. Fowler, N. J. Thomas, *Thin Solid Films*, **1985**, 132, 113.

[18] M. J. Cook, A. J. Dunn, F. M. Daniel, R. C. O. Hart, R. M. Richardson, S. J. Roser, *Thin Solid Films*, **1988**, 159, 395.

[19] M. A. Mohammad, P. Ottenbreit, W. Prass, G. Schnurpfeil, D. Wöhrle, *Thin Solid Films*, **1992**, 213, 285.

[20] D. Wöhrle, O. Suvorowa, R. Gerdes, O. Bartels, L. Lapok, N. Baziakina, S. Makarov, A. Slodek, *J. Porphyrins Phthalocyanines*, **2004**, 8, 1020.

[21] M. T. Riou, C. Clarisse, *J. Electroanal. Chem.*, **1988**, 249, 181.

[22] D. Schlettwein, D. Wöhrle, N. I. Jäger, *J. Electrochem. Soc.*, **1989**, 136, 2882.

[23] J. F. Van der Pol, E. Neelman, J. W. Zwickker, R. J. M. Nolte, W. Drenth, J. Aerts, R. Visser, S. J. Picken, *Liq. Cryst.*, **1989**, 6, 577.

[24] A. Braun, J. Tcherniac, *Ber. Deut. Chem. Ges.*, **1907**, 40, 2709.

[25] J. M. Robertson, *J. Chem. Soc.*, **1935**, 615.

[26] J. M. Robertson, *J. Chem. Soc.*, **1936**, 1195.

[27] J. M. Robertson, I. Woodward, *J. Chem. Soc.*, **1937**, 219.

[28] A. Tomoda, S. Saito, S. Ogawa, S. sShiraishi, *Chem. Lett.*, **1980**, 1277.

[29] P. A. Barret, C. E. Dent, R. P. Linstead, *J. Chem. Soc.*, **1936**, 1719.

[30] A. W. Snow, N. L. Jarvis, *J. Am. Chem. Soc.*, **1984**, 106, 4706.

[31] P. J. Brach, S. J. Grammatica, O. A. Ossanna, L. Weiberger, *J. Heterocycl. Chem.*, **1970**, 7, 1403.

[32] C. C. Leznoff, D. M. Drew, *Can. J. Chem.*, **1996**, 74, 307.

[33] G. Pawlowski, M. Hanack, *Synthesis*, **1980**, 287.

[34] S. A. Mikhalenko, E. A. Luk'yanets, *Zh. Obshch. Khim.*, **1969**, 39, 2129.

[35] A. Kempa, J. Dobrowolski, *Can. J. Chem.*, **1988**, 66, 2553.

[36] A. Shaabani. *J. Chem. Res.*, **1998**, 672.

[37] M. K. Lowery, A. J. Starshak, J. N. Esposito, P. C. Krueger, M. E. Kenney, *Inorg. Chem.*, **1965**, 4, 128.

[38] C. W. Derk, T. Inabe, K. F. Schoch, J. Marks, T. J. Marks, *J. Am. Chem. Soc.*, **1983**, 105, 1539.

[39] R. D. Joyner, M. E. Kenney, *J. Am. Chem. Soc.*, **1960**, 82, 5790.

[40] W. J. Kroenke, M. E. Kenney, *Inorg. Chem.*, **1964**, 3, 251.

[41] S. Hayashida, N. Hayashi, *Mat. Chem.*, **1991**, 3, 92.

[42] S. Hayashida, N. Hayashi, *Synt.Met.*, **1991**, 41, 1243.

[43] V. F. Borordkin, *Zh. Prikl. Khim.,* **1958**, 31, 813; *J. Appl.Chem. USSR (Engl. Trans.)*, **1958**, 31, 803.

[44] T. J. Hurley, M. A. Robinson,S. I. Trotz, *Inorg. Chem.*, **1967**, 6, 389.

[45] F. Baumann, B. Bienert, G. Rösch, H. Vollmann, W. Wolf, *Angew. Chem.*, **1956**, 68, 133.

[46] I. Chambrier, M. J. Cook, *J. Chem. Res. (S)*, **1990**, 322.

[47] S. Rodriguez-Morgade, M. Hanack, *Chem. Eur. J.*, **1997**, 3, 1042.

[48] C. D. Molek, J. A. Halfen, J. C. Loe, E. W. McGaff, *Chem. Commun.*, **2001**, 2644.

[49] J. F. Van der Pol, E. Neelman, J. W. Zwickker, R. J. M. Nolte, W. Drenth, J. Aerts, R. Visser, S. J. Picken, *Makromol. Chem.*, **1989**, 190, 2727.

[50] S. Basu, *Indian J. Phys.*, **1954**, 28, 511.

[51] M. Kasha, H. R. Rawls, M. Ashrat El-Bayoumi, *Pure and Appl. Chem.*, **1965**, 11, 371.

[52] M. Fujiki, H. Tabei, T. Kurihara, *J. Phys. Chem.*, **1988**, 9, 1281.

[53] E. Ciliberto, K. A. Doris, W. J. Pietro, G. M. Reisner, D. E. Ellis, I. Fragala, F. H. Herbstein, M. A. Ratner, T. J. Marks, *J. Am. Chem. Soc.*, **1984**, 106, 7748.

[54] B. Simic-Glavaski, A. A. Tanaka, M. E. Kenney, E. Yeager, *J. Electroanal. Chem. Interf*acial *Electrochem.*, **1987**, 229, 285.

[55] S. Hayashida, N. Hayashi, *Synthetic Metals*, **1991**, 41, 1243.

[56] J. H. Sharp, M. Lardon, *J. Phys. Chem.*, **1968**, 72, 3230.

[57] L. E. Lyons, J. R. Walsh, J. W. White, *J. Chem. Soc.*, **1960**, 167.

3. Nonlinear optical properties of phthalocyanines

Nonlinear optical (NLO) occurrence deals with changes in the optical properties of materials, which are exposed to light [1]. Many optical devices such as optical switches [2], dynamic holography [3], and optical data-recording [4] are based on the nonlinear optical effects. For NLO applications practical are molecular materials which can display large nonlinearities, small losses, fast response time and small dielectric constants [5]. Among the large numbers of NLO absorbers such as porphyrins [6, 7], fullerenes [8-10].and other materials [11-16], phthalocyanines (Pc) and their derivatives have recently emerged as most promising materials due to their extended delocalized π–electron structure leading to strong excited-state absorptions, high triplet yields, fast NLO response times, large nonlinear susceptibilities and easy processing [17-21]. Through both axial (via the central metal) and peripheral (at the ligand) substitutions of the basic Pc structure has led to a large control and improvement of their NLO properties.

3.1 Optical limiting phenomenon

Between many nonlinear optical properties of phthalocyanines, the optical limiting (OL) belongs to the most intensively investigates. Devices based on nonlinear optical phenomena are of special interest due to their abilities to protect light-sensitive elements in many instruments, human eyes, light sensors, sky analyzers and optical apparatus against the high intensity light sources, which can irreversibly destroy such delicate instruments when the safety threshold is transcended [22, 23].

For instance, the ANSI (American National Standards Institute) standard for the maximum permitted exposure for human eyes to nanosecond pulses in the visible is ≤ 0.2 μJ [24], where the Nd:YAG laser produces 4 or 6 orders of magnitude higher energy.

Many mechanisms based on optical processes are involved to achieve a nonlinear response. A perturbation of the electronic distribution in the material by the electric field of the incident light and a molecular reorientation are mechanisms that can contribute to the nonlinear response. An optical pumping is another mechanism for a third-order NLO response that is often noticed in phthalocyanines. Initially, molecules are energized from the ground state to the excited state by the absorption of a light. The optical properties of an excited state are significant different from those of a ground state. The population of molecules in the excited state causes the changes in the optical properties of the material and high optical nonlinearities. The optical pumping is the mechanism evoking a saturable and reverse

saturable absorption. Processes such as nonlinear scattering or nonlinear diffraction may also generate the OL effect. The two-photon absorption (TPA) can as well contribute to a third-order NLO response. TPA is a nonlinear optical process. In particular, the imaginary part of the third-order nonlinear susceptibility is related to the extent of TPA in a given molecule. The main mechanisms to accomplish OL effect are based on nonlinear absorption and nonlinear refraction. Most important to achieve OL is the sequential two-photon absorption.

Materials with an effective OL effect often display a so-called reverse saturable absorption (RSA) [25]. The reverse saturable absorption phenomenon appears when transmission decrease with increasing incident intensity of light. This contrasts to the more common process of saturable absorption (SA) where the transmission increases with incident intensity, the absorbance bleaches with increasing incident intensity.

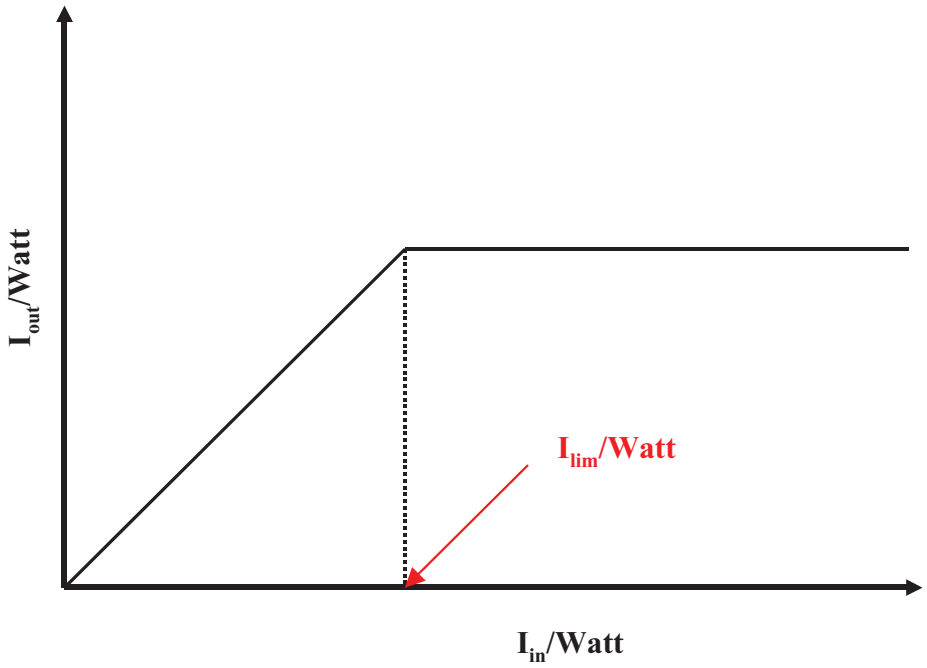

Figure 3.1 Function of an ideal optical limiter; light intensity I_{out} transmitted versus incoming light intensity I_{in}; threshold intensity I_{lim} at which I_{out} saturates.

The optical limiting phenomenon takes place when the intensity of the light beam is strongly suppressed by the optical limiter system while the input intensity is over a certain threshold value (I_{lim}). The function of an idealized optical limiter is shown in **Figure 3.1**. The I_{out} and I_{in} are the intensity of the light beam transmitted by the optical limiter and of incoming light, respectively. The output intensity of an ideal limiter ascends linearly with the input intensity until the threshold is reached. When the threshold value is achieved, the output intensity

becomes a constant value for any larger input light energy. The transmission for an ideal optical limiter is high at normal light intensities and low for intense light intensities. In fact, for the real limiter the threshold is not sharp.

The variable transmission as a function of the light intensity allows us to understand that different processes of the light absorption exist in the system at miscellaneous irradiation levels [26]. The five-level diagram (**Figure 3.2**) in which the absorption of excited state is considered can be used to discuss nonlinear absorption of phthalocyanines.

In **Figure 3.2**, the red and black arrows indicate absorption from ground and excited states and relaxations, respectively. After excitation, the first excited singlet state S_1 is populated by undergoing of the molecules from the ground state S_0 into S_1. From S_1 level the molecules may decay into S_0 or may be excited to upper second singlet excited state S_2.

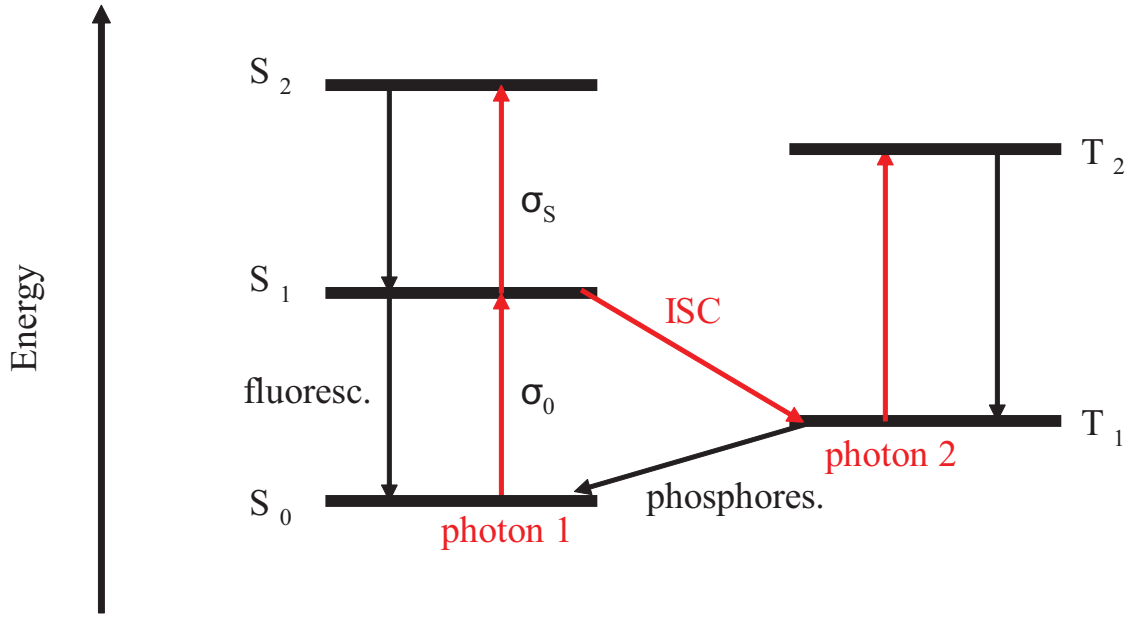

Figure 3.2 Five-level energy diagram.

The molecules from level S_2 rapidly relax to the first excited singlet state S_1. From the S_1 state the molecules can go through an intersystem crossing (ISC) with a time constants τ_{ISC} to the first excited triplet state T_1. Here molecules may go by excitation to the upper second triplet excited state T_2 and than fast relax to lower energy level T_1 through fluorescence. If the molecule has an excited state (S_1 or T_1) absorption cross section ($\sigma_{ex,S}$ or $\sigma_{ex,T}$) larger than the ground state cross section σ_0 including high populations, the effective absorption of the molecule increases and RSA takes place (values of $\sigma_{ex,S}/\sigma_0$ or $\sigma_{ex,T}/\sigma_0 > 1$).

The intersystem crossing transition $S_1 \rightarrow T_1$ and fluorescence transition $T_2 \rightarrow T_1$ are expected to be fast processes. The fast intersystem crossing is necessary to populate the excited triplet state T_1 and furthermore to obtain efficient $T_1 \rightarrow T_2$ transitions of molecules.

The net absorption coefficient α in the five-level system is given in the **Equations 3.1** [27, 28].

$$\alpha = \alpha_{S_0 S_1} + \beta I_{in} \qquad (\mathbf{3.1})$$

The **Equation 3.1** entails the modification of the Lambert-Beer law for a two-photon absorption process where z is the direction of light propagation through a material (**Equation 3.2**).

$$-\frac{\partial I_{in}}{\partial z} = \alpha_{S_0 S_1} I_{in} + \beta I_{in}^2 \qquad (\mathbf{3.2})$$

Hence the five-level diagram explains the variation of the absorption coefficient α with the incident light intensity I_{in}. Moreover, it is expected that the saturation threshold I_{lim} decreases with increasing of the absorption cross section for the transition from the ground state and with the lifetime of the phosphorescence $T_1 \rightarrow S_0$ [27-29]. The nonlinear absorption coefficient β is straight correlated with the generalized optical susceptibility $\chi^{(3)}$ as expressed in **Equation 3.3** [30, 31], where c represents the speed of the light (3×10^8 m s^{-1}), n_0 represents the linear refractive index of the system, and ω^* refers to the excitation light frequency.

$$\mathrm{Im}\left[\chi^{(3)}\right] = \frac{2c^2 n_0^2 \beta}{\pi \omega^*} \times 10^{-22} C \cdot m \cdot V^{-3} \qquad (\mathbf{3.3})$$

The **Equation 3.3** indicates that the optical limiting effect is an example of a third-order NLO property of the system.

Optical limiter based on RSA should possess the high ratio of excited state to ground state cross section (σ_{ex}/σ_0), a fast intersystem crossing transition, the long excited state lifetime. The large exited state absorption and the long excited state lifetime are required to achieve a strong nonlinear absorption. In fact, in materials exposed to laser irradiation two situations can occur. First, when the duration of the incoming light pulses is shorter than the time required populating the first excited singlet state S_1. Then the singlet-singlet absorption occurs

before the expected population of the first excited triplet state T_1. Under these conditions, the simplest three-level system (S_0, S_1, and S_2, **Figure 3.2**) can be considered to discuss the experimental results. On the other hand, when the lifetime of the first excited triplet state T_1 is much longer than the light pulses duration, the excited state T_1 is significantly populated and triplet-triplet transition $T_1 \rightarrow T_2$ occurs. Moreover, the optical limiting response is fluence (J cm^{-2}) not intensity (W cm^{-2}) dependent [32]. With regard to phthalocyanines, the last situation is more preferable, since the absorption cross section of the transition $T_1 \rightarrow T_2$ is greater than the absorption cross section of the $S_1 \rightarrow S_2$ transition.

A number of various parameters have been determined and cited in literature to estimate the effectiveness of optical limiting materials. The threshold fluence has been considered as the best parameter to compare the efficacy of optical limiting materials by some authors. The threshold fluence is defined as that fluence at which the transmission drops to half of its linear value. The saturation fluence has been also made use of quantitative interpretation of the optical limiting response. Moreover, McLean *et al*. [33] put other fluence parameter, F_c, as a figure of merit for OL in nanosecond case. F_c is defined by **Equation 3.4** where *hv* is the photon energy, σ_{ex} and σ_0 are excited and ground state absorption cross section.

$$F_c = h\nu/(\sigma_{ex} - \sigma_0) \qquad (\mathbf{3.4})$$

The materials considering as efficient optical limiters should possess a broad spectral bandwidth for limiting, a low threshold for nonlinear response, a high threshold for the damage, a low transmission to high energy beams, and a fast response times in sub-nanosecond regime. Notwithstanding, the most acceptable indicator of limiting power is κ value *e.i.* the ratio between the excited state absorption cross section and that of the ground state (σ_{ex}/σ_0). Thus, it implies that both, a large excited state absorption cross section and a large difference between the ground and excited state cross section, are required. Unfortunately, a quantification of the magnitude of the optical limiting action is not easily possible because often different mechanisms are involved or measurement techniques are used.

3.2 Experimental techniques

The main techniques which have been successfully employed to study the optical limiting effect in phthalocyanines are third harmonic generation (THG) [34-36], degenerate four wave mixing (DFWM) [37-40] and z-scan methods [32, 41]. All these methods include determination of the third-order optical nonlinearities $\chi^{(3)}$, which is of major interest in phthalocyanines. The THG technique measures the $\chi^{(3)}$ of a material at the incident laser frequency. The $\chi^{(3)}$ is determined from the relative intensity of the third harmonic of the sample and the substrate related to a standard (silica or quartz plate). An Nd:YAG laser with the wavelength of 1064 nm is usually used in THG measurement. A perturbation of the electron distribution by the electric field of the light is the mechanism in THG experiments [42]. The DFWM experiment is based on measuring the $\chi^{(3)}$ while the polarization of the incident beam is changing. In this measurement, when three input beams of the equal frequency, derived from short pulses from an Nd:YAG laser, interact in a nonlinear sample, they give rise to a fourth beam possessing the same frequency as the incident light. If all the beams are parallel polarized to each other, the experiment determines $\chi^{(3)}$. The DFWM experiment is performed similarly as THG relative to a standard, usually carbon disulphide (CS_2) is used. In DFWM experiments the fast distortion of the electronic cloud, the reorientation and optical pumping are involved mechanisms. The THG and DFWM experiments measure slightly different components of third-order nonlinearity $\chi^{(3)}$. Moreover, the $\chi^{(3)}$ measured in a DFWM experiment is commonly larger than that measured by using a THG technique due to more mechanisms contributed. A very convenient and fast experimental method to assess materials for optical limiting is the open-aperture *z*-scan experiment [41]. This measures the total transmittance through the sample as a function of incident laser intensity while the sample is gradually moved through the focus of a lens (along the *z*-axis). The set-up is shown schematically in **Figure 3.3**.

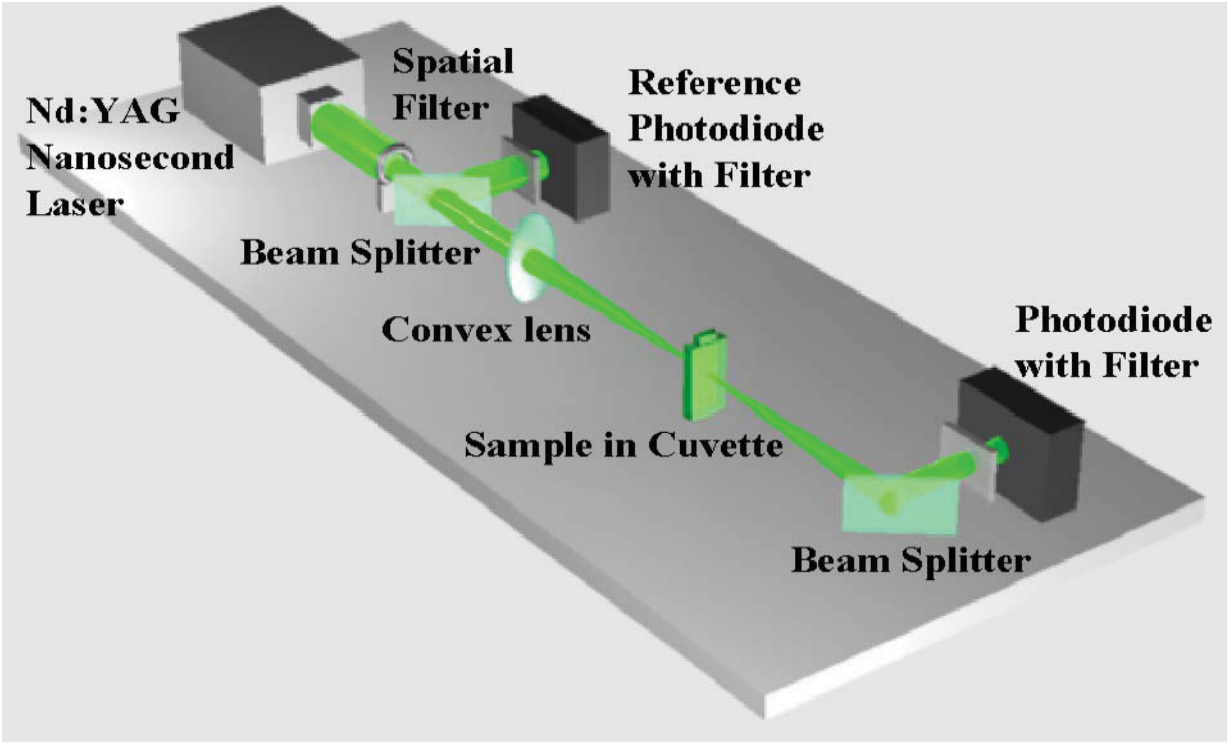

Figure 3.3 Open-aperture z-scan experiment.

The z-scan experiment determines the magnitude of real $\chi^{(3)}$ (the nonlinear refraction) and imaginary part of $\chi^{(3)}$ (the nonlinear absorption).

The z-scan method supplements both, the THG and the DFWM methods, and indicates whether the investigated material fulfils the requirements for a good optical limiter or not. Furthermore, for both the z-scan and DFWM experiments the ratio of the laser pulse width to the excited state lifetime should be taken into account in interpreting optical pumping nonlinearities.

3.3 Phthalocyanines as optical limiters

Among the large numbers of NLO absorbers, phthalocyanines (Pcs) have recently emerged as the most promising materials. The phthalocyanines are a highly conjugated π-electron macrocycle that can give rise to a large optical nonlinearity with sub-nanosecond response times [17]. In comparison with inorganic materials they possess small dielectric constant which is useful for optical switching fabrications. Moreover, the phthalocyanines are stable compounds with ability for incorporating more than 70 elements into the ring cavity.

The modification of the macrocycle by peripheral and axial substitutions along with the great variety of central metals incorporated into the macrocycle is of particular importance for tailoring their nonlinear optical properties. Moreover, the phthalocyanines exhibit the strong Q-band centred in the region of 700 nm and a B-band near the UV (**Figure 2.8**, Chapter 2.4.1). In the spectral region, between the Q- and Soret bands, the absorption is comparatively weak. It is in this region where phthalocyanines act as attractive limiters of visible light (~ 420 - 650 nm). Such properties make the phthalocyanines the most appealing candidates in NLO investigations (**Figure 3.4**) [23, 43-49].

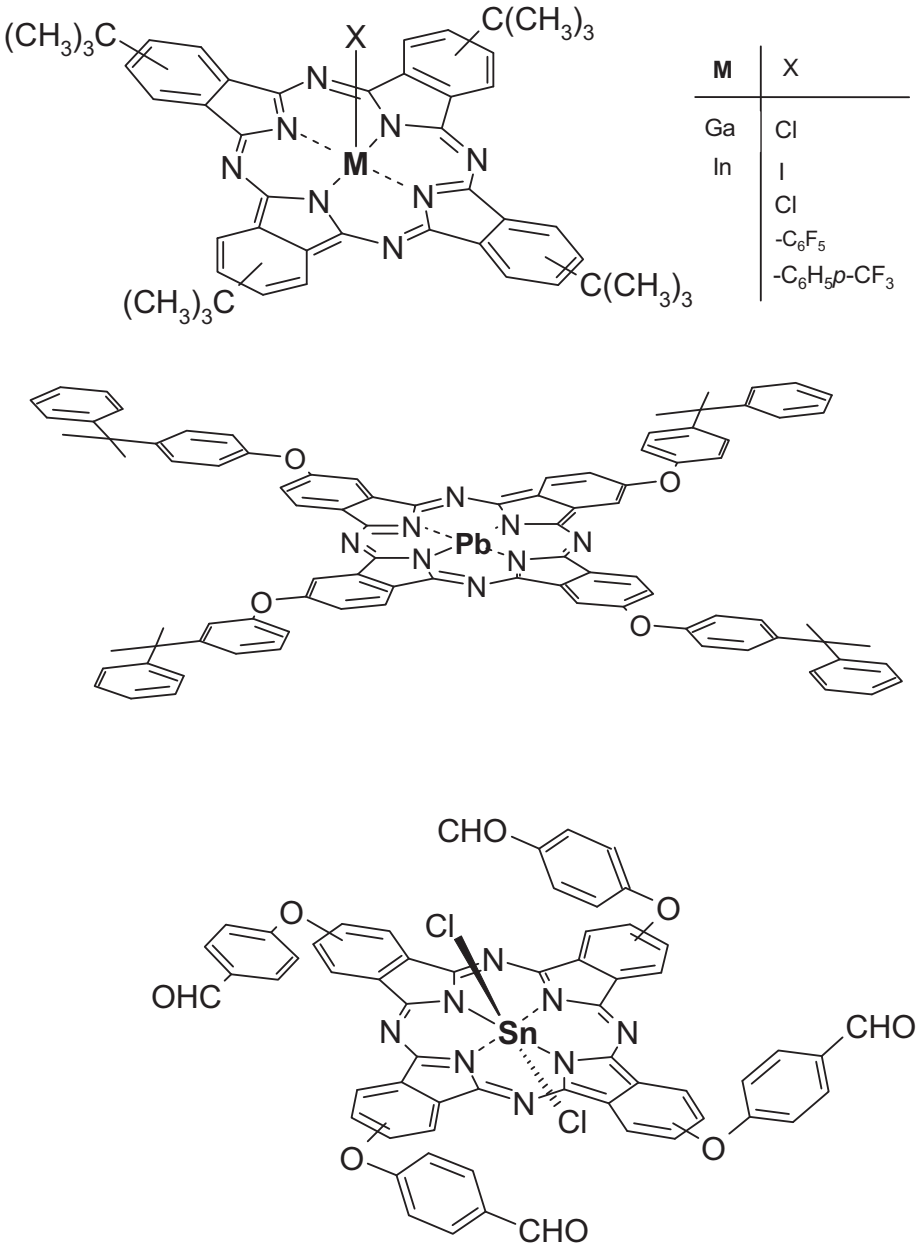

Figure 3.4 Examples of phthalocyanines for optical limiting.

3.3.1 Structural factors affecting optical liming properties of phthalocyanines

The chemical modification of phthalocyanines can affect of their electronic structure and thus their NLO properties. The substitution at the various benzene ring positions of macrocycle, the possibility of exchanging the central metal coordinated within the ring cavity, and the introduction of an axial ligands bound to the central metal can considerably alter the electronic and molecular properties of phthalocyanines. Knowledge of the correlation existing between the electronic structure of the phthalocyanine and its response to light can then allow the synthesis of molecules possessing the required features. The NLO data of several phthalocyanines reported in the literature are collected in **Table 3.1**.

Table 3.1 The NLO data of various phthalocyanines.

Compound	Im$\{\chi^{(3)}\}$ [esu]	λ [nm]	κ $[\sigma_{ex}/\sigma_0]$	method	references
$(CP)_4PcH_2$	4.0e-12	1064		DFWM	52, 53
PcPb	2.0e-11	1064		DFWM	54
$(CP)_4PcPb$	2.0e-11	1064		DFWM	52, 53
$(CP)_4PcPt$	2.0e-10	1064		DFWM	52, 53
$(CP)_4PcPd$	2.0e-11	1064		DFWM	52, 53
$(CP)_4PcZn$	7.0e-12	1064		DFWM	52, 53
$(CP)_4PcCu$	4.0e-11	1064		DFWM	52, 53
$(CP)_4PcNi$	6.0e-11	1064		DFWM	52, 53
$(CP)_4PcCo$	8.0e-11	1064		DFWM	52, 53
PcInCl	1.3e-10	1900		THG	52, 53
(*t*-Bu)$_4$PcGaCl	1.2e-11	532	13.5	z-scan	17
(*t*-Bu)$_4$PcGa(*p*-TMP)	1.1e-11	532	13.6	z-scan	17
(*t*-Bu)$_4$PcInCl	1.6e-11	532	27.4	z-scan	17
(*t*-Bu)$_4$PcZn	1.1e-11	532	11.3	z-scan	17

(*t*-Bu)$_4$PcCo	3.5e-13	532	6.5	z-scan	17
(C$_6$H$_{13}$)$_8$PcInCl	1.2e-11	532	16.1	z-scan	17
(C$_6$H$_{13}$)$_8$PcPd	3.6e-11	532	5.9	z-scan	17
(C$_6$H$_{13}$)$_8$PcZn	1.5e-11	532	11.4	z-scan	17
(C$_6$H$_{13}$)$_8$PcNi	5.9e-13	532	2.4	z-scan	17
(C$_6$H$_{13}$)$_8$PcPb	1.1e-11	532	16.1	z-scan	17
(C$_6$H$_{13}$)$_8$PcH$_2$	6.6e-12	532	14.5	z-scan	17
(C$_{10}$H$_{21}$)$_8$PcH$_2$	5.8e-12	532	14.4	z-scan	17, 57
(Ciso$_5$H$_{11}$)$_8$PcH$_2$	5.9e-12	532	11.3	z-scan	17, 57
(C$_{10}$H$_{21}$)$_8$PcZn	9.1e-12	532	11.7	z-scan	17, 57
(Ciso$_5$H$_{11}$)$_8$PcZn	1.5e-11	532	12.2	z-scan	17, 57
(fPhO)$_4$PcH$_2$	4.4e-12	532	5.7	z-scan	55
(fPhO)$_4$PcGeCl$_2$	7.2e-12	532	13.0	z-scan	55
(fPhO)$_4$PcSnCl$_2$	1.1e-11	532	16.9	z-scan	55
PcNi	1.6e-12	2100		THG	59
(NH$_2$)$_4$PcNi	1.63e-12	2100		THG	58
PcCu	1.1e-12	2100		THG	59
(NH$_2$)$_4$PcCu	2.0e-12	2100		THG	58
(SC$_8$H$_{17}$)$_4$PcCu	5.0e-11	2100		THG	59

In addition, the low symmetry of phthalocyanines can fluctuate the electronic structure of macrocycle and consequently the optical properties [50]. Thus, unsymmetrically substituted phthalocyanines are another tool to modulate the optical limiting properties. Probably due to

the difficulty in the preparation of pure unsymmetrically substituted phthalocyanines, only a few papers described the NLO properties of this kind of compounds [51].

3.3.1.1 Effect of the central metal atom on optical limiting properties of phthalocyanines

The systematic study on the NLO properties of phthalocyanines with different central metals in Pc cavity appeared in 1991 [52]. A series of metallotetrakis(cumylphenoxy)phthalocyanines $(CP)_4PcM$ with the following central atom: M = Pb, Zn, Cu, Ni, Co, Pd and Pt were investigated at 1064 nm by the degenerate four wave mixing (DFWM) measurement [52, 53]. It was found that the value of $\chi^{(3)}$ decreases with increasing atomic number of the metal in a series: $Co(d^7) < Ni(d^8) < Cu(d^9) < Zn(d^{10})$ where **$(CP)_4$PcCo** exhibits the highest value of $\chi^{(3)}$ determined to be 8.0×10^{-11} esu and **$(CP)_4$PcZn** the lowest value of $\chi^{(3)}$ being 7.0×10^{-12} (**Table 3.1**). This indicates that the transition metals with unfilled d-orbital can induce larger third-order optical nonlinearity. In the series of $(CP)_4PcM$ with M = Pt, Ni, Pd where central metals possess the same electronic configuration *i.e.* d^8, the $\chi^{(3)}$ increases in the following order **PcPt** > **PcNi** > **PcPd**. An anticipation of increasing of $\chi^{(3)}$ with an increase of the atomic polarizability of central metal due to the magnification of the electronic cloud in a row from Ni to Pt was not found [7]. In a series of MPcs where the central metal has f-type configuration (M = Sc, Lu, Yb, Y, Gd, Eu, Nd), no strong dependence of the third-order optical properties was found [53].

The linear and nonlinear properties of large number of different metallophthalocyanines have been recently reported [17]. Optical limiting of several phthalocyanine compounds with great diversity of peripheral substituents, central metal M and axial ligands as well as some naphthalocyanines and dimeric Pcs was investigated with the open-aperture z-scan [17]. It was presented that the largest values of κ were found for complexes RPcM with M = In, Zn, Ga, 2H, Pd and Pb, whereas M = Ni, Co and Zn complexes displayed lower values (**Table 3.1**). The observed κ value of metallated tetrakis(*tert*-butyl)phthalocyanines $(t\text{-Bu})_4PcM$ where M = In, Zn, Ga and Co diminished in a series: κ (**$(t\text{-Bu})_4$PcInCl**) < κ (**$(t\text{-Bu})_4$PcGaCl**) < κ (**$(t\text{-Bu})_4$PcZn**) < κ (**$(t\text{-Bu})_4$PcCo**) where the **$(t\text{-Bu})_4$PcInCl** exhibited the highest value of κ determined to be 27.4 in the entire study (**Table 3.1**). Comparison of indium and palladium octaalkyl-substituted phthalocyanines $(C_6H_{13})_8PcM$ showed that much larger value of κ was obtained for **$(C_6H_{13})_8$PcInCl** than for the corresponding palladium compound **$(C_6H_{13})_8$PcPd** (**Table 3.1**). The opposite situation was observed in comparison of nonlinear absorption

coefficient β_I, where **$(C_6H_{13})_8$PcPd** possessed ~ 3 times higher value of β_I than **$(C_6H_{13})_8$PcInCl** [17]. Moreover, the highest value of the saturation energy density F_{Sat} was found for In, Ga and Co phthalocyanine complexes. Interestingly, the study [17] includes MPcs with both the lowest κ factor (PcCo) and the highest κ factor (PcIn). In general, no clear relation between the central metal's atomic mass and the κ value was found. On the other hand, it was proved that the κ values show a regular dependence on the absorption coefficient α_0 of the Pc in the ground state at the same wavelength. Moreover, a linear relationship between log(κ) and log(α_0) was found [17].

The optical limiting of tetrakis(*p*-formylphenoxy)phthalocyanines $(fPhO)_4PcM$ with M = Sn, Ge and 2H was investigated by the use of the open-aperture z-scan [55]. The magnitude of the third-order optical nonlinearities $\chi^{(3)}$ considerably rose with an increase in the size of the central metal as follows: 2H < Ge(IV) < Sn(IV). The same trend was observed in the κ value, where **$(fPhO)_4PcSnCl_2$** exhibited the highest κ value of the others (**Table 3.1**).

3.3.1.2 Effect of peripheral substituents on nonlinear properties of phthalocyanines

Peripheral substituents in phthalocyanines can also influence the NLO properties by altering the electronic structure of the molecule, or by modification of the spatial relationship between adjacent molecules. Moreover, the nature of the peripheral substituents can intensely affect the aggregation and the supramolecular structure of the aggregates and, consequently, change the nonlinear optical properties of phthalocyanines. The metal-free phthalocyanines with different peripheral substituents (tetrakis(*t*-butyl) and hexadeca(trifluoroethoxy)) were investigated [56]. It was found that, since the concentration of **$(t\text{-}Bu)_4PcH_2$** was higher than 0.5 wt. %, the nonlinear absorption coefficient began to decrease, whereas metal-free phthalocyanine **$(CF_3CH_2O)_{16}PcH_2$** displayed almost constant nonlinear absorption coefficient within the same range of concentration [56]. The CF_3CH_2O peripheral groups strongly diminish the molecular aggregation. This study showed evidently that aggregation has an influence on NLO properties.

NLO properties of a series of metallated and metal-free 1,4-octaalkyl-substituted phthalocyanines R_8PcM were recently investigated [17, 57]. The peripheral substituents in nonperipheral positions induce a partial distortion of the ring (**Figure 3.5**), thus, they significantly suppress the aggregation.

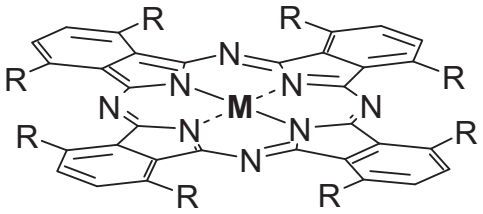

R = CnHm
$5 \leq n \leq 10$
$11 \leq m \leq 21$
M = 2H, Ni, Zn, Cu, Pd, Pb, InCl

Figure 3.5 Octaalkyl-substituted phthalocyanines for optical limiting.

The magnitude of $\chi^{(3)}$ was found to be similar for **$(C_6H_{13})_8$PcZn** and **$(Ciso_5H_{11})_8$PcZn** while for **$(C_{10}H_{21})_8$PcZn** the value of $\chi^{(3)}$ was lower (**Table 3.1**) [17]. Those zinc phthalocyanine complexes exhibit relatively similar and high value of κ, indicating that the variation of length of alkoxy chain in peripheral positions of macrocycle does not significantly contribute to better optical limiting. Moreover, octaalkyl-substituted PcIns exhibit the highest κ values whereas alkyl-substituted PcPds are the compounds with the largest values of β_I [17, 57].

The $\chi^{(3)}$ values of copper and nickel phthalocyanines containing NH_2 and SC_8H_{17} peripheral substituents were measured by THG experiment [58, 59]. The values of $\chi^{(3)}$ for copper and nickel tetraamino-substituted (**$(NH_2)_4$PcCu** and **$(NH_2)_4$PcNi**) complexes were slightly larger than for unsubstituted compounds, **PcCu** and **PcNi** [59]. Moreover, compound **$(SC_8H_{17})_4$PcCu** exhibited the $\chi^{(3)}$ value an order of magnitude higher compared to **PcCu** (**Table 3.1**) [59].

The effect of peripheral substituents was investigated for substituted titanyl phthalocyanines containing alkyl and electron-withdrawing groups (**Figure 3.6**) [60].The compound **A** (**Figure 3.6**) showed very low value of transmittance at high levels of irradiation [60].

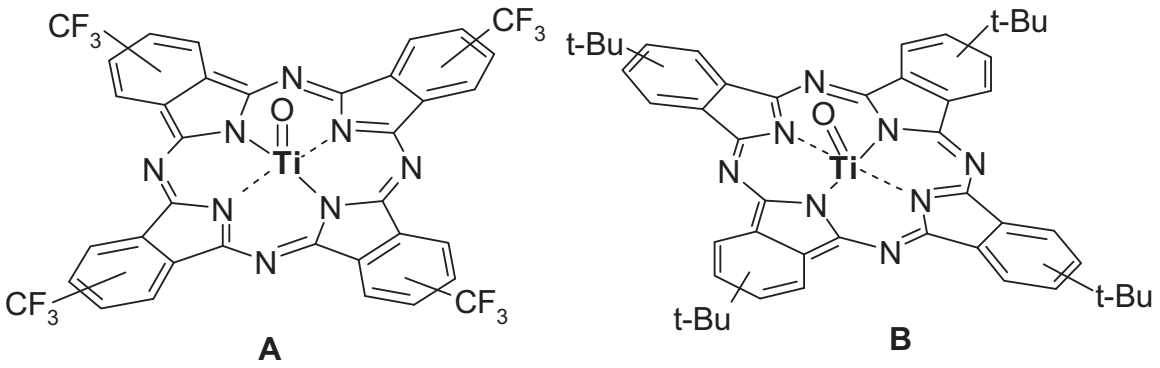

Figure 3.6 2,3-Tetra-trifluoromethylphthalocyaninato titanium oxide (**A**) and 2,3-tetra-*tert*-butylphthalocyaninato titanium oxide (**B**).

It was discussed that species with an electron-withdrawing groups display a more effective OL because these groups produce larger variations of the transition dipole moments in correspondence to the electronic transition responsible for the OL effect [61]. Presumably this effect can increase the excited state absorption cross section and the κ factor, since the ground state absorption cross section is not as influenced as the excited state cross section by the presence of electron-withdrawing substituents.

3.3.1.3 Effect of the axial substitution on optical limiting properties of phthalocyanines

The attachment of the axial ligands X to the central atom M may significantly alter the third-order phthalocyanine optical properties [62, 63]. It was shown that variation of axial substituents at metal M = VO, TiO, GaCl, AlCl and InCl of phthalocyanines noticeably changes their NLO properties [62-64]. The significant enhancement of $\chi^{(3)}$ of PcMXs is explained by the introduction of the dipole moment perpendicularly oriented to the Pc ring plane by the presence of axial ligands at the central atom M, which vary the electronic structure of the Pcs in the ground and excited states, and the introduction of new steric effects, which modify the aggregation properties of PcMX's [46].

The first comparative study on the effect of axial substituents X in MPc's on the OL properties was described by Shirk and Hanack group for (*t*-Bu)$_4$PcInX with X = Cl, Br, I, *p*-trifluorophenyl (*p*-TMP), *m*-trifluorophenyl (*m*-TMP), phenyl, pentafluorophenyl (PFP) and *p*-fluorophenyl (*p*-FP) [23, 46, 65-68] (**Figure 3.7**).

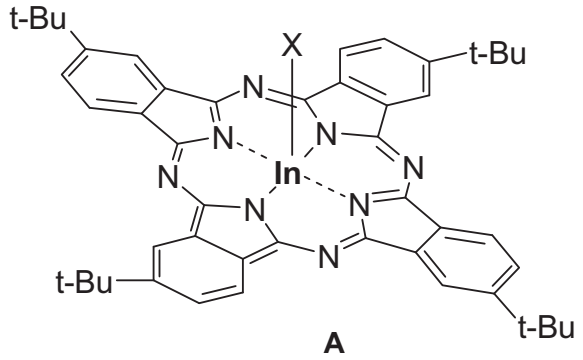

	X	abbrevation
1	-Cl	
2	-Br	
3	-I	
4	$-C_6F_5$	(PFP)
5	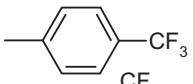	(*p*-TMP)
6	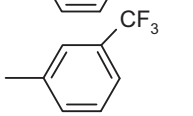	(*m*-TMP)
7	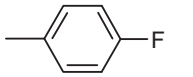	(*p*-FP)

Figure 3.7 (*t*-Bu)$_4$PcInX with different axial substituents X for optical limiting.

The aryl-substituted indium complexes display high solubility in common organic solvents and remarkably diminish the aggregation in solution. It was found that the aryl-substituted indium complexes (**A4** and **A5** in **Figure 3.7**) exhibited higher nonlinear absorption coefficients, lower limiting thresholds, and lower transmission at high fluences compared to **(*t*-Bu)$_4$PcInCl** compound [23, 46]. The transient absorption study of compounds **A1**, **A4**, and **A5** (**Figure 3.7**) showed that incident light in the region between 420 and 600 nm provoked excitation of the system to the singlet state, which was converted into excited triplet state with an ISC time in the range of 300 ps [46]. Thus, the materials behaved as reverse saturable absorbers in the 420 - 600 nm range. The nonlinear absorption coefficients α for all axially substituted indium complexes were found to be the largest ever measured in various phthalocyanines [65-68]. The **(*t*-Bu)$_4$PcInI** displayed higher intersystem crossing rate than **(*t*-Bu)$_4$PcInCl**. However, the quantum yields of the excited triplet state were the same for both compounds [46, 65-68]. It can be explained by heavy atom effect of the iodine axial ligand, which enhances the formation of triplet excited state in the nonlinear optical window [69].

The NLO properties of oxotitanium tetrakis(*t*-butyl)Pc (**Figure 3.8**) have been investigated in order to explain how the differently substituted axial aromatic ligands affect the reverse saturable absorption [65-68].

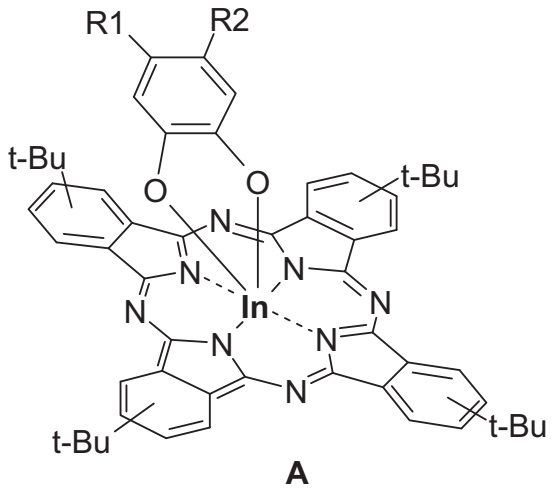

A

	R1	R2
1	H	H
2	H	CHO
3	H	*t*-Bu
4	CN	CN
5	H	CH_2CN

Figure 3.8 Axially catechol-substituted (*t*-Bu)$_4$PcTi for optical limiting.

It was proved that the molecules with electron-withdrawing substituents at the axial ligands displayed much better optical limiting response [65-68]. The electron-withdrawing groups such as CN, CHO, CH_2CN, and Br attached to the axial catechol additionally give rise to the dipole moment perpendicular to the macrocycle. It was found that with increasing the dipole moment the better OL effect was obtained. This indicates that the magnitude of the imaginary nonlinear responses at presented intensities considerably rises with increase of the electron-withdrawing character of the groups in the axial catechol ligand as follows: **A3** < **A2** < **A5** < **A4** [65-68]. Furthermore, the bulky functionalized catechol ligands induce a steric crowding and significantly reduce aggregation. For the first time the authors showed that the NLO properties could be altered by electron-withdrawing substituents at axial ligand in the oxotitanium phthalocyanines.

The optical liming effect of (*t*-Bu)$_4$PcGaX with X = Cl and *p*-trifluorophenyl (*p*-TMP) was also investigated. Both compounds, **(*t*-Bu)$_4$PcGaCl** and **(*t*-Bu)$_4$PcGa(*p*-TMP)**, displayed high and similar $\chi^{(3)}$ and κ values (**Table 3.1**) [17, 43]. However, the saturation energy density F_{Sat} value for **(*t*-Bu)$_4$PcGa(*p*-TMP)** was ~ 3 times smaller than for **(*t*-Bu)$_4$PcGaCl**, implied that the **(*t*-Bu)$_4$PcGa(*p*-TMP)** compound containing the bulky *p*-TMP axial ligand which suppresses molecular aggregation, attenuated laser pulses of much lower energies than **(*t*-Bu)$_4$PcGaCl** did.

3.3.2 Optical limiting properties of phthalocyanines in thin films

The nonlinear optical properties of a wide variety of phthalocyanines were mainly investigated in solution (references cited in Chapter 3.3.1). However for practical and

commercial applications it is essential to analyse the optical limiting of phthalocyanine compounds in solid-state.

Optical limiting properties of axial and peripheral substituted PcMXs with M = Si, Ge, Sn, In, Al, Ga and Pb were reported (**Figure 3.9**) [70]. An important result is that MPcs in PMMA (poly (methylmethacrylate)) and in organically modified sol gel films (ORMOSIL) possessed similar excited state properties (triplet-triplet absorption spectra, triplet quantum yields) and ratios of σ_{ex}/σ_0 as in toluene solution. The cross section ratios (σ_{ex}/σ_0) were determined to range from 10 to ~ 30 depending on the central metal of phthalocyanines. The highest values of σ_{ex}/σ_0 and saturation fluence F_{Sat} for phthalocyanines containing heavy atoms (Sn, Pb) in toluene solution as well as in films were obtained [70].

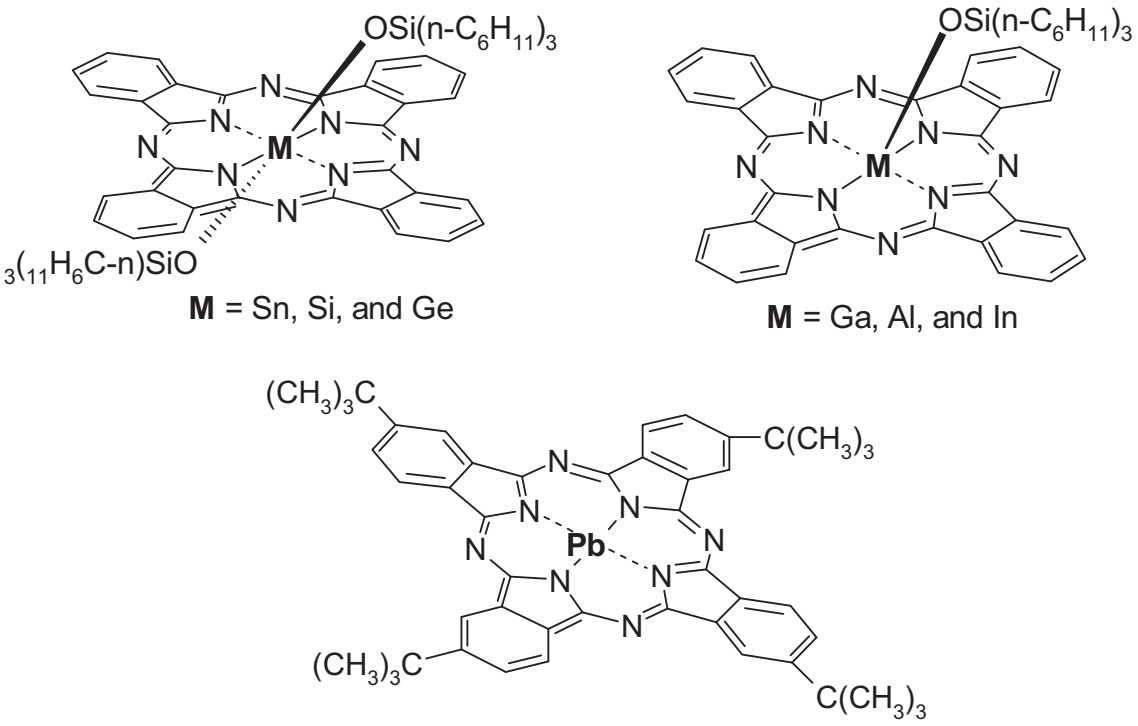

Figure 3.9 A molecular structure of MPc's doped in PMMA.

Spin coated thin films of PcCu and PcVO with tetraalkylthio peripheral substituents were examined by THG technique showing values of $\chi^{(3)}$ of the order of 10^{-11} esu at 1900 and 2100 nm [59, 71]. SHG experiment for unsymmetrically substituted vanadyl phthalocyanines with twelve 2,2,2-trifluoroethoxy groups and one nitro directly at the Pc macrocycle or one exocyclic conjugated nitro group doped in PMMA film showed higher second harmonic signals for the MPc with exocyclic conjugated nitro group which was explained by a more extended π-conjugated system [72]. The third-order susceptibility $\chi^{(3)}$ of phthalocyanines with

tetra-*t*-butyl substituents (*t*-Bu)$_4$PcM with M = 2H, VO, Pb embedded in PMMA thin films was measured [73, 74]. It was found that **(*t*-Bu)$_4$PcH$_2$** complex showed much lower $\chi^{(3)}$ than (*t*-Bu)$_4$PcMs (M= VO, Pb). Also a tendency of the kind of metal on the value $\chi^{(3)}$ was observed [73-75]. Comparison of $\chi^{(3)}$ values of PMMA films of **(*t*-Bu)$_4$PcVO** with unsubstituted **PcVO** showed lower values of $\chi^{(3}$ for **(*t*-Bu)$_4$PcVO** explained by difference in molecular packing caused by the peripheral substituents [74]. OL properties of silicon phthalocyanines either embedded in PMMA or included in copolymers of methylmethacrylate and silicon phthalocyanines axially substituted by methacrylate groups were investigated by DFWM experiment at 598 nm [76]. The results indicated that the value of $\chi^{(3)}$ for the copolymers was higher compared to the value of the Pc embedded in PMMA. In one case a third-order nonlinear optical response of an axial substituted silicon phthalocyanine in a polysiloxane network was described [77].

3.4 References

[1] P. N. Prasad, D. J. Williams, *Introduction to Nonlinear Optical Effects in Molecules and Polymers.* John Wiley & Sons, New York, **1991**.

[2] S. M. Jensen, *IEEE J. Quant. Electron.,* **1982**, QE-18, 1580.

[3] B. Kraabel, A. Malko, J. Hollingsworth, V. I. Klomov, *Appl. Phys. Lett.,* **2001**, 78, 1814.

[4] S. V. Serak, A. V. Agashkov, V. Y. Reshetnyak, *Quantum Electron.,* **2001**, 31, 273.

[5] R. G. Denning, *J. Mat. Chem.,* **1995**, 5, 365.

[6] G. L. Wood, M. J. Miller, A. G. Mott, *Opt. Lett.*, **1995**, 20, 973.

[7] F. Z. Henari, J. Callaghan, W. J. Blau, P. Haisch, M. Hanack, *Pure Appl. Opt.*, **1997**, 6, 741.

[8] F. Z. Henari, J. Callaghan, H. Stiel, W. J. Blau, D. J. Cardin, *Chem. Phys. Lett.*, **1992**, 199, 144.

[9] J. Barroso, A. Costela, I. Garcai-Moreno, J. L. Saiz, *J. Phys. Chem. A*, **1998**, 102, 2527.

[10] J. Callaghan, W. J. Blau, *J. Nonlinear Opt. Phys. Mater.*, **2000**, 9, 505.

[11] L. W. Tutt, S. W. McCahon, M. B. Klein, *SPIE Proc.*, **1990**, 1307, 315.

[12] B. L. Justus, Z. H. Kafafi, A. L. Huston, *Opt. Lett.*, **1993**, 18, 1603.

[13] A. Hochlbaum, Y. Y. Hsu, J. L. Fergason, *SPIE Proc.*, **1994**, 2229, 48.

[14] A. Kost, J. E. Jensen, M. B. Klein, S. W. McCoahon, *SPIE Proc.*, **1994**, 2229, 78.

[15] W. Ji, S. Shi, H. J. Du, *J. Phys. Chem.*, **1995**, 99, 17297.

[16] L. Vivien, D. Riehl, P. Lancon, F. Hache, E. Anglaret, *Opt. Lett.*, **2001**, 26, 223.

[17] S. M. O'Flaherty, S. V. Hold, M. J. Cook, T. Torres, Y. Chen, M. Hanack, W. J. Blau, *Adv. Mater.,* **2003**, 15, 19.

[18] J. Zyss, Nonlinear Optics: Materials*, Physics and Devices*, Academic Press, Boston, MA **1993**.

[19] J. L .Bredas, C. Adant, P. Tackx, A. Persoons, B. M. Pierce, *Chem.Rev*., **1994**, 94, 243.

[20] H. S. Nalwa & S. Miyata, *Nonlinear Optics of Organic Molecules and Polymers*, CRC Press, Boca Raton, FL, **1997**.

[21] G. de la Torre, P. Vazquez, F. Agullo-Lopez, T. Torres, *Chem. Rev*., **2004**, 104, 3723.

[22] J. S. Shirk, A. Rosenberg, *Laser Focus World,* **2000**, 36, 121.

[23] J. W. Perry, K. Mansour, I. Y. S. Lee, X. L. Wu, P. V. Bedworth, C. T. Ng. D. Chen, S. R. Marder, P. Miles, T. Wada, M. Tian, H. Sasabe, *Science,* **1996**, 273, 1533.

[24] D. Sliney, M. Wolbarsht, *Safety with Lasers and other Optical Sensors*. Plenum, New York, **1980**.

[25] D. J. Harter, M. L. Shand, Y. B. Band, *J. Appl. Phys.*, **1984**, 56, 865.

[26] P. Chen, I. V. Tomov, A. S. Dvornikov, M. Nakashima, J. F. Roach, D. M. Alabran, P. M. Rentzepis, *J. Phys. Chem.,* **1996**, 100, 17507.

[27] S. Couris, E. Koudoumas, A. A. Ruth, S. Leach, *J. Phys. B: At. Mol. Opt. Phys. Lett.,* **1995**, 28, 4537.

[28] B. Taheri, H. Liu, B. Jassemnejad, D. Appling, R. C. Powell, J. J. Song, *Appl. Phys. Lett.,* **1996**, 68, 1317.

[29] M. Hercher, *Appl. Opt.,* **1967**, 6, 94.

[30] Y. Prior, H. Vogt, *Phys. Rev. B,* **1979**, 19, 5388.

[31] I. M. Skinner, S. J. Garth, *Am. Phys.,* **1990**, 58, 177.

[32] E. W. Van Stryland, M. Sheik-Bahae, A. A. Said, D. J. Hagan, *Prog. Crystal Growth and Charact.*, **1993**, 27, 279.

[33] D. G. McLean, R. L. Southerland, M. C. Brant, D. M. Brendelik, P. A. Fleitz, T. Pottenger, *Opt, Lett.,* **1993**, 18, 858.

[34] F. Kajzar, J. Messier, *Phys. Rev. A,* **1985**, 32, 2352.

[35] F. Kajzar, J. Messier, C. Rosilio, *J. Appl. Phys.,* **1986**, 60, 3040.

[36] G. R. Meredith, B. Buchalter, C. Hanzlik, *J. Chem. Phys.,* **1983**, 78, 1533.

[37] A. Yariv, *IEEE J. Quantum Eletron.,* **1978**, QE-14, 650.

[38] C. R. Guiliano, *Physics Today,* **1981**, 27.

[39] R. C. Lind, D. G. Steel, G. J. Dunning, *Opt. Eng.,* **1982**, 21, 190.

[40] J. F. Reintjes, *Nonlinear Optical Parametric Processes in Liquids and Gases,* Academic Press, New York, **1984**, Chapter 5, 327ff.

[41] M. Sheik-Bahae, A. A. Said, T.-H. Wei, D. J. Hagan, and E. W. Van Stryland, *IEEE Journal of Quantum Electronics,* **1990**, 26**,** 760.

[42] J. R.Heflin, D. C. Rodenberger, R. F. Shi, M. Wu, N. Q. Wang, Y. M. Cai, A. F. Garito, *Phys. Rev. A,* **1992**, 45, 4233.

[43] Y. Chen, L. R. Subramanian, M. Barthel, M. Hanack, *Eur. J. Inorg. Chem.*, **2002**, 1032.

[44] Y. Chen, M. Barthel, M. Seiler, L. R. Subramanian, S. Vagin, M. Hanack, *Angew. Chem.,* **2002**, 114, 3373.

[45] Y. Chen, M. Barthel, M. Seiler, L. R. Subramanian, S. Vagin, M. Hanack, *Angew. Chem. Int. Ed.*, **2002**, 41, 3239.

[46] J. S. Shirk, R. G. S. Pong, S. R. Flom, H. Heckmann, M. Hanack, *J. Phys. Chem. A.*, **2000**, 104, 1438.

[47] Y. Chen, L. R. Subramanian, M. Fujitsuka, O. Ito, S.O'Flaherty, W. J. Blau, T. Schneider, D. Dini, M. Hanack, *Chem. Eur. J.,* **2002**, 8, 4248.

[48] J. S. Shirk, R. G. S. Pong, F. J. Bartolo, A. W. Snow, *Appl. Phys. Lett.*, **1993**, 63, 1880.

[49] J. S. Shirk, R. G. S. Pong, S. R. Flom, R. J. Bartoli, M. E. Boyle, A. W. Snow, *Pure Appl. Opt.*, **1996**, 5, 701.

[50] G. de la Torre, P. Vasquez, F. Agullo-Lopez, T. Torres, *J. Mat.Chem.,* **1998**, 8, 1671.

[51] Y. Liu, Y. Xu, D. Zhu, X. Zhao, *Thin Films Solid,* **1996**, 289, 282.

[52] J. S. Shirk, J. R. Linde, F. J. Bartoli, Z. H. Kafafi, A. W. Snow, In *Materials for Nonlinear Optics-Chemical Perspectives.* S. R. Mareder, J. E. Sohn, G. D. Stucky, *Eds., ACS Symposium*, **1991**, Series 445; Chapter 42, 626.

[53] J. S. Shirk, J. R. Lindle, F. J. Bartoli, Z. H. Kafafi, *International J. Nonlinear Opt.*, **1992**, 1, 699.

[54] J. S. Shirk, J. R. Lindle, F. J. Bartoli, C. A. Hoffman, Z. H. Kafafi, A. Snow, *Appl. Phys. Lett.*, **1989**, 55, 1287.

[55] A. Slodek, D. Wöhrle, J. J. Doyle, W. Blau, *Macromol. Symp.*, **2006**, 235, 9.

[56] T. Wada, S. Yanagi, H. Kobayashi, J. Kumar, K. Sasaki, H. Sasabe, *SPIE*, **1994**, 2143, 172.

[57] A. Auger, W. Blau, P. M. Burnham, I. Chambrier, M. J. Cook, B. Isaure, F. Nekelson, S. M. O'Flaherty, *J. Mat. Chem.*, **2003**, 13, 1042.

[58] H. S. Nalwa, A. Kakuta, *Thin Solid Films*, **1995**, 254, 218.

[59] H. Matsuda, S. Okada, A. Masaki, H. Nakanishi, Y. Suda, K. Shigehara, A. Yamada, *SPIE Proc.*, **1990**, 1337, 105.

[60] D. Dini, M. Barthel, M. Hanack, T. Schneider, M. Ottmar, S. Serma, *Sol. St. Ionics,* **2003**, 165, 289.

[61] D. Dini, G. Y. Yang, M. Hanack, *J. Chem. Phys.*, **2003**, 119, 4857.

[62] J. L. Petersen, C. S. Schramm, D. R. Stojakovic, B. M. Hoffma, T. J. Marks, *J. Amer. Chem. Soc.*, **1997**, 99, 286.

[63] R. S. Gairns, In *The Chemistry and technology of Printing and Imaging System.* Blackie:London, **1996**, 76.

[64] H. S. Nalwa, S. Kobayashi, A. Kakuta, *Nonlinear Optics*, **1993**, 6, 169.

[65] M. Hanack, T. Schneider, M. Barthel, J. S. Shirk, S. R. Flom, R. G. S. Pong, *Coord. Chem. Rev.*, **2001**, 219, 235.

[66] M. Hanack, D. Dini, M. Barthel, S. Vagin, *Chem. Rec.*, **2002**, 2, 129.

[67] D. Dini, M. Hanack, M. Barthel, *Eur. J. Org. Chem.*, **2001**, 3759.

[68] M. Calvete, G. Y. Yang, M. Hanack, *Synth. Met.*, **2004**, 141, 231.

[69] N. J. Turro, *Modern Molecular Photochemistry,* Benjamin/Cummings: Menlo Park, **1978**.

[70] K. Mansour, P. D. Fuqua, S. R. Marder, B. Dann, J. W. Perry, *SPIE Proc.*, **1994**, 2143, 239.

[71] Y. Suda, K. Shigenhara, A. Yamada, H. Matsuda, S. Okada, A. Masaki, H. Nakanishi, *SPIE Proc.*, **1991**, 1560, 75.

[72] M. Tian, T. Wada, H. Kimura-Suda, H. Sasabe, *J. Mater. Chem.*, **1997**, 7, 861.

[73] T. Wada, S. Yanagi, H. Kobayashi, J. Kumor, K. Sasaki, H. Sasabe, *SPIE*, **1994**, 2143, 172.

[74] H. Sasabe, T. Wada, M. Hosoda, H. Ohkawo, M.Hara, A. Yamada, A. F. Garito, *SPIE*, **1990**, 1337.

[75] M. Sanghadasa, B. Wu, R. D. Clarck, H. Guo, B.G. Penn, *Proc. SPIE-Ins. Soc. Opt. Eng.,* **1997**, 3147, 185.

[76] R. A. Norwood, J. R. Sounik, J. Popolo, D. R. Holcomb, *SPIE*, **1991**, 1560, 55.

[77] B. K. Mandal, B. Bihari, A. K. Sinha, M. Kamath, *Appl. Phys. Lett.*, **1995**, 68, 932.

4. Synthesis and characterization of phthalocyanine complexes

The aim of synthesis was to prepare phthalocyanines (Pcs) that will be used as optical limiters. The tin and germanium were chosen as atoms incorporated in the phthalocyanine ring. The Sn and Ge ions incorporated to the phthalocyanine cavity with the charge of +4 enable axial substitution and furthermore, enhance the solubility. The heavy metal as tin was especially chosen due to increase of intersystem crossing rate from the first excited singlet state to the first excited triplet state $S_1 \rightarrow T_1$. Additionally, syntheses of phthalocyanines were intended to introduce electron-withdrawing groups in annulene rings in order to alteration the electronic properties and transition dipole moment. Phthalocyanines with these features were synthesized and then their nonlinear optical (NLO) properties were investigated.

Many tetra-, one octa-, and hexadeca-substituted phthalocyanines with different electron-withdrawing groups attached to the phthalocyanine macrocycle and with the variation of axial ligands were prepared. All analytical data are presented in Chapter 6th. Some of the tin and germanium phthalocyanine complexes enough soluble were used for preparation of films (Chapter 7.3). The NLO properties of all synthesized metal-free, germanium and tin phthalocyanines were investigated in solutions. Enough soluble Pcs were used for preparation of films in different matrixes and with various numbers of layers. Optical limiting of eight phthalocyanines was examined in detail in films. NLO properties of synthesized phthalocyanines in solution and in films are presented and discussed in Chapter 8th.

4.1 Synthesis of phthalonitriles

Substituted phthalonitriles are good starting materials for preparation of the phthalocyanines. The phthalonitriles: 4-(4-nitrophenoxy)phthalonitrile (**1**) and 4-(4-formylphenoxy)phthalonitrile (**2**) were used as the precursors in the preparation of the phthalocyanines **3** and **4**, and thus their synthesis will be discussed.

Commercially available 4-nitrophthalonitrile (**I**) was used as starting material for preparation of both substituted phthalonitriles **1** and **2**. Synthesis by a typical base catalyzed nucleophilic aromatic substitution (S_NAr) was introduced (**Figure 4.1**). Generally, the nitro group is after fluorine [1] the best leaving group in S_NAr. The S_NAr mechanism depends in first step on formation of a tetrahedral intermediate (**Figure 4.1**) and its creation is contributed by leaving groups possessing strong *-I* effects (the electron-withdrawing inductive effect) [2].

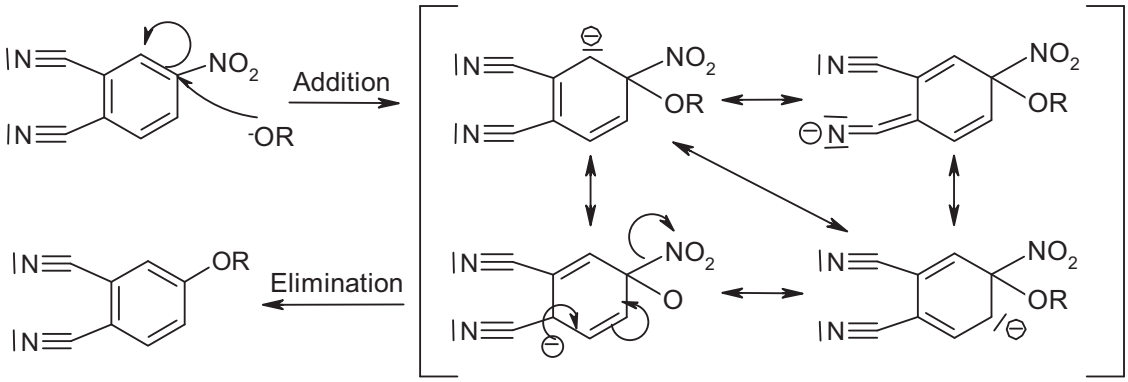

Figure 4.1 Mechanism of nucleophilic aromatic substitution.

The nitro group in 4-nitrophthalonitrile (**I**) is very mobile and undergoes easily nucleophilic replacement. The 4-(4-nitrophenoxy)phthalonitrile (**1**) was synthesized according to the method used by A. A. Hirth [3]. The reaction of 4-nitrophthalonitrile (**I**) with 4-nitrophenol (**II**) in polar aprotic solvent dimethylsulfoxide (DMSO) with twice addition of potassium carbonate (K_2CO_3) at room temperature under stirring led to **1** (**Figure 4.2**). According to method described by A. A. Hirth the reaction should be stirred for additional 96 hours but it was found that same yield was obtained if the reaction was allowed to carry on for just another 48 hours.

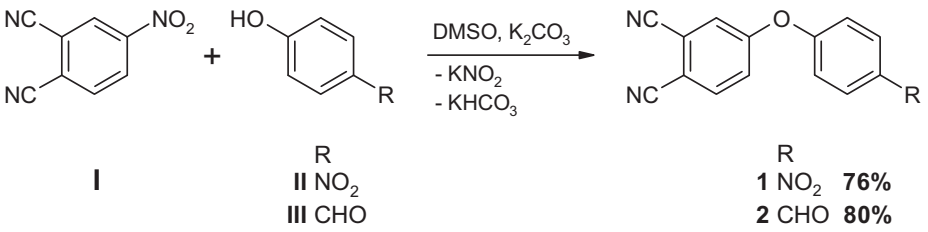

Figure 4.2 Synthesis of phthalonitriles **1** and **2**.

The synthesis of 4-(4-formylphenoxy)phthalonitrile (**2**) was carried out by nucleophilic displacement of nitro group in 4-nitrophthalonitrile (**I**) by formylphenoxy group from 4-formylphenol (**III**) in dry DMSO and with addition of K_2CO_3 (three times) in every 24 hours (**Figure 4.2**). The reaction was carried out under nitrogen at room temperature with gentle stirring for 72 hours. The crude products **1** and **2** were few times recrystallized from methanol (MeOH). Good purity and nice yields (76% for **1** and 80% for **2**) were obtained. The compounds were characterized by IR and MS spectroscopy. The IR spectrum of **1** was verified with intense C≡N vibration at 2234 cm^{-1}, C-O-C in the range 1225-1157 cm^{-1}, and

NO_2 stretches at 1513 cm^{-1}. The IR spectrum of **2** clearly indicates the presence of C≡N at 2230 cm^{-1}, C-O-C at 1232-1178 cm^{-1}, and C=O at 1698 cm^{-1} (detailed analytical data in Chapter 6.3).

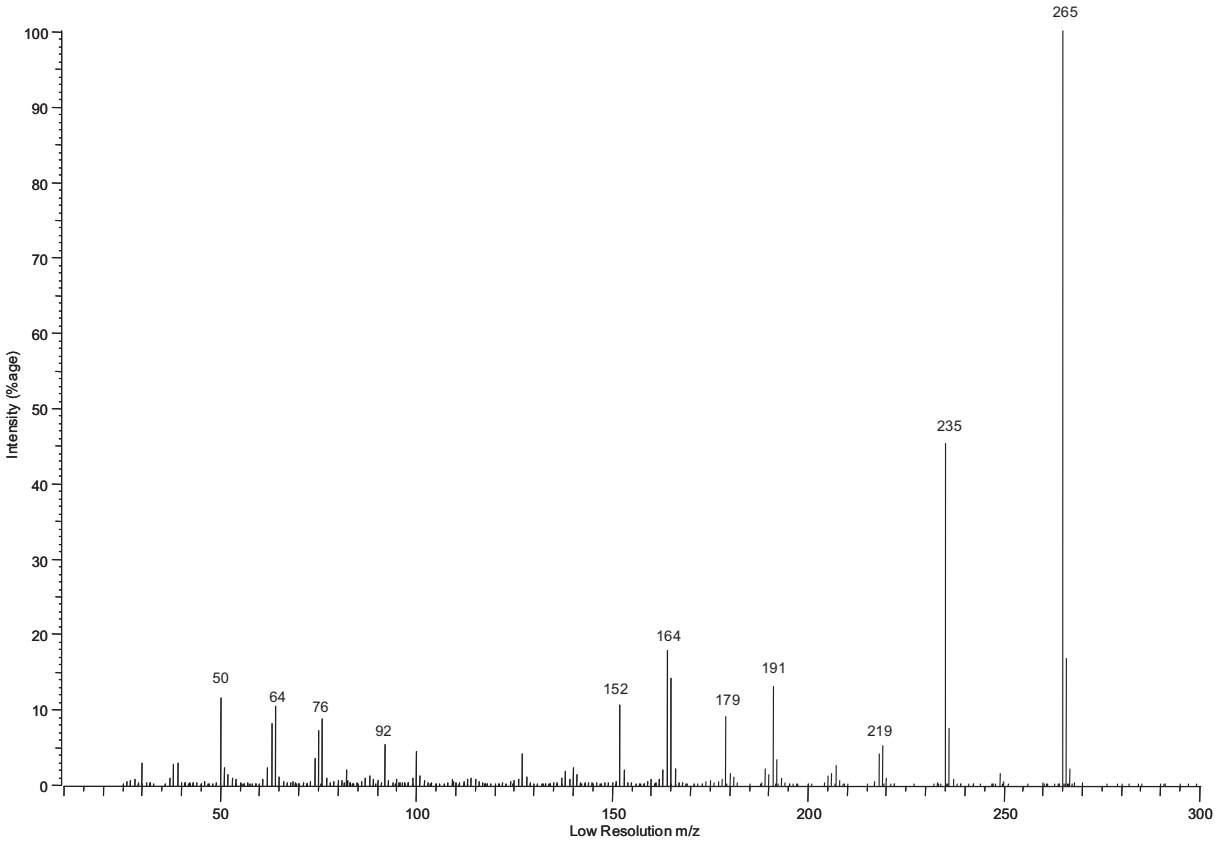

Figure 4.3 EI-MS spectrum of 4-(4-nitrophenoxy)phthalonitrile (**1**).

The Electron Impact Ionization (EI) mass spectra (**Figure 4.3** and **4.4**) confirm the identity of compounds **1** and **2**. In the EI-MS spectrum of compound **1** molecular ion appears at 295 *m/z* and the fragmentation pattern shows the sequential loss of the ligands: NO (235 *m/z*) and NO_2 (219 *m/z*). The peaks at 191 and 179 *m/z* correspond to fragments $C_{12}H_3N_2O^+$ and $C_{11}H_3N_2O^+$ (**Figure 4.3**). The EI-MS spectrum of **2** (**Figure 4.4**) displays main peak at 248 *m/z*, and peaks at 247 and 219 *m/z* represent the loss of hydrogen (H) and formyl (CHO) group, respectively (IR and MS data in Chapter 6.3).

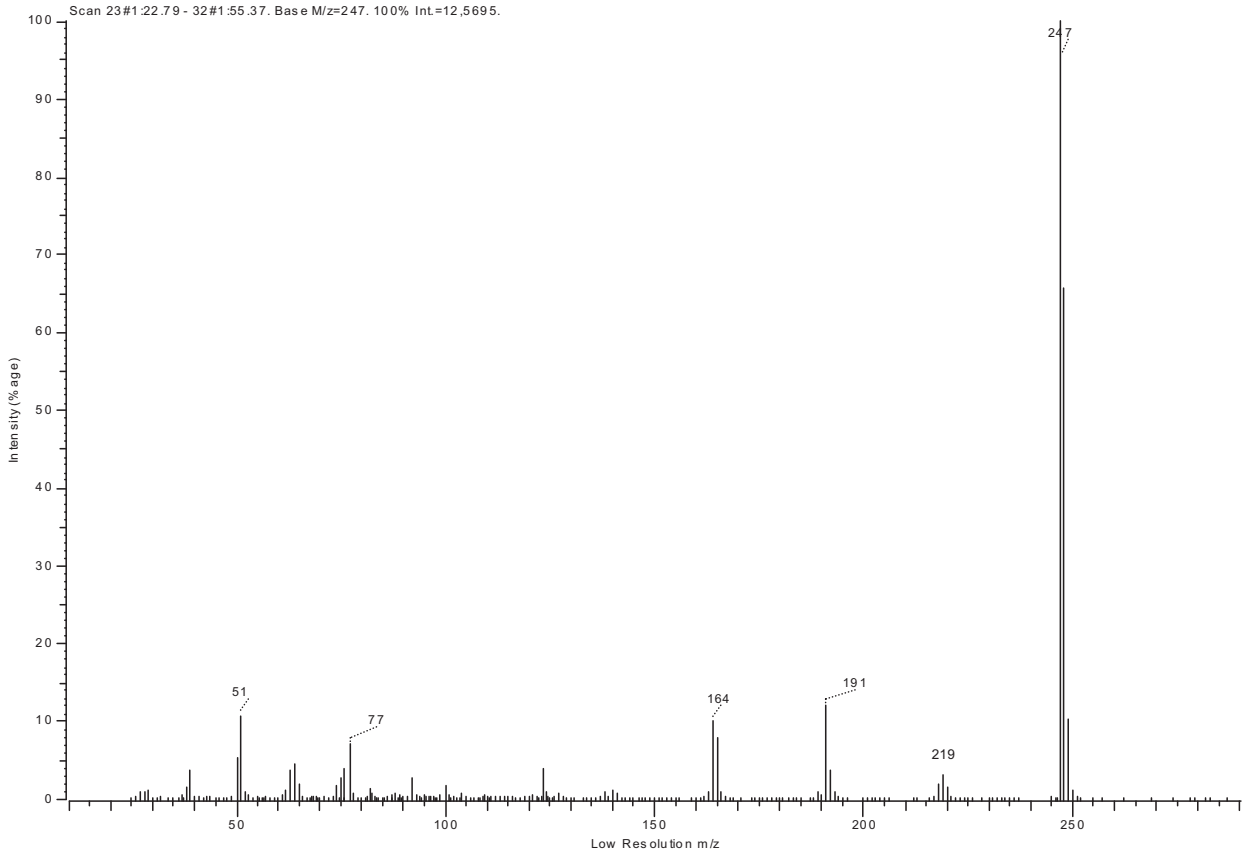

Figure 4.4 MS- spectrum (EI) of 4-(4-formylphenoxy)phthalonitrile (**2**).

4.2 Synthesis of tetra- and octa-substituted phthalocyanines

The metal-containing tetrasubstituted phthalocyanines were obtained from monosubstituted phthalonitriles or by metallation of metal-free tetrasubstituted phthalocyanines as a mixture of four regioisomers of C_{4h}, D_{2h}, C_{2h}, and C_s symmetry (**Figure 4.5**).The mixture of similar isomers enhance the solubility of tetrasubstituted phthalocyanines [4]. The separation of tetrasubstituted phthalocyanines into constitutional isomers was achieved analytically by high performance liquid chromatography (HPLC) and in a preparative scale with medium pressure liquid chromatography (MPLC) by Hanack [5-7].

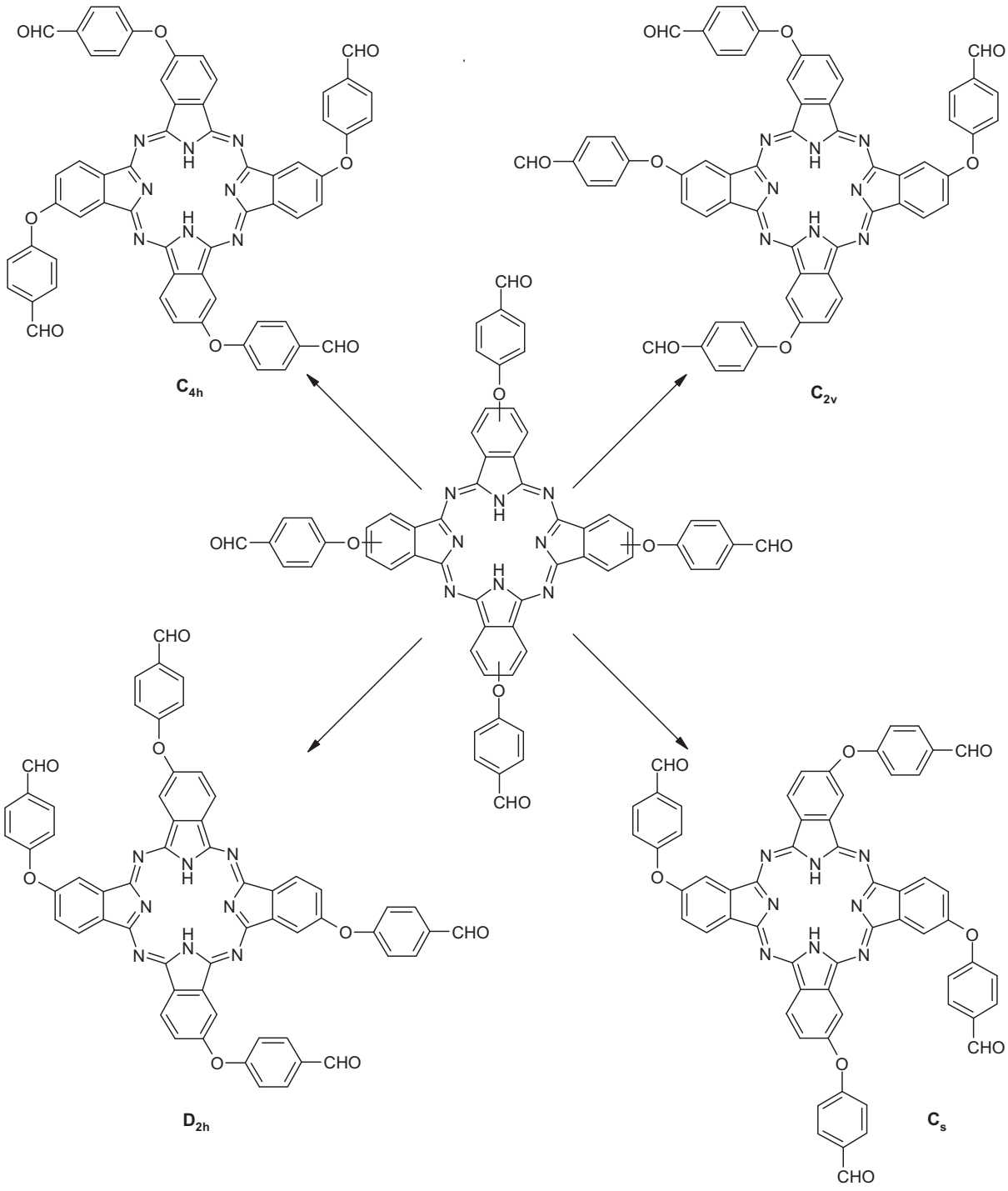

Figure 4.5 The stereoisomers of 2,9,16,23-tetrakis(4-formylphenoxy)phthalocyanine (**3**).

The all tetrasubstituted phthalocyanines presented in the study are a mixture of the four isomers. The presented figures of routes of synthesis of phthalocyanines contain one of the four isomers in order to be clear. The names, abbreviations, numbers, peripheral and axial substituents, molecular weights, yields and analytical data discussed in this subchapter phthalocyanines are presented in **Table 4.1** and **4.2**.

Table 4.1 Abbreviations, numbers, and peripheral and axial substituents of tetra- and octasubstituted phthalocyanines.

Compound	Abbreviation	No	Peripheral substituent	Axial substituent
2,9,16,23-tetrakis(4-formylphenoxy)phthalocyanine	**(fPhO)$_4$PcH$_2$**	**3**	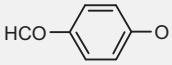 *p*-formylphenoxy	
2,9,16,23-tetrakis(4-nitrophenoxy)phthalocyanine	**(nPhO)$_4$PcH$_2$**	**4**	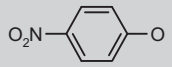 *p*-nitrophenoxy	
dichlorotin(IV) 2,9,16,23-tetrakis(4-nitrophenoxy)phthalocyanine	**(nPhO)$_4$PcSnCl$_2$**	**5**	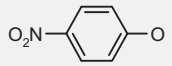	Cl
dichlorotin(IV) 2,9,16,23-tetrakis(4-formylphenoxy)phthalocyanine	**(fPhO)$_4$PcSnCl$_2$**	**6**	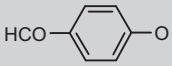	Cl
dichlorogermanium(IV) 2,9,16,23-tetrakis(4-formylphenoxy)phthalocyanine	**(fPhO)$_4$PcGeCl$_2$**	**7**	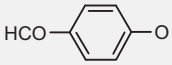	Cl
dichlorotin(IV) 2,9,16,23-tetranitrophthalocyanine	**(*β*NO$_2$)$_4$PcSnCl$_2$**	**18**	NO_2	Cl
dichlorotin(IV) 1,8,15,22-tetranitrophthalocyanine	**(*α*NO$_2$)$_4$PcSnCl$_2$**	**19**	NO_2	Cl
dichlorogermanium(IV) 2,9,16,23-tetranitrophthalocyanine	**(*β*NO$_2$)$_4$PcGeCl$_2$**	**20**	NO_2	Cl
dihydroxygermanium(IV) 2,9,16,23-tetranitrophthalocyanine	**(*β*NO$_2$)$_4$PcGe(OH)$_2$**	**21**	NO_2	OH
dichlorogermanium(IV) 1,8,15,22-tetranitrophthalocyanine	**(*α*NO$_2$)$_4$PcGeCl$_2$**	**22**	NO_2	Cl
bis(3,5-di-*tert*-butylphenoxy)germanium(IV) 2,9,16,23-tetranitrophthalocyanine	**(*β*NO$_2$)$_4$PcGe(*t*Bu$_2$P)$_2$**	**23**	NO_2	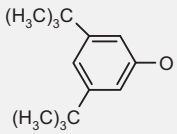
chloroindium(III) 2,9,16,23-tetrakis(*tert*-butyl)phthalocyanine	**(*t*-Bu)$_4$PcInCl**	**25**	$C(CH_3)_3$	Cl
dichlorotin(IV) 2,3,9,10,16,17,23,24-octacyanophthalocyanine	**(CN)$_8$PcSnCl$_2$**	**24**	CN	Cl

Table 4.2 Molecular weights (**M**), yields, spectral and mass data of tetra- and octasubstituted phthalocyanines.

Compound	**M** [g mol^{-1}]	Yield %	ESI-MS (*m/z*) 100%	IR (KBr, cm^{-1})
(fPhO)$_4$PcH$_2$ (3)	994	39	negative 994.3	1633 (C=O), 1254 and 1022 (C-O-C)
(nPhO)$_4$PcH$_2$ (4)	1062	42	negative 1061.1	1349 (NO_2), 1252 and 1020 (C-O-C)
(nPhO)$_4$PcSnCl$_2$ (5)	1250	54	negative 1050 positive 1215.2	1519 and 1348 (NO_2), 1249 and 1022 (C-O-C)
(fPhO)$_4$PcSnCl$_2$ (6)	1182	38	negative 1182.1 positive 1147.3	1692 (C=O), 1237 and 1023 (C-O-C)
(fPhO)$_4$PcGeCl$_2$ (7)	1136	24	negative 1136.1 positive 1101.3	1633 (C=O), 1254 and 1023 (C-O-C)
(βNO$_2$)$_4$PcSnCl$_2$ (18)	882	76	negative 881.8	3013, 1527 and 1352 (NO_2)
(αNO$_2$)$_4$PcSnCl$_2$ (19)	882	23	negative 881.8	3131, 1537 and 1359 (NO_2)
(βNO$_2$)$_4$PcGeCl$_2$ (20)	836	58	negative 835.9	3095, 1528 and 1350 (NO_2)
(βNO$_2$)$_4$PcGe(OH)$_2$ (21)	800	75	negative 799.9 positive 783.1	3383 (OH), 3094, 1526 and 1346 (NO_2)
(αNO$_2$)$_4$PcGeCl$_2$ (22)	836	14	negative 836	3021, 1537 and 1361 (NO_2)
(βNO$_2$)$_4$PcGe(*t*Bu$_2$P)$_2$ (23)	1176	25	negative 1176.3	2965, 2866, 1532 and 1351 (NO_2), 800
(*t*-Bu)$_4$PcInCl (25)	886	47	negative 886.3	2964, 2865, 1364 ($(CH_3)_3$)
(CN)$_8$PcCl$_2$ (24)	902	63	negative 831.9	2233 (C≡N)

The metal-free phthalocyanines **3** and **4** were prepared as precursors in the synthesis of the metal-containing phthalocyanines **5**, **6** and **7**. The direct synthesis of **(nPhO)$_4$PcSnCl$_2$** (**5**), **(fPhO)$_4$PcSnCl$_2$** (**6**) and **(fPhO)$_4$PcGeCl$_2$** (**7**) from phthalonitriles, **1** and **2**, with appropriate metal chloride even easier and faster was failed.

The metal-free 2,9,16,23-tetrakis(4-formylphenoxy)phthalocyanine (**3**) and 2,9,16,23-tetrakis(4-nitrophenoxy)phthalocyanine (**4**) were prepared by reaction of the corresponding

phthalonitriles, **2** and **1**, in 1-pentanol in the presence of the strong organic base 1,8-diazabicyclo[5.4.0]undec-7-ene (DBU) for 14 hours in case of **3** and 17 hours in case of **4** (**Figure 4.6**). The crude products were washed with organic solvents such as methanol, acetone and diethyl ether. Finally, the column chromatography in pyridine/MeOH gave desired complexes: **(fPhO)$_4$PcH$_2$** (**3**) and **(nPhO)$_4$PcH$_2$** (**4**) in 39 and 42 % yield, respectively (**Table 4.2**).

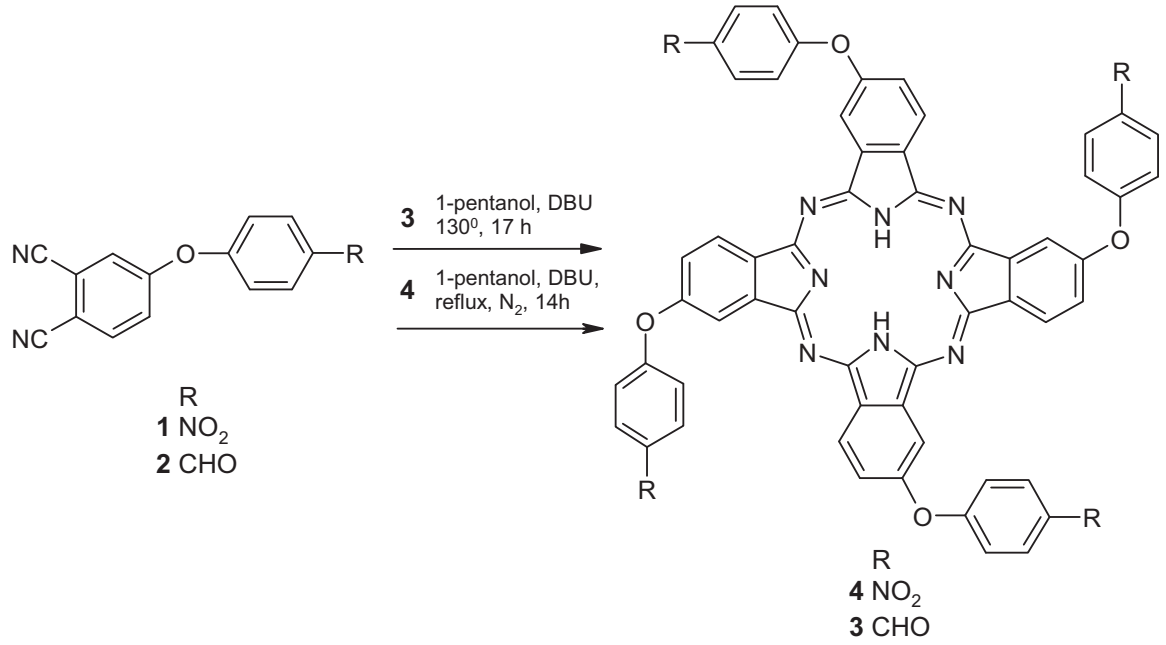

Figure 4.6 Route of the synthesis of 2,9,16,23-tetrakis(4-nitrophenoxy)phthalocyanine (**4**) and 2,9,16,23-tetrakis(4-formylphenoxy)phthalocyanine (**3**).

Compounds **(fPhO)$_4$PcH$_2$** (**3**) and **(nPhO)$_4$PcH$_2$** (**4**) are soluble in tetrahydrofuran (THF), dimethylformamide (DMF), DMSO and pyridine. Absorption spectra (**Figure 4.7 A** and **B**) of **3** and **4** in THF and pyridine solution show the characteristic split of Q-band absorption (**Table 4.3**) of metal-free phthalocyanine.

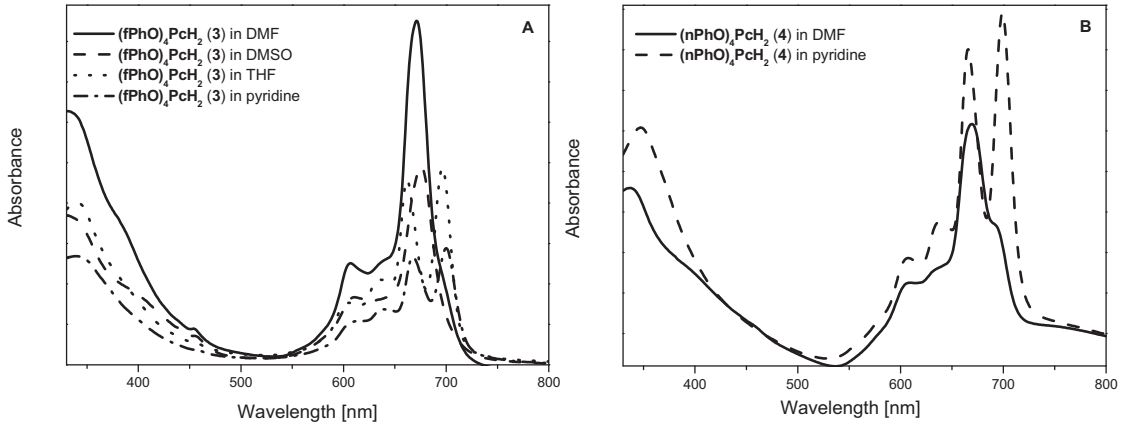

Figure 4.7 Absorption spectra of **(fPhO)$_4$PcH$_2$** (**3**) (**A**, left) and **(nPhO)$_4$PcH$_2$** (**4**) (**B**, right) in different solvents.

However, absorption spectra in DMSO and DMF display only one strong band, suggesting the complex formation with the solvent molecules observed also in the other macrocyclic compounds [8].

Table 4.3 Absorption band maxima for **(fPhO)$_4$PcH$_2$** (**3**) and **(nPhO)$_4$PcH$_2$** (**4**).

Compound	Solvent	λ_{max} [nm]
(fPhO)$_4$PcH$_2$ (**3**)	THF	697, 662, 602, 635, 341
	pyridine	700, 668, 636, 608, 341
	DMF	672, 606, 334
	DMSO	675, 609, 340
(nPhO)$_4$PcH$_2$ (**4**)	THF	694, 660, 634, 603, 342
	pyridine	698, 665, 638, 606, 337
	DMF	669, 636, 606, 337

Compared to the IR spectra of phthalonitriles (**1** and **2**), the spectra of phthalocyanines **3** and **4** show the disappearance of the C≡N stretch. The IR spectrum of **3** exhibits the ketone carbonyl stretch at 1633 cm^{-1} and the ether C-O-C stretch in the range of 1289-1254 cm^{-1}. The characteristic NO_2 stretch at ~ 1349 cm^{-1} is observed in the IR spectrum of **4** as well as in phthalonitrile **1**. Compounds **(fPhO)$_4$PcH$_2$** (**3**) and **(nPhO)$_4$PcH$_2$** (**4**) characterized by mass

spectrometry gave molecular ion peaks consistent with proposed structure. Mass spectrum of **(fPhO)$_4$PcH$_2$** shows main peak at 994.3 *m/z* and of **(nPhO)$_4$PcH$_2$** (**4**) at 1061.1 *m/z* (**Figure 4.8**) without additional fragmentation.

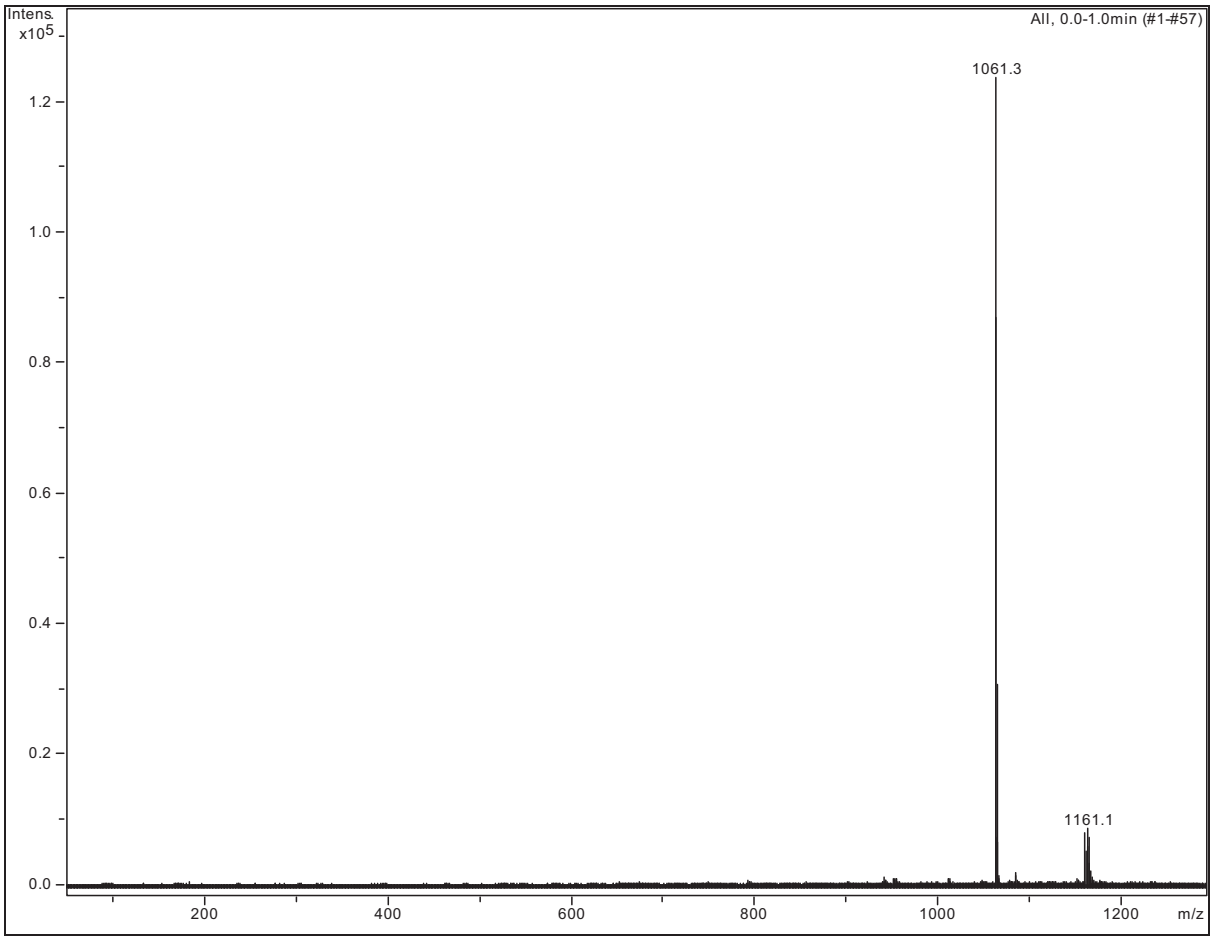

Figure 4.8 ESI-MS spectrum of **(nPhO)$_4$PcH$_2$** (**4**).

The **(nPhO)$_4$PcSnCl$_2$** (**5**), **(fPhO)$_4$PcSnCl$_2$** (**6**) and **(fPhO)$_4$PcGeCl$_2$** (**7**) compounds were obtained by metallization **4** or **3** with germanium(IV) chloride ($GeCl_4$) and tin(IV) chloride ($SnCl_4$) used as the metal sources, in an appropriate solvent (**Figure 4.9**). The preparation of tin complexes needs to apply a high-boiling solvent because insertion of so large atom into phthalocyanine ring requires higher energy. Thus, the synthesis of **(nPhO)$_4$PcSnCl$_2$** (**5**) and **(fPhO)$_4$PcSnCl$_2$** (**6**) was carried out in 1-chloronaphthalene. In both cases, the reactions were monitored by UV/Vis spectroscopy and stopped when the split of Q-band changed into one.

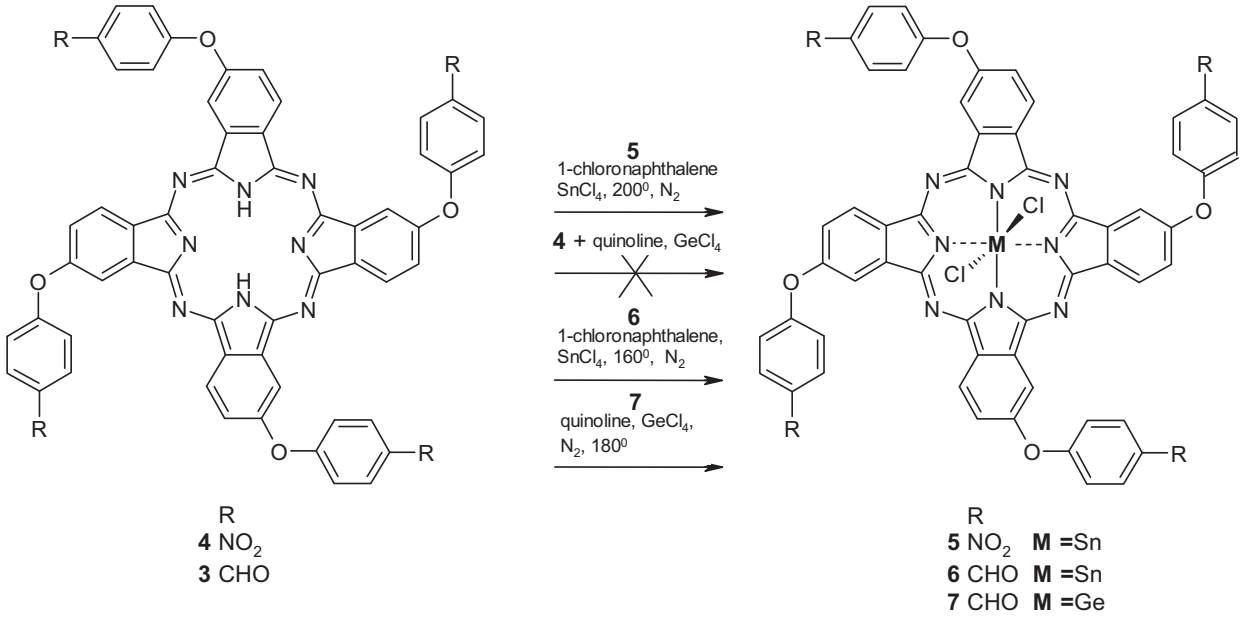

Figure 4.9 Synthesis of **(nPhO)$_4$PcSnCl$_2$** (**5**), **(fPhO)$_4$PcSnCl$_2$** (**6**) and **(fPhO)$_4$PcGeCl$_2$** (**7**).

The synthesis of **5** and **6** took approximately 1.5 hour. A removal of so high-boiling solvent like a 1-chloronaphthalene was achieved by precipitation of phthalocyanines by addition of hexane; furthermore, the precipitate was repetitively washed with diethyl ether until the 1-chloronaphthalene could not be longer smelled. The compounds **5** and **6** were purified by column chromatography on silica gel. Both compounds, **5** and **6**, were initially chromatographed using a THF as an eluent in order to remove first impurities and finally, chromatography with mixture of chloroform ($CHCl_3$)/methanol gave pure desired products.

The synthesis of **(fPhO)$_4$PcGeCl$_2$** (**7**) was performed by metallization of **3** by addition of $GeCl_4$ in quinoline. Quinoline is the solvent preferable in this reaction because of its alkalinity, it neutralizes the chloride acid (HCl) created during the reaction. The reaction progress has been checked by UV/Vis spectroscopy. The insertion of germanium into **3** took approximately 2 hours.

Unfortunately, attempts to synthesize the dichlorogermanium(IV) 2,9,16,23-tetrakis(4-nitrophenoxy)phthalocyanine were failed. The reaction either of **(nPhO)$_4$PcH$_2$** (**4**) with $GeCl_4$ in quinoline or 4-(4-nitrophenoxy) phthalonitrile (**1**) with $GeCl_4$, urea and catalyst in bomb vessel gave just traces of phthalocyanine but compound decomposed during the workup procedure. Furthermore, the reaction of **1** with $GeCl_4$ in solution did not work as well.

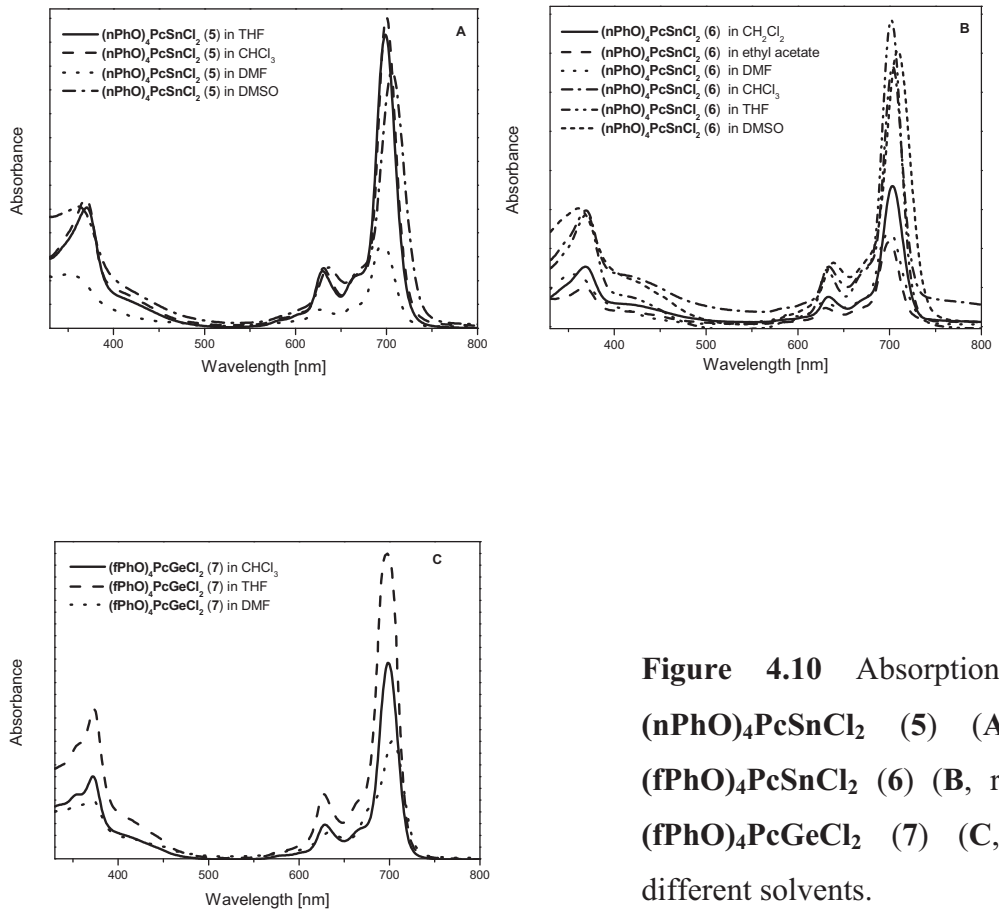

Figure 4.10 Absorption spectra of **(nPhO)$_4$PcSnCl$_2$** (**5**) (**A**, left top), **(fPhO)$_4$PcSnCl$_2$** (**6**) (**B**, right top) and **(fPhO)$_4$PcGeCl$_2$** (**7**) (**C**, bottom) in different solvents.

The synthesized phthalocyanines **5**, **6** and **7** exhibit a good solubility in most organic solvents *e.g.* $CHCl_3$, dichloromethane (CH_2Cl_2), THF, ethyl acetate, DMF, DMSO. They are less soluble in toluene and roughly insoluble in hexane, methanol, and acetone. The measured absorption spectra of **5**, **6** and **7** in different solvents are shown in **Figure 4.10**.

Table 4.4 contains the prominent B- and Q-bands of **5**, **6** and **7** in nonpolar ($CHCl_3$) and polar (THF) solvent. The spectral features of **5**, **6** and **7** are similar either in polar and nonpolar solvents exhibiting independence on the solvent.

Table 4.4 Absorption band maxima for **(nPhO)$_4$PcSnCl$_2$** (**5**), **(fPhO)$_4$PcSnCl$_2$** (**6**) and **(fPhO)$_4$PcGeCl$_2$** (**7**).

Compound	Solvent	λ_{max} [nm]
(nPhO)$_4$PcSnCl$_2$ (**5**)	$CHCl_3$	700, 631, 370
	THF	699, 630, 371
(fPhO)$_4$PcSnCl$_2$ (**6**)	$CHCl_3$	704, 634, 368
	THF	702, 632, 370
(fPhO)$_4$PcGeCl$_2$ (**7**)	$CHCl_3$	699, 629, 372
	THF	698, 627, 373

The Q-band peak is observed at approximately 700 nm for each compound. It was not observed a considerable shift of Q-band towards longer wavelengths between **6** and **7** due to decreasing the electronegativity of the metal M [9] though the Q-band of **6** was ~ 4 nm red-shifted compared to compound **7**. The absorption spectra of **5**, **6** and **7** show typical patterns of metallated phthalocyanines with single peak for Q- and B-bands. The shapes of the absorption bands indicate that the compounds exist in nonaggregated state in the used solvents likely due to the presence of two chlorine atoms at the axial positions and four bulky peripheral substituents as well as the very structural isomers.

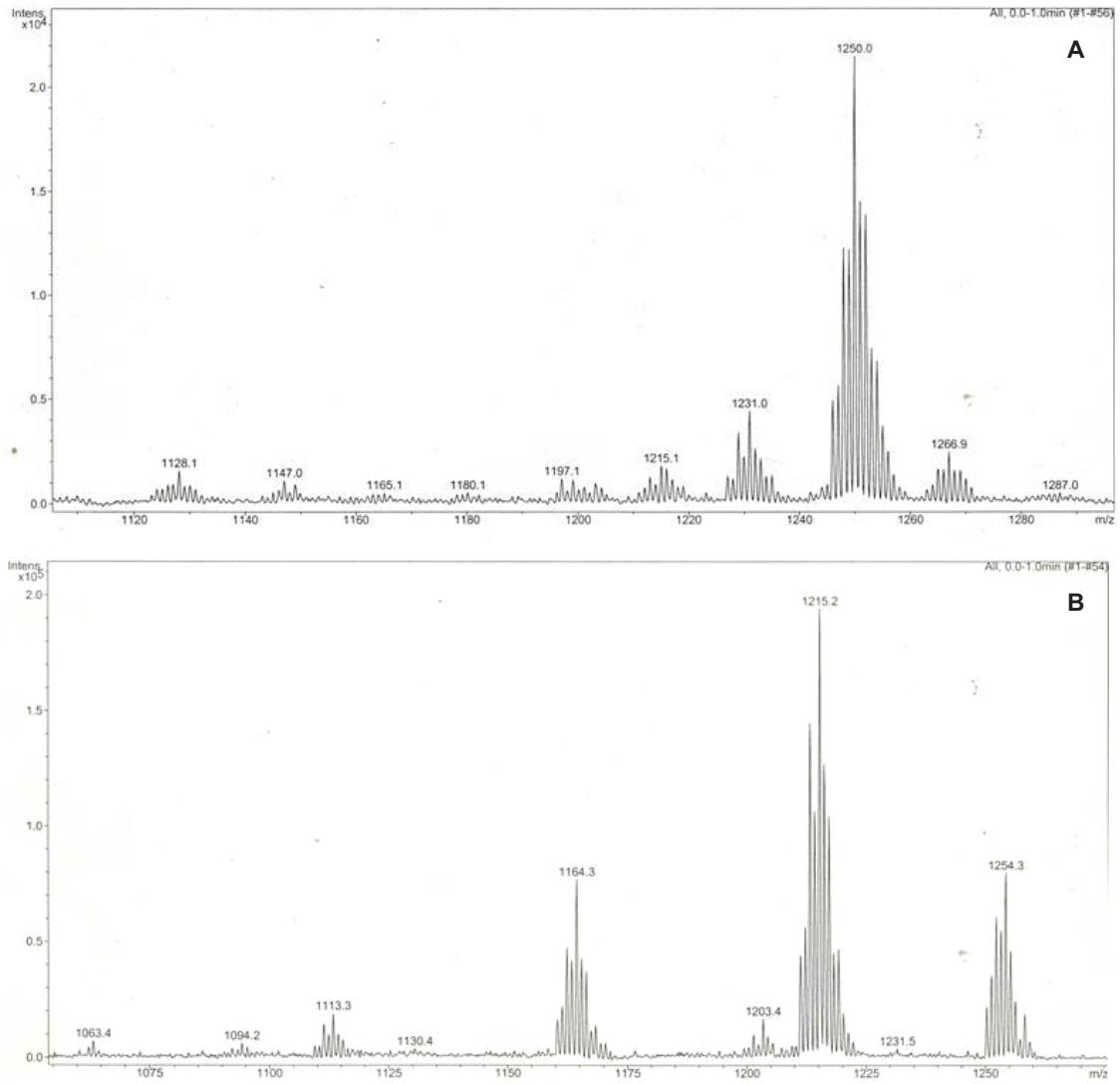

Figure 4.11 ESI-MS (negative ion mode) (**A**, top) and (positive ion mode) (**B**, bottom) spectra of **(nPhO)$_4$PcSnCl$_2$** (**5**).

The obtained ESI-MS (negative ion mode) spectra of **5**, **6** and **7** confirm the proposed structures of the complexes (**Table 4.2** and Chapter 6.4). The ESI-MS (negative ion mode) spectrum of **(nPhO)$_4$PcSnCl$_2$** (**5**) consists of the molecular ion at 1250 *m/z* and peaks at 1215.1 and 1180.1 *m/z*, showing loss of two axial chlorine atoms (**Figure 4.11 A**). However, the ESI-MS (positive ion mode) spectrum of **5** shows the main peak at 1215 *m/z* corresponding to the molecular ion without one chlorine atom and further fragmentation is observed (**Figure 4.11 B**).

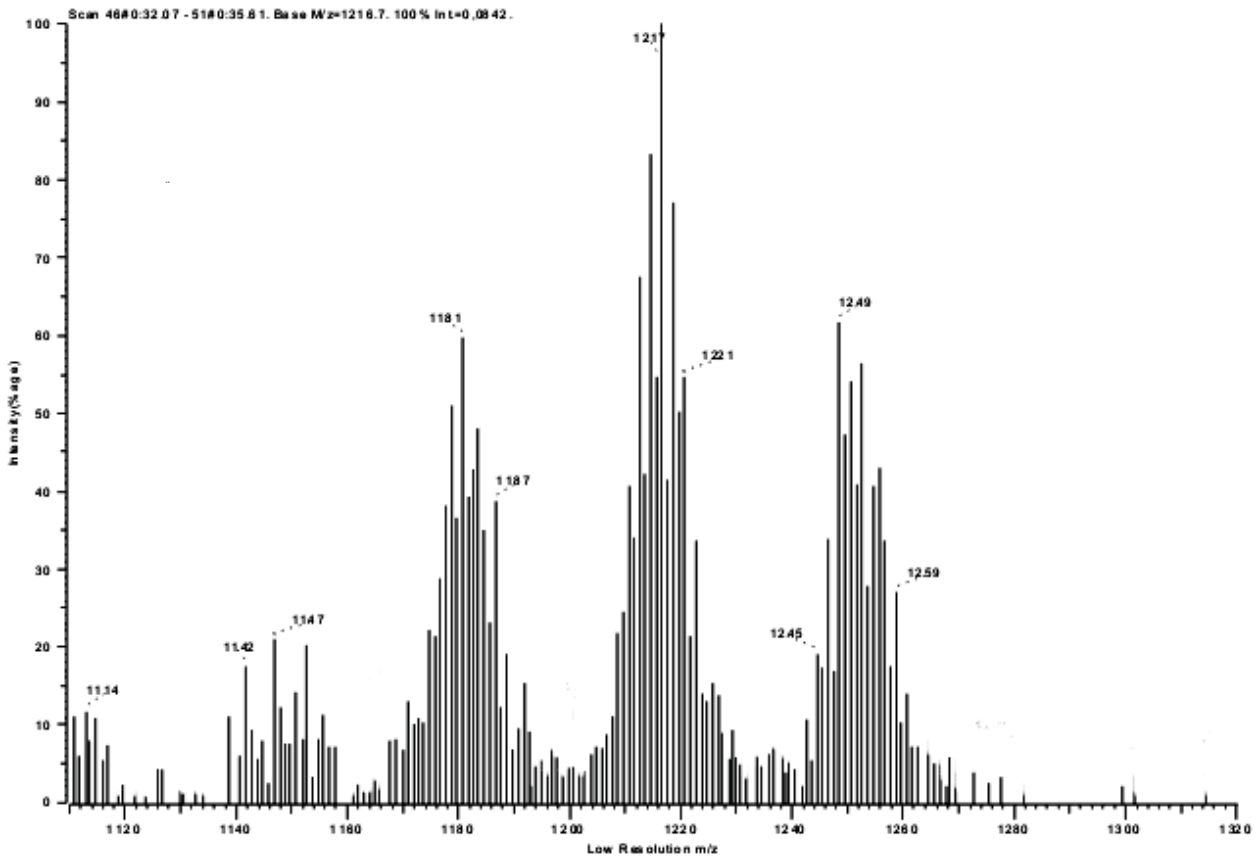

Figure 4.12 ESI-MS spectrum of **(fPhO)$_4$PcSnCl$_2$** (**6**).

The ESI-MS (positive ion mode) spectra of **6** and **7** gave main peaks at 1147.3 and 1101.3 *m/z*, respectively, assigned to $[M - Cl^-]^+$, and additional loss of the second chlorine atom at 1112.4 *m/z* $[M - 2Cl^-]^+$ for **6** and 1083.3 *m/z* $[M - 2Cl^- + OH^-]^+$ for **7** appeared. The metallization of crude metal-free phthalocyanine **3** (just after Soxhlet extraction with methanol) with $SnCl_4$ and $GeCl_4$ gave interesting results. Beside the peaks corresponded to molecular ions of **6** and **7** in ESI-MS spectra, the peaks differ by 86 units from peaks assigned to molecular ions of **6** and **7** were observed. The ESI-MS spectra obviously showed beside main complexes **6** and **7**, the side phthalocyanine products. The attachment of a *p*-formylphenoxy group to the central tin and germanium ion of tetrakis(*p*-formylphenoxy)phthalocyanines (**Figure 4.12** and **Figure 4.13**) was observed. The peaks at 1268.1 and 1352.2 *m/z* in ESI-MS (negative ion mode) spectrum of **6** correspond to monochloromono(4-formylphenoxy)tin(IV) tetrakis(*p*-formylphenoxy)phthalocyanine and di(*p*-formylphenoxy)tin(IV) tetrakis(*p*-formylphenoxy)phthalocyanine, respectively. The nucleophile $^-$OPhCHO that displaced axial chloride ion was observed as traces in ESI-MS spectrum obtained after synthesis of **6** and **7** (**Figure 4.13**). The same situation was observed

in case of **(fPhO)$_4$PcGeCl$_2$** (**7**). The ESI-MS spectrum displays peaks at 1222.1 and 1309.2 *m/z* explained as the replacement of one and two chloride ions in axial position by *p*-formylphenoxy group. Additionally, a peak at 121 *m/z* corresponds to a *p*-formylphenoxy group (**Figure 4.13**) with low intensity was observed.

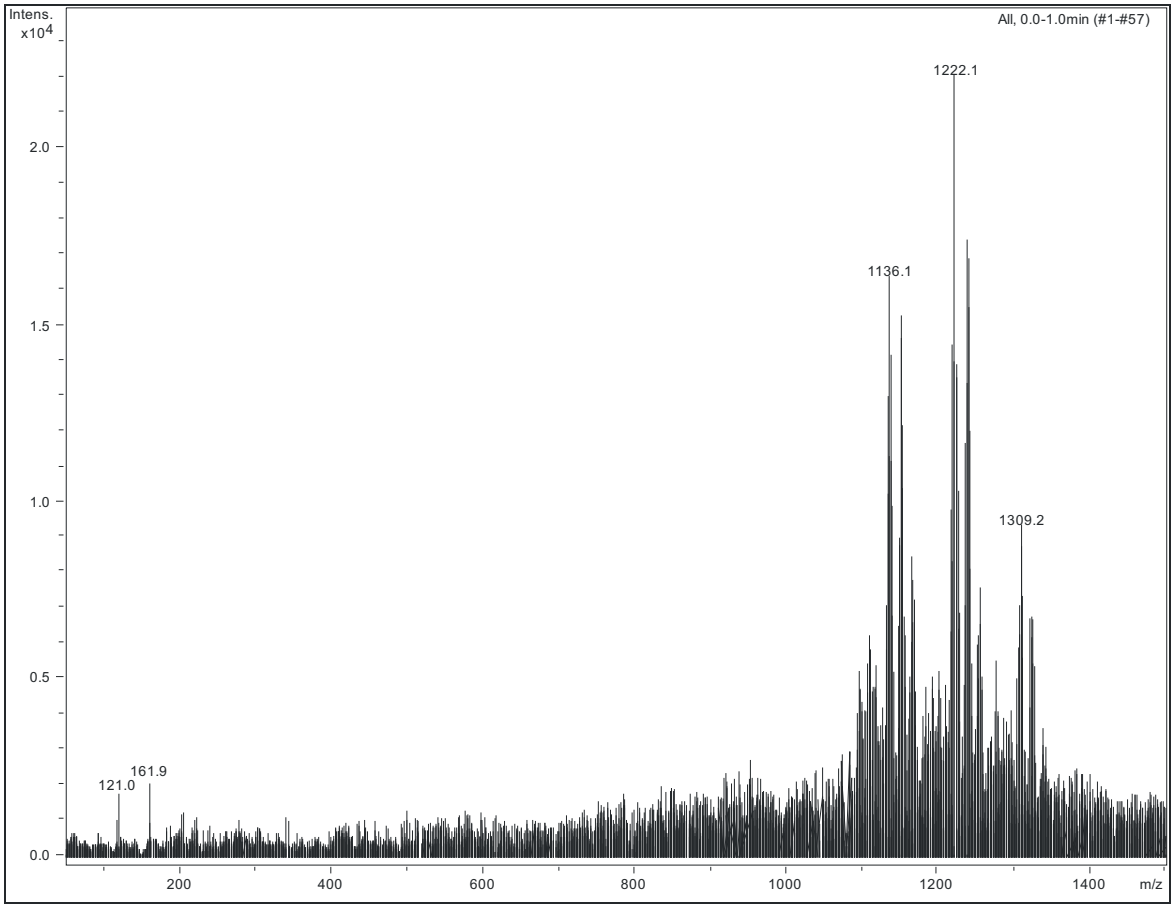

Figure 4.13 ESI-MS spectrum of **(fPhO)$_4$PcGeCl$_2$** (**7**).

The germanium and tin tetranitro-substituted phthalocyanines were prepared by using phthalic anhydrides [10] as a starting material. The phthalocyanines substituted at 1,8,15,22-positions of the macrocycle by nitro groups in this study are termed α-substituted Pcs and at 2,9,16,23-positions are termed β-substituted Pcs (**Figure 4.14** and **4.15**). The condensation of 4-nitrophthalic anhydride (**IV**) or 3-nitrophthalic anhydride (**V**) and urea as a source of nitrogen in the presence of ammonium molybdate as a catalyst with $SnCl_4$ or $GeCl_4$ led to **(*β*NO$_2$)$_4$PcSnCl$_2$** (**18**), **(*α*NO$_2$)$_4$PcSnCl$_2$** (**19**), **(*β*NO$_2$)$_4$PcGeCl$_2$** (**20**) and **(*α*NO$_2$)$_4$PcGeCl$_2$** (**22**), respectively (**Figure 4.14** and **4.15**). The nitrobenzene was used as a solvent in reactions of **18**, **20** and **22** whereas synthesis of **19** was performed in 1-chloronaphthalene.

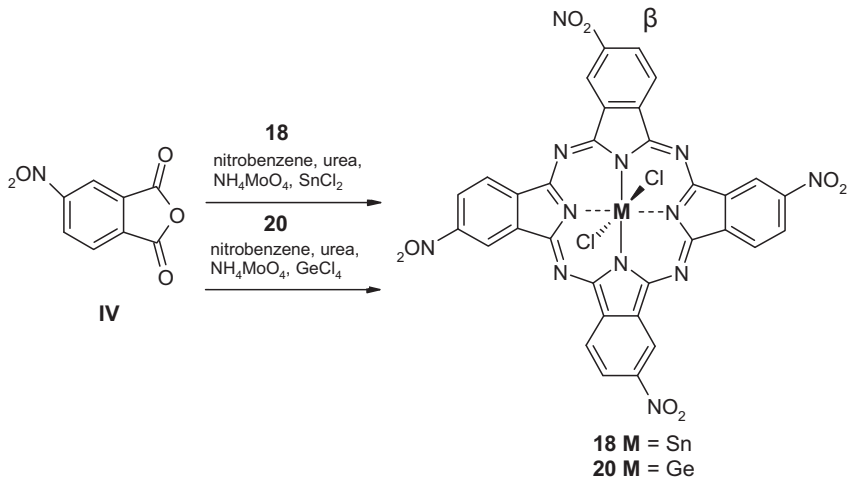

Figure 4.14 Route of synthesis of tetra-β-nitro-substituted phthalocyanines **18** and **20**.

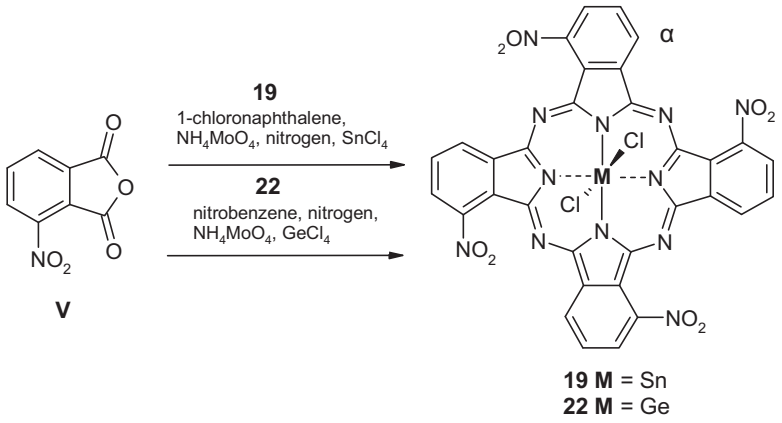

Figure 4.15 Synthesis of tetra-α-nitro-substituted phthalocyanines **19** and **22**.

The obtained olive-brown suspensions after synthesis of β-nitro-substituted phthalocyanines **18** and **20** were diluted with ethanol (EtOH), filtered, and washed with EtOH, MeOH and acetone. The residue was placed in the thimble of a Soxhlet extractor and treated consecutively with petroleum ether, MeOH and acetone. Finally, the products were dried in vacuum and yielded 76% (compound **18**) and 58% (compound **20**) of a blue powder (**Table 4.2**).

In the case of phthalocyanines substituted at α-positions of the aromatic rings, **19** and **22**, the suspension was treated by hexane, precipitate filtered off and washed with petroleum ether. The Soxhlet extraction consecutively with petroleum ether, diethyl ether and ethyl acetate removed first brown and yellow impurities. The products were further redissolved in small amount of THF, precipitated with methanol and centrifuged. This procedure was repeated until the supernatant was colorless. Finally, the products were dried in vacuum to give ~ 20%

of a dark blue powder (**Table 4.2**). The tin and germanium tetra-α-nitro-substituted phthalocyanines exhibit better solubility in organic solvents than those substituted at β-positions. Thus, the trial of purification of compounds **(αNO$_2$)$_4$PcSnCl$_2$** (**19**) and **(αNO$_2$)$_4$PcGeCl$_2$** (**22**) by column chromatography was performed. Unfortunately, phthalocyanines complexes showed high affinity for silica gel and just small amounts of **19** and **22** could be eluted.

MALDI-MS (Matrix:DCTD) spectrum confirmed the identity of **(βNO$_2$)$_4$PcSnCl$_2$** (**18**) compound. The main peak appears at 882.92 and two peaks at 845.94 and 812.99 correspond to one and two lost axial ligands (**Figure 4.16**).

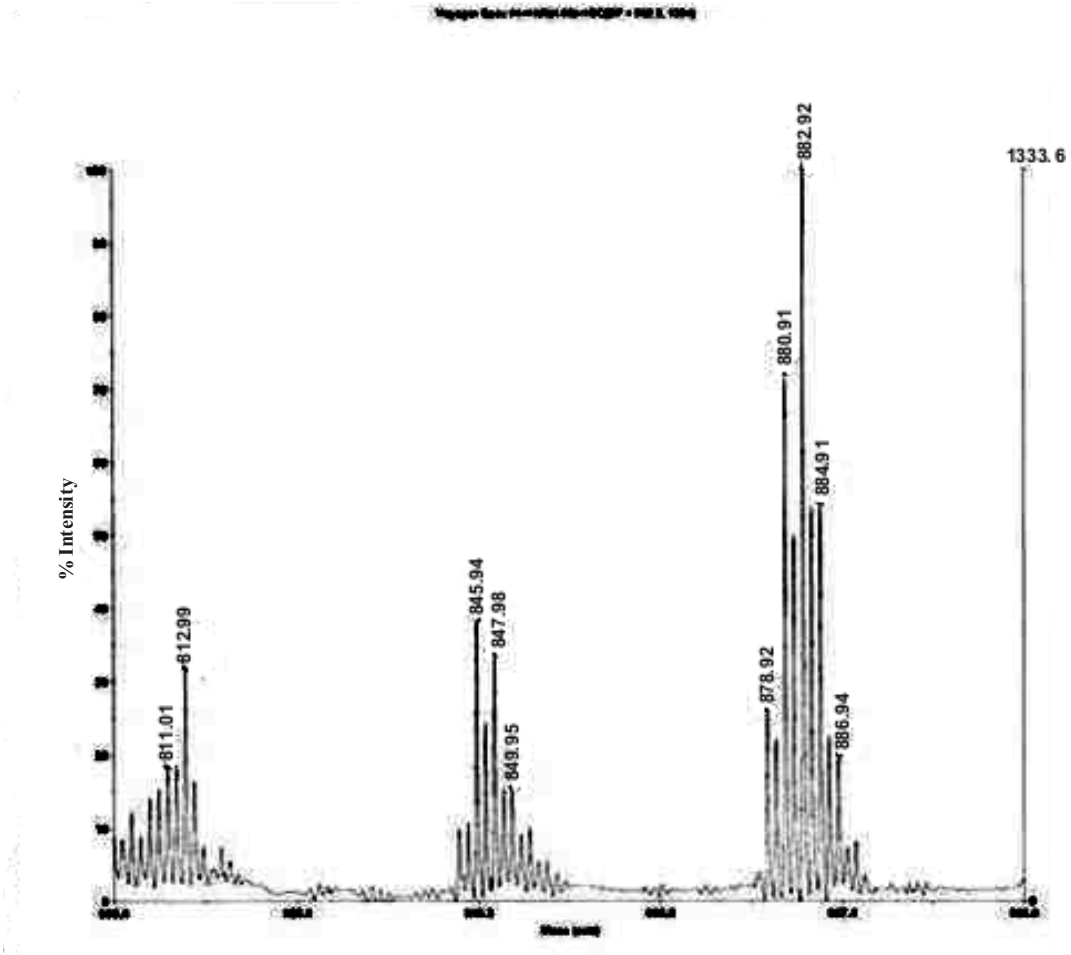

Figure 4.16 MALDI-MS spectrum of **(βNO$_2$)$_4$PcSnCl$_2$** (**18**).

The data obtained from mass spectra for **(αNO$_2$)$_4$PcSnCl$_2$** (**19**), **(βNO$_2$)$_4$PcGeCl$_2$** (**20**) and **(αNO$_2$)$_4$PcGeCl$_2$** (**22**) (**Table 4.2** and Chapter 6.4) tallied with their molecular formulas. The ESI-MS spectrum of **(αNO$_2$)$_4$PcSnCl$_2$** (**19**) shows peaks at 881.8, 846.9 and 812 *m/z* being the molecular ion, **(αNO$_2$)$_4$PcSnCl$^-$** and **(αNO$_2$)$_4$PcSn^{2-}** species, respectively (**Figure 4.17**).

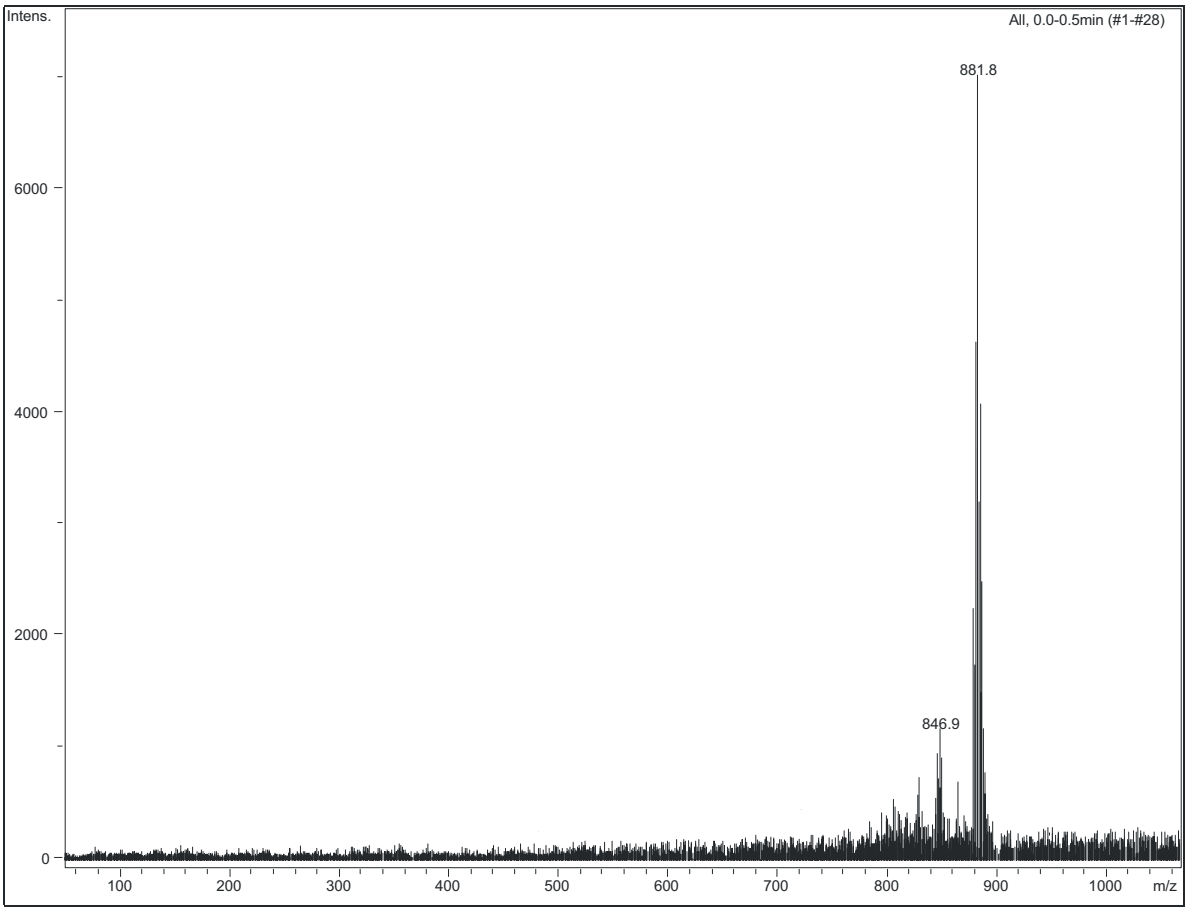

Figure 4.17 ESI negative-MS spectrum of **(αNO$_2$)$_4$PcSnCl$_2$** (**19**).

The ESI-MS spectrum of compound **(βNO$_2$)$_4$PcGeCl$_2$** (**20**) shows molecular peak at 835.9 *m/z* and signal at 800 *m/z* corresponds to loss of one axial chlorine atom or molecule **(βNO$_2$)$_4$PcGe(OH)$_2$** (hydrolyzed compound **20**), and at 817 *m/z* corresponds to [M – 2Cl$^-$ +O$^-$]$^-$ *i.e.* molecule without one chlorine atom and with one oxygen atom in axial position (**Figure 4.18**). In case of **(αNO$_2$)$_4$PcGeCl$_2$** (**22**) ESI-MS spectrum depicts the molecular ion at 836 *m/z* and any further fragmentation was observed.

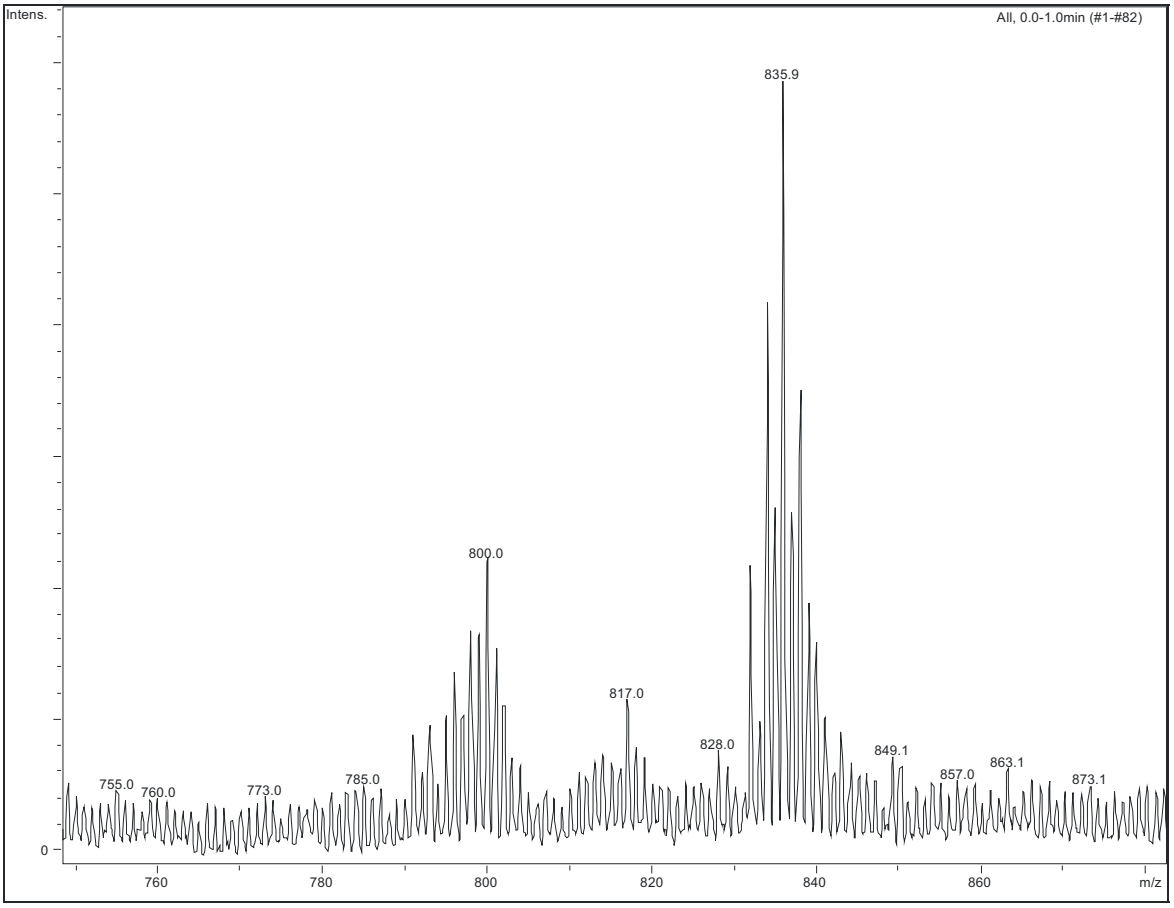

Figure 4.18 ESI negative-MS spectrum of **(βNO$_2$)$_4$PcGeCl$_2$** (**20**).

The IR spectra (Chapter 6.4) of tin and germanium tetra-α-nitro-substituted phthalocyanines slightly differ from complexes substituted at β-position of the phthalocyanine ring. For **18** and **20** compounds band of NO_2 appeared at ~ 1527 (asymmetric stretching vibration) and at ~ 1352 cm^{-1} (symmetric stretching vibration) whereas complexes **19** and **22** substituted at α-positions demonstrated the 10 cm^{-1} red shift of the NO_2 vibration in comparison with **18** and **20** substituted at β-positions (**Table 4.2**).

The UV/Vis data display the bathochromic shift of Q-bands of tin phthalocyanine complexes, **18** and **19**, in comparison with germanium analogues, **20** and **22** (**Table 4.5**). Moreover, comparing the absorption spectra of **(βNO$_2$)$_4$PcSnCl$_2$** (**18**) and **(βNO$_2$)$_4$PcGeCl$_2$** (**20**) with **(αNO$_2$)$_4$PcSnCl$_2$** (**19**) and **(αNO$_2$)$_4$PcGeCl$_2$** (**22**) a hypsochromic shift of Q-band for β-nitro-substituted derivates is observed. The Q-band of tin complexes **18** and **19** is ~ 20 nm blue-shifted in comparison with germanium complexes **20** and **22**.

Table 4.5 Absorption band maxima for tin and germanium tetranitro-substituted phthalocyanines.

Compound	λ_{max} [nm] DMF	λ_{max} [nm] pyridine	λ_{max} [nm] $CHCl_3$
($\beta$$NO_2$)$_4$PcSn$Cl_2$ (18)	701, 348	713, 357	-
($\alpha$$NO_2$)$_4$PcSn$Cl_2$ (19)	693, 345	686	-
($\beta$$NO_2$)$_4$PcGe$Cl_2$ (20)	680, 344	694	-
($\beta$$NO_2$)$_4$PcGe$(OH)_2$ (21)	-	682, 358	-
($\alpha$$NO_2$)$_4$PcGe$Cl_2$ (22)	671, 338		-
($\beta$$NO_2$)$_4$PcGe($t$$Bu_2$P)$_2$ (23)			687, 622, 354

Furthermore, the Q-band is ~ 10 nm blue-shifted in complexes substituted at α-positions compared to Q-band in complexes substituted by electron-withdrawing nitro substituents at β-position (**Table 4.5**). The electron-withdrawing nitro groups lower the energy level of the highest occupied molecular orbital (HOMO) and cause a hypsochromic shift of the Q-band depending on their positions. The shift of Q-band causing by the positions of the peripheral substituents was observed in octa-substituted phthalocyanines [11]. The Q-band was more bathochromic shifted in case of phthalocyanines substituted at the 1,4-positions than of those at the 2,3-positions by alkoxy groups [11]. The bathochromic shift of the Q-band in octa-substituted phthalocyanines with alkoxy groups in peripheral positions is caused by the electron-donating alkoxy chain depending on the positions of the substituents. The phthalocyanines substituted at the 1,4-positions exhibit a more red-shifted Q-band than those at the 2,3-positions because of the electron-donating alkoxy groups attached to the benzene carbons closest to the phthalocyanine core [12]. The Q-band in 1,4-octasubstitued nickel phthalocyanines with alkoxy groups at the inner benzo substitution positions is ~ 60 nm red-shifted in comparison with those in 2,3-octasubstituted ones [13]. Dihydroxygermanium(IV) 2,9,16,23-tetranitrophthalocyanine (**21**) was obtained by treatment **($\beta$$NO_2$)$_4$PcGe$Cl_2$** (**20**) with ammonium hydroxide in pyridine under reflux for 17 hours. The solution formed was evaporated and Soxhlet extraction with methanol and acetone yielded 75% of a dark blue powder. Hydrolysis of **($\beta$$NO_2$)$_4$PcSn$Cl_2$** (**18**) by ammonium hydroxide or sodium hydroxide (NaOH) was failed. The mass spectroscopy after hydrolysis of dichlorotin(IV) 2,9,16,23-tetranitrophthalocyanine (**18**) clearly exhibited the demetallization of the compound.

Compound **(βNO$_2$)$_4$PcGe(OH)$_2$** (**21**) shows lower solubility and higher aggregation tendency in comparison with compound **20**. The ESI-MS spectrum of **21** shows the molecular peak at 800 *m/z* and the peak at 783 *m/z* corresponds to the loss of one hydroxyl axial ligand (**Figure 4.19**).

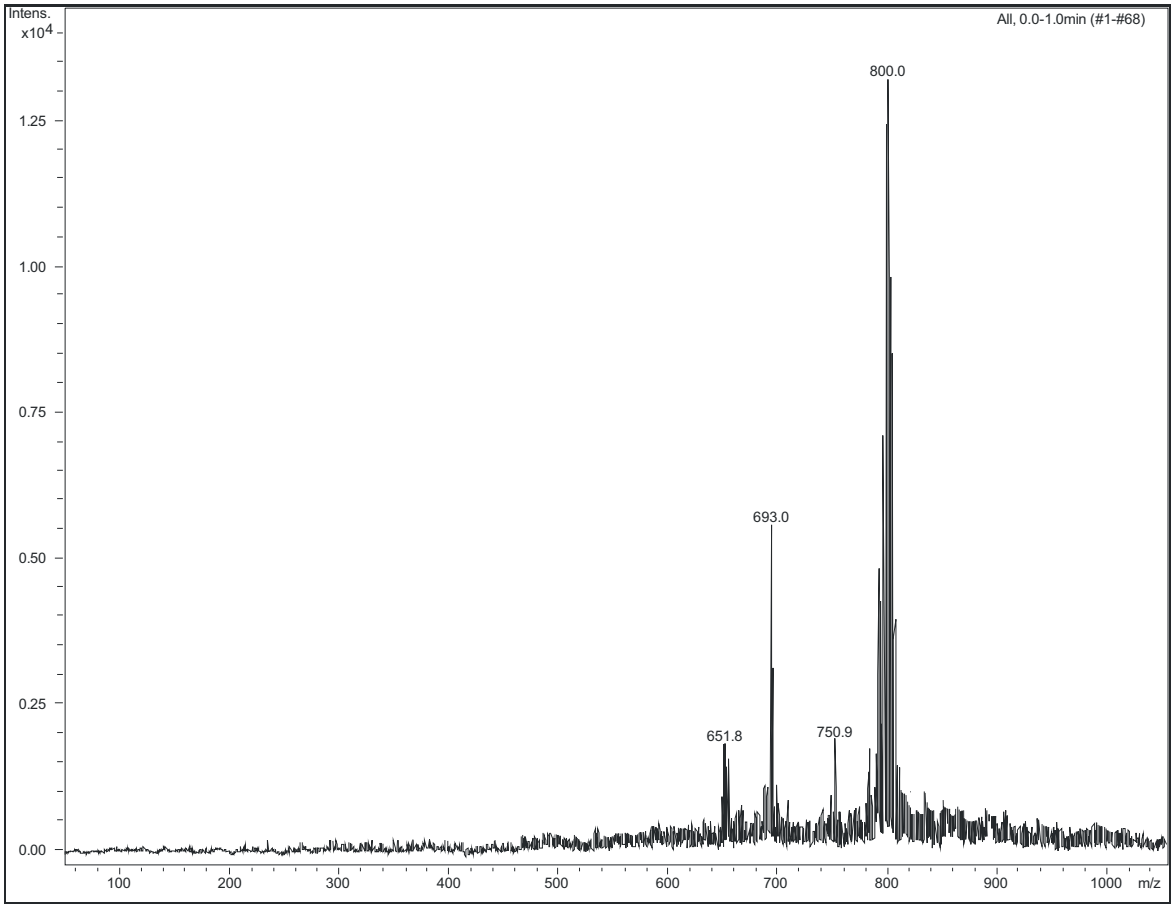

Figure 4.19 ESI negative-MS spectrum of **(βNO$_2$)$_4$PcGe(OH)$_2$** (**21**).

The replacement of the chlorine ligands by bulky groups in tetra-β-nitro-substituted phthalocyanines **18** and **20** was intended to enhance their solubility. The bulky di(*tert*-butyl)phenoxy group introduces steric hindrance and better suppresses the aggregation compared to the small chlorine atoms. Unfortunately, any attempt to substitute the chlorine atoms in complex **18** by bulky di(*tert*-butyl)phenoxy groups was unsuccessful.

Bis(3,5-di-*tert*-butylphenoxy)germanium(IV) 2,9,16,23-tetranitrophthalocyanine (**23**) was synthesized by treating **(βNO$_2$)$_4$PcGeCl$_2$** (**20**) with 3,5-di-*tert*-butylphenol, powdered K_2CO_3 and 1,4,7,10,13,16-hexaoxacyclooctadecane (18-crown-6) in a molar ratio 1:2:2. The reaction was carried out in 1,2,4-trimethylbenzene under argon atmosphere (**Figure 4.20**). Crown ethers possess a high ability to solvate alkali, alkaline-earth and transition-metal cations in

nonpolar, aprotic solvents. [14-16]. When a salt is dissolved in aprotic solvent using crown ether, the anion is separated in such a way that it becomes highly reactive. The 18-crown-6 as a catalyst is used to activate the nucleophilic species as a naked anion. After activation, the nucleophile (t-Bu)$_2$C$_6$H$_4$O$^-$ attacks germanium atom, the stable Ge-O bond is formed and the chloride ions are leaving groups.

The suspension was heated and monitored by TLC (silica gel/$CHCl_3$) and stopped when all of **(βNO$_2$)$_4$PcGeCl$_2$** (**20**) had been consumed. The crude product was twice purified by column chromatography using THF and CH_2Cl_2 as eluent. First column chromatography with THF allowed removing large amount of impurities and finally elution with CH_2Cl_2 on a short column gave the desired blue product.

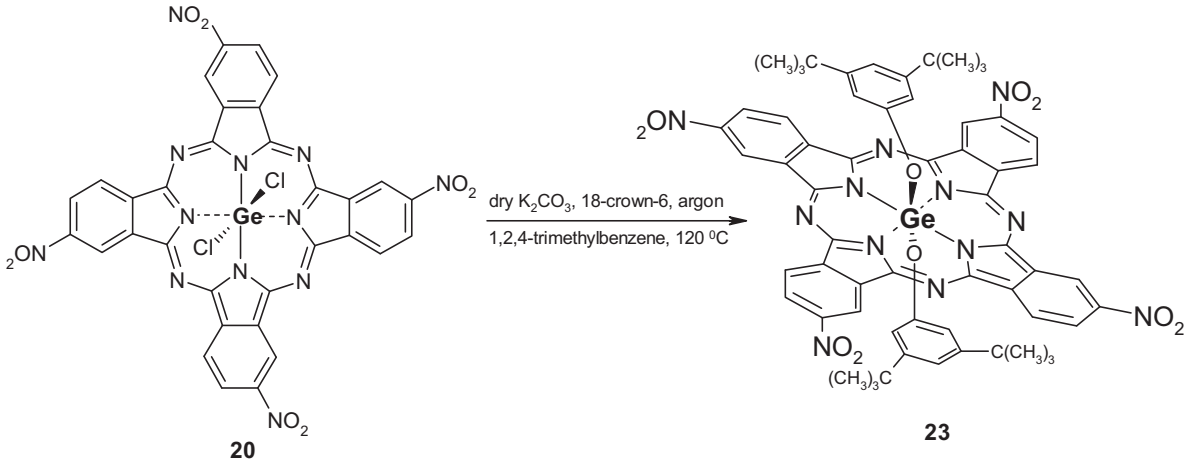

Figure 4.20 Synthesis of **(βNO$_2$)$_4$PcGe(tBu$_2$P)$_2$** (**23**).

The obtained compound **23** is highly soluble in organic solvents such as $CHCl_3$, CH_2Cl_2 and THF and surprisingly shows tendency to aggregate in DMF solution. The mass spectrometry of **(αNO$_2$)$_4$PcGe(tBu$_2$P)$_2$** (**23**) showed intense peak at 1176.3 *m/z* in ESI-MS spectrum (**Figure 4.21**) for **(αNO$_2$)$_4$PcGe(tBu$_2$P)$_2^-$** and peak at 971.1 *m/z* for [M – $C_{14}H_{21}O^-$]$^-$. The observed peak at 1335.5 *m/z* suggests the substitution of a nitro peripheral group by di(*tert*-butyl)phenoxy group.

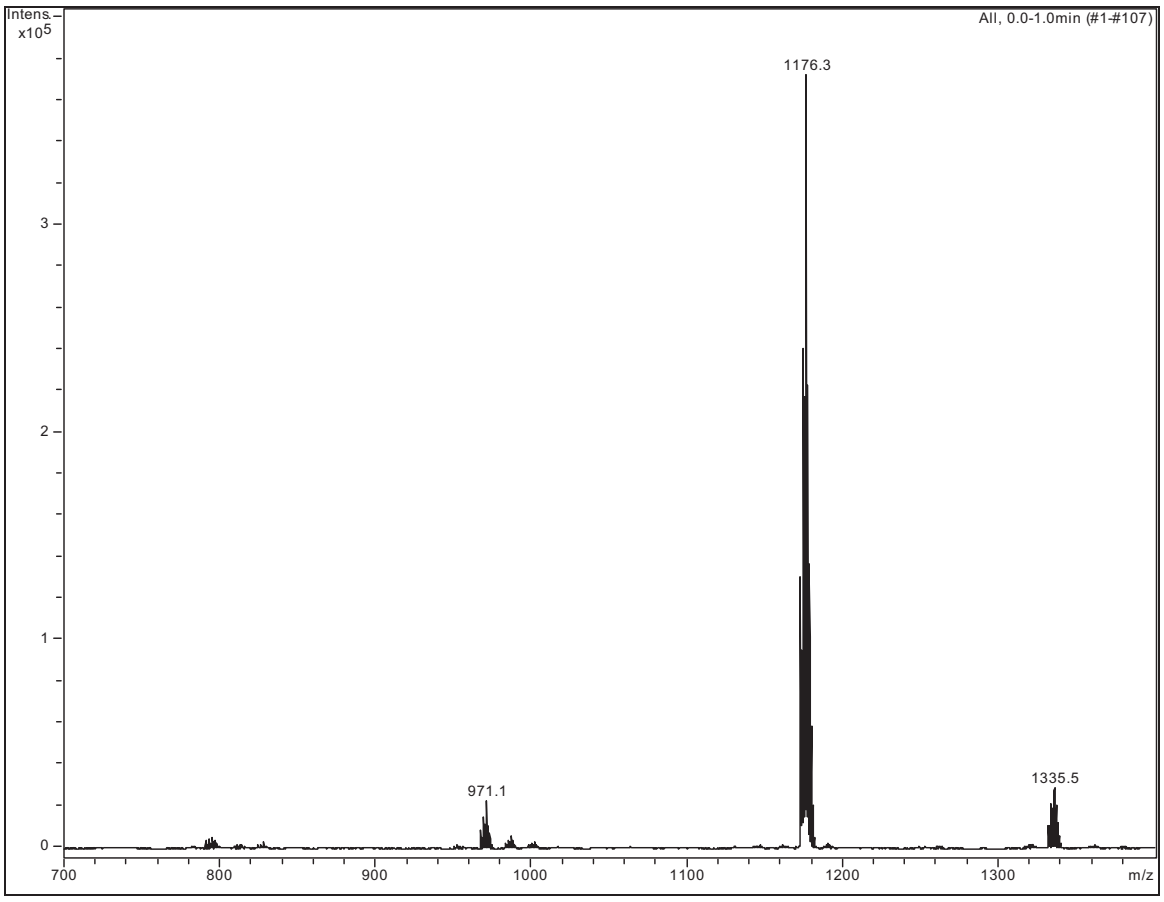

Figure 4.21 ESI negative-MS spectrum of **(βNO$_2$)$_4$PcGe(tBu$_2$P)$_2$** (**23**).

Additionally, the chloroindium(III) 2,9,16,23-tetrakis(*tert*-butyl)phthalocyanine (**25**) was synthesized according to the Hanack method [17]. The **(*t*-Bu)$_4$PcInCl** (**25**) is a well-known phthalocyanine possessing a very good nonlinear optical properties. The preparation of thin films of **25** and comparison its NLO properties with synthesized in this study phthalocyanines was an aim. The complex **25** was used here as a comparative pattern. The cyclotetramerization of 4-*tert*-butylphthalonitrile (**VI**) with $InCl_3$ in freshly distilled quinoline in the presence of a strong base (DBU) led to chloroindium(III) 2,9,16,23-tetrakis(*tert*-butyl)phthalocyanine (**25**) (**Figure 4.22**). The compound was purified by column chromatography using $CHCl_3$ as an eluent and than was recrystallized from mixture of CH_2Cl_2/MeOH to give 47% of a blue microcrystals.

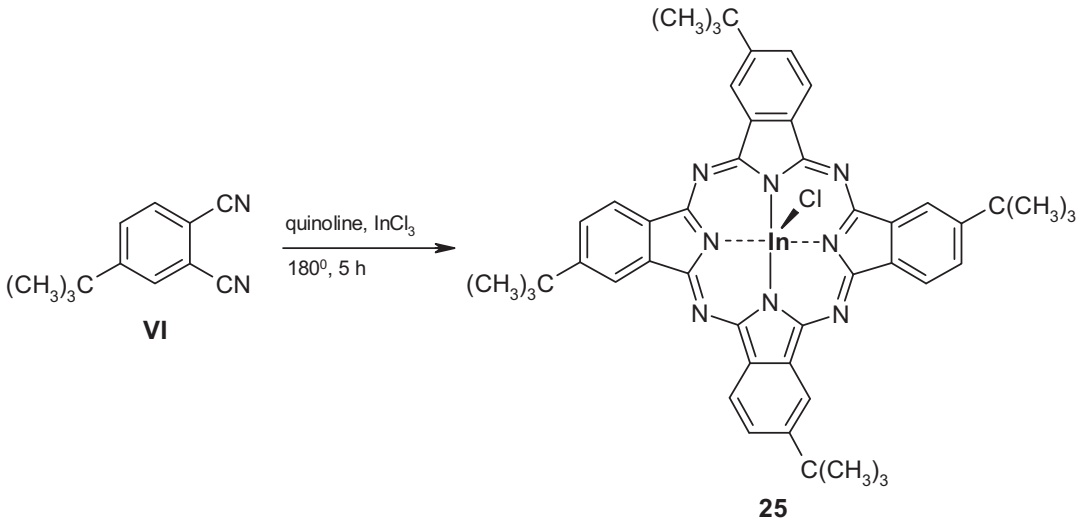

Figure 4.22 Synthesis of **(*t*-Bu)$_4$PcInCl** (**25**).

The chloroindium(III) 2,9,16,23-tetrakis(*tert*-butyl)phthalocyanine (**25**) is soluble in most common organic solvents *e.g.* chloroform, toluene, tetrahydrofuran, dichloromethane and does not exhibit any tendency to aggregation. The UV/Vis and IR data correlate with previously described by ones M. Hanack and H. Heckmann [17]. The main peak at 886.3 *m/z* in ESI-MS spectrum was related to the **(*t*-Bu)$_4$PcInCl** (**25**) and additional further fragmentation was not observed (**Figure 4.23**).

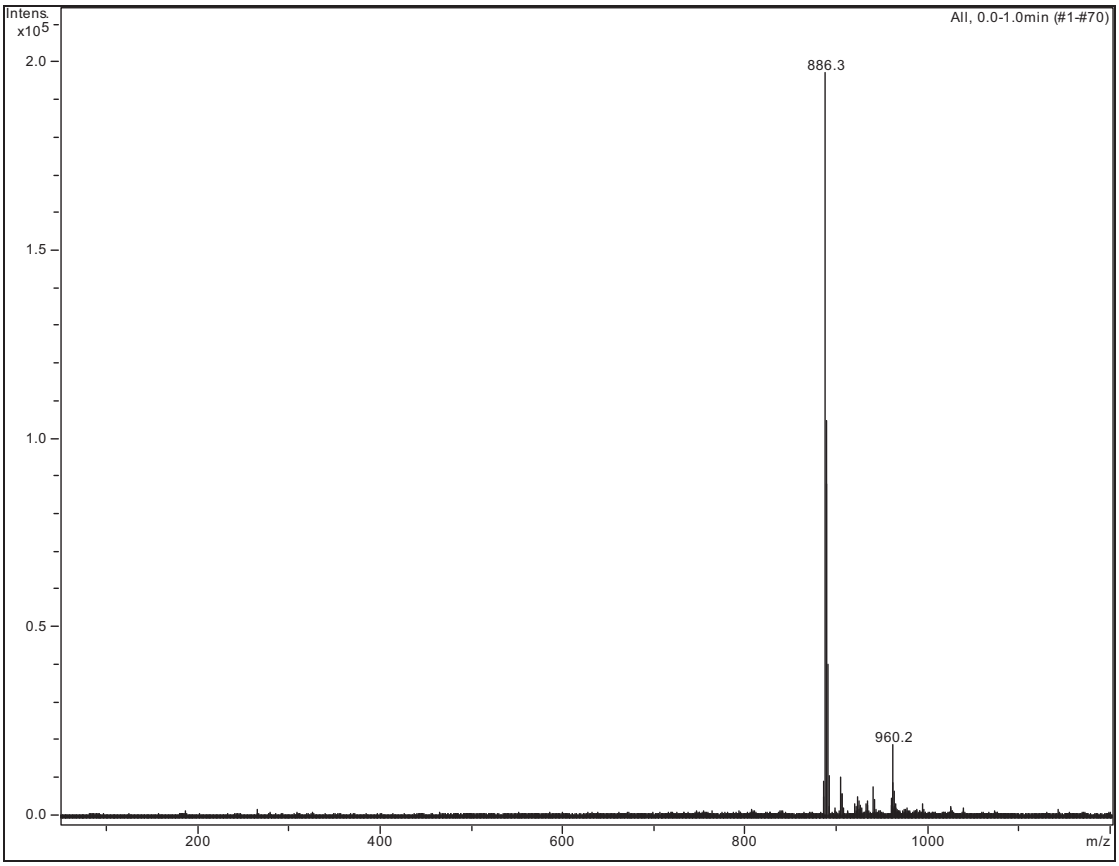

Figure 4.23 ESI negative-MS spectrum of **(*t*-Bu)$_4$PcInCl** (**25**).

The dichlorotin(IV) 2,3,9,10,16,17,23,24-octacyanophthalocyanine (**24**) was obtained by reaction of tetracyanobenzene (**X**) with anhydrous tin(II) chloride ($SnCl_2$) (**Figure 4.24**) in a closed glass ampoule for 2 hours at 200 °C. Soxhlet extraction with acetone and methanol, and afterwards air dryness gave blue product in satisfactory yield (63%) (**Table 4.2**).

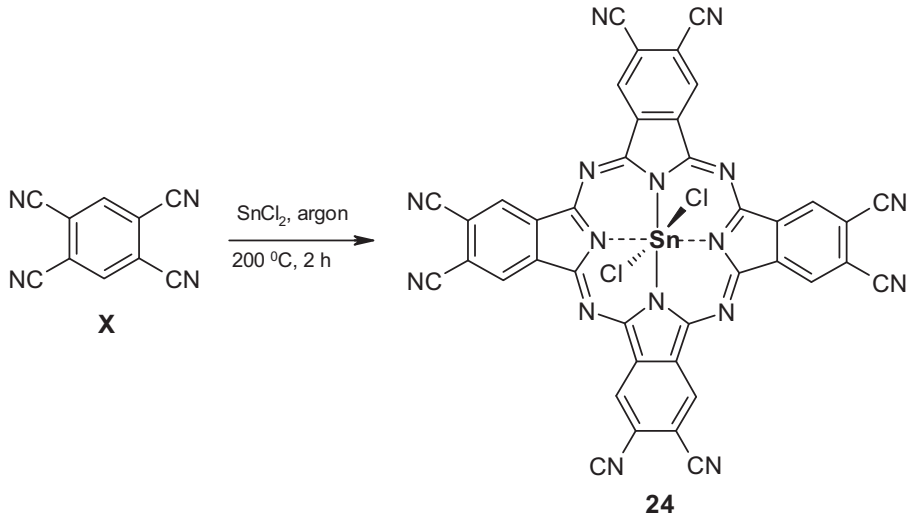

Figure 4.24 Synthesis of **(CN)$_8$PcSnCl$_2$** (**24**).

Unfortunately, any attempts to synthesize the dichlorogermanium(IV) 2,3,9,10,16,17,23,24-octacyanophthalocyanine either in solution or in the bulk were unsuccessful. Synthesis of **$(CN)_8PcSnCl_2$** (**24**) in the solution was not successful as well. A dark polymer was formed after reactions and traces of unknown purple-red product characterized by bands in the region 400 - 500 nm by UV/Vis spectroscopy was obtained.

The IR spectrum of **$(CN)_8PcSnCl_2$** (**24**) displays the characteristic nitrile stretch (C≡N) at 2233 cm^{-1} and vibrational bands representative for phthalocyanine complex (Chapter 6.4).

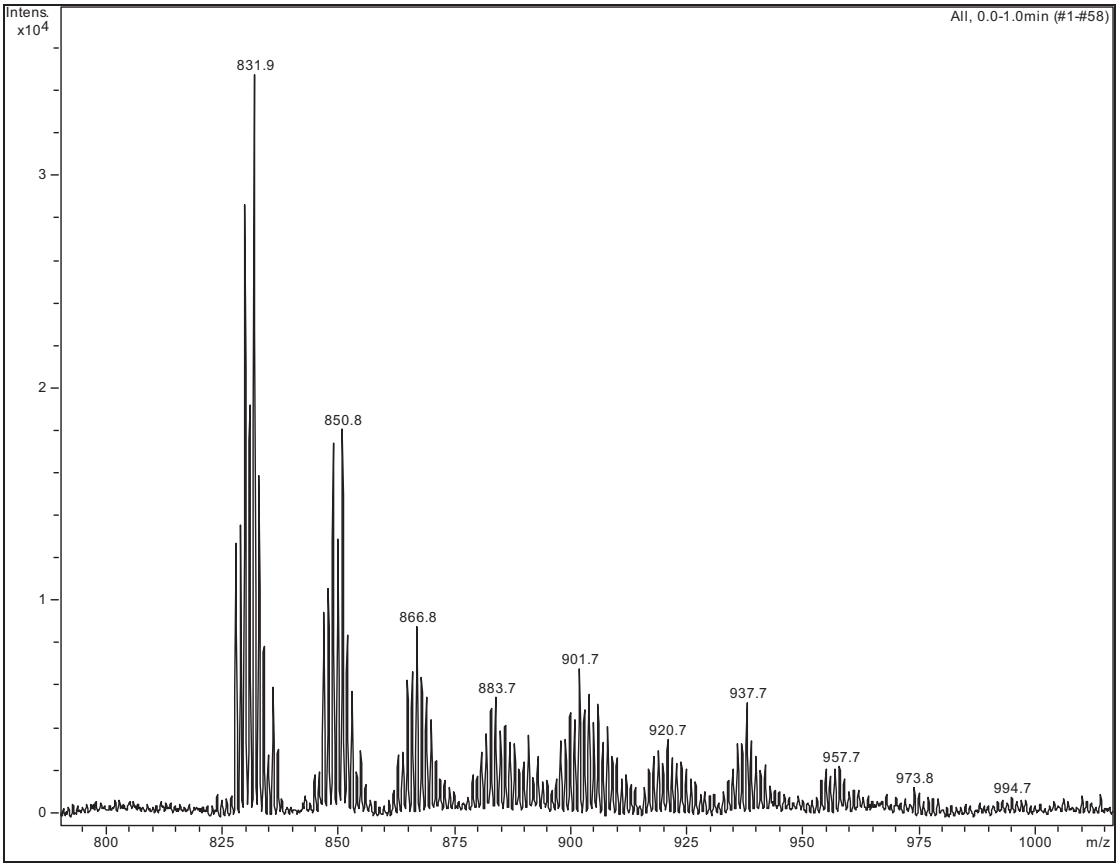

Figure 4.24 ESI-MS spectrum of **$(CN)_8PcSnCl_2$** (**24**).

The complex **24** is soluble in DMF, DMSO, pyridine and THF. The mass spectrum (**Figure 4.24**) shows the main peak at 831.9 *m/z*-suggesting loss of two axial chlorine atoms, the loss of one chlorine atom is observed at 866.8 *m/z*. Also the peak of the molecular ion is visible at 901.7 *m/z*.

4.3 Synthesis of hexadeca-substituted phthalocyanines

The synthesis of tin and germanium hexadeca-substituted (per-substituted) phthalocyanines were performed. The electron-withdrawing fluorine and chlorine groups were chosen as the peripheral substituents. The small chlorine atoms are not bulky enough to increase the solubility of phthalocyanines. Hence, in case of the low soluble tin and germanium hexadecachloro-substituted phthalocyanines different in size axial ligands were employed. Different approaches of phthalocyanines such as electron-withdrawing groups, small tendency to aggregate and good solubility are desired for preparation of good optical limiting devices. A variety of axial ligands at tin and germanium perchloro-substituted phthalocyanines were employed to check the fluence of different sizes and electronegativities of the axial groups on NLO properties of phthalocyanines.

The names, abbreviations and numbers of phthalocyanines, and their peripheral and axial substituents are presented in **Table 4.6**.

Table 4.6 Abbreviations, numbers, and peripheral and axial substituents of hexadeca-substituted phthalocyanines.

Compound	Abbreviation	No	Peripheral substituent	Axial substituent
dichlorotin(IV) hexadecachlorophthalocyanine	**$Cl_{16}PcSnCl_2$**	**8**	Cl	Cl
dichlorogermanium(IV) hexadecachlorophthalocyanine	**$Cl_{16}PcGeCl_2$**	**9**	Cl	Cl
dihydroxytin(IV) hexadecachlorophthalocyanine	**$Cl_{16}PcSn(OH)_2$**	**10**	Cl	OH
dihydroxygermanium(IV) hexadecachlorophthalocyanine	**$Cl_{16}PcGe(OH)_2$**	**11**	Cl	OH
difluorotin(IV) hexadecachlorophthalocyanine	**$Cl_{16}PcSnF_2$**	**12**	Cl	F
difluorogermanium(IV) hexadecachlorophthalocyanine	**$Cl_{16}PcGeF_2$**	**13**	Cl	F
bis(3,5-di-*tert*-butylphenoxy)tin(IV) hexadecachlorophthalocyanine	**$Cl_{16}PcSn(tBu_2P)_2$**	**14**	Cl	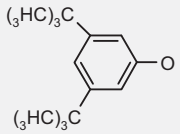
bis(3,5-di-*tert*-butylphenoxy)germanium(IV) hexadecachlorophthalocyanine	**$Cl_{16}PcGe(tBu_2P)_2$**	**15**	Cl	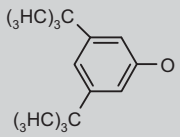
dichlorotin(IV) hexadecafluorophthalocyanine	**$F_{16}PcSnCl_2$**	**16**	F	Cl
dichlorogermanium(IV) hexadecafluorophthalocyanine	**$F_{16}PcGeCl_2$**	**17**	F	Cl

The molecular weights, yields and analytical data of hexadeca-substituted phthalocyanines are presented in **Table 4.7**.

Table 4.7 Molecular weights (**M**), yields, spectral and mass data of hexadeca-substituted phthalocyanines.

Compound	**M** [g mol^{-1}]	Yield %	MS (*m/z*) 100%	IR (KBr, cm^{-1})
8	1246	65 (Method I) 92 (Method II)	ESI-MS (negative) 1253.3	1633, 1094, 786, 766
9	1200	37 (Method I) 74 (Method II)	DCI-MS (negative) 1208 DCI-MS (positive) 1207	1633, 1105, 785, 746
10	1210	60	DCI-MS (negative) 1217 DCI-MS (positive) 1181	3408 (OH), 1634, 783, 765
11	1164	63	DCI-MS (negative) 1171.8 ESI-MS (negative) 1169.4	3400 (OH), 1633, 1060, 798, 746
12	1214	83	ESI-MS (negative) 1219.3	1633, 1178, 1139, 1106, 747,
13	1168	93	ESI-MS (negative) 1173.4	1633, 1147, 1106, 746
14	1586	22	ESI-MS (negative) 1591.6	2965, 2867, 1351, 791, 746
15	1540	25	ESI-MS (negative) 1545.7	2966, 2867, 1362, 747, 704
16	990	42	ESI-MS (negative) 989.7	1634, 1455, 1302, 1255
17	944	28	ESI-MS (negative) 943.6	1633, 1455, 1301, 1255

The synthesis of dichlorotin(IV), and dichlorogermanium(IV) hexadecachlorophthalocyanines was performed by a reaction of phthalonitrile in bulk (method I) as well as from phthalic anhydride or phthalonitrile in solution (method II). Formation of **$Cl_{16}PcSnCl_2$** (**8**) was achieved by refluxing in dry 1-chloronaphthalene the mixture of dry tetrachlorophthalonitrile (**VII**) with anhydrous $SnCl_2$ for 2 hours (method II). In addition, tetrachlorophthalonitrile (**VII**) heated with anhydrous $SnCl_2$ in closed glass ampoule at 250 °C for 5 hours gave desired **$Cl_{16}PcSnCl_2$** (**8**) as well (method I). The preparation of **$Cl_{16}PcGeCl_2$** (**9**) from **VII** and $GeCl_4$ at 300 °C within 5 hours succeeded (method I). In case of the bulk reaction (without solvent) of **$Cl_{16}PcSnCl_2$** (**8**) and **$Cl_{16}PcGeCl_2$** (**9**), multiple flushing with argon is needed, and afterwards the glass vessel was sealed under 1.33 Pa. Routes of synthesis of **8** and **9** are presented in **Figure 4.25** and **Figure 4.26**.

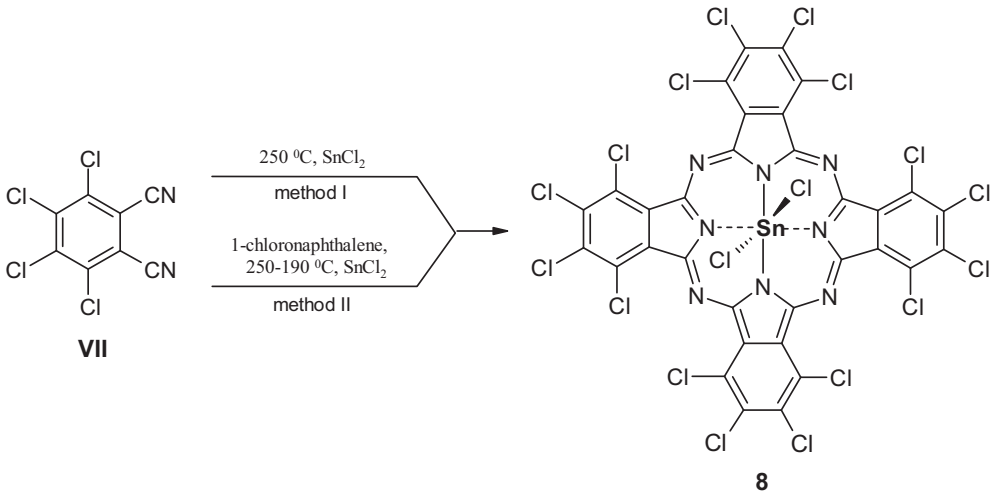

Figure 4.25 Routes of synthesis of **$Cl_{16}PcSnCl_2$** (**8**).

The synthesis of **$Cl_{16}PcGeCl_2$** (**9**) was also achieved by using as a starting material tetrachlorophthalic anhydride (**VIII**), beside $GeCl_4$ addition of urea is required as a source of nitrogen and ammonium molybdate as a catalyst (method II; **Figure 4.26**).

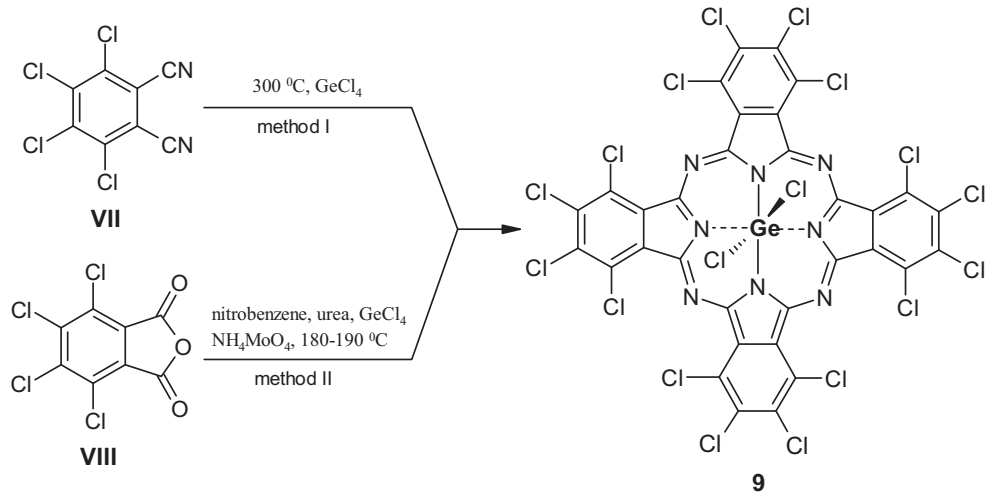

Figure 4.26 Two methods of synthesis of **$Cl_{16}PcGeCl_2$** (**9**).

The phthalocyanines, **8** and **9**, prepared by method I were purified by successive washing with acetone, methanol and diethyl ether; hence, the insoluble products were obtained. In case of **8** prepared by method II, the removal of 1-chloronaphthalene was achieved in the same way as in case of compound **5** and **6**. Afterwards Soxhlet extraction with diethyl ether, acetone and methanol gave dark bluish-green product. The **$Cl_{16}PcGeCl_2$** (**9**) synthesized by method II was precipitated by addition of ethanol and successive washing with hot water, diethyl ether, methanol, acetone and dichloromethane. UV/Vis absorption spectra of **$Cl_{16}PcSnCl_2$** (**8**) and

$Cl_{16}PcGeCl_2$ (**9**) show characteristic Q- and B-bands for metallated phthalocyanines. The Q-band of complexes **8** and **9** is located at longer wavelength: at 755 and 751 nm, respectively. The bathochromic shift of the Q-band of (hexadecachlorophthalocyaninato)iron(II) ~ 5 nm in comparison with unsubstituted PcFe was observed [18]. Furthermore, the halogenation on the peripheral positions of the phthalocyanines generally causes a bathochromic shift of the absorption bands [19]. The Q-band of germanium complex **9** is ~ 5 nm red–shifted than that of tin complex **8** in 1-chloronaphthalene (**Figure 4.27**). This is caused by raising the energy level of the $a_{2u}(\pi)$ HOMO with the transition Si → Ge → Sn [9].

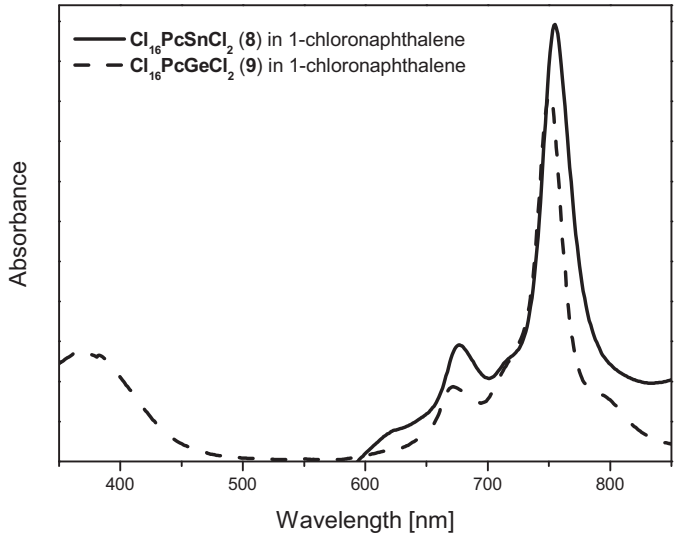

Figure 4.27 UV/Vis spectra of **$Cl_{16}PcSnCl_2$** (**8**) and **$Cl_{16}PcGeCl_2$** (**9**) in 1-chloronaphthalene.

The perchloro-substituted **$Cl_{16}PcSnCl_2$** (**8**) and **$Cl_{16}PcGeCl_2$** (**9**) phthalocyanines are soluble in 1-chloronaphthalene and 1,2,4-trimethylbenzene, and only slightly soluble in pyridine, and nearly insoluble in DMF and DMSO. Sonification in pyridine, DMF and DMSO of the compounds **8** and **9** gave colored solutions and allowed to take their absorption spectra. Absorption spectra of **8** and **9** taken in pyridine were dominated by aggregation suggesting that compounds were not truly soluble in these solvents. Furthermore, the solutions of **$Cl_{16}PcSnCl_2$** (**8**) and **$Cl_{16}PcGeCl_2$** (**9**) in pyridine, DMF and DMSO after approximately one hour became colorless.

Table 4.8 Absorption band maxima for hexadeca-substituted phthalocyanines

Compound	Solvent	λ_{max} [nm]
$Cl_{16}PcSnCl_2$ (8)	1-chloronaphthalene	755, 677, 380
$Cl_{16}PcGeCl_2$ (9)	1-chloronaphthalene	751, 671, 375
$Cl_{16}PcSn(OH)_2$ (10)	1-chloronaphthalene	750, 674, 365
$Cl_{16}PcGe(OH)_2$ (11)	1-chloronaphthalene	748, 672, 368
$Cl_{16}PcSnF_2$ (12)	1-chloronaphthalene	746, 712, 671, 364
$Cl_{16}PcGeF_2$ (13)	1-chloronaphthalene	739, 667, 359
$Cl_{16}PcSn(tBu_2P)_2$ (14)	CH_2Cl_2	733, 699, 661, 380
$Cl_{16}PcGe(tBu_2P)_2$ (15)	CH_2Cl_2	731, 695, 659, 367
$F_{16}PcSnCl_2$ (16)	$CHCl_3$	708, 678, 637, 368
$F_{16}PcGeCl_2$ (17)	$CHCl_3$	697, 666, 627, 357

The ESI-MS spectrum of **$Cl_{16}PcSnCl_2$ (8)** (**Figure 4.28**) shows the molecular ion at 1253.3 *m/z* and signals at 1218.3 $[M - Cl^-]^-$, 1183.3 $[M - 2Cl^-]^-$, 1150 $[M - 3Cl^-]^-$ and 1115.4 *m/z* $[M - 4Cl^-]^-$, exhibiting the sequential loss of two axial ligands and additional two chlorine atoms from peripheral positions of the macrocycle.

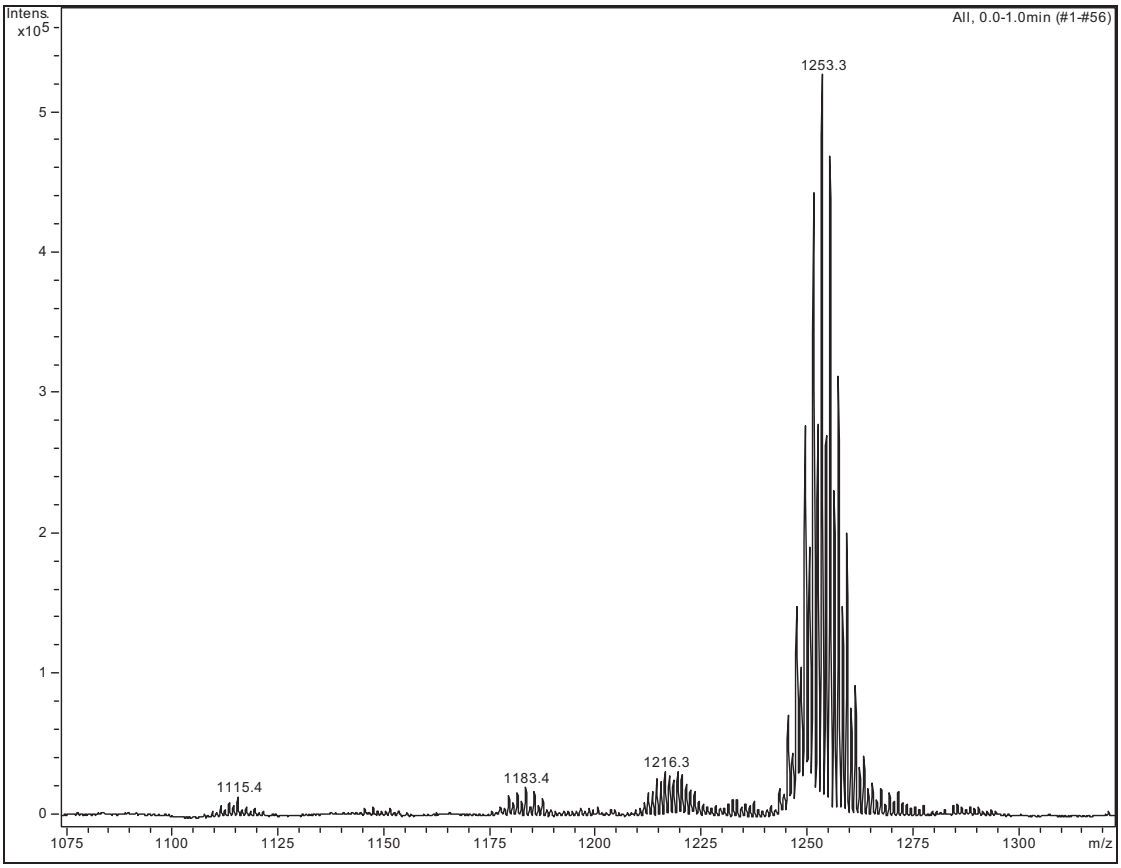

Figure 4.28 ESI negative-MS spectrum of $\mathbf{Cl_{16}PcSnCl_2}$ (**8**).

The nominal mass weight of $\mathbf{Cl_{16}PcSnCl_2}$ (**8**) and $\mathbf{Cl_{16}PcGeCl_2}$ (**9**) is 1246 and 1200, respectively, but average mass weight taking into account Ge's and Sn's isotopes is determined to be 1253.3 and 1207.2, respectively. The isotopic distribution of **8** and **9** is presented in **Figure 4.29 A** and **B**. The obtained ESI-MS spectrum for **8** and DCI-MS for **9** (**Figure 4.30**) are consistent with the theoretical isotopic patterns.

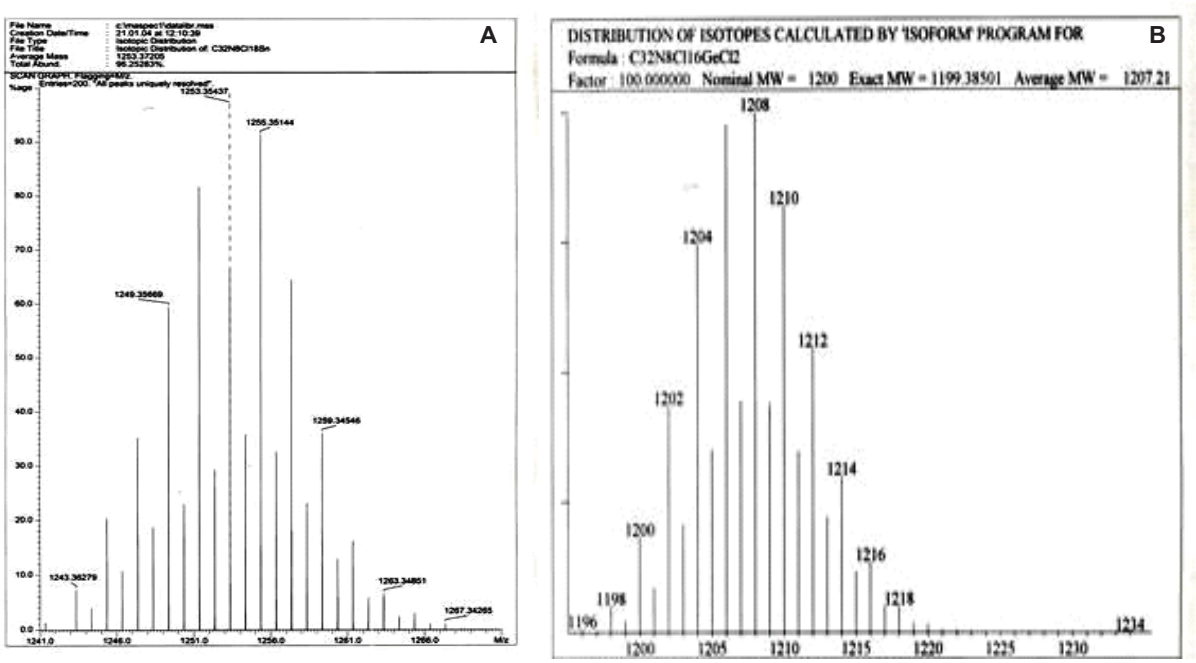

Figure 4.29 The isotopic distribution of $\mathbf{Cl_{16}PcSnCl_2}$ (**8**) (**A**, left) and of $\mathbf{Cl_{16}PcGeCl_2}$ (**9**) (**B**, right).

Figure 4.30 A shows the DCI-MS spectrum of the raw product of **9** prepared by method I. The mass spectrum evidently shows unreacted tetrachlorophthalonitrile and the phthalocyanine **9**. The mass spectrum presented in **Figure 4.30 B** shows prepared by method II the $\mathbf{Cl_{16}PcGeCl_2}$ (**9**) after purification. The molecular ion appears at 1208 *m/z* and the loss of one of the two axial chlorine substituents is demonstrated at 1173 *m/z*.

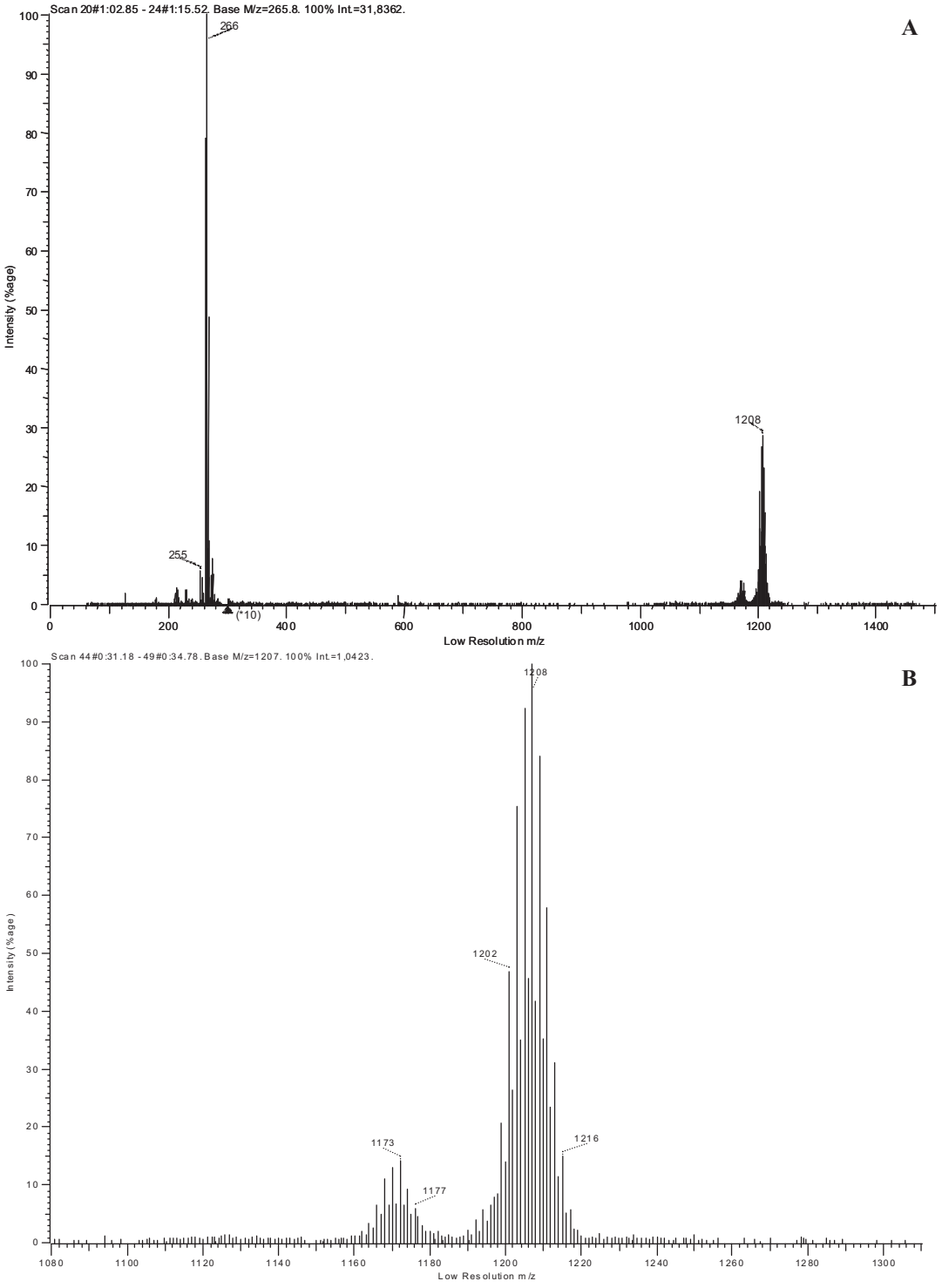

Figure 4.30 DCI-MS spectrum of $\mathbf{Cl_{16}PcGeCl_2}$ (**9**) after reaction (**A**, top) and after purification (**B**, bottom).

The dihydroxytin(IV) hexadecachlorophthalocyanine (**10**) and dihydroxygermanium(IV) hexadecachlorophthalocyanine (**11**) were synthesized by the hydrolysis of $\mathbf{Cl_{16}PcSnCl_2}$ (**8**) and $\mathbf{Cl_{16}PcGeCl_2}$ (**9**) (**Figure 4.31**). The crude products were filtered off and washed

intensively with organic solvents. Finally, after Soxhlet extraction with methanol and acetone bluish compounds, **10** and **11** were obtained in good yields between 60.5 – 63 % (**Table 4.7**). The UV/Vis spectra of **$Cl_{16}PcSn(OH)_2$** (**10**) and **$Cl_{16}PcGe(OH)_2$** (**11**) are slightly blue-shifted by ~ 5 nm for **10** and ~ 3 nm for **11** in comparison with **$Cl_{16}PcSnCl_2$** (**8**) and **$Cl_{16}PcGeCl_2$** (**9**) in 1-chloronaphthalene. It is the consequence of exchange of axial ligands from hydroxyl to chlorine groups. On the other hand, the Q-band of the perchloro-substituted complexes **10** and **11** in 1-chloronaphthalene solution is significantly red-shifted (~ 50) relating to the unsubstituted derivatives **$PcSn(OH)_2$** and **$PcGe(OH)_2$** in pyridine [20], showing a significant influence of chlorine peripheral substituents on optical properties of phthalocyanines.

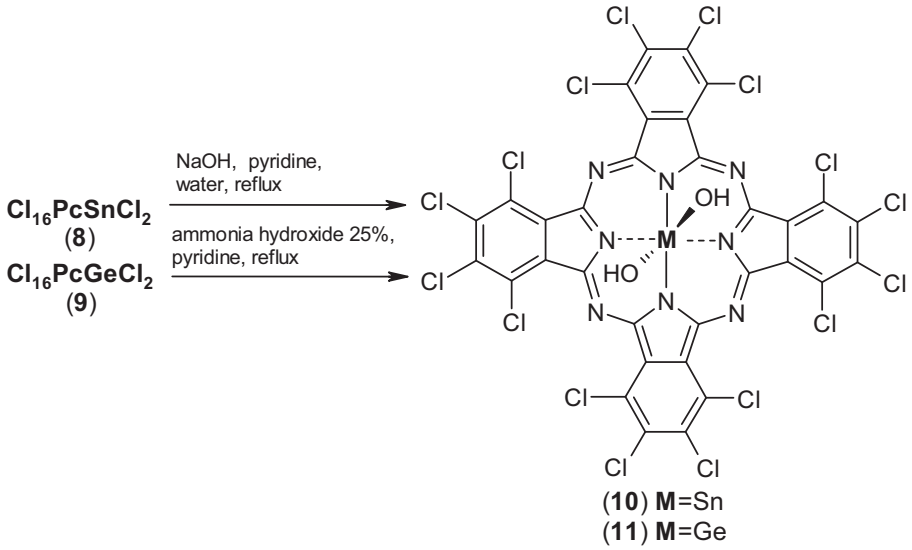

Figure 4.31 Route of synthesis of **$Cl_{16}PcSn(OH)_2$** (**10**) and **$Cl_{16}PcGe(OH)_2$** (**11**).

The **$Cl_{16}PcSn(OH)_2$** (**10**) and **$Cl_{16}PcGe(OH)_2$** (**11**) exhibit similar solubility like **$Cl_{16}PcSnCl_2$** (**8**) and **$Cl_{16}PcGeCl_2$** (**9**). They are very less soluble in pyridine and additionally the UV/Vis spectra of **10** and **11** in pyridine were much broader than that of their dichloride axially substituted analogues, **8** and **9**, in the same solvent.

The molecular ion at 1216 *m/z* in the DCI-MS (negative ion mode, NH_3) spectrum of **$Cl_{16}PcSn(OH)_2$** (**10**) (**Figure 4.32 A**) is in the agreement with the theoretical isotopic distribution calculated for compound **10** (**Figure 4.33 A**). The DCI-positive spectrum of **10** consists of the main peak at 1181 *m/z* corresponding to $[M + H^+ - 2OH^-]^+$, the molecular ion at 1217 *m/z* and the peak at 1252 *m/z* being the unreacted complex **8.**

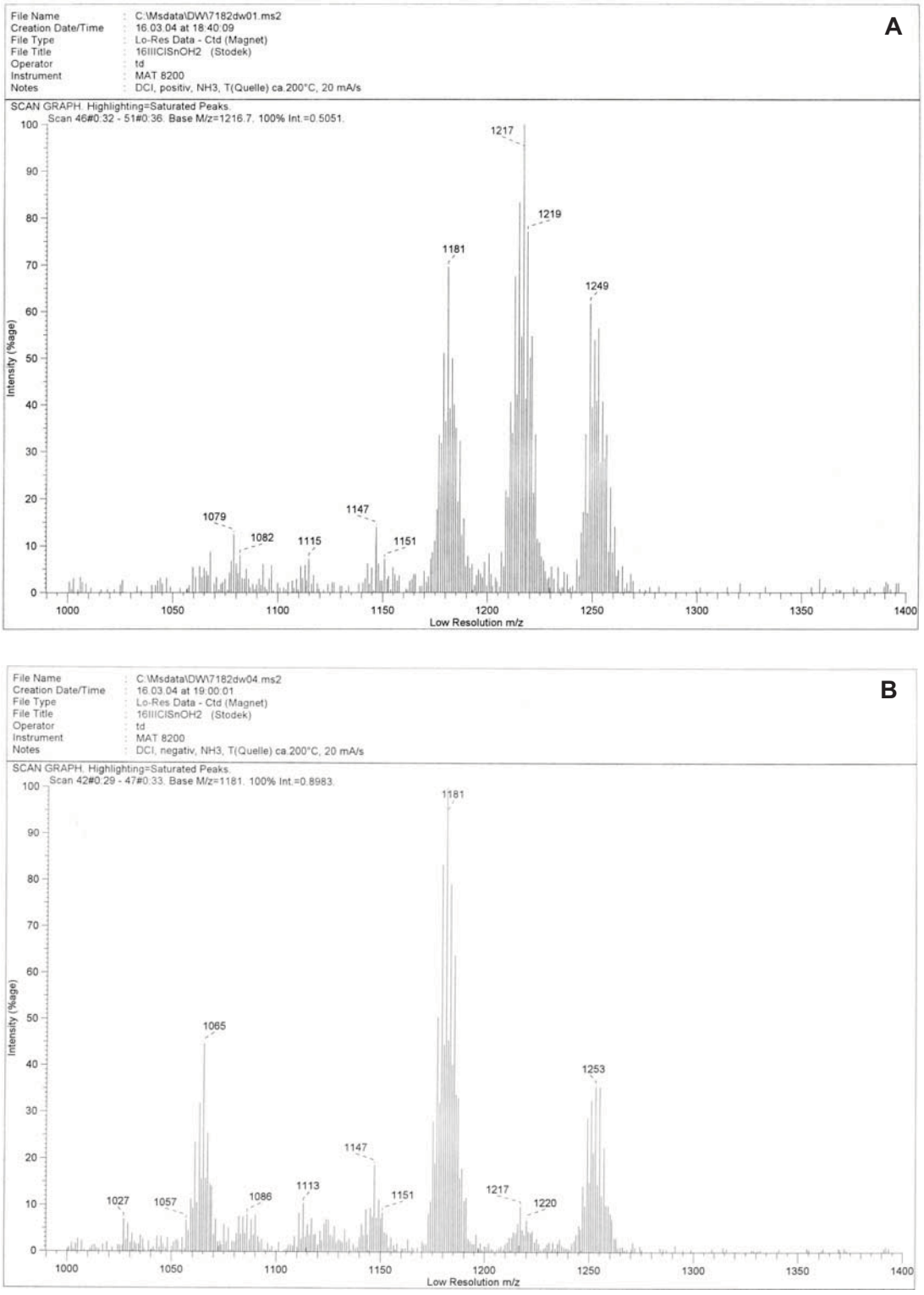

Figure 4.32 DCI-MS (negative ion mode, NH_3) spectrum (**A**, top) and (positive ion mode, NH_3) spectrum of **$Cl_{16}PcSn(OH)_2$** (**10**) (**B**, bottom).

The additional fragmentation of the complex **11** was observed in every case of the DCI method. The successive loss of one, two and three peripheral chlorine atoms of $[M - 2OH^-]^+$ is seen at 1147, 1113, 1079 *m/z* and the loss of the central metal is observed at 1065 *m/z* ($[M - 2OH^- - Sn]^+$) (**Figure 4.32 B**). The theoretical isotopic distribution of $\mathbf{Cl_{16}PcGe(OH)_2}$ (**11**) presented in **Figure 4.33 B** corresponds to DCI-MS spectrum of **11** (**Figure 4.34 A**).

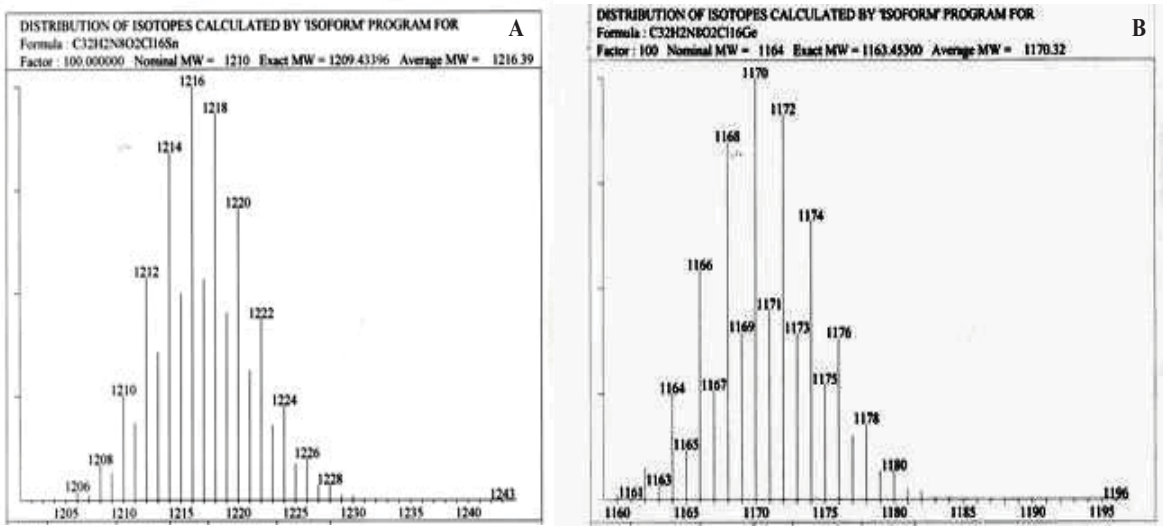

Figure 4.33 The isotopic distribution of dihydroxytin(IV) hexadecachlorophthalocyanine (**10**) (**A**, left) and dihydroxygermanium(IV) hexadecachlorophthalocyanine (**11**) (**B**, right).

The DCI-MS spectrum shows the molecular ion at 1171.8 *m/z*, and in the ESI-MS spectrum (**Figure 4.34 B**) of compound **11** the molecular ion is seen at 1169.4 *m/z*, and species at 1152.4 and 1135.4 *m/z* correspond to the loss of axial hydroxyl groups.

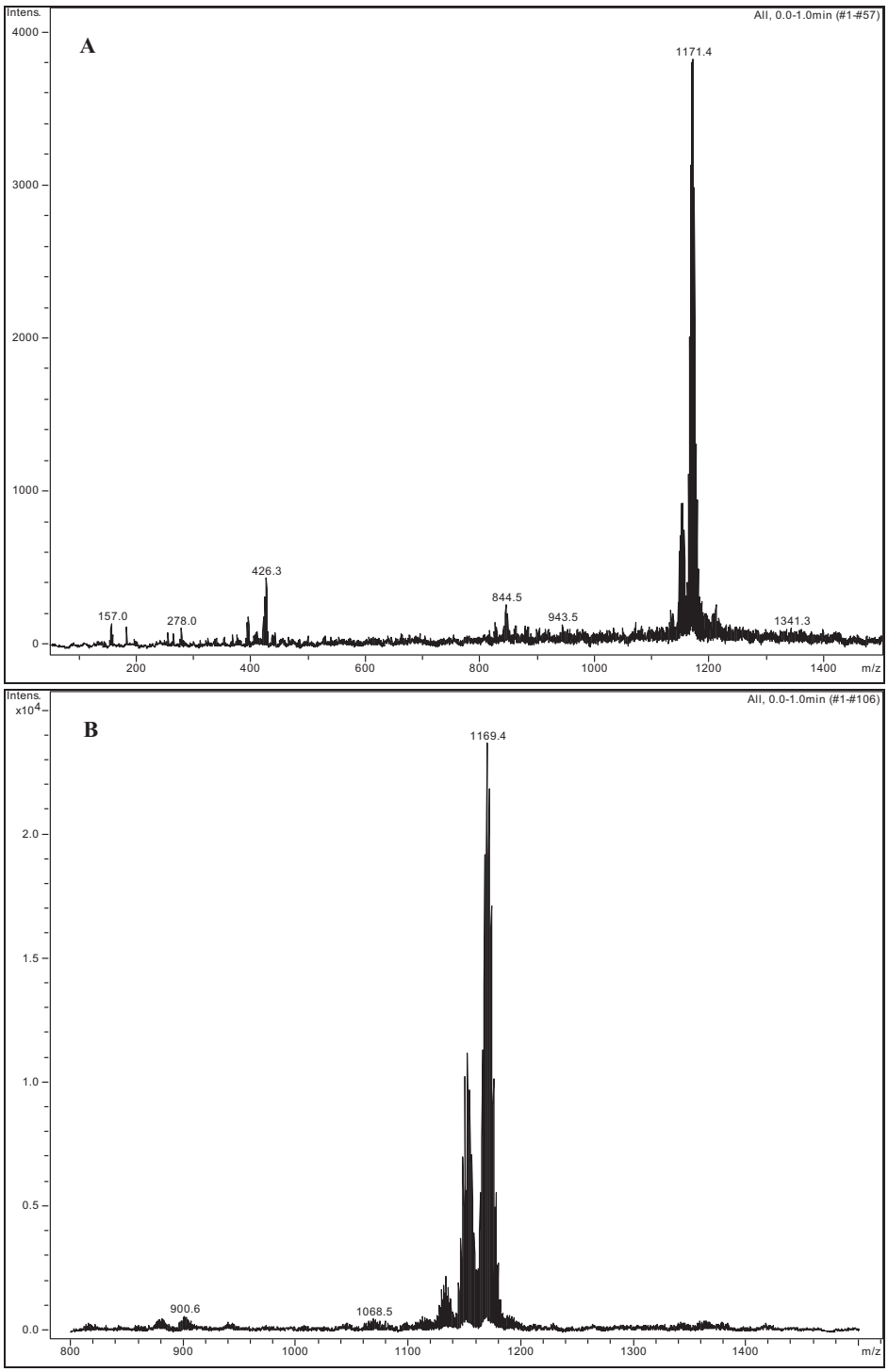

Figure 4.34 DCI-MS (**A**, top) and ESI-MS (**B**, bottom) of $\mathbf{Cl_{16}PcGe(OH)_2}$ (**11**).

The difluorotin(IV) hexadecachlorophthalocyanine (**12**) and difluorogermanium(IV) hexadecachlorophthalocyanine (**13**) were synthesized by treatment of $\mathbf{Cl_{16}PcSn(OH)_2}$ (**10**) and $\mathbf{Cl_{16}PcGe(OH)_2}$ (**11**) with 40% fluoric acid. The purification of $\mathbf{Cl_{16}PcSnF_2}$ (**12**) and $\mathbf{Cl_{16}PcGeF_2}$ (**13**) by Soxhlet extraction with organic solvents (methanol, acetone, pyridine) gave bluish products in good yields (**Table 4.7**).

The solubility of the complexes **12** and **13** decreases in comparison with complexes with the dichloro axially substituted compounds **8** and **9**. A shift of the Q-band ~ 5 nm to shorter wavelengths of complexes **12** and **13** compared with complexes **8** and **9** in 1-chloronaphthalene solutions is observed. The mass spectrum of $\mathbf{Cl_{16}PcSnF_2}$ (**12**) shows the molecular ion at 1219.3 *m/z* and peaks at 1200.4 and 1181.4 *m/z* correspond to the loss of axial fluorine ligands (**Figure 4.35 A**).

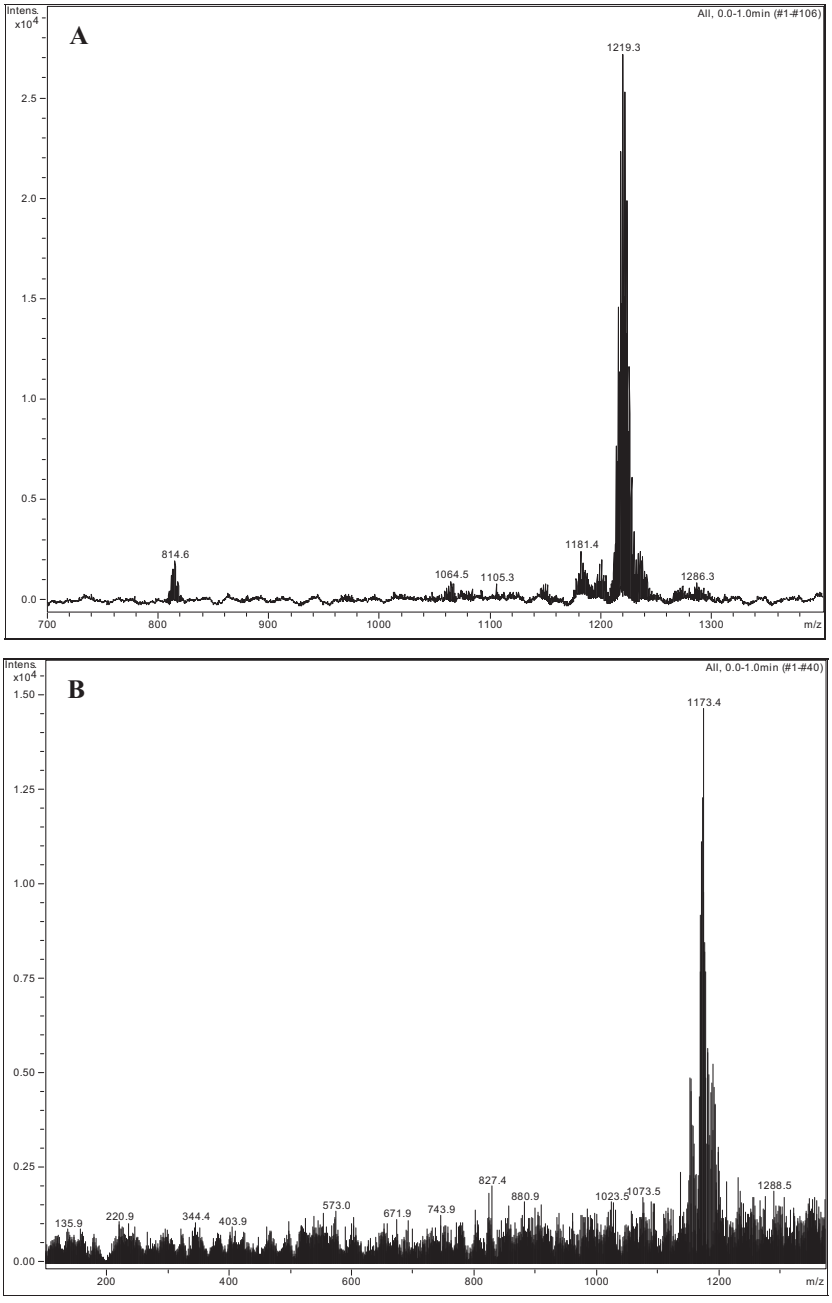

Figure 4.35 ESI-MS spectrum of $\mathbf{Cl_{16}PcSnF_2}$ (**12**) (**A**, top) and $\mathbf{Cl_{16}PcGeF_2}$ (**13**) (**B**, bottom).

In case of **$Cl_{16}PcGeF_2$** (**13**) the ESI–MS spectrum (**Figure 4.35 B**) displays the main peak at 1173.4 *m/z* and a signal at 1156.4 *m/z* is assigned to a loss of one fluorine axial ligand.

In order to prepare films of tin(IV) and germanium(IV) perchloro-substituted phthalocyanines, it was necessary to increase their solubility. It was decided to substitute axial chlorine atoms of **$Cl_{16}PcSnCl_2$** (**8**) and **$Cl_{16}PcGeCl_2$** (**9**) phthalocyanines by di(*tert*-butyl)phenoxy groups as it was performed in case of compound **23**. The bulky substituents in the axial position increase solubility in organic solvents and polymers and by steric hindrance prevent the aggregation.

The **$Cl_{16}PcSn(tBu_2P)_2$** (**14**) and **$Cl_{16}PcGe(tBu_2P)_2$** (**15**) were synthesized by mixing appropriate **$Cl_{16}PcSnCl_2$** (**8**) or **$Cl_{16}PcGeCl_2$** (**9**) with 3,5-di-*tert*-butylphenol, powdered K_2CO_3 and 18-crown-6 (molar ratio, 1:2:2) in 1,2,4-trimethylbenzene under argon atmosphere (**Figure 4.36**). The resulting suspension was heated at 140 °C with stirring. The reaction was monitored by TLC and UV/Vis spectroscopy and stopped when all of the complexes **8** and **9** have been consumed. The duration of the axial substitution for **$Cl_{16}PcGe(tBu_2P)_2$** (**15**) took around 50 minutes and in case of **$Cl_{16}PcSn(tBu_2P)_2$** (**14**) approximately 1.5 hour. The attempt of axial substitution of **$Cl_{16}PcSnCl_2$** (**8**) or **$Cl_{16}PcGeCl_2$** (**9**) by di(*tert*-butyl)phenoxy groups without using a catalyst gave partial substitution and took around 18 hours. The dark greenish-blue solutions were poured into hexane; the precipitate formed was collected by centrifugation and washed with hexane. The crude products were chromatographed on silica gel using toluene in case of **14** and CH_2Cl_2 in case of **15** as an eluent. Removal of the solvent and drying in vacuum at 60 °C gave green products in ~ 20 % yield (**Table 4.3**).

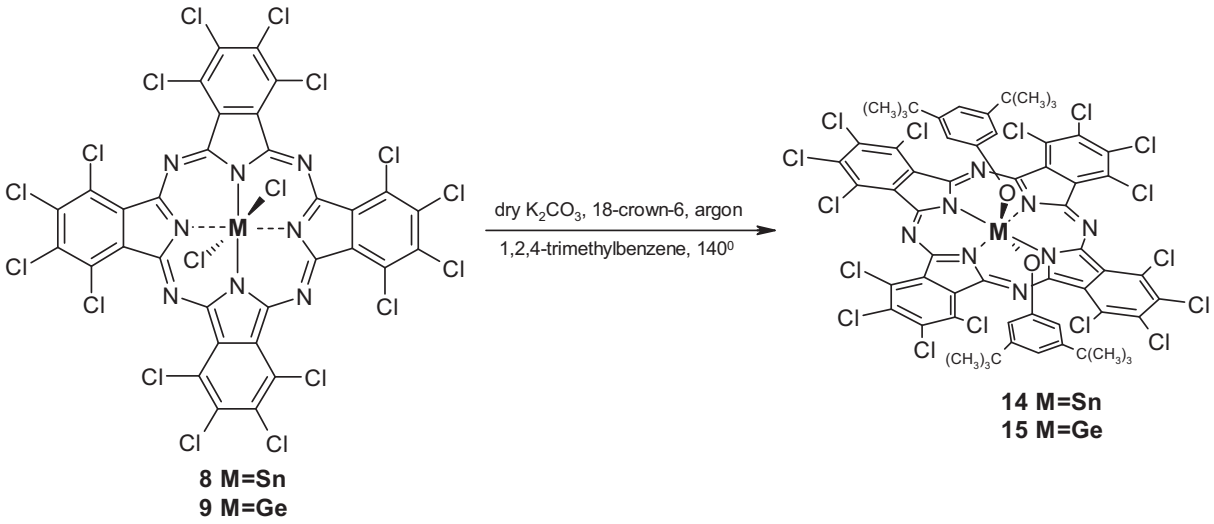

Figure 4.36 Route of synthesis of **$Cl_{16}PcSn(tBu_2P)_2$** (**14**) and **$Cl_{16}PcGe(tBu_2P)_2$** (**15**).

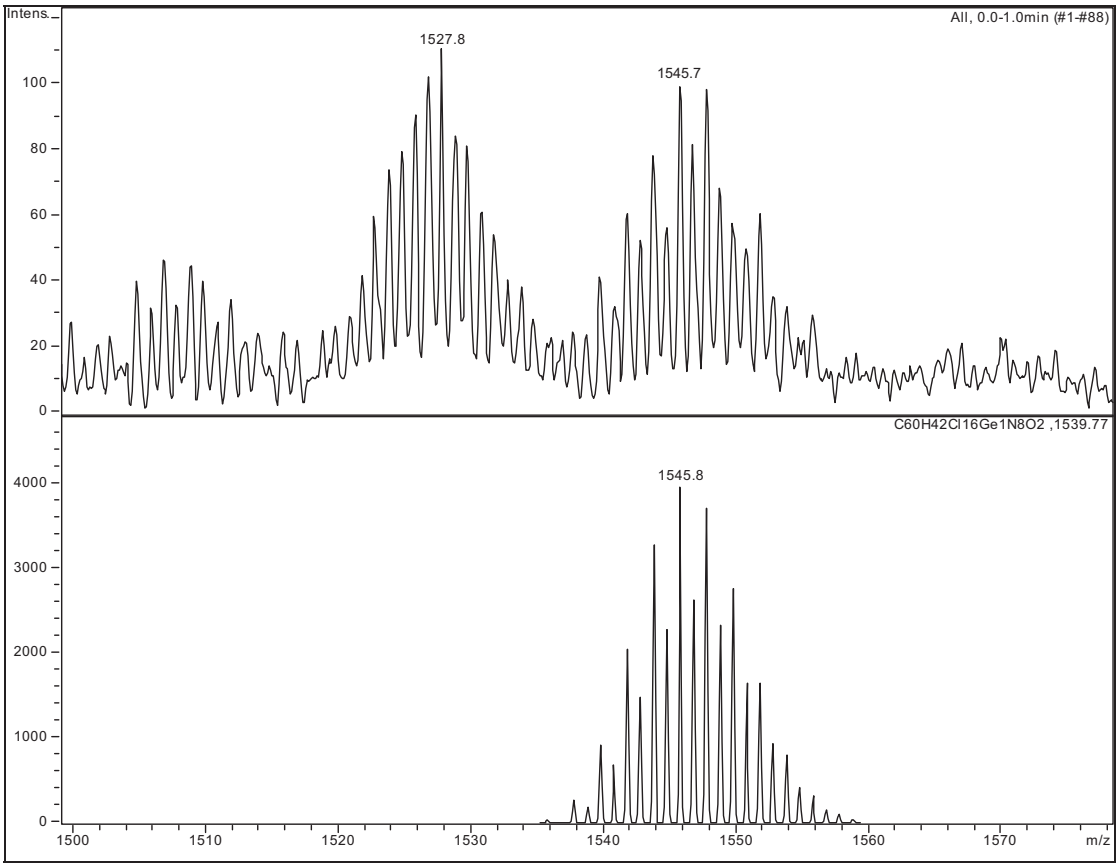

Figure 4.37 ESI-MS spectrum of **$Cl_{16}PcGe(tBu_2P)_2$** (**15**) in comparison with isotopic pattern of **15** (bottom).

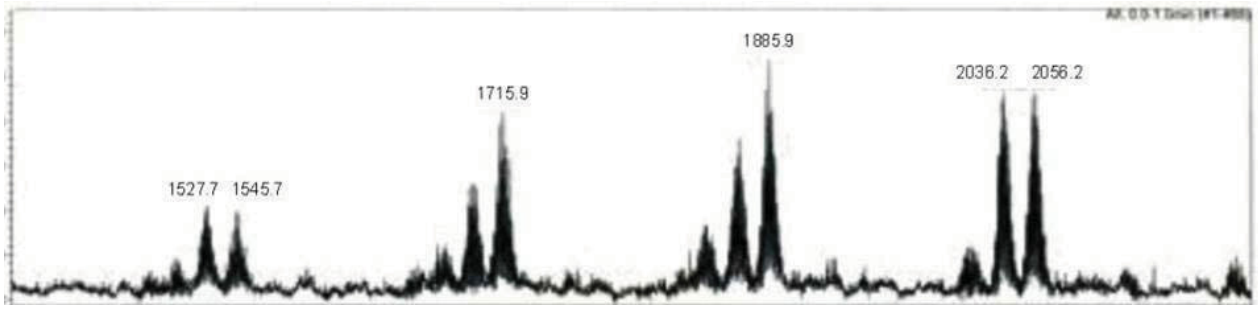

Figure 4.38 ESI-MS spectrum of **$Cl_{16}PcGe(tBu_2P)_2$** (**15**).

The ESI-MS spectra of **$Cl_{16}PcSn(tBu_2P)_2$** (**14**) and **$Cl_{16}PcGe(tBu_2P)_2$** (**15**) (**Figure 4.37**) show a cluster of peaks almost identical in intensity to that calculated for its respective isotopic composition. The ESI-MS spectra shows the peak at 1591.6 *m/z* attributed to **$Cl_{16}PcSn(tBu_2P)_2$** and at 1545.7 *m/z* attributed to **$Cl_{16}PcGe(tBu_2P)_2$** (**15**). The loss of one of the axial group $C_{14}H_{21}0$, in ESI-MS spectra of **14** and **15** is observed. It is interesting to note that the extension of the time of the reaction of **$Cl_{16}PcSn(tBu_2P)_2$** (**14**) and **$Cl_{16}PcGe(tBu_2P)_2$** (**15**) to 5 hours and mole ratio of phthalocyanine:3,5-di-*tert*-butylphenol:18-crown-6 to 1:4:4

gave peaks in the mass spectra with a difference by 170 units, suggesting substitution of peripheral chlorine groups by di(*tert*-butyl)phenoxy ($C_{14}H_{21}0$) groups (**Figure 4.38**).

The substitution of the small chlorine ligands of **8** and **9** by bulky di(*tert*-butyl)phenoxy groups improved significantly solubility of **14** and **15**. The complexes **14** and **15** are well soluble in chloroform (**Figure 4.39**), tetrahydrofuran, dichloromethane and toluene. In DMSO and DMF both compounds **14** and **15** are partly soluble and exhibit partial aggregation.

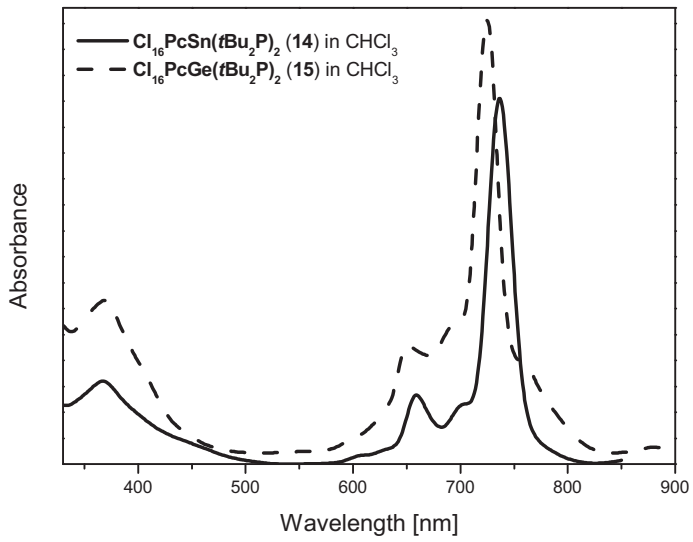

Figure 4.39 UV/Vis spectra of **$Cl_{16}PcSn(tBu_2P)_2$** (**14**) and **$Cl_{16}PcGe(tBu_2P)_2$** (**15**) in $CHCl_3$.

Dichlorotin(IV) hexadecafluorophthalocyanine (**16**) was prepared by a modified version of the synthesis described by Birchall [21]. The cyclotetramerization reaction to obtain **$F_{16}PcSnCl_2$** (**16**) was performed by refluxing tetrafluorophthalonitrile (**IX**) and anhydrous $SnCl_2$ in dry 1-chloronaphthalene under nitrogen atmosphere for 2 hours (**Figure 4.40**). After removal of the high-boiling solvent by precipitation with hexane, the product was repetitively washed with diethyl ether in order to remove first impurities. Afterwards the crude product was placed in a sublimation apparatus to remove yellow-white impurities. Soxhlet extraction with petroleum ether was performed in order to remove all unreacted tetrafluorophthalonitrile (**IX**).

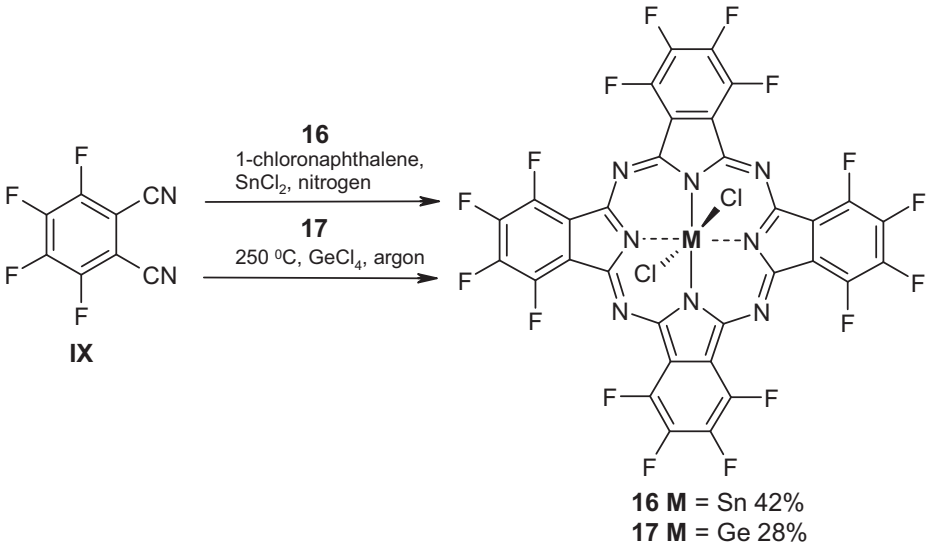

Figure 4.40 Synthesis of $\mathbf{F_{16}PcSnCl_2}$ (**16**) and $\mathbf{F_{16}PcGeCl_2}$ (**17**).

Purification by column chromatography gave large losses of the product pointing out a high affinity of compound **16** to the sol gel material. The obtained product after chromatography showed high aggregation in the absorption spectrum. The ESI-MS spectrum (negative ion mode) gave peaks at 953.9, 936.9, and 936.9 *m/z* attributed to $F_{16}PcSn(OH)_2$ (dihydroxytin(IV) hexadecafluorophthalocyanine), $F_{16}PcSn(OH)^-$ and $F_{16}PcSn^{2-}$, respectively. Thus, the solid was redissolved in small amount of THF, precipitated with hexane, then with methanol, and centrifuged off. This was repeated until the supernatant was colorless. Finally, the product was vacuum dried to give 42% of a dark blue powder.

The preparation of dichlorogermanium(IV) hexadecafluorophthalocyanine (**17**) was only achieved by heating at 250 °C tetrafluorophthalonitrile (**IX**) with $GeCl_4$. The product was purified by column chromatography on silica gel using chloroform as an eluent, leading to a blue product. The cyclotetramerization of neither tetrafluorophthalonitrile (**IX**) nor tetrafluorophthalic anhydride with $GeCl_4$ in quinoline or nitrobenzene with addition of urea and ammonium molybdate was unsuccessful.

The $\mathbf{F_{16}PcSnCl_2}$ (**16**) (**Figure 4.41**) and $\mathbf{F_{16}PcGeCl_2}$ (**17**) compounds are highly soluble in many solvents such as chloroform (**Figure 4.42**), dichloromethane, toluene, tetrahydrofuran, dimethylsulfoxide, ethyl acetate and even slightly soluble in acetone and methanol.

Figure 4.41 shows that the absorption spectra of **16** are independent on the solvent, with the Q-band ranging from 703 nm in ethyl acetate till 708 nm in $CHCl_3$. The same independence on the solvent is observed in the case of $\mathbf{F_{16}PcGeCl_2}$ (**17**) as well. The spectral features of vanadyl hexadecafluorophthalocyanine ($\mathbf{F_{16}PcVO}$) [22], contrary to compounds, **16** and **17**,

are dependent on the solvent. The phthalocyanine complex **F_{16}PcVO** exhibits the Q-band ~ 710 nm in nonpolar solvents whereas in polar solvents the Q-band is shifted ~ 60 nm to shorter wavelength [22].

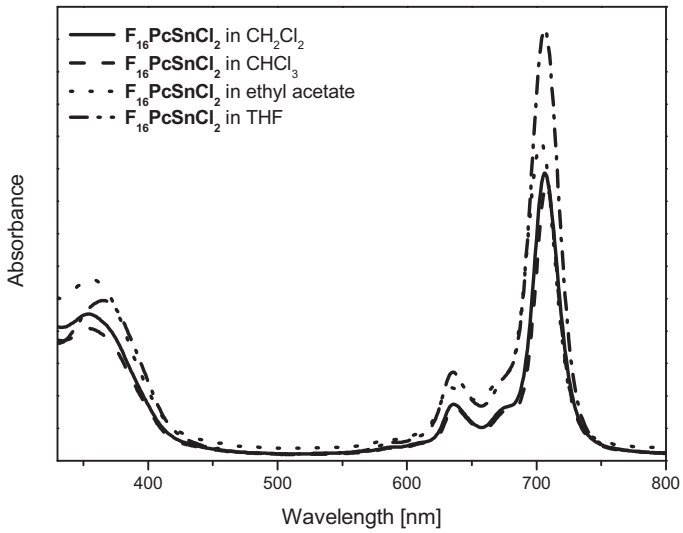

Figure 4.41 Absorption spectra of **F_{16}PcSnCl$_2$** (**16**) in different solvents.

The Q-band of **F_{16}PcSnCl$_2$** (**16**) is approximately 10 nm blue-shifted than that of **F_{16}PcGeCl$_2$** (**17**) caused by decreasing electronegativity of central metal Ge → Sn which shifts charge into the ring and raises the energy of the $a_{2u}(\pi)$ HOMO [9, 23].

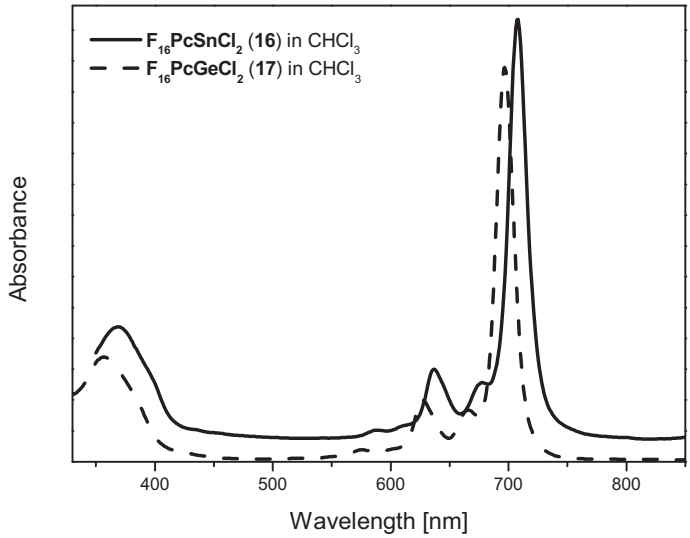

Figure 4.42 Absorption spectra of **F_{16}PcSnCl$_2$** (**16**) and **F_{16}PcGeCl$_2$** (**17**) in $CHCl_3$.

However, the difference in the shift of the Q-band between tin and germanium tetrakis*(p*-formylphenoxy)-substituted phthalocyanines, **6** and **7**, related to decreased electronegativity of the M is two times smaller (see **Table 4.4** in Chapter 4.2) than that of hexadecafluoro-substituted compounds **16** and **17**.

The ESI negative-mass spectrum (**Figure 4.43**) confirm the presence of the desired $\mathbf{F_{16}PcSnCl_2}$ (**16**) compound. The molecular ion is observed at 989.7 *m/z*. The peaks at 954.8 and 919.8 *m/z* exhibit the loss of one and two chlorine atoms, respectively. The peak at 970.8 *m/z* suggests the substitution of chlorine atom by oxygen atom ($[M - Cl^- + O^-]^-$).

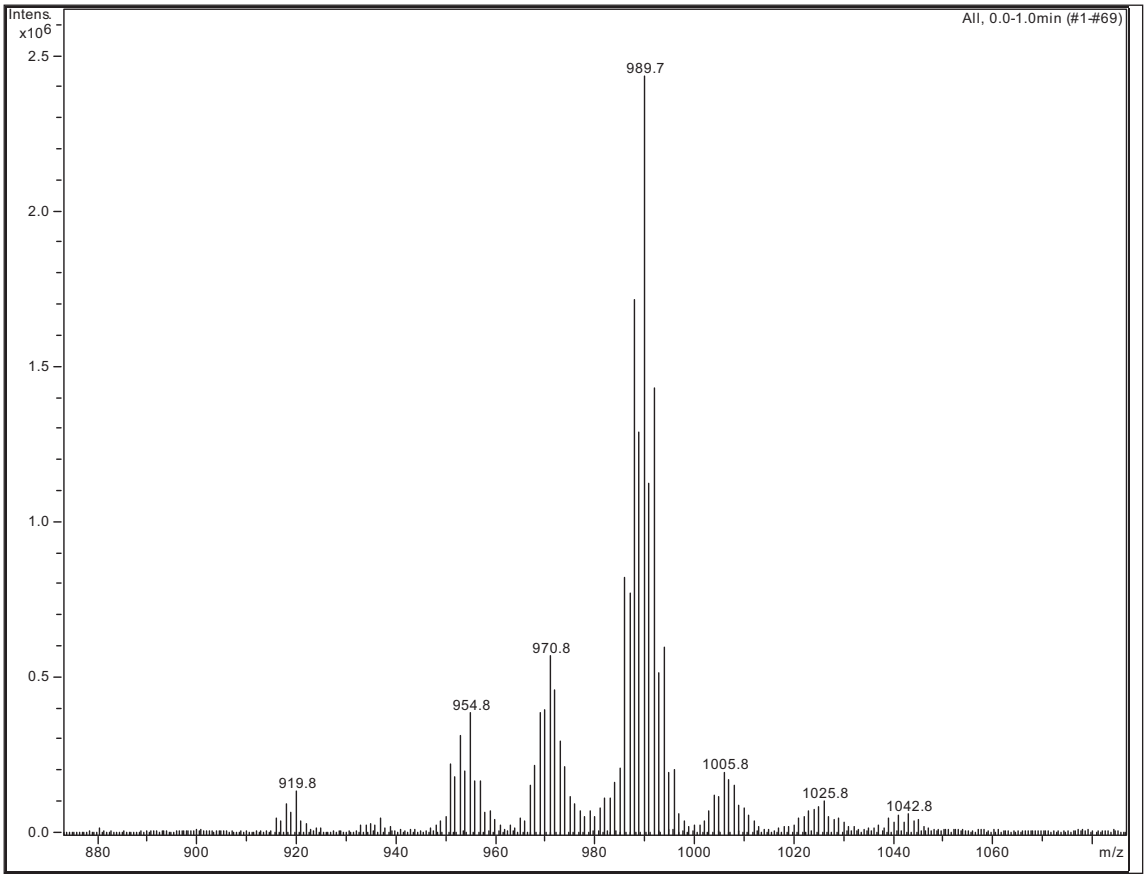

Figure 4.43 ESI-MS spectrum of $\mathbf{F_{16}PcSnCl_2}$ (**16**)

The synthesis of dichlorotin(IV) hexadecafluorophthalocyanine (**16**) carried out with a great excess of tin(II) chloride, beside main product *i.e.* $\mathbf{F_{16}PcSnCl_2}$ (**16**), gave some other side products detected by mass spectrometry. **Figure 4.44** presents main peak at 989.7 *m/z* corresponding to $\mathbf{F_{16}PcSnCl_2}$ (**16**) and additional peaks are visible at 1005.7, 1024.7, 1038.7, 1054.7, 1070.7, 1091.7, 1107.7 *m/z*.

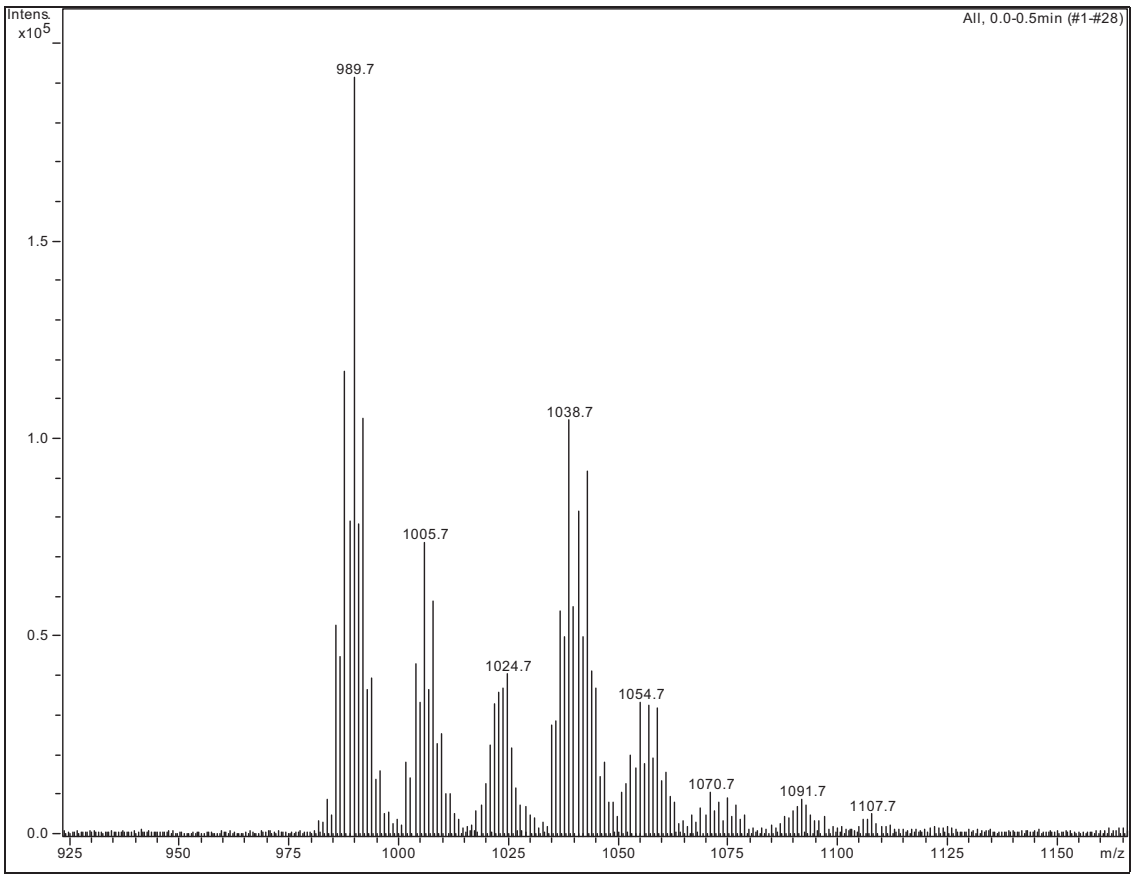

Figure 4.44 ESI-MS spectrum of $\mathbf{F_{16}PcSnCl_2}$ (**16**) and side products.

Those peaks are correlated to different phthalocyanines as presented in **Figure 4.45**. The mass spectrum of the obtained products (**Figure 4.44**) during the reaction between tetrafluorophthalonitrile (**IX**) and $SnCl_2$ suggests a nucleophilic substitution of fluoride by chloride ions. It means that nucleophilic attack by chloride ions distinctly takes place during reaction and the cleavage of the bond C-F easily occurs.

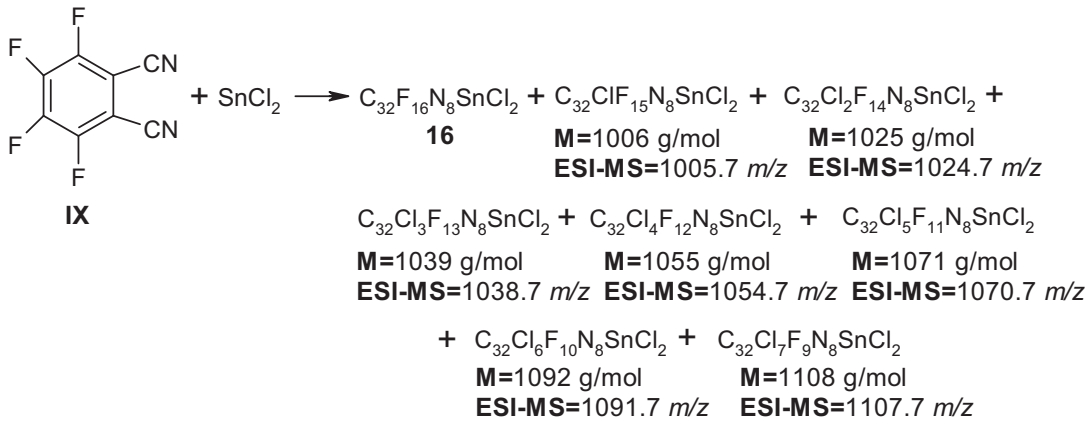

Figure 4.45 Mixture of phthalocyanines obtained during the reaction of tetrafluorophthalonitrile (**IX**) with big excess of $SnCl_2$.

J. M. Birchall and *et al.* [21] reported the displacement of fluoride by chloride ion during reaction of tetrafluorophthalonitrile with zinc chloride suggesting the nucleophilic attack by chloride ion at tetrafluorophthalonitrile or at zinc hexadecafluorophthalocyanine already formed. The exchange of fluoride from the 4- and 5-positions of tetrafluorophthalonitrile by lithium chloride in aprotic solvents [24] indicated that the halogenation took place before formation of the phthalocyanine [24]. The displacement of fluoride by chloride ion during synthesis of dichlorotin(IV) hexadecafluorophthalocyanine (**16**) was not reported before.

The ESI negative-mass spectrum of dichlorogermanium(IV) hexadecafluorophthalocyanine (**17**) is presented in **Figure 4.46**.

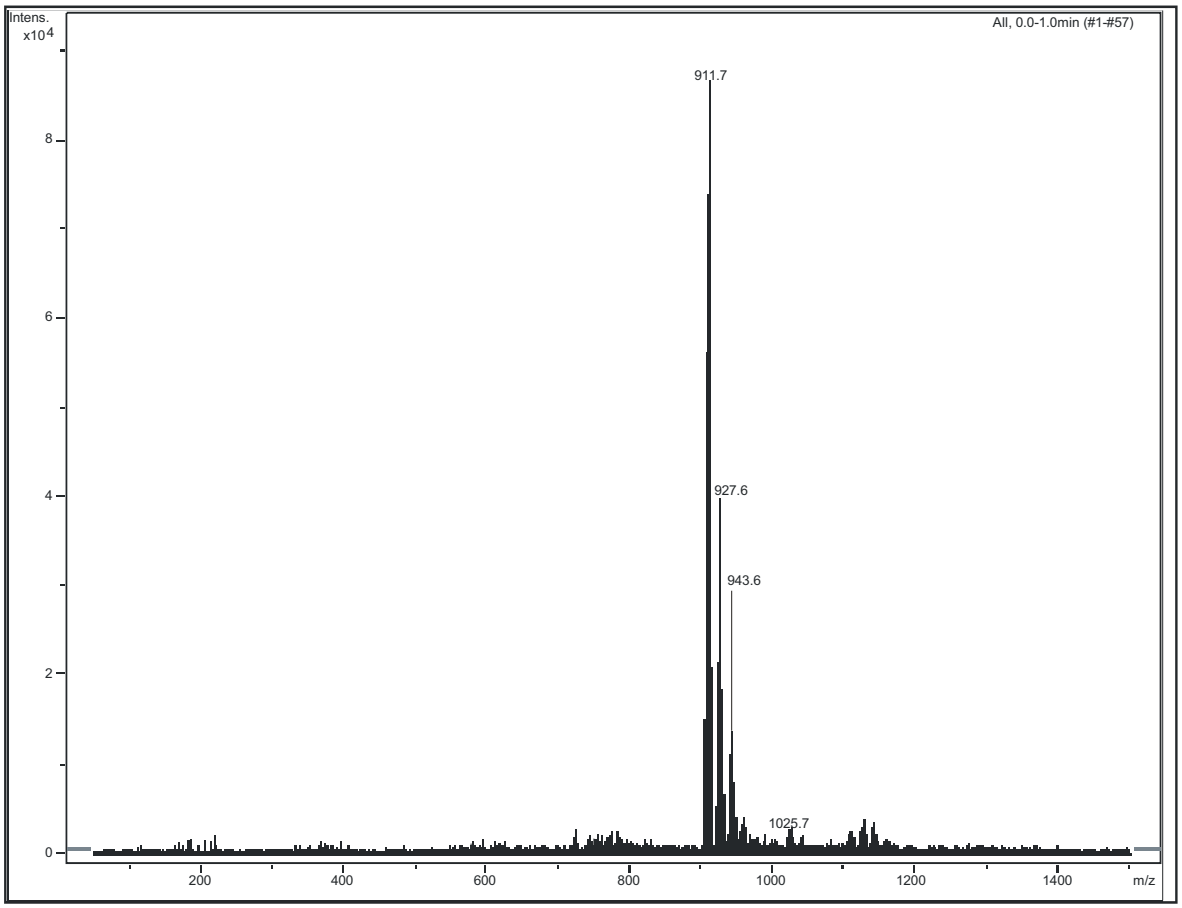

Figure 4.46 ESI negative-MS spectrum of $\mathbf{F_{16}PcGeCl_2}$ (**17**)

The molecular ion is observed at 943.6 *m/z*. Surprisingly the substitution of fluoride by chloride ion was not noticed. However, the opposite situation was observed, the peaks at 927.6 and 911.7 *m/z* suggest substitution of two axial chlorine ligands by fluorine atoms.

4.4 Conclusion

A series of metal-free, tin and germanium tetra-, hexadeca- and one octa-substituted phthalocyanines containing various electron-withdrawing groups as peripheral and axial substituents were synthesized and characterized. The phthalocyanines were prepared in order to check the influence of different substituents in peripheral and axial positions on their nonlinear optical (NLO) properties in solution of organic solvents. The enhancement of solubility of tin and germanium hexadecachloro- and tetranitro-substituted phthalocyanines *i.e.* **$Cl_{16}PcSnCl_2$** (**8**), **$Cl_{16}PcSnCl_2$** (**9**) and **$(\alpha NO_2)_4PcGeCl_2$** (**20**) was attained by the introduction of the bulky substituent such as di(*tert*-butyl)phenoxy group in the axial positions. The di(*tert*-butyl)phenoxy group was chosen as axial substituent due to its bulkiness that should reduce the tendency to form aggregates in solution. In addition, di(*tert*-butyl)phenoxy group as axial ligand introduces a dipole moment perpendicular to the macrocycle, which alters the electronic structure of the macrocycle and furthermore gives rise to a better optical limiting effect in the phthalocyanine. The phthalocyanines were characterized by IR, UV/Vis and mass spectroscopy. The absorption spectra of synthesized Pcs mainly show the red shift of the Q- and B-bands which is usually associated with the presence of electron-withdrawing groups at the periphery of the macrocycle. During synthesis of **$Cl_{16}PcSn(tBu_2P)_2$** (**14**), **$Cl_{16}PcGe(tBu_2P)_2$** (**15**), **$F_{16}PcSnCl_2$** (**16**) and **$F_{16}PcGeCl_2$** (**17**) occurred some side reactions that led to replacement of some peripheral groups by others. The side products were not separated and remained as impurities. Few well in organic solvents soluble and pure phthalocyanines were used for the preparation of multi-layer polymeric films (Chapter 7) and their optical limiting properties were further investigated (Chapter 8).

4.5 References

[1] J. D. Loudon, N. Shulman, *J. Chem. Soc.*, **1941**, 772.

[2] J. March, Williams, *Advanced Organic Chemistry: Reactions, Mechanism and Structure.* John Wiley & Sons: New York, **1992**.

[3] A. A. Hirth, *Biotinylierte Phthalocyanine für die Polyphasisische Photodynamische Tumortherapie*, Mai **1999**, Bremen.

[4] C. C. Leznoff, S. M. Marcuccio, S. Greenberg, A. B. P. Lever, K. B. Tomer, *Can. J. Chem.*, **1985**, 63, 623.

[5] M. Hanack, G. Schmid, M. Sommerauer, *Angew. Chem.,* **1993**, 105, 1540.

[6] M. Hanack, G. Schmid, M. Sommerauer, *Angew. Chem., Int. Ed. Eng.*, **1993**, 32, 1422.

[7] M. Hanack, D: Meng; A. Beck, M. Sommerauer, L. R. Subramanian, *J. Soc. Chem. Commun.,* **1993**, 58.

[8] M. Whalley, *J. Chem. Soc.,* **1961**, 866.

[9] M. Gouterman, *J. Chem. Phys.*, **1959**, 30, 1139.

[10] A. Shaabani, *J. Chem. Res. (S).*, **1998**, 672.

[11] G. Schmid, E. Witke, U. Schlick, S. Knecht, M. Hanack, *J. Mat. Chem.*, **1995**, 5, 855.

[12] N. Kobayashi, N. Sasaki, Y. Higashi, T. Osa, *Inorg. Chem.*, **1995**, 34, 1636.

[13] T. G. Linssen, M. Hanack, *Chem. Ber.*, **1994**, 157, 2051.

[14] C. Pedersen, .J. *Aldrichimica Acta*, **1971**, *4*, 1.

[15] G. W. Gokel; H. D. Durst, *ibid*., **1976**, *9*, 3.

[16] J. S. Valentine, A. B. Curtis, *J. Am. Chem. Soc*., **1975**, *97*, 224.

[17] M. Hanack, H. Heckmann, *Eur. J. Inorg. Chem.*, **1998**, 367.

[18] J. Metz, O. Schneider, M. Hanack, *Inorganic Chemistry*, **1984**, 23, 8.

[19] T. Takeuchi, H. B. Gray, W. A. Goddard, *J. Am. Chem. Soc.*, **1994**, 9730, 116.

[20] C.W. Dirk, T. Inabe, K. F. Schoch, T. J. Marks, *J. Am. Chem. Soc.*, **1983**, 1539, 105.

[21] J. M. Birchall, R. N. Haszeldine, J. O. Morley, *J. Chem. Soc. (C),* **1970**, 2667.

[22] M. Gouterman, F. P. Schwarz, P. D. Smith, D. Dolphin, *J. Chem. Phys.*, **1973**, 59, 676.

[23] M. Handa, A. Suzuki, S. Shoji, K. Kasuga, K. Sogabe, *In. Chimica Acta*, **1995**, 230, 41.

[24] J. M. Birchall, R. N. Haszeldine, J. O. Morley, *J. Chem. Soc. (C),* **1970**, 456.

5. Preparation and characterization of films of phthalocyanines embedded in different polymers

Phthalocyanines (Pcs) are very promising materials for optical liming as described in Chapter 3rd. However for practical application it is essential to investigate the optical limiting of phthalocyanine complexes in solid state. In this chapter solid-state films of various phthalocyanine compounds embedded in different polymers on glass or sapphire substrates will be discussed. Their preparation via spin casting and drop casting techniques will be described. Films were prepared on glass slides and sapphire substrates. Both substrates are enough resistant to heat through laser irradiation. Furthermore, fabricated single-layer and multi-layer films were prepared. For practical application in optical limiting devices the thickness of films should be very high in order to reduce the harmful effects associated with the overheating of the sample by irradiation with the intense laser light. Thus, optically homogenous multi-layer films till 7-layer possessing deep glassy blue or green appearance were obtained.

The solid-state samples were characterized by their absorption spectra and thicknesses. Absorption spectra are very important to see whether the phthalocyanines in the films are aggregated or not. In the case of aggregation, the Q-band of monomolecular distributed Pcs at ~ 670 nm shifts clearly to shorter wavelength at ~ 620 - 640 nm. Monomolecular distributed Pcs in the films are crucial for their good optical limiting properties (Chapter 8.4).

In the study, there are designations that will be utilized to abbreviate names of multi-layer films of phthalocyanines in polymers. For instance, **5PVC4** determines a 4-layer film of phthalocyanine **5** in PVC *i.e.* **5** is a number ascribed to a phthalocyanine, **PVC** is a polymer, and **4** represents number of layers of film.

5.1 Methods of preparation of phthalocyanine films

Films of phthalocyanine were prepared applying two methods: spin coating and drop coating. Both drop and spin coating techniques require satisfactorily soluble compounds.

- The spin coating is plain and successful method of obtaining a relatively thin and uniform film on a given substrate. The selected well soluble phthalocyanines and following polymers: poly (methylmethacrylate) (PMMA), poly(vinylchloride) (PVC) and poly(styrene) (PS) were used to produce thin films (see Chapter 7.3). The solvent should be volatile, providing for its simultaneous evaporation. Thus, the

phthalocyanines were dissolved in toluene, chloroform ($CHCl_3$) or in tetrahydrofuran (THF). Methylcyclohexanone was used as a solvent for preparation all polymer solutions. A range of concentrations of phthalocyanine in polymer solution was from 1×10^{-3} till 5×10^{-3} mol L^{-1}. Approximately 0.3 mL of the polymer-phthalocyanine composite was dropped on the glass substrate. The substrate was then rotated with speed of 3000 rpm for 5 minutes in order to spread the fluid by centrifugal force (**Figure 5.1**). Polymer phthalocyanine films were deposited by spin coating polymer solutions on the glass or sapphire substrate as shown in **Figure 5.1**. The uniform and thin film obtained by spin coating can be further processed. This means preparation of multilayer films by a sequential deposition and spin casting process. The films were dried at high temperature (100 ^{0}C) for 1 hour between successive layers of film preparation. Films till 7 layers were obtained.

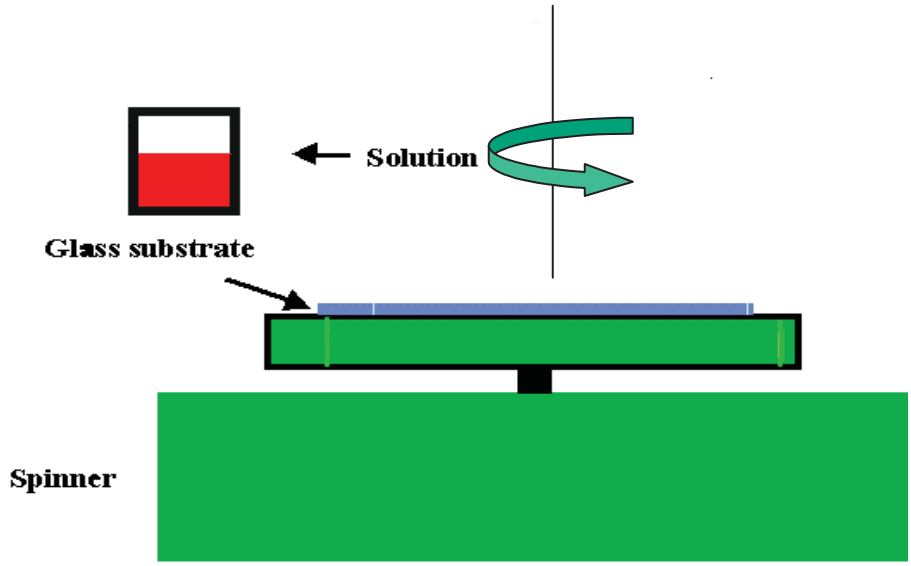

Figure 5.1 Spin coating technique.

- The drop casting procedure is straightforward method applying stationary deposition of solution onto sapphire substrate (**Figure 5.2**). 3 mL of the polymer-phthalocyanine solution containing 1×10^{-3} mol L^{-1} of a Pc was poured onto a sapphire substrate using a syringe. The majority of the organic solvent in the cast films is slowly evaporated at room temperature over 2 days and additionally films were dried at 100 ^{0}C for around 5 hours.

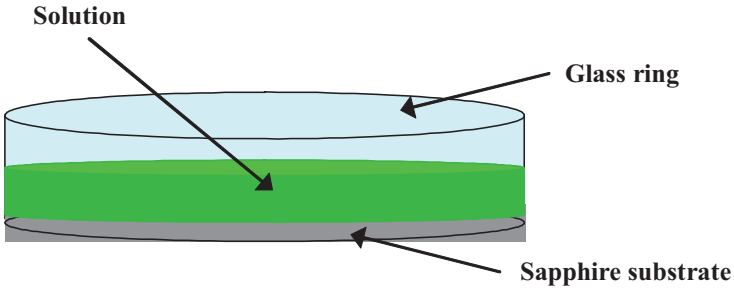

Figure 5.2 Drop coating method.

The advantage of drop casting is one-step procedure where films achieve thickness (*d*) up to several hundred μm. The cast films were prepared on sapphire substrates.

5.2 Characterization of phthalocyanine films prepared by spin casting method

5.2.1 Films of tetra-substituted phthalocyanines

The following tetrasubstituted phthalocyanines **(nPhO)$_4$PcSnCl$_2$** (**5**), **(nPhO)$_4$PcSnCl$_2$** (**6**), **(fPhO)$_4$PcGeCl$_2$** (**7**), **(*β*NO$_2$)$_4$PcGe(*t*Bu$_2$P)$_2$** (**23**), **(*t*-Bu)$_4$PcInCl** (**25**) [1], **(PhO)$_4$PcH$_2$** (**26**) [2], **(*t*-BuPhO)$_4$PcH$_2$** (**27**) [2] were used for fabrication of spin coated films. Phthalocyanines used for films formation differ in size, the central metal, and type of peripheral substituent groups. The relationship between the absorption spectra of phthalocyanines in solution and film, and between different films of phthalocyanines will be discussed. Clear homogeneously colored films of **(nPhO)$_4$PcSnCl$_2$** (**5**), **(fPhO)$_4$PcSnCl$_2$** (**6**), **(fPhO)$_4$PcGeCl$_2$** (**7**), **(*β*NO$_2$)$_4$PcGe(*t*Bu$_2$P)$_2$** (**23**), **(*t*-Bu)$_4$PcInCl** (**25**), **(PhO)$_4$PcH$_2$** (**26**), **(*t*-BuPhO)$_4$PcH$_2$** (**27**) in polymers were obtained by spin coating on glass substrates. Mono-layer films were prepared from methylcyclohexanone solution containing appropriate phthalocyanine and polymer. Prior to this, the composite solution was gently stirred in order to get homogeneous solution. Multi-layer films were obtained by repeated spin coating on the previously prepared and dried films. Multi-layer films with 3 to 6 layers in PMMA and films with 4 to 7 layers in PVC were obtained from methylcyclohexanone solutions containing the following phthalocyanines **(nPhO)$_4$PcSnCl$_2$** (**5**), **(fPhO)$_4$PcSnCl$_2$** (**6**), **(fPhO)$_4$PcGeCl$_2$** (**7**), **(*β*NO$_2$)$_4$PcGe(*t*Bu$_2$P)$_2$** (**23**), **(*t*-Bu)$_4$PcInCl** (**25**) and adequate polymer. The double layer (two-side) films were fabricated from metal-free phthalocyanines **(PhO)$_4$PcH$_2$** (**26**) and **(*t*-BuPhO)$_4$PcH$_2$** (**27**) on sapphire substrates. In this case the polymer-phthalocyanine composite was deposited on the reverse side under the same conditions as mentioned above. The 2,9,16,23-

tetraphenoxyphthalocyanine (**26**) was embedded in PVC to obtain film with 3 layers and 3 layer of film in PS was prepared from 2,9,16,23-tetrakis(4-*tert*-butylphenoxy)phthalocyanine (**27**) as well.

Figure 5.3 presents the absorption spectra of **(nPhO)$_4$PcSnCl$_2$** (**5**) with *p*-nitrophenoxy and **(fPhO)$_4$PcSnCl$_2$** (**6**), **(fPhO)$_4$PcGeCl$_2$** (**7**) with *p*-formylphenoxy peripheral substituents in multi-layer films in PMMA compared to that of the corresponding spectra in chloroform solutions.

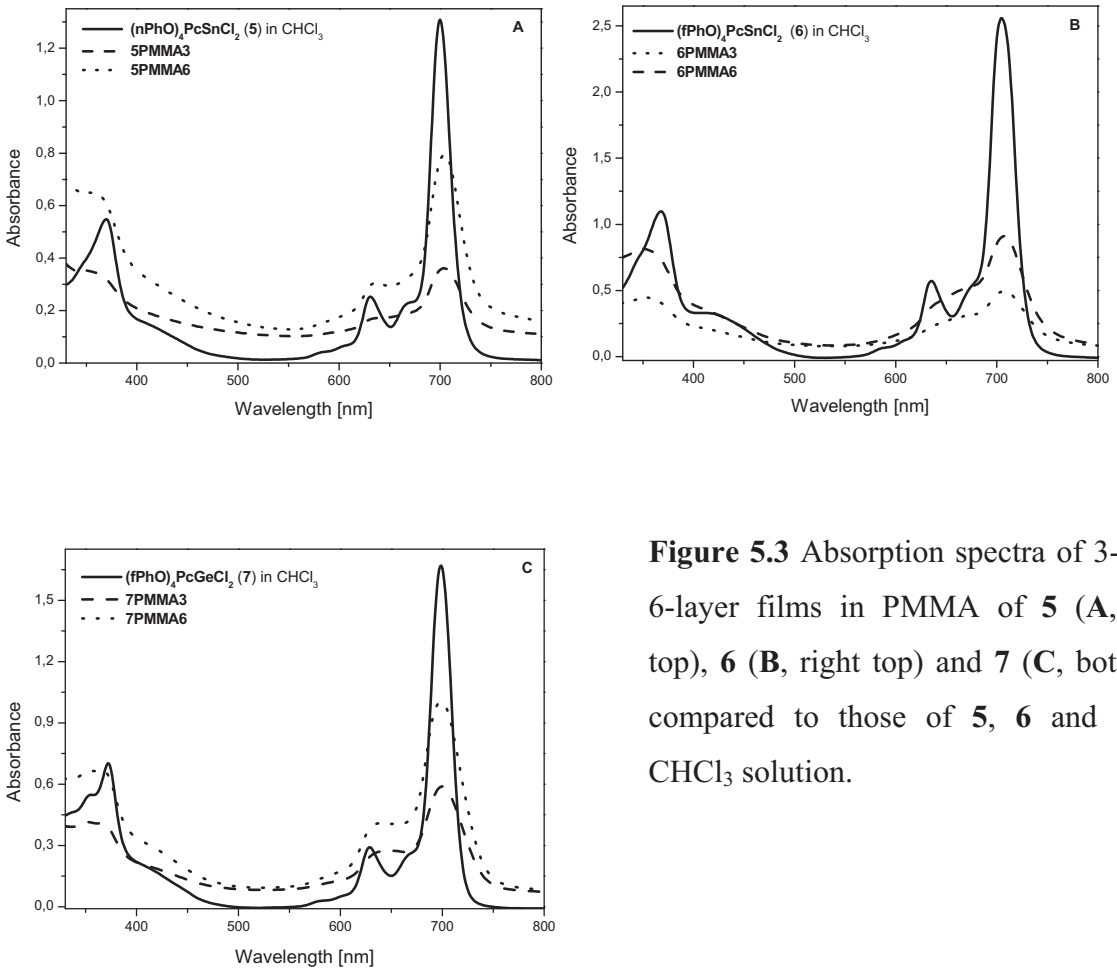

Figure 5.3 Absorption spectra of 3- and 6-layer films in PMMA of **5** (**A**, left top), **6** (**B**, right top) and **7** (**C**, bottom) compared to those of **5**, **6** and **7** in $CHCl_3$ solution.

As shown by the spectra of films in PMMA: **5PMMA3**, **5PMMA6**, **6PMMA3** and **6PMMA6** films are only slightly red-shifted (~ 5 nm in case of **5** and **6**) in comparison with spectra of **5** and **6** in chloroform solutions (**Table 5.1**, **Figure 5.3 A** and **B**). However, maxima of absorption of **(fPhO)$_4$PcGeCl$_2$** (**7**) films in PMMA (**7PMMA3** and **7PMMA6**) are same as in chloroform solution (**Table 5.1**, **Figure 5.3 C**). Interestingly, comparison of absorption spectra of multi-layer PMMA films of phthalocyanines with the same peripheral

substituents *i.e p*-formylphenoxy and different central metal, **(fPhO)$_4$PcSnCl$_2$** (**6**) and **(fPhO)$_4$PcGeCl$_2$** (**7**), results in broader and slightly red-shifted Q-band of PMMA films of **6** than those of **7**. The observed shift of the Q-band of films of **6** containing Ge as central metal compared to films of **7** with Sn as central atom indicates that heavier cental atom *i.e* Sn complexed in Pc is more effective in suppressing aggregation.

Table 5.1 UV/Vis data of tetra-substituted phthalocyanines in $CHCl_3$ and in solid-state.

Compound	λ_{max} [nm] $CHCl_3$		Films in PMMA			Films in PVC		
	Q-band	Soret band	No of layers	Q-band	Soret band	No of layers	Q-band	Soret band
(nPhO)$_4$PcSnCl$_2$ (**5**)	700, 631	370	3	705, 634	360	4	708, 637	363
			6	705, 634	360	7	708, 637	363
(fPhO)$_4$PcSnCl$_2$ (**6**)	704, 634	368	3	708, 651	352	4	710, 640	364
			6	708, 651	352	7	710, 640	364
(fPhO)$_4$PcGeCl$_2$ (**7**)	699, 629	372	3	699, 633	367	4	702, 632	370
			6	699, 633	367	7	702, 632	370
(βNO$_2$)$_4$PcGe(tBu$_2$P)$_2$ (**23**)	687, 621	354	3	713, 658	352	4	695	347
			6	707	352	7	693	347
(t-Bu)$_4$PcInCl (**25**)	699, 622	358	3	693, 626	360	4	702, 632	369
			6	694, 626	360	7	701, 632	369

The absorption spectra of mono-layer till 6-layer PMMA films of **5** (**Figure 5.4 A**, top), **6** (**Figure 5.4 B**, middle) and **7** (**Figure 5.4 C**, bottom) are presented in **Figure 5.4**. The absorption spectra of multi-layer films of **(nPhO)$_4$PcSnCl$_2$** (**5**) and **(fPhO)$_4$PcGeCl$_2$** (**7**) show a Q-band in successive films similar to those in chloroform solutions, though a wing beyond 340 nm appears in case of films with compound **5**.

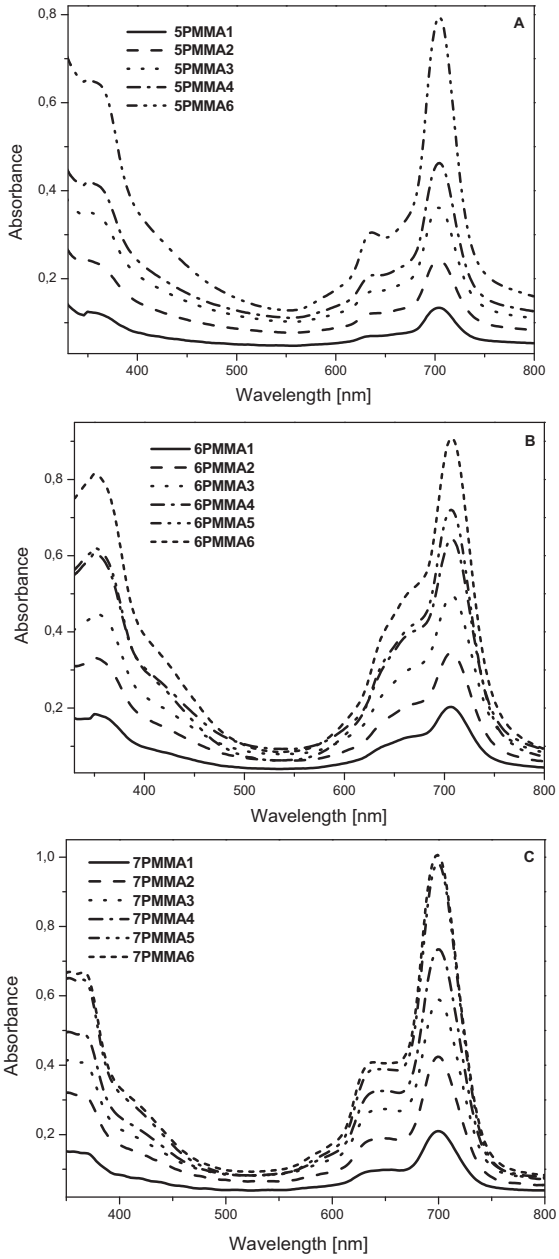

Figure 5.4 Absorption spectra of multi-layer **(nPhO)$_4$PcSnCl$_2$** (**5**) (**A**, top) **(fPhO)$_4$PcSnCl$_2$** (**6**) (**B**, middle) and **(fPhO)$_4$PcGeCl$_2$** (**7**) (**C**, bottom) films in PMMA.

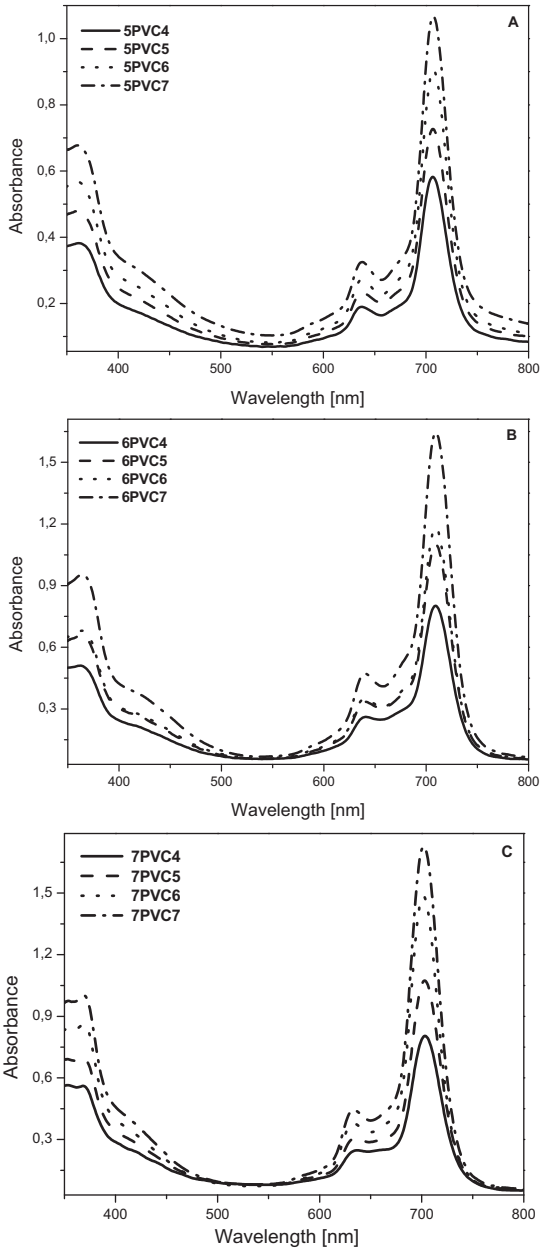

Figure 5.5 Absorption spectra of multi-layer **(nPhO)$_4$PcSnCl$_2$** (**5**) (A, top) **(fPhO)$_4$PcSnCl$_2$** (**6**) (B, middle) and **(fPhO)$_4$PcGeCl$_2$** (**7**) (C, bottom) films in PVC.

When the films are made of **(fPhO)$_4$PcSnCl$_2$** (**6**), the Q-bands are slightly broader and the gentle slope of the shorter wavelength of Q-band in absorption spectra of films appears in

comparison with the Q-band of **$(fPhO)_4PcSnCl_2$** (**6**) in $CHCl_3$ solution. This issue is observed in each multi-layer PMMA films of **6** and it does not change with increasing thickness of films. Qualitatively, the films show no obvious spectral changes at over range of concentration of doped phthalocyanines. This indicates that the behavior of **6** in PMMA films can be mainly caused by influence of a polar environment of a host lattice. Moreover, higher amount of **6** in 5- or 6-layer films compared to 1- or 3-layer films in PMMA does not affect plainly on Q-band shapes.

Figure 5.4 and **Figure 5.5** demonstrate nicely that the absorbance of **$(nPhO)_4PcSnCl_2$** (**5**), **$(fPhO)_4PcSnCl_2$** (**6**) and **$(fPhO)_4PcGeCl_2$** (**7**) in the PMMA and PVC films increases proportional and continuously with increasing film thickness. The considerable increase in layers (from 1 to 6 for PMMA films and 1 till 7 layers for PVC films) of films of compounds **$(nPhO)_4PcSnCl_2$** (**5**), **$(fPhO)_4PcSnCl_2$** (**6**) and **$(fPhO)_4PcGeCl_2$** (**7**) does not cause any evident shifts of Q-band in absorption spectra of each films between mono-layer and multi-layer polymeric films (**Figure 5.4** and **5.5**). This indicates that the bulky *p*-formylphenoxy and *p*-nitrophenoxy peripheral groups successfully suppress molecular aggregation, even at high concentration of **5**, **6** and **7** in films.

The films of **5**, **6** and **7** produced in PMMA on glass substrate are green colored. It can be satisfactorily seen in **Figure 5.6** that with increasing thickness of films the color of films becomes deeper green. The thickness (*d*) of the films (**Table 5.2**), measured by a Dektak, increases linearly, *i.e.* the thickness of 3-layer film is approximately half the thickness of the 6-layer film.

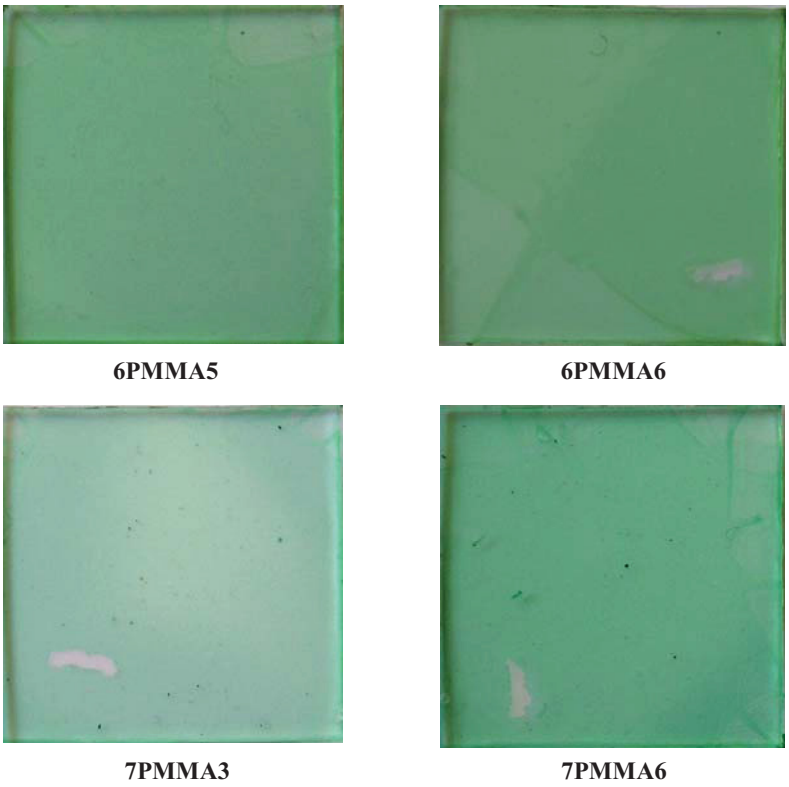

Figure 5.6 Photos of multi-layer films of **6** and **7** in PMMA.

Table 5.2 Thickness (*d*) of phthalocyanine films in polymers.

Solid-state sample	Films in PMMA		Solid-state sample	Films in PVC	
	No of layers	*d* [μm]		No of layers	*d* [μm]
5PMMA3	3	0.9	**5PVC4**	4	0.9
5PMMA6	6	1.8	**5PVC7**	7	1.8
6PMMA3	3	1.0	**6PVC4**	4	1.0
6PMMA6	6	2.3	**6PVC7**	7	2.3
7PMMA3	3	1.0	**7PVC4**	4	1.0
7PMMA6	6	1.9	**7PVC7**	7	1.9
23PMMA3	3	0.8	**23PVC4**	4	0.8
23PMMA6	6	1.5	**23PVC7**	7	1.5
25PMMA3	3	0.9	**25PVC4**	4	0.8
25PMMA6	6	1.9	**25PVC7**	7	1.4

Figure 5.7 shows electronic absorption spectra of films of **(nPhO)$_4$PcSnCl$_2$** (**5**) and **(fPhO)$_4$PcSnCl$_2$** (**6**) in PVC in comparison with related spectra of **5** and **6** in solution. The absorption spectra of **5** with *p*-nitrophenoxy peripheral substituents in PVC films are slightly more bathochromic shifted (~ 8 nm) in comparison with spectrum of **5** in solution than **6** and **7** with *p*-formylphenoxy peripheral groups (**Figure 5.7 B** and **5.8**) in PVC films in comparison with spectra of **6** and **7** in solutions. For both compounds, **(fPhO)$_4$PcSnCl$_2$** (**6**) and **(fPhO)$_4$PcGeCl$_2$** (**7**) with *p*-formylphenoxy peripheral substituents (**Figure 5.7 B** and **5.8**), the absorption spectra of films in PVC appear at slightly longer wavelength (~ 4 nm) than that of **6** and **7** in chloroform solution. Absorption spectra in transmission of the spin coated films of **5**, **6** and **7** in PVC show the Q-band at ~ 708, 710 and 702 nm, respectively, which is characteristic for monomolecular distributed phthalocyanines as in solution (**Figure 5.7** and **5.8**).

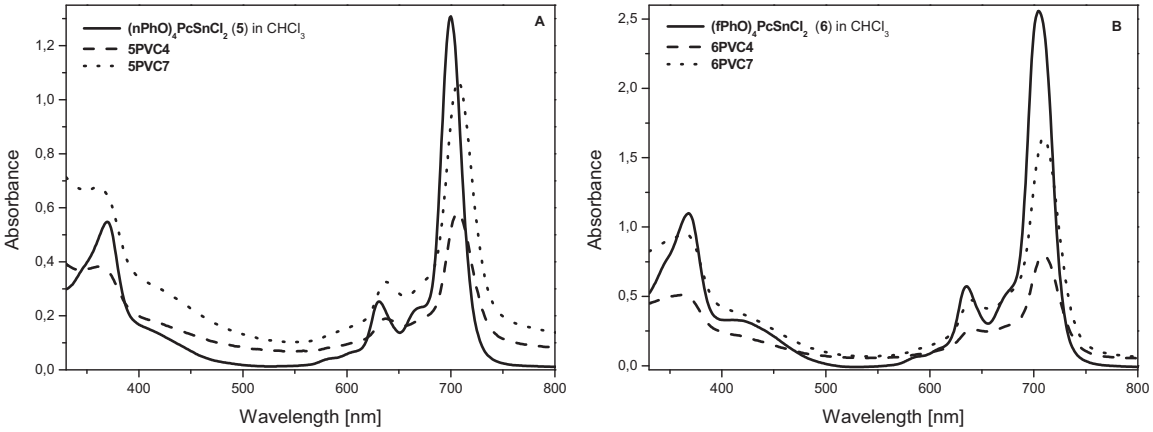

Figure 5.7 Absorption spectra of multi-layer **(nPhO)$_4$PcSnCl$_2$** (**5**) (**A**, left) and **(fPhO)$_4$PcSnCl$_2$** (**6**) (**B**, right) films in PVC, compared to those of **5** and **6** in $CHCl_3$ solution.

The position of Soret band of **5**, **6** and **7** in PVC films resembles the Soret band adequate to spectra in solution whereas in PMMA films the position of Soret band is shifted by ~ 10 nm to the shorter wavelength in comparison with solution spectra.

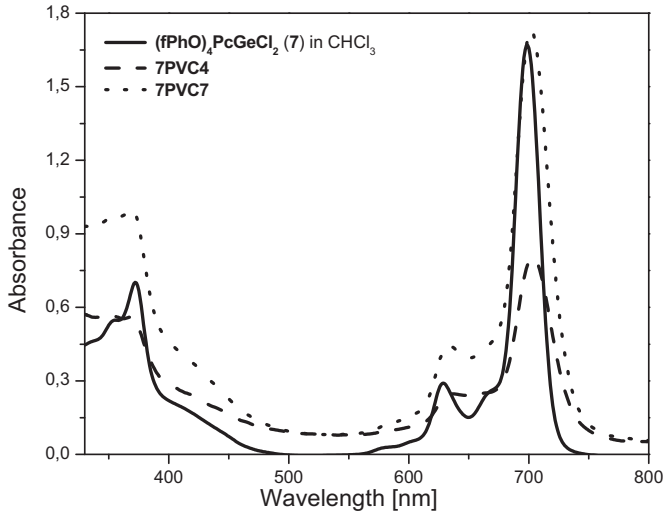

Figure 5.8 Comparison of absorption spectra of **$(fPhO)_4PcGeCl_2$** (**7**) in multi-layer PVC films and in $CHCl_3$ solution.

Qualitatively, this spectral evidence shows that compounds **5**, **6** and **7** in PVC films do not exhibit tendency to aggregate even in thick films *i.e.* 7-layer films (**Figure 5.5**). As shown in **Figure 5.5**, the spectra of **5**, **6** and **7** in PVC films represent phthalocyanines in the non-aggregated or "monomeric" state. Although, the absorption spectra of PMMA films of compounds **5**, **6** and **7** are slightly broader than those of PVC films.

The films of **5**, **6** and **7** in PVC possess green color and good uniformity without any cracks (**Figure 5.9**). The thicknesses of films range from 0.9 μm in case of 4-layer films in PVC to 2.3 μm for 7-layer films (**Table 5.2**).

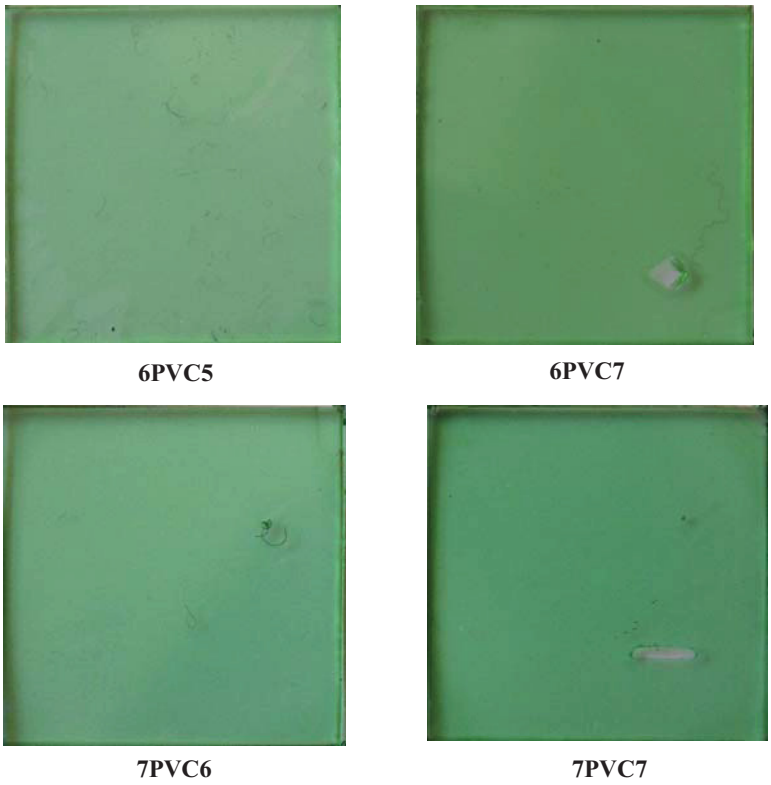

Figure 5.9 Photos of multi-layer thin films of **6** and **7** in PVC.

Absorption spectra of multi-layer films of tetra-substituted phthalocyanines, **(nPhO)$_4$PcSnCl$_2$** (**5**), **(fPhO)$_4$PcSnCl$_2$** (**6**) and **(fPhO)$_4$PcGeCl$_2$** (**7**) show the Q-band which is characteristic for a monomolecular distributed phthalocyanine, suggesting that bulky peripheral substituents and two axial chlorine ligands successfully prevent cofacial aggregation. Moreover, the shift of the Q-band in PVC films to the red region is slightly greater than in adequate PMMA films (**Table 5.1**). The absorption spectra of films in PMMA show slightly more prominent spectral changes than in PVC films what can be caused by influence of an environment of a host lattice but the vibrational structure of the Q-bands is remained.

Figure 5.10 shows spectra of compound **(*β*NO$_2$)$_4$PcGe(*t*Bu$_2$P)$_2$** (**23**), having bulky axial groups, di(*tert*-butyl)phenoxy, in 6-layer PMMA (**23PMMA6**) and 7-layer PVC (**23PVC7**) films and, for comparison, the spectrum of **23** in chloroform solution. For **23PVC7**, the Q-band is broader and shifts to longer wavelength, but to a lesser extent than for **23PMMA6**. The absorption spectra of the films in PVC (**Figure 5.11 A**) differ from the corresponding spectrum of **23** in solution, suggesting that aggregation is not enough suppressed by two bulky axial ligands (di(*tert*-butyl)phenoxy). The main maximum in all multi-layer PVC films is only slightly red-shifted by ~ 5 nm against Q-band in chloroform solution. In each spectrum of PVC films of **23** the spectral features around Q-band are smoothed out and a shoulder at ~

620 nm appears, suggesting that some part of phthalocyanine exists in an aggregated state. Therefore, the Soret band position of **23** in films is essentially comparable to that in solution. The thickness of the films was estimated to be 0.8 μm for **23PVC4** and 1.5 μm for **23PVC7**. (**Table 5.2**).

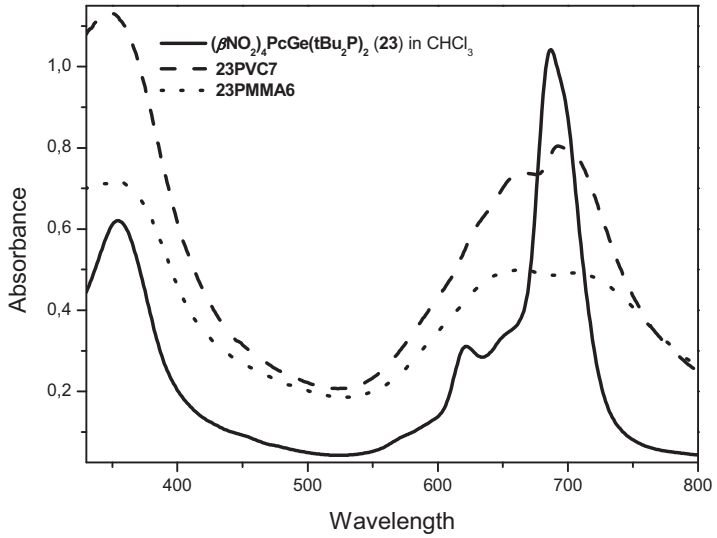

Figure 5.10 Absorption spectra of **(βNO$_2$)$_4$PcGe(*t*Bu$_2$P)$_2$** (**23**) in $CHCl_3$ solution and in PVC and PMMA films.

Absorption spectra of **23** in PMMA films (**Figure 5.10** and **5.11 B**), contrary to spectra of **23** in PVC films, display a high aggregation. The electronic absorption spectra of PMMA films demonstrate the split Q-band absorption at 660 and 707 nm. The similar type of behavior in film has been observed for a cast film prepared from 2,3-tetraquinoxalinotetraazaporphyrinatozinc onto ITO (indium tin oxide) by Yanagi *et al.* [3]. The authors concluded that it could be caused by a columnar stacking structure similar to that found in β-crystals. This phenomenon does not take place when PVC is used as polymer for preparation films of **23**.

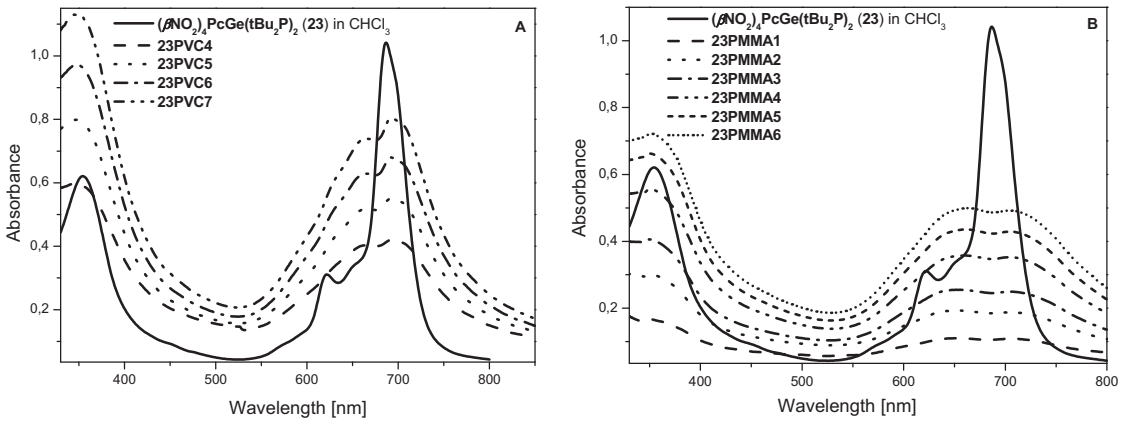

Figure 5.11 Absorption spectra of **(βNO$_2$)$_4$PcGe(tBu$_2$P)$_2$** (**23**) in PVC (**A**) and in PMMA (**B**) films in comparison with **23** in $CHCl_3$ solution.

Figure 5.12 shows the spectra of chloroindium(III) 2,9,16,23-tetrakis(*tert*-butyl)phthalocyanine (**25**) [1] in PMMA and PVC thin films. The absorption spectra of films in PVC as well as in PMMA show no sign of intermolecular aggregation even at high amount of **25** in multi-layer films *i.e.* in **25PVC7** and **25PMMA6**. The Q-band is slightly red-shifted by ~ 3 nm in PVC films, in PMMA films the Q-band appears at shorter wavelength (shift ~ 6 nm), in comparison with **25** in chloroform solution. Moreover, the Soret band in PMMA films is unchanged whereas in PVC films is red-shifted by ~ 10 nm in relation to spectrum of **25** in solution. The vibrational structure of Q-band is nicely retained and its position does not change with the increasing in layers of films.

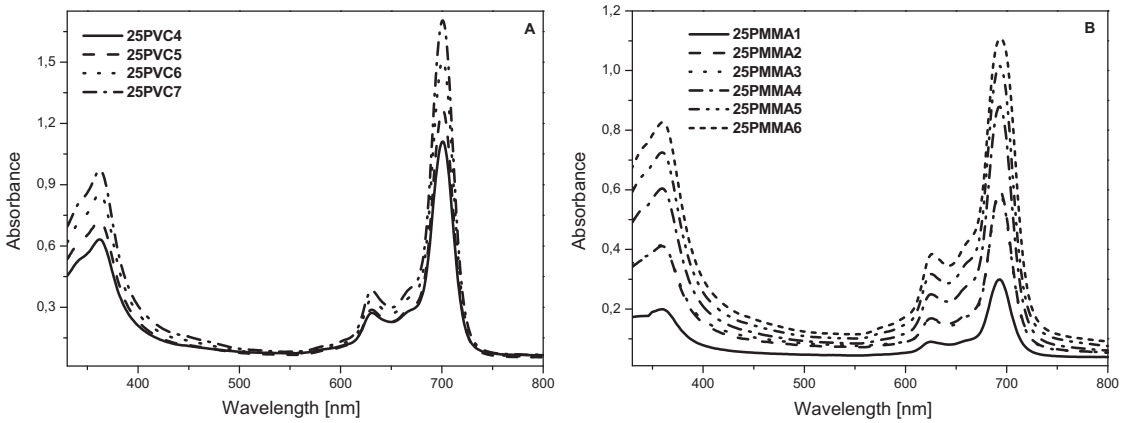

Figure 5.12 Absorption spectra of (**t-Bu)$_4$PcInCl** (**25**) in PVC (**A**) and PMMA (**B**) films.

Spin coated film of related compound, *p*-(trifluoromethyl)phenylindium(III) tetrakis(*tert*-butyl)phthalocyanine (**(*t*-Bu)$_4$PcIn(*p*-TMP)**) has been prepared [4]. The absorption spectrum of **(*t*-Bu)$_4$PcIn(*p*-TMP)** in film is broader and Q-band is slightly red-shifted relative to chloroform solution. The spectrum of film of **(*t*-Bu)$_4$PcIn(*p*-TMP)** is broader than spectra of **25** in PMMA and PVC films. Compound **25** produced uniform greenish, transparent (**Figure 5.13**) films with thicknesses from 0.8 to 1.9 μm (**Table 5.2**).

25PMMA4 **25PVC7**

Figure 5.13 Photos of PVC and PMMA films of **25**.

Spin coated films of **(PhO)$_4$PcH$_2$** (**26**) and **(*t*-BuPhO)$_4$PcH$_2$** (**27**) were prepared on two sides of sapphire windows. In both cases, 3 layers of films were prepared, 2 layers on one side and 1 layer on reverse side of sapphire substrate. The film of 2,9,16,23-tetraphenoxyphthalocyanine (**26**) was obtained in PVC whereas the film of 2,9,16,23-tetrakis(4-*tert*-butylphenoxy)phthalocyanine (**27**) in PS polymer. In both cases metal-free phthalocyanines **26** and **27** yielded less rough films than previously discussed films of metallated tetra-substituted phthalocyanines. **Figure 5.14** depicts absorption spectra for solutions and films of **26** and **27**. The spectral features of both phthalocyanine films, **26PVC3** and **27PS3**, demonstrate noteworthy changes relative to corresponding spectra in solutions.

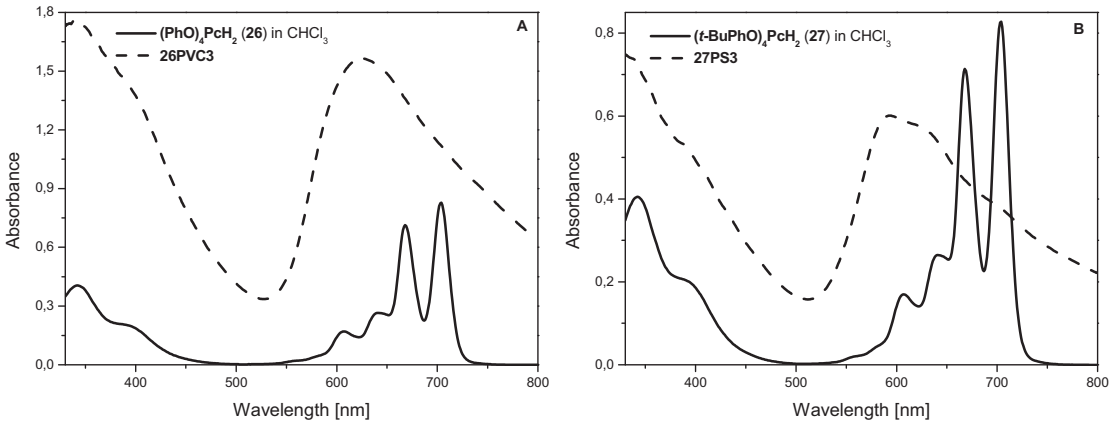

Figure 5.14 Absorption spectra of **$(PhO)_4PcH_2$** (**26**) in $CHCl_3$ and in PVC film (**A**). Spectra of **$(t\text{-}BuPhO)_4PcH_2$** (**27**) in $CHCl_3$ and in PS film (**B**).

The Q-band of **26** in film (**Figure 5.14 A**) broadens and shifts to a shorter wavelength. For **26** in PVC film, the Q-band vanished and new broad band appears at ~ 620 nm (**Table 5.3**). Spin coated film of **27** in PS (**Figure 5.14 B**) also displays blue-shifted Q-band but remarkably bigger than in film of **26**. Interestingly, the concentration of **26** in polymer solution taking for preparation of film was higher than that of **27**, determined to be 5×10^{-3} for **26** and 1×10^{-3} mol L^{-1} for **27**, what is noticeable in decrease in absorption (**Figure 5.14**). The absorption spectrum of **27PS3** shows broad Q-band which is widely blue-shifted by ~ 100 nm (**Table 5.3**) in comparison with Q-band of **27** in chloroform solution. The higher aggregation and bigger shift of Q-band in film of **27** can be explained by less polar polymer *i.e.* poly(styrene) which causes appearance of phthalocyanines in higher aggregated state in film. The changes of the absorption maximum observed in polymeric films of **26** and **27** can be explained by cofacial arrangement of molecules as dimmers or higher aggregates [5].

Table 5.3 Comparison of UV/Vis data of compounds **26** and **27** in $CHCl_3$ and in solid-state.

Compound	λ_{max} [nm] $CHCl_3$		Film in PS			Film in PVC		
	Q-band	Soret band	No of layers	Q-band	Soret band	No of layers	Q-band	Soret band
$(PhO)_4PcH_2$ (26)	667, 702	348				3	626	339
$(t\text{-}BuPhO)_4PcH_2$ (27)	668, 704	342	3	594				

The broad and blue-shifted Q-band was also observed in metal-free tetrakis(*tert*-butyl)phthalocyanines in the condensed state [6]. Spin coated films of metal-free tetra(2,6-di-*tert*-butyl-4-methylphenyl-oxy)phthalocyanine (**TTB_2MePcH_2**) show a blue shift of Q-band [7], suggesting formation of cofacial type of aggregation, likewise in films of **26** and **27**. The well-defined characteristic peaks, and no aggregation were noticed in case of solution spectrum of **TTB_2MePcH_2** [7], similarly to solution spectra of **26** and **27**.

5.2.2 Films of octa-substituted phthalocyanines

The following series of octabutoxy-substituted phthalocyanines **$(BuO)_8PcZn$** (**29**) [2, 8], **$(BuO)_8PcPb$** (**30**) [2, 8] and **$(BuO)_8PcCu$ (31)** [2, 8] were chosen for the film preparations. Films were prepared by spin coating method on sapphire substrates. In those cases, films were produced on both sides of sapphire substrates. The Q-bands position, thicknesses and used polymer for preparation double layer films are presented in **Table 5.4** and **5.5**.

Table 5.4 Characterization of metallated octabutoxy-substituted phthalocyanines in toluene solution and in solid-state.

Compound	λ_{max} [nm] toluene		Film in PMMA			Films in PVC			Film in PS		
	Q-band	Soret band	No of layers	Q-band	Soret band	No of layers	Q-band	Soret band	No of layers	Q-band	Soret band
$(BuO)_8PcZn$ (29)	678, 612	356				4	678	355			
$(BuO)_8PcZn$ (29)	678, 612	356							3	677, 629	342
$(BuO)_8PcPb$ (30)	714, 643	404				5	719, 647	405			
$(BuO)_8PcCu$ (31)	677, 609	345	7	615	337						

Figure 5.15 demonstrates the absorption spectra of compound **29** in PVC and in PS films relative to spectrum of **29** in diluted solution. **Figure 5.15 A** shows spectrum of **29PVC2** film which is prepared on both sides of sapphire, and afterwards **29PVC2** was covered by further two layers to produce the final **29PVC4** film. The electronic spectra of **29PVC2** and **29PVC4** are slightly broader than the solution spectrum of **29**, as expected, but position of Q-bands in films is same (in **29PVC2** and in **29PVC4** determined to be 678 nm). The Q- and Soret bands position of films are consistent with **29** dissolved in chloroform solution (**Table 5.4**). This implies that shape of Q-band of **29** even in thicker polymeric film, **29PVC4**, does not change considerably in comparison with its Q-band in film which possesses fewer layers, **29PVC2**.

This shows that **29** does not show aggregation tendency in PVC films and behaves as monomolecular distributed.

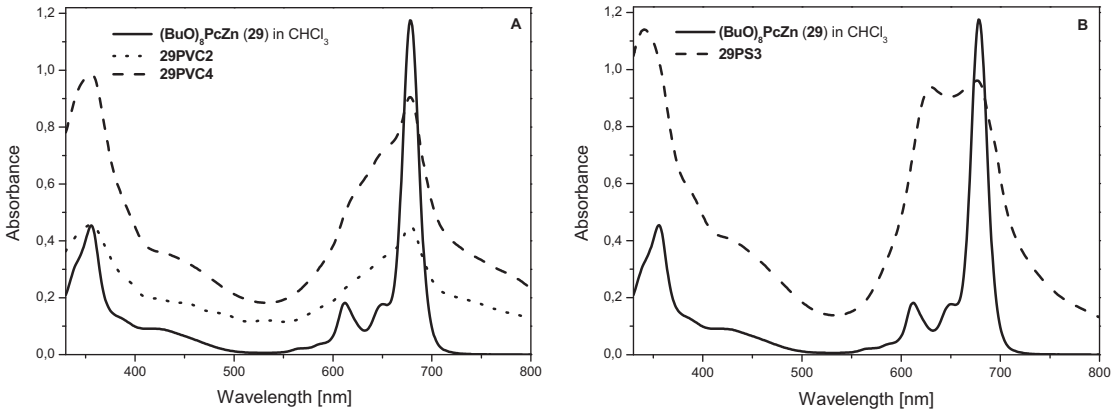

Figure 5.15 Absorption spectra of **29** in $CHCl_3$ and in PVC film (**A**) and PS film (**B**).

In contrast, when the film is made in PS (**Figure 5.15 B**), the Q-band broadens and its position is only slightly blue-shifted (~ 2 nm), whereas the slope of the shorter wavelength side of the Q-band appears. The shoulder exists at ~ 620 nm pointing out cofacial aggregation. Comparison of behavior of **29** in two different polymers indicates that compound **29** in less polar poly(styrene) exhibits tendency to form aggregates. The thickness of **29PVC4** and **29PS3** was determined to be 0.6 and 0.5 nm, respectively (**Table 5.5**).

Table 5.5 Thickness (*d*) and number of layers of double layer phthalocyanine films in polymers.

Compound	Solid-state sample	No of layers	*d* [μm]		
			one side	other side	total
$(BuO)_8$PcZn (29)	**29PS3**	3	0.3	0.3	0.6
$(BuO)_8$PcZn (29)	**29PVC4**	4	0.3	0.2	0.5
$(BuO)_8$PcPb (30)	**30PVC5**	5	0.4	0.3	0.7
$(BuO)_8$PcCu (31)	**31PMMA7**	7	0.6	0.3	0.9

The electronic spectrum of spin coated film with 5 layers of compound **30** in PVC prepared on both sides of sapphire, 3 layers on one and 2 on another, is presented in **Figure 5.16**. It is nicely seen that the shape of Q-band is distinctly similar to that of **30** in toluene solution.

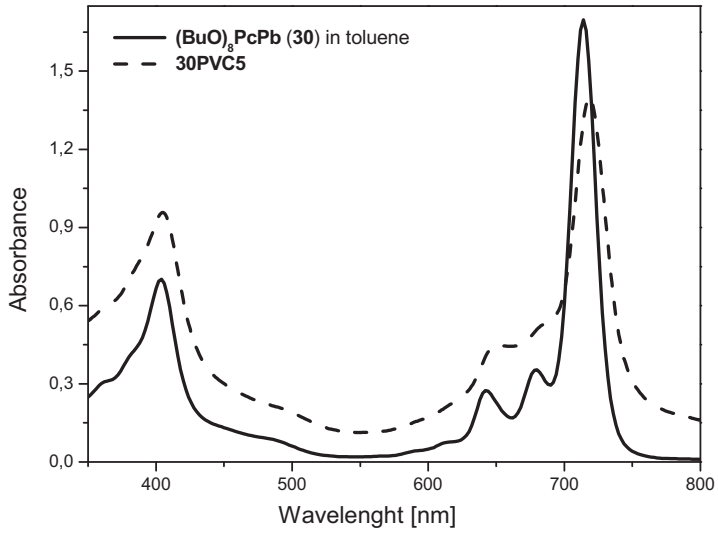

Figure 5.16 Absorption spectra of **30** in toluene and in **30PVC5** film.

The Q-band of **30PVC5** film is merely shifted by ~ 2 nm to red region whereas the Soret band has the same position in relation to spectrum of **30** in solution. This phenomenon firmly indicates that **(BuO)$_8$PcPb** (**30**) behaves non-aggregated in solid state. Interestingly, the film spectrum of **(BuO)$_8$PcZn** (**29**) in PVC (**29PVC4**) slightly differs in shape from spectrum of **30PVC5** in spite of possessing the same butoxy peripheral substituent, suggesting that the large ion Pb^{2+} which is displaced 0.4 Å from the plane of macrocycle and distorts the ring from planarity [9, 10] additionally prevents formation of aggregates. Flom *et al.* [11] prepared thin film of lead tetrakis(4-(3-aminophenoxy))phthalocyanine-butanediol-urethane copolymer with 5.9% by weight of Pc. The Q- and B-bands in the polymer are slightly broader than those in solution. Furthermore, the position of the Q- and B-bands resembles those observed in $CHCl_3$ solution of Pb tetrakis(cumylphenoxy)phthalocyanine [12]. The absorption spectrum of lead tetrakis(4-(3-aminophenoxy))phthalocyanine-butanediol- urethane copolymer is only slightly broader than this for solution that is comparable to distribution of compound **30** in PVC film and in solution. Spin coated film of Pb tetrakis(*tert*-butyl)phthalocyanine in PMMA on glass substrate was obtained [6], exhibiting the absorption spectrum broader and somewhat red-shifted in comparison with solution spectra.

The concentration of **$(BuO)_8$PcPb** (**30**) in the film was determined by comparing their optical absorption spectra in spin coated films with those measured in toluene solution at known concentrations (**Figure 5.17**). It is satisfactorily perceived that the absorption in dependence of the phthalocyanine **30** concentration in films grows linearly.

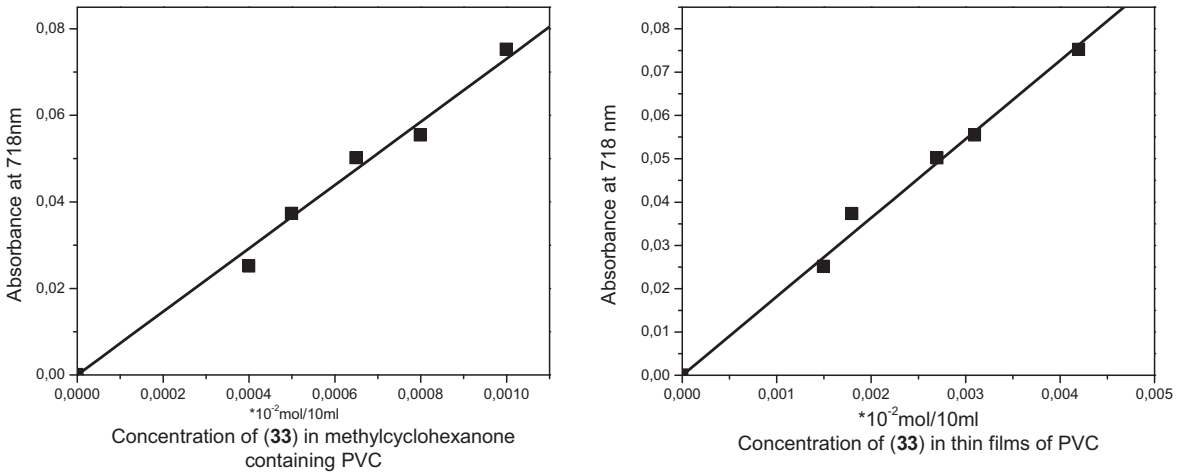

Figure 5.17 Concentration dependence of **30** in films.

Figure 5.18 presents the spectrum of **$(BuO)_8$PcCu** (**31**) in solution and its film in PMMA. The film consists of 3 layers laid on one side and 4 layers on reverse side of sapphire substrate and with total thickness determined to be 0.9 μm (**Table 5.5**). In case of film of compound **31** in PMMA, the absorption spectrum is dominated by aggregation. Shape of Q-band of **31PMMA7** is widely shifted to blue region. Change of the absorption maximum observed in polymeric film of **31** to ~ 620 nm can be explained by cofacial arrangement of Pc as dimmers [5]. The blue shift of Q-band has been observed for film of copper tetra(2,6-dimethylphenoxy)phthalocyanine [13] prepared on silver surface, suggesting also a cofacial arrangement of molecules.

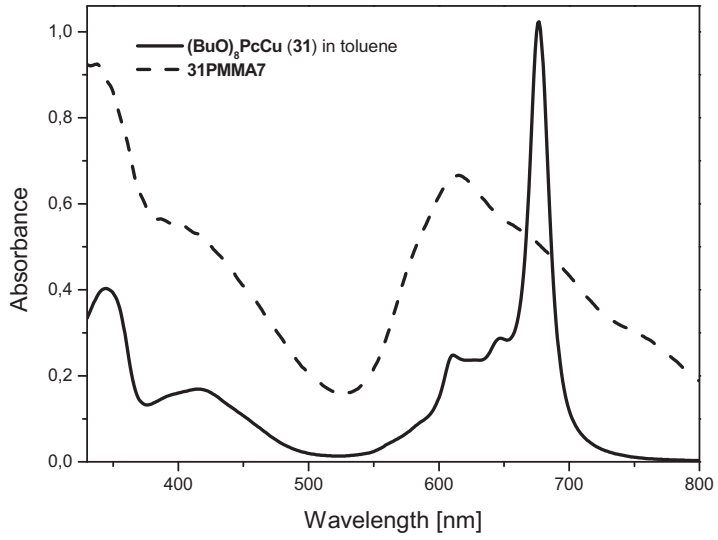

Figure 5.18 Absorption spectra of **31** in toluene and in PMMA film.

Furthermore, cast films of copper peripherally octasubstituted phthalocyanines bearing amide and ester groups, from $CHCl_3$ solution, depending on their thickness show red or blue shifts [14, 15]. Thin films exhibit a slightly red-shifted Q-band and thicker films show blue-shifted Q-bands in relation to the solution spectra.

5.2.3 Thin films of hexadeca-substituted phthalocyanines

Dichlorotin(IV) hexadecafluorophthalocyanine **$F_{16}PcSnCl_2$** (**16**) [16] and germanium and tin hexadecachlorophthalocyanine, **$Cl_{16}PcSn(tBu_2P)_2$** (**14**) and **$Cl_{16}PcGe(tBu_2P)_2$** (**15**) were used for spin coated film preparations. The series of hexadeca-substituted phthalocyanines, **14**, **15** and **16**, produced smooth uniform, and transparent films with deep glassy blue (**$F_{16}PcSnCl_2$** (**16**)) and green color (**$Cl_{16}PcSn(tBu_2P)_2$** (**14**) and **$Cl_{16}PcGe(tBu_2P)_2$** (**15**)). The compounds were deposited as spin coated films in PMMA as well as in PVC on glass substrates.

Table 5.6 Comparison of UV/Vis data of **14**, **15** and **16** in $CHCl_3$ solution and in solid-state.

Compound	λ_{max} [nm] $CHCl_3$		Films in PMMA			Films in PVC		
	Q-band	Soret band	No of layers	Q-band	Soret band	No of layers	Q-band	Soret band
$Cl_{16}PcSn(tBu_2P)_2$ (14)	737, 660	367	3	736, 681	365	4	738, 683	365
			6	736, 681	366	7	738, 686	366
$Cl_{16}PcGe(tBu_2P)_2$ (15)	726, 651	368	3	728, 660	367	4	732, 665	369
			6	728, 661	367	7	732, 665	370
$F_{16}PcSnCl_2$ (16)	708, 637	370	3	707, 666	359	4	712, 669	360
			6	708, 664	359	7	713, 669	360

Figure 5.19 demonstrates the absorption spectra of compound **$Cl_{16}PcSn(tBu_2P)_2$ (14)** in chloroform solution and its 7-layer film in PVC as well as 6-layer film in PMMA. As shown by the spectra in films, both films exhibit the position of Q- and Soret bands essentially similar relative to spectrum of **14** in chloroform solution.

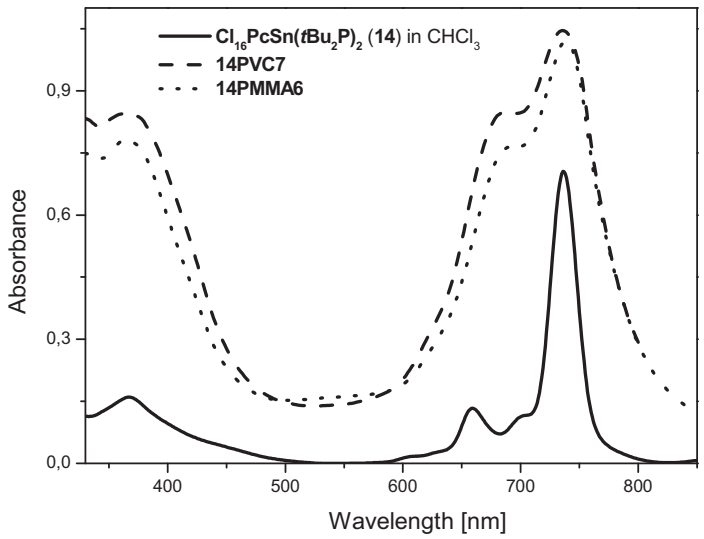

Figure 5.19 Absorption spectra of **$Cl_{16}PcSn(tBu_2P)_2$ (14)** in PMMA and in PVC films in comparison with spectrum of **14** in $CHCl_3$ solution.

The absorption spectra of films are slightly broader than that of solution, and the shoulder on the shorter wavelength side of the Q-band appears, suggesting that some part of compound **14** exists in aggregated state. Multi-layer films of **14** in PVC are relatively narrower and slightly more batochromic shifted than those in PMMA, indicating the influence of the host lattice.

As shown in **Figure 5.20 A** and **B**, with the increasing layers of films the significant increase in absorption can be seen in electronic spectra of films in PMMA as well as in PVC. Furthermore, the Q-band position of films does not change with the growth of their thickness. Besides, no meaningful changes of the shape of Q-bands can be seen from the comparison of 1-layer with 6-layer film in PMMA, and 4-layer with 7-layer film in PVC, respectively.

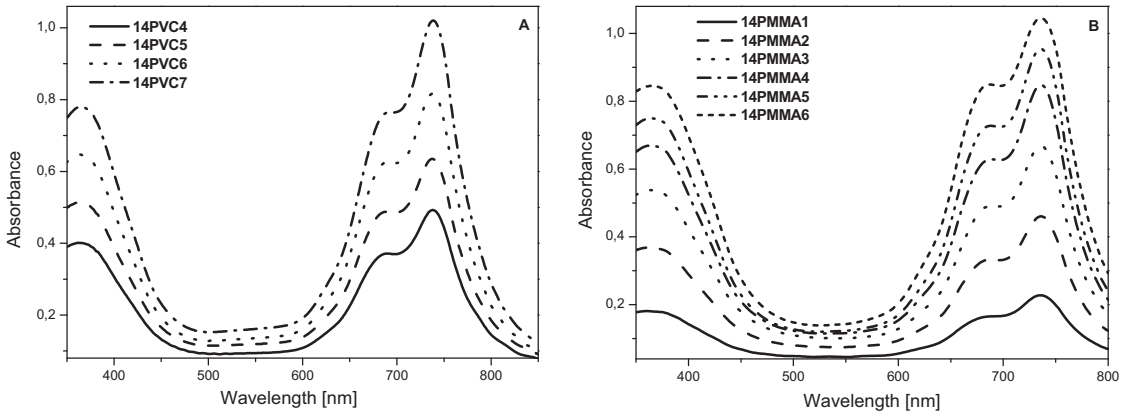

Figure 5.20 Absorption spectra of **14** in PVC (**A**) and in PMMA (**B**) films.

This phenomenon points out that even many layers of doped phthalocyanine does not influence remarkably on phthalocyanine-phthalocyanine interactions. The thicknesses of the films (**Table 5.7**) measured by Dektak, were determined to be 0.9, 2.0, 0.9 and 1.6 μm for **14PMMA3**, **14PMMA6**, **14PVC4** and **14PVC7**, respectively.

Table 5.7 Thickness (*d*) of metallated hexadecasubstituted phthalocyanine films in polymers.

Solid-state sample	Films in PMMA		Solid-state sample	Films in PVC	
	No of layers	*d* [μm]		No of layers	*d* [μm]
14PMMA3	3	0.9	**14PVC4**	4	0.9
14PMMA6	6	2.0	**14PVC7**	7	1.6
15PMMA3	3	0.9	**15PVC4**	4	0.8
15PMMA6	6	1.9	**15PVC7**	7	1.5
16PMMA3	3	0.8	**16PVC4**	4	0.9
16PMMA6	6	1.8	**16PVC7**	7	1.9

The absorption spectra of compound **$Cl_{16}PcGe(tBu_2P)_2$** (**15**) in chloroform solution and its **15PMMA6** and **15PVC7** films are presented in **Figure 5.21**. The spectrum of 7-layer film in PVC (**15PVC7**) essentially resembles the spectrum of **15** in solution while the spectrum of 6-layer film in PMMA (**15PMMA6**) is slightly broader than that of chloroform solution. Though, the maximum peak of Q-band of PMMA film (**15PMMA6**) appears almost at same wavelength like this of corresponding solution. The Q-band is slightly red-shifted by ~ 6 nm in case of **15PVC7** compared to the chloroform solution (**Table 5.6**). Moreover, the position of Soret bands of **15PMMA6** as well as **15PVC7** is unchanged in relation to the chloroform solution of **15**.

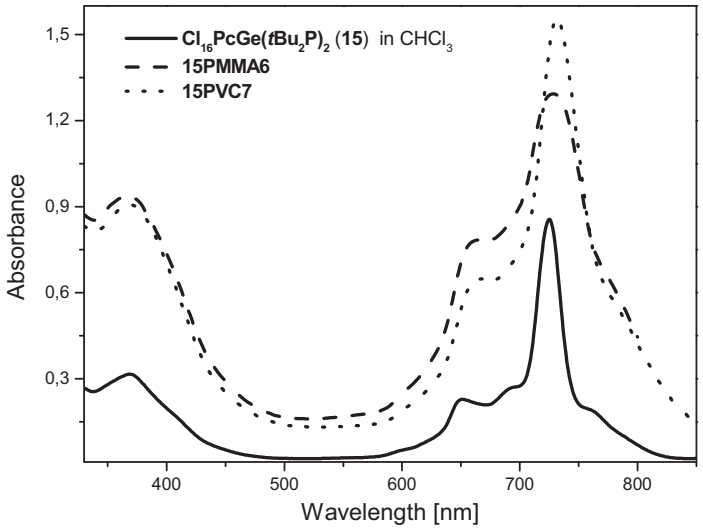

Figure 5.21 Absorption spectra of **$Cl_{16}PcGe(tBu_2P)_2$** (**15**) in PMMA and in PVC films in comparison with **15** in $CHCl_3$ solution.

Figure 5.22 satisfactorily demonstrates that the absorbance of **$Cl_{16}PcGe(tBu_2P)_2$** (**15**) either in PVC (**Figure 5.22 A**) or in PMMA (**Figure 5.22 B**) films increases continuously with increasing film thicknesses. Optically homogenous with deep green color films containing compound **15** in PMMA and PVC with a thickness from 0.8 till 1.9 μm (**Table 5.7**) were obtained.

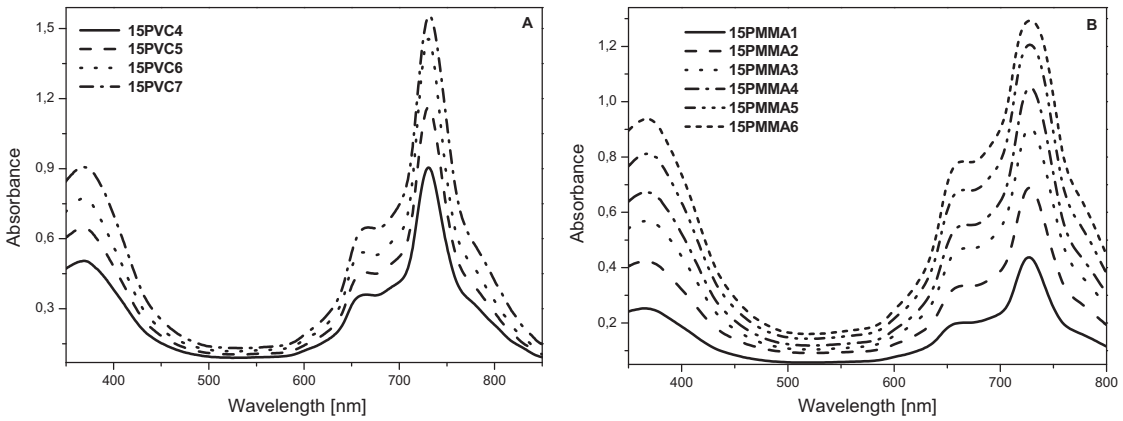

Figure 5.22 Absorption spectra of **$Cl_{16}PcGe(tBu_2P)_2$** (**15**) in PVC (**A**) and PMMA (**B**) films.

The presented phthalocyanines **14** and **15** possess small chlorine peripheral groups and bulky di(*tert*-butyl)phenoxy groups in axial positions. The absorption spectra of **14** and **15** in films show a slightly red-shifted or unchanged Q-band, indicating that the bulky axial groups successfully diminish cofacial arrangement of molecules. The bathochromic shift of the Q-band has been observed for spin coated films of hexadecasubstituted phthalocyanines, *p*-8OMe-np-8$C_{12}PcH_2$, *p*-8Me-np-8C_8OPcH_2, and *p*-[OCO]*c*C_6-np-$C_{12}PcH_2$ [17]. The absorption spectra of those films were almost same as in solution, only somewhat red-shifted and broadened [17].

Figure 5.23 presents the absorption spectra of dichlorotin(IV) hexadecafluorophthalocyanine (**16**) in chloroform solution and of spin coated 6-layer PMMA and 7-layer PVC films. Both films exhibit the absorption spectra slightly broader with the shoulder at ~ 670 nm (suggesting the existence some part of **$F_{16}PcSnCl_2$** (**16**) in aggregated state) compared to that of spectrum in solution. The position of the Q-band of **16PMMA6** film corresponds approximately to that of the compound **16** dissolved in chloroform. Furthermore, the Q-band of **16PVC7** is somewhat red-shifted by ~ 4 nm (**Table 5.7**) compared to the Q-band of **16** in chloroform solution.

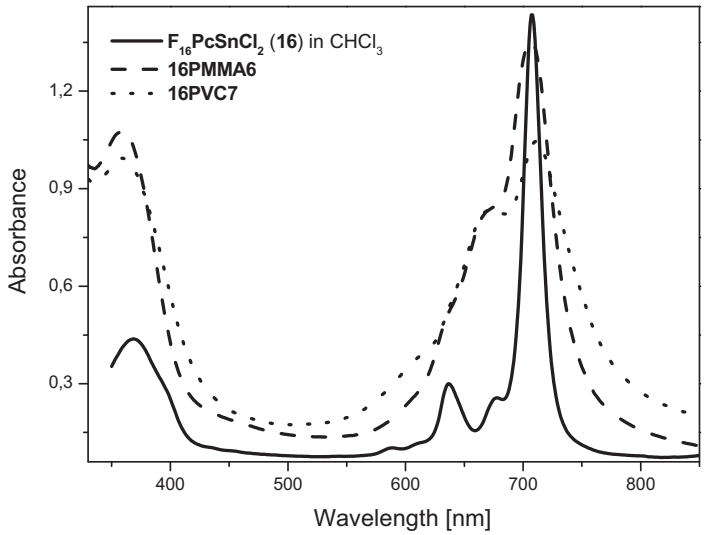

Figure 5.23 Absorption spectra of **$F_{16}PcSnCl_2$** (**16**) in PMMA and in PVC films in comparison with spectrum of **16** in $CHCl_3$ solution.

The position of the Soret band is shifted to the shorter wavelength by ~ 10 nm between the films (**Table 5.7**) and chloroform solution. In spite of the blue shift of the Soret band in films,

16PMMA6 and **16PVC7**, the shape of the Soret band is preserved. The electronic spectrum of film of hexadecamethylphthalocyaninatoiron (II) (**$_{16}$(Me)FePc**) [18] with small peripheral substituents shows a red-shifted Q- and Soret bands in relation to solution. Furthermore, the absorption spectrum of **$_{16}$(Me)FePc** in film is much broader than that of **$F_{16}PcSnCl_2$** (**16**) either in PVC or in PMMA relative to their solutions. The absorption spectra of multi-layer films containing **16** in PVC and in PMMA are presented in **Figure 5.24 A** and **B**. Similarly to polymeric films of compounds **14** and **15**, the substantial increase in absorption with increasing film thicknesses is observed for films containing compound **16**. The thicknesses of polymeric films containing **16** range from 0.8 to 1.9 μm (**Table 5.7**).

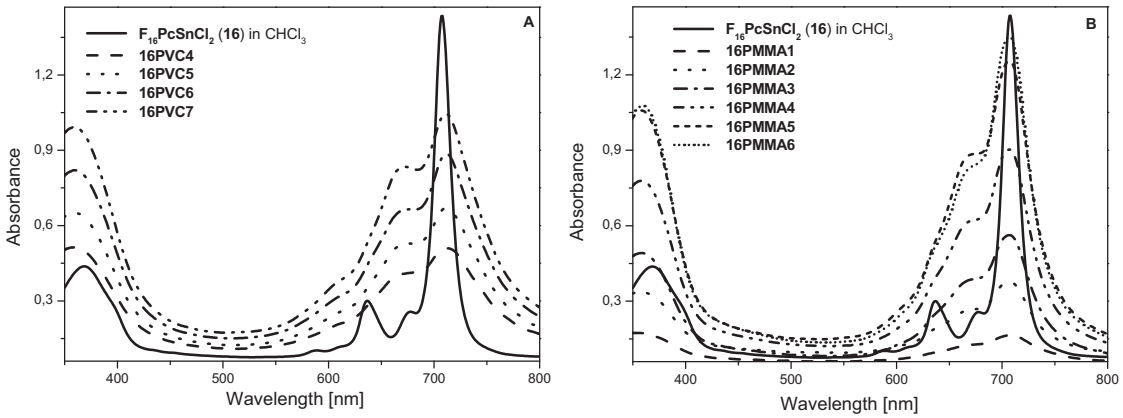

Figure 5.24 Absorption spectra of **$F_{16}PcSnCl_2$** (**16**) in PVC (**A**) and in PMMA (**B**) films.

Comparison of the electronic spectra of polymeric films containing compound **$F_{16}PcSnCl_2$** (**16**) with axial chlorine groups with films of **15** possessing bulky di(*tert*-butyl)phenoxy axial substituents shows that the bulky ligands nicely prevent cofacial aggregation in films; moreover small chlorine axial groups lessen aggregation as well.

5.3 Characterization of phthalocyanine films prepared by drop casting method

The following series of octabutoxy-substituted phthalocyanines **$(BuO)_8PcZn$** (**29**) [2, 8], **$(BuO)_8PcPb$** (**30**) [2, 8], and **$(BuO)_8PcCu$** (**31**) [2, 8] was deposited as drop casted films from the polymer-phthalocyanine solution. A drop of polymer-phthalocyanine solution containing 1×10^{-3} mol L^{-1} of an appropriate phthalocyanine was poured onto a sapphire substrate using a syringe. The majority of the organic solvent in the cast films was slowly evaporated at room temperature during few days, and afterwards the films were dried at 100 ^{0}C for additional 5

hours. The cast films of octa-substituted phthalocyanines, **29**, **30** and **31** were prepared in PMMA and PS polymers (**Table 5.8**). In addition, the hydrophilic tetraanionic tetrasulfophthalocyanine **(Sul)$_4$PcGa** (**28**) [19] was included in a cast film of silica gel. The drop casting method easily allows preparing in one-step procedure films with a thickness up to several hundred μm (**Table 5.8**). The concentrations of the examined phthalocyanines in cast films were determined to be 0.436, 0.430, 0.435, and 0.432 mol L^{-1} for **28**, **29**, **30** and **31** in cast films (**Table 5.8**), respectively.

Table 5.8 Thickness (*d*) and UV/Vis data of drop coated phthalocyanine films in polymers and in solutions.

Compound	λ_{max} [nm] toluene	Cast films			
	Q-band	Solid-state sample	Concentration Pc in film [mol L^{-1}]	*d* [μm]	Q-band
(Sul)$_4$PcGa (28)	681, 613	**28GaPcGel**	0.436	109.0	672
(BuO)$_8$PcZn (29)	678	**29PMMA1**	0.430	244.0	642
(BuO)$_8$PcPb (30)	715	**30PS1**	0.435	205.0	631
(BuO)$_8$PcCu (31)	677	**31PMMA1**	0.432	117.0	662

The sol gel of compound **(Sul)$_4$PcGa** (**28**) was prepared by mixing appropriate monomeric precursors such as tetraethoxysilane (TEOS) and phenyltriethoxysilane (PhTriEOS), ethanol, and HCl, and then aqueous solution of **28** was added. The mixture was stirred for few hours, and finally poly(ethylene glycol) (PEG) was added, and the solution was further stirred [20-22]. Upon addition of PEG, mechanically stable and crack-free films of the sol-gel material were obtained.

Absorption spectrum of sol gel of compound **28** (**28GaPcGel**) prepared by drop casting method relative to aqueous solution of **28** is shown in **Figure 5.25 B**. Besides, only for comparison, the spectrum of sol gel of **(Sul)$_4$PcGa** (**28**) prepared by spin coating method is presented (**Figure 5.25 A**). The sol gel of compound **28** obtained by spin coating was not further investigated. The shape of absorption spectrum of sol gel prepared by spin coated method resembles the aqueous solution, indicating that compound **28** occurs in the film in monomeric state.

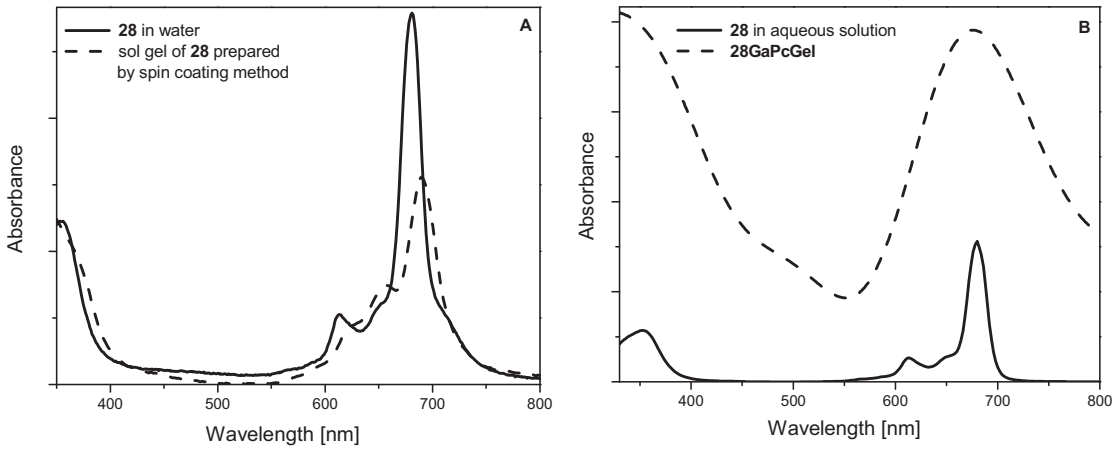

Figure 5.25 Absorption spectra of sol gel of **(Sul)$_4$PcGa** (**28**) prepared by spin coating (**A**) and drop coating method (**B**) in relation to aqueous solution.

In general, sulfonated phthalocyanines containing bivalent metal like Zn(II) are strongly aggregated in aqueous solution. In contrast sulfonated phthalocyanines with tri- or tetravalent metals like Al(III)OH, Ga(III)OH, Si(IV)(OH)$_2$ are more monomeric [23]. Compound **28** is monomericaly dissolved in films prepared by spin coating which is due to axial substitution which decreases the formation of aggregates either in solution or in solid state. However, the Q-band of the **28** in the sol gel film obtained by drop casting technique broadens on both sides of the Q-band of solution. Interestingly, even though the sharpness of the Q-band is completely lost in film, the Q-band shifts to a shorter wavelength just by ~ 8 nm. This comparison of two films of compound **28** prepared by two different methods clearly shows that the drop casting method is more preferable for preparation of aggregates than spin coating.

In case of cast films of compound **(BuO)$_8$PcZn** (**29**) in PMMA and **(BuO)$_8$PcPb** (**30**) in PS (**Figure 5.26**) the absorption spectra are dominated by aggregation. The Q-bands of **29PMMA1** and **30PS1** films are widely shifted to the blue region, by ~ 36 nm for **29PMMA1** against Q-band in toluene solution, and by ~ 80 nm for **30PS1** in comparison with the Q-band of compound **30** in toluene solution. The absorption spectra of both films are significantly broader than those of the corresponding spectra in solutions. The thicknesses of **29PMMA1** and **30PS1** films were determined to be 244 and 205 μm (**Table 5.8**), respectively.

Interestingly, the lead tetrakis(cumylphenoxy)phthalocyanine (**PbPc(β-CP)$_4$**) at very high concentrations in chloroform solution show tendency to form aggregates, observed as considerable red shift of Q-band in its absorption spectrum [24].

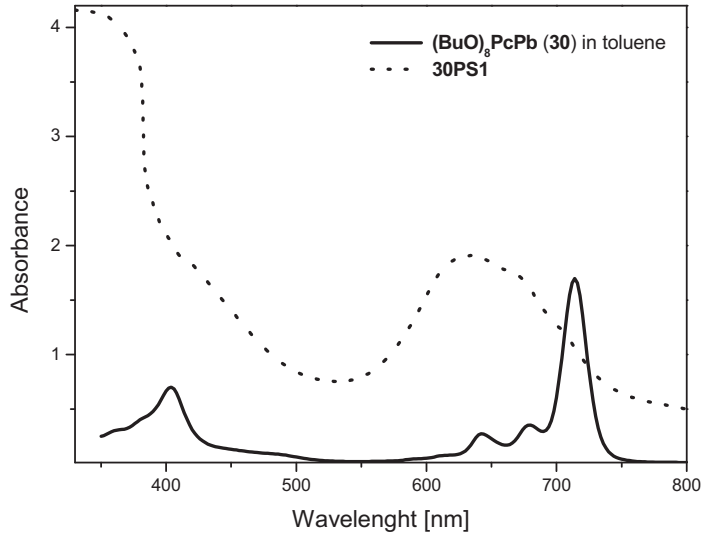

Figure 5.26 Absorption spectra of **(BuO)$_8$PcPb** (**30**) in toluene and in cast film.

Figure 5.27 presents the absorption spectrum of cast film of compound **(BuO)$_8$PcCu** (**31**) in relation to spectrum in toluene solution. As shown by the spectrum of **31PMMA1**, the Q-band of **31** in film considerably broadens on both side of the solution Q-band. This indicates existing of **31** in an aggregated state in film. The films of **31** in PMMA prepared either by spin or drop coating method show absorption spectra dominated by aggregation. Shapes of Q-bands of both films are notably broader compared to that of toluene solution.

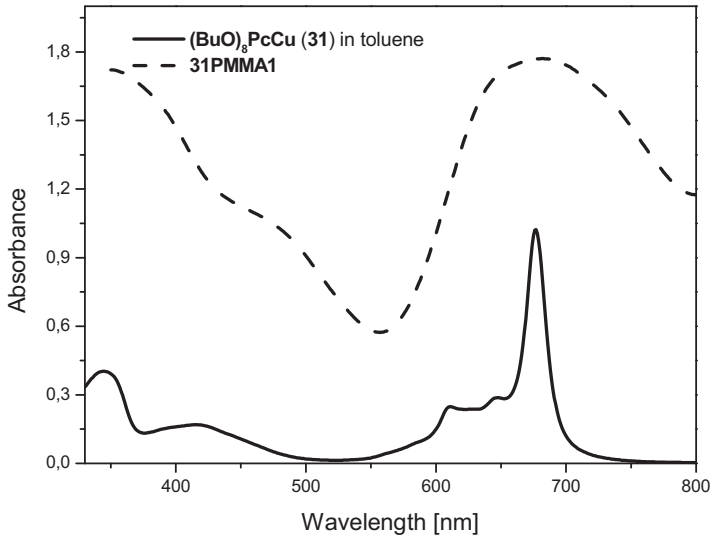

Figure 5.27 Absorption spectra of **$(BuO)_8PcCu$** (**31**) in toluene and in cast film.

The tendency to form aggregates in drop coated films from polymeric solution takes place due to slow evaporation of the solvents (few days at room temperature) so that strong molecular interactions and big packing of Pc occur. This is in contrast to the spin coating method where solvent is rapidly evaporated .and then the Pcs usually remain in a monomolecular state.

5.4 Conclusion

Multi-layer films of different polymers containing soluble phthalocyanines were obtained by spin coating on glass or sapphire substrates. Films by drop casting method were also prepared. The electronic absorption spectra of films for several compounds were compared and discussed in relation to solution spectra. The films were characterized with regard to their thickness, concentration, and electronic data. Tetra-substituted, **$(nPhO)_4PcSnCl_2$** (**5**), **$(fPhO)_4PcSnCl_2$** (**6**), **$(fPhO)_4PcGeCl_2$** (**7**), **$(t\text{-}Bu)_4PcInCl$** (**25**), octa-substituted **$(BuO)_8PcZn$** (**29**), **$(BuO)_8PcPb$** (**30**), and hexadeca-substituted **$Cl_{16}PcSn(tBu_2P)_2$** (**14**), **$Cl_{16}PcGe(tBu_2P)_2$** (**15**), **$F_{16}PcSnCl_2$** (**16**) phthalocyanines, either in PVC or PMMA films exhibit tendency that those Pcs are monomolecular distributed. The bulky peripheral substituents, *p*-nitrophenoxy and *p*-formylphenoxy, and axial groups effectively diminish cofacial aggregation. The Q-band position of phthalocyanines in spin coated films is similar or slightly blue- or red-shifted compared to Q-band in solutions. The shape and position of Q-band of multi-layer films do not differ in particular from mono-layer films. The metal-free tetra-substituted

phthalocyanines, **(PhO)$_4$PcH$_2$** (**26**), **(*t*-BuPhO)$_4$PcH$_2$** (**27**), germanium phthalocyanine, **(αNO$_2$)$_4$PcGe(*t*Bu$_2$P)$_2$** (**23**) and copper phthalocyanine **(BuO)$_8$PcCu** (**31**) exhibit a clear tendency to form cofacial aggregates in spin coated films. Every of drop coated film of **(BuO)$_8$PcZn** (**29**), **(BuO)$_8$PcPb** (**30**), **(BuO)$_8$PcCu** (**31**) and **(Sul)$_4$PcGa** (**28**) shows domination of aggregation. The Q-band in drop coated films is significantly broader and blue-shifted compared to solution spectra. This is caused by strong molecular interactions and big packing of phthalocyanines during long time of their drying. Phthalocyanines in films prepared by the drop casting method tend to aggregate whereas in spin coated films most phthalocyanines are totally monomeric and not aggregated.

In summary, several phthalocyanines are monomeric distributed in films prepared by the spin coating technique. Such films are suitable for being good optical limiters (Chapter 8.4).

5.5 References

[1] M. Hanack, H. Heckmann, *Eur. J. Inorg. Chem.*, **1998**, 367.

[2] D. Wöhrle, G. Schnurpfeil, G. Knothe, *Dyes and Pigments*, **1992**, 18, 91.

[3] H. Yanagi, Y. Kanbayashi, D. Schlettwein, D. Wöhrle, N. R. Armstrong, *J. Chem. Phys.*, **1994**, 98, 4760.

[4] J. S. Shirk, R. G. S. Pong, S. R.Flom, H. Heckmann, M. Hanack, *J. Phys. Chem. A*, **2000**, 104, 1438.

[5] A. Schmidt, L. K. Chau, A. Back, N. R. Armstong, in *Phthalocyanines – Properties and Applications*, vol. 4, eds. C. C. Leznoff and A. B. P. Lever, VCH, New York, **1996**, 307.

[6] S. Yanagi, T. Wada, J. Kumor, H. Sasabe, K. Sasaki, *Mol. Cryst. Liq. Cryst*., **1994**, 255, 167.

[7] B. M. Hassan, H. Li, N. B. McKeown, *J. Mater. Chem.*, **2000**, 10, 39.

[8] D. Wöhrle, V. Schmidt, J.Chem.Soc., Dalton Trans., **1988**, 549.

[9] K. Ukei, *Acta Crystallogr., Sect. B*, **1973**, B29, 2290.

[10] K. Ukei, *J. Phys. Chem. Jpn.*, **1976**, 40, 140.

[11] S. R. Flom, J. S. Shirk, R. G. S. Pong, J. R. Lindle, F. J. Bartoli, M. E. Boyle, J. D. Adkins, A. W. Snow, *SPIE Proc.,* **1994**, 229, 2143.

[12] J. S. Shirk, R. G. S. Pong, F. J. Bartoli, *Appl. Phys. Lett.,* **1980**, 63, 1880.

[13] T. Kudo, M. Kimura, K. Hanabusa, K. Shirai, T. Sakaguchi, *J. Porphyrins Phthalocyanines,* **1999**, 3, 65.

[14] L. K. Chau, E. J. Osburn, N. R. Armstrong, D. F. O'Brien, B. A. Parkinson, *Langmuir*, **1994**, 10, 351.

[15] E. J. Osburn, L. K. Chau, S. Y. Chen, N. Collins, D. F. O'Brien, N. R. Armstrong, *Langmuir*, **1996**, 12, 4784.

[16] J. M. Birchall, R. N. Haszeldine, J. O. Morley, *J. Chem. Soc. (C),* **1970**, 2667.

[17] B. M. Hassan, H. Li, N. B. McKeown, *J. Mater. Chem.*, **2000**, 10, 39.

[18] H. Ogata, R. Higashi, N. Kobayashi, *J. Porphyrins Phthalocyanines*, **2003**, 7, 551.

[19] G. Schneider, D. Wöhrle, W.Spiller, J. Stark, G. Schulz-Ekloff, *Photochem. Photobiol.*, **1994**, 60, 333.

[20] K. Mansour, P. D. Fuqua, S. R. Marder, B. Dann, J. W. Perry, *SPIE Proc.,* **1994**, 2143, 239.

[21] R. A. Norwood, J. R. Sounik, J. Popolo, D. R. Holcomb, *SPIE*, **1991**, 1560, 55.

[22] M. Sheik-Bakue, A. A. Said, T. H. Wei, D. J .Hagan, E. W. Van Stryland, *IEEE Journal of Quantum Electronic*, **1990**, 26, 760.

[23] R. Gerdes, O. Bartels, G. Schneider, D. Wöhrle, G. Schulz-Ekloff, *Polym. Adv. Technol*., **2001**, 12, 1.

[24] A. W. Snow, in *The Porphyrin Handbook– Phthalocyanines: Properties and Materials*, vol. 17, eds. K. M. Kadish, K. M. Smith, R. Cuilard, **2003**, 129.

6. Experimental part

6.1 Materials

All reactions were carried out under dry nitrogen or argon atmosphere. Dimethylsulphoxide (DMSO) was dried over alumina. 1-Chloronaphthalene, 1,2,4-trimethylbenzene, nitrobenzene, and dimethylformamide (DMF) were distilled under vacuum and inert gas atmosphere. Quinoline was always freshly distilled under vacuum and inert gas atmosphere prior to use. Tetrafluorophthalonitrile purchased from Aldrich was purified in a sublimation apparatus at 10^{-2} Torr (1.33 Pa) at a bath temperature of 90-100 °C. All other chemicals were commercially available and used without further purification.

6.2 Instrumental methods

Electronic spectra were obtained on Perkin Elmer Lambda 2 Lambda 9. FT-IR spectra were recorded on Biorad-SPC-3200 as KBr pellets. Electrospray mass spectra (ESI) were recorded using the Bruker Esquire-LC that is a HPLC/MS system consisting of an Agilent/HP 1100 liquid chromatography system and an ion trap mass detector. Both components can be used separately. Electron Impact (EI) and Direct Chemical Ionization (DCI), mass spectra with ammonia as a reacting gas were recorded on Finnigan MAT 8200, which is double-focusing instrument with reverse Nier-Johnson geometry.

6.3 Synthesis of phthalonitriles

6.3.1 Synthesis of 4-(4-nitrophenoxy)phthalonitrile (1)

A solution of the 4-nitrophthalonitrile (**I**) (5.0 g, 28 mmol) and 4-nitrophenol (**II**) (7.8 g, 56 mmol) in 100 ml of dry DMSO was stirred under nitrogen. Stirring was continued while dry fine, powdered potassium carbonate (K_2CO_3) (7.7 g, 56 mmol) was added. After 24 hours stirring at room temperature the next portion of dry K_2CO_3 (7.7 g, 56 mmol) was added. The mixture was stirred for an additional 24 hours and added to 250 ml water thereafter. The precipitate was filtered off and washed thoroughly with water. The product was three times recrystallized from methanol yielding 5.76 g (76%) of a yellow-white microcrystalline solid.

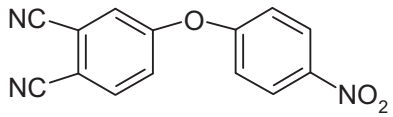

M = 265 g mol^{-1}

1

IR (KBr): ν (in cm^{-1}) = 3109, 3078, 2851, 2234 (C≡N), 1684, 1513, 1426, 1346 (NO_2), 1225 (C-O-C), 1157 (C-O-C), 1047, 1005, 951, 893, 854, 755, 723, 712, 689, 621, 593, 552, 525.

EI-MS (70 eV) *m/z* = 265[M^+], 235[M – NO^+]$^+$, 191[M – $C_2H_4NO_2^+$]$^+$, 179[M – $C_3H_4NO_2^+$]$^+$, 164[M_{191} – CHN]$^+$, 152[$C_{12}H_4NO^+$], 76[$C_6H_4^+$], 50[$C_6H_2^+$].

6.3.2 Synthesis of 4-(4-formylphenoxy)phthalonitrile (2)

4-Nitrophthalonitrile (**I**) (6.92 g, 40 mmol) and 4-formylphenol (**III**) (9.76 g, 80 mmol) were dissolved in 100 ml of dry DMSO under nitrogen at room temperature. Dry, powdered K_2CO_3 (3 × 80 mmol, 11.12 g every 24 hours) was added. After 72 hours stirring, the reaction mixture was put into 500 ml of ice water. The precipitate was filtered off, washed copiously with water, recrystallized twice from methanol dried in vacuum.

Yield: 7.92 g (80%) of a yellowish powder.

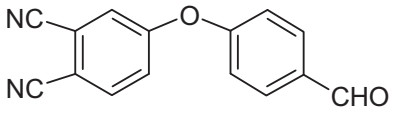

M = 248 g mol^{-1}

2

IR (KBr): ν (in cm^{-1}) = 2230 (C≡N), 1698 (C=O), 1513, 1496, 1232 (C-O-C), 1178 (C-O-C), 1047, 1005, 951, 893, 854, 755, 723, 712, 689, 621, 593, 552, 525.

EI-MS (70 eV, 200°C) *m/z* = 248[M^+], 247[M – H^+]$^+$, 219[M – CHO]$^+$, 191[M – $C_2H_4CHO^+$]$^+$, 164[M_{191} – CHN]$^+$, 77[$C_6H_5^+$], 51[$C_6H_3^+$].

6.4 Synthesis of phthalocyanines

All tetra-substituted phthalocyanines are mixtures of regioisomers, although only the C_{4v} structures are presented.

6.4.1 Synthesis of 2,9,16,23-tetrakis(4-formylphenoxy)phthalocyanine (3)

4-(4-Formylphenoxy)phthalonitrile (**2**) (5 g, 20 mmol) was refluxed in 100 ml of dry 1-pentanol in the presence of 1,8-diazabicyclo[5.4.0]undec-7-ene (DBU) (3 g, 20 mmol) under

nitrogen for 14 hours. The resulting greenish suspension was cooled, and the product was precipitated by addition of 150 ml of petroleum ether. The precipitate was filtered off and washed successively with petroleum ether, methanol, and acetone. The product then was chromatographed on silica gel using pyridine/MeOH (20:1) as the mobile phase. The compound was dried in vacuum at 60 °C (6 h) to give 1.95 g (39%) of a blue powder.

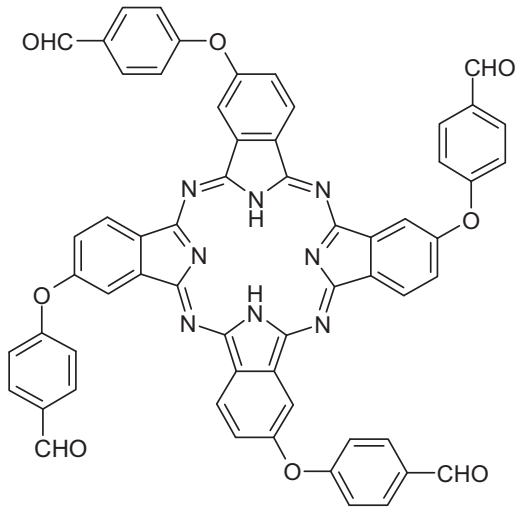

M = 994 g mol^{-1}
$(fPhO)_4PcH_2$ (**3**)

UV/Vis (pyridine): λ (in nm) = 700, 668, 636, 608, 341.

IR (KBr): ν (in cm^{-1}) = 3013, 2841 (CHO), 1748, 1633 (CO), 1519, 1492, 1453, 1426, 1365, 1289, 1254 (C-O-C), 1177, 1138, 1106, 1063, 1022 (C-O-C), 968, 923, 882, 859, 777, 748, 466.

ESI-MS (negative ion mode) *m/z* = 994.3[M$^-$].

6.4.2 Synthesis of 2,9,16,23-tetrakis(4-nitrophenoxy)phthalocyanine (4)

4-(4-Nitrophenoxy)phthalonitrile (**1**) (2 g, 7.55 mmol) was dissolved in 50 ml of dry 1-pentanol. The organic base, DBU (1.13 g, 7.55 mmol) was added, and the mixture was heated at 130 °C under nitrogen for 17 hours. After being cooled to room temperature, the mixture was poured into 200 ml of methanol. The precipitate formed was collected by filtration and washed sequentially with methanol, acetone, and diethyl ether to remove first impurities. The crude compound was further Soxhlet extracted with methanol (4 hours) and then with acetone (2 hours). Finally, the product was dissolved in pyridine and loaded onto short silica column. Elution with pyridine afforded the desired compound as blue band, which upon removal of the solvent under reduced pressure and drying in a vacuum at 60 °C for 8 hours gave of a blue solid.

Yield: 0.85 g (42%).

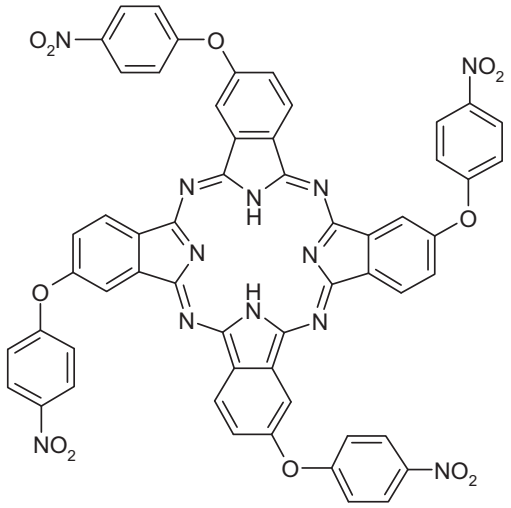

M = 1062 g mol^{-1}
(nPhO)$_4$PcH$_2$ (**4**)

UV/Vis (pyridine): λ (in nm) = 698, 665, 638, 606, 337.

IR (KBr): ν (in cm^{-1}) = 2840, 1754, 1632, 1612, 1586 (C=N), 1518, 1490, 1455, 1424, 1349 (NO_2), 1323, 1252 (C-O-C), 1177, 1145, 1110, 1063, 1020 (C-O-C), 1005, 927, 863, 748, 715, 631.

ESI-MS (negative ion mode) *m/z* = 1061.1[M$^-$].

6.4.3 Synthesis of dichlorotin(IV) 2,9,16,23-tetrakis(4-nitrophenoxy)phthalocyanine (5)

A solution of the 2,9,16,23-tetrakis(4-nitrophenoxy)phthalocyanine (**4**) (1.5 g, 1.4 mmol) and anhydrous tin(II) chloride ($SnCl_2$) (1.27 g, 7 mmol) or $SnCl_4$ (3.7 g, 14 mmol) in 30 ml of dry 1-chloronaphthalene was heated at 200 °C with stirring under nitrogen atmosphere. The reaction was monitored by UV/Vis and stopped when the split Q-band collapsed into one (it took approximately 1.5 hour). After cooling, the resulting greenish suspension was poured into 50 ml of hexane, and the precipitate was collected by filtration. The 1-chloronaphthalene was removed by repetitively washing with diethyl ether until the 1-chloronaphthalene could no longer be smelled. The crude compound was redissolved in tetrahydrofuran (THF) and chromatographed on silica gel. After removal of the solvent, second column chromatography was applied using mixture of $CHCl_3$/MeOH (5:1). Removal of the solvent and drying in a vacuum (60 °C, 12 h) gave 0.95 g (54%) of a deep green solid.

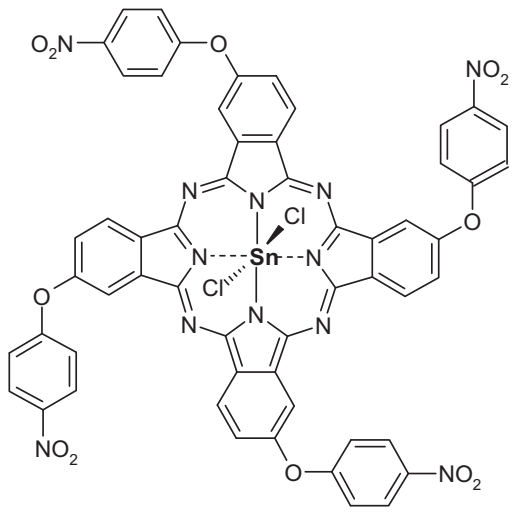

M = 1250 g mol^{-1}
(nPhO)$_4$PcSnCl$_2$ (5)

UV/Vis ($CHCl_3$): λ (in nm) = 700, 667, 631, 370.

IR (KBr): ν (in cm^{-1}) = 2841, 1748, 1652 (C=N), 1611, 1587 (C=N), 1519 (NO_2), 1489, 1429, 1348 (NO_2), 1291, 1249 (C-O-C), 1213, 1176, 1138, 1111, 1063, 1022 (C-O-C), 997, 966, 901, 863, 750, 697.

ESI-MS (negative ion mode) *m/z* = 1250[M^-], 1215.1[$M - Cl^-]^-$, 1180.1[$M - 2Cl^-]^-$.

ESI-MS (positive ion mode) *m/z* = 1215.2[$M^+ - Cl^-]^+$, 1164.3[$M^+ - 2Cl^- - O^-]^+$.

6.4.4 Synthesis of dichlorotin(IV) 2,9,16,23-tetrakis(4-formylphenoxy)phthalocyanine (6)

A sample of 2,9,16,23-tetrakis(4-formylphenoxy)phthalocyanine (**3**) (1.5 g, 1.5 mmol) was dissolved in 20 ml of dry 1-chloronaphtahlene under the flow of dry inert gas. The flask was placed in a metal bath at 160 °C, and then 0.88 ml of tin(IV) chloride ($SnCl_4$) (1.95 g, 7.5 mmol) was transferred into solution via syringe. Heating was carried on for approximately 1.5 hour until the split Q-band in the UV/Vis spectrum (solvent: THF or chloroform ($CHCl_3$)) collapses to a single Q-band. After being cooled, 50 ml of hexane was added, and the precipitate was collected by filtration. The 1-chloronaphthalene was removed by repetitively washing with diethyl ether until the 1-chloronaphthalene could not be smelled. The green residue was chromatographed on silica gel using THF as an eluent in order to remove large amounts of the impurities. The solvent was removed by distillation and the second column chromatography was applied using mixture of $CHCl_3$/MeOH (20:1). Elution with $CHCl_3$/MeOH (20:1) afforded a green band, which upon removal of the solvent and drying in a vacuum (60 °C, 3 hours) gave 0.68 g (38%) of a deep-green solid.

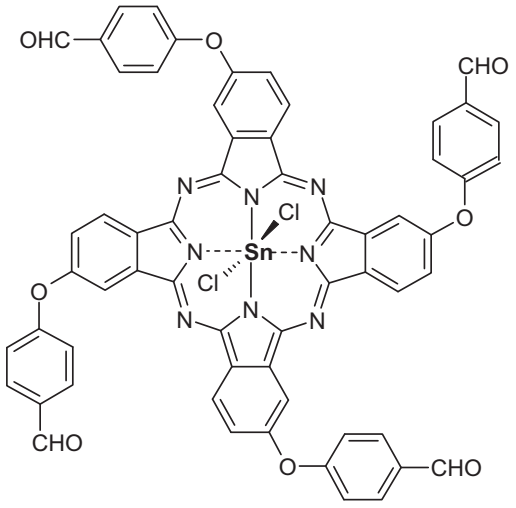

M = 1182 g mol^{-1}
(fPhO)$_4$PcSnCl$_2$ (**6**)

UV/Vis ($CHCl_3$): λ (in nm) = 704, 633, 368.

IR (KBr): ν (in cm^{-1}) = 1760, 1692 (C=O), 1594, 1583, 1528, 1513, 1480, 1443, 1399, 1342, 1281, 1237 (C-O-C), 1207 (C-O-C), 1163, 1122, 1093, 1023 (C-O-C), 952, 848, 790, 768, 735, 658, 411.

ESI-MS (negative ion mode) *m/z* = 1182.1[M$^-$].

ESI-MS (positive ion mode) *m/z* = 1147.3[M – Cl$^-$]$^+$, 1112.4[M – 2Cl$^-$]$^+$.

6.4.5 Synthesis of dichlorogermanium(IV) 2,9,16,23-tetrakis(4-formylphenoxy)phthalocyanine (7)

A sample of 2,9,16,23-tetrakis(4-formylphenoxy)phthalocyanine (**3**) (2 g, 2.27 mmol) was dissolved in 20 ml of freshly distilled quinoline under inert gas atmosphere. The flask was placed in a metal bath at 180 °C, and then 0.45 ml of germanium(IV) chloride ($GeCl_4$) (0.83 g, 3.87 mmol) was added to the flask via syringe. The reaction was allowed to proceed at 180 °C with magnetic stirring, and the reaction progress has been checked by UV/Vis and stopped when the split Q-band collapsed into one (it took approximately 2 hour). The mixture was cooled, 50 ml of chloroform was added, and the solution was filtered off. The chloroform layer was washed 4 times with 10% HCl (100 ml each time) and evaporated to a solid with a rotary evaporator. The crude product was purified using column chromatography (silica gel) with THF to remove first impurities. After evaporation of the solvent, second column chromatography was performed using mixture of $CHCl_3$/hexane (1:5). Drying in vacuum at 60 °C (6 h) gave 0.61 (24%) of a deep green microcrystals.

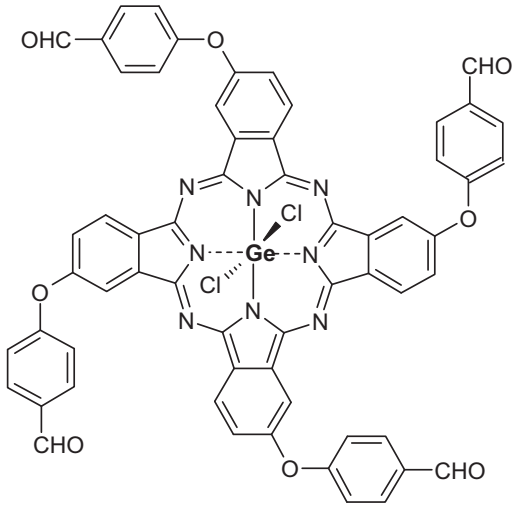

M = 1136 g mol^{-1}
$(fPhO)_4PcGeCl_2$ (**7**)

UV/Vis ($CHCl_3$): λ (in nm) = 699, 668, 629, 372.

IR (KBr): ν (in cm^{-1}) = 2970, 1766, 1737, 1633 (C=O), 1584, 1516, 1492, 1427, 1415, 1361, 1301, 1290, 1254 (C-O-C), 1178, 1145, 1106, 1060, 1023 (C-O-C), 996, 968, 923, 860, 746, 524, 470.
ESI-MS (negative ion mode) *m/z* = 1136.1[M$^-$].

ESI-MS (positive ion mode) *m/z* = 1101.3[M – Cl$^-$]$^+$,
1083.3[M – 2Cl$^-$ + OH$^-$]$^+$.

6.4.6 Synthesis of dichlorotin(IV) hexadecachlorophthalocyanine (8)

Method 1. Fine, dry powdered of tetrachlorophthalonitrile (**VII**) (0.15 g, 0.57 mmol) was mixed with anhydrous $SnCl_2$ (0.22 g, 0.14 mmol) and transferred to a glass ampoule. After multiple flushing with argon and evacuating, the glass vial was sealed under vacuum (10^{-2} Torr = 1.33 Pa). The ampoule was heated at 250 °C for 5 hours. The solid product was crushed and washed sequentially with dichloromethane (CH_2Cl_2) (4 h), acetone (8h), and methanol (8 h) yielded 0.11 (65%) of a bluish-green powder.

Method 2. A mixture of dry tetrachlorophthalonitrile (**VII**) (5 g, 17 mmol) and anhydrous $SnCl_2$ (1.6 g, 8.5 mmol) was dissolved in 50 ml of dry 1-chloronaphthalene under inert gas atmosphere. The mixture was kept under reflux within 2 hours. The greenish-brown solution was held at 190 °C for further 20 hours. After cooling, the resulting greenish-brown suspension was poured into 100 ml of hexane, and the precipitate was collected by filtration. The 1-chloronaphthalene was removed by repetitively washing with diethyl ether until the 1-chloronaphthalene could no longer be smelled. The product was placed in the thimble of a Soxhlet extractor and washed sequentially with diethyl ether (12 h), acetone (8 h) and methanol (8 h). After being dried at 70 °C in vacuum, a dark bluish-green powder was obtained. Yield: 4.9 g (92%).

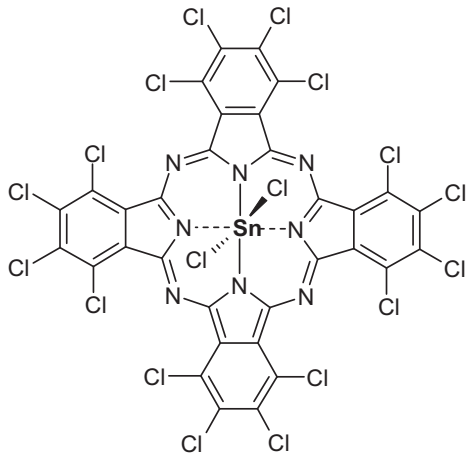

M = 1246 g mol^{-1}
$Cl_{16}PcSnCl_2$ (**8**)

UV/Vis (1-chloronaphthalene): λ (in nm) = 755, 677, 380.

IR (KBr): ν (in cm^{-1}) = 1754, 1633, 1537, 1492, 1427, 1365, 1331, 1106, 1295, 1254, 1201, 1180, 1134, 1094, 1062, 995, 968, 944, 786 (C-Cl), 766 (C-Cl), 518.

ESI-MS (negative ion mode) *m/z* = 1253.3[M$^-$], 1218.3[M – Cl$^-$]$^-$, 1183.3[M – 2Cl$^-$]$^-$.

6.4.7 Synthesis of dichlorogermanium(IV) hexadecachlorophthalocyanine (9)

Method 1. A dry powder of tetrachlorophthalonitrile (**VII**) (0.46 g, 1.7 mmol) was placed into an ampoule. The vial was repeatedly flushing with argon and then a $GeCl_4$ (0.12 g, 0.55 mmol) was injected into the ampoule with a hypodermic needle. The tube was sealed under vacuum (10^{-2} Torr = 1.33 Pa) and heated at 300 °C for 5 hours. The solid product was crushed, placed in the thimble of a Soxhlet extractor, and treated with dichloromethan (8 h), acetone (12 h), and methanol (12 h). The product was dried in vacuum at 70 °C (14 h) and obtained in a yield of 0.19 g (37%) as dark green powder.

Method 2. Tetrachlorophthalic anhydride (**VIII**) (2 g, 7 mmol), urea (1.4 g, 20 mmol), and ammonium molybdate (0.009 g) were suspended in 15 ml of dry nitrobenzene in a two-necked round-bottomed flask with stirring. Then 0.26 ml of $GeCl_4$ (0.49 g, 2.26 mmol) was transferred to the flask with the aid of syringe under nitrogen. The reaction mixture was stirred at 190 °C within 2 hours and was then held at 180 °C for an additional 14 hours. The viscous brown-olive suspension was cooled to 90 °C, diluted with 60 ml of ethanol and filtered hot. The residue was washed copiously with hot water. The crude product was further washed with diethyl ether (6 h), methanol (12 h), acetone (6 h) and dichloromethane (6 h). The desired product was dried at 70 °C in vacuum for 12 hours.

Yield: 1.5 g (74 %) of a bluish-green powder.

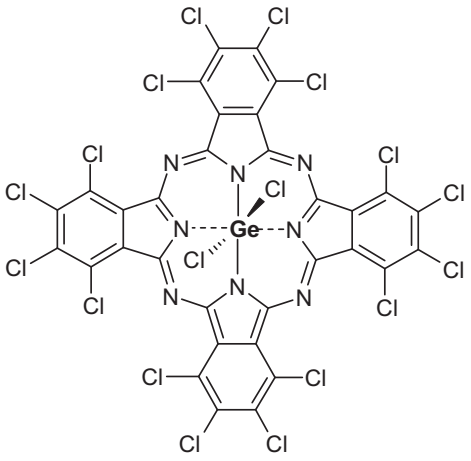

M = 1200 g mol^{-1}
$Cl_{16}PcGeCl_2$ (**9**)

UV/Vis (1-chloronaphthalene): λ (in nm) = 751, 671, 605, 375.

IR (KBr): ν (in cm^{-1}) = 1745, 1633, 1537, 1492, 1427, 1365, 1317, 1303, 1255, 1213, 1179, 1149, 1105, 1062, 1022, 994, 965, 956, 920, 785 (C-Cl), 746 (C-Cl), 512.

DCI-MS (negative ion mode, NH_3) *m/z* = 1208[M^-], 1175[M – Cl^-]$^-$, 1138[M – 2Cl^-]$^-$.

DCI-MS (positive ion mode, NH_3) *m/z* = 1207[M^+], 1173[M – Cl^-]$^+$, 1138[M – 2Cl^-]$^+$, 1064[M – 2Cl^- –Ge]$^+$.

6.4.8 Synthesis of dihydroxytin(IV) hexadecachlorophthalocyanine (10)

A 0.5 g sample of dichlorotin(IV) hexadecachlorophthalocyanine (**8**) (0.4 mmol) and 0.06 g of NaOH (1.6 mmol) were suspended in 5 ml of pyridine and 20 ml of water. The mixture was refluxed for 20 hours and then allowed to cool slowly. The brownish-blue solid was filtered off and washed copiously with water. The residue was placed in the thimble of a Soxhlet extractor and treated with methanol (8 h) and then with acetone (8 h). Drying in vacuum at 70 °C for 8 hours gave 0.29 g (60%) of a blue powder.

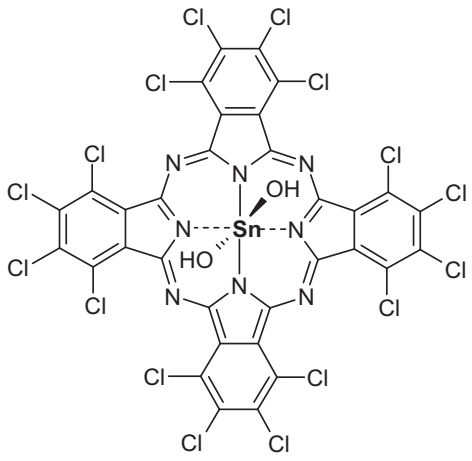

M = 1210 g mol^{-1}
$Cl_{16}PcSn(OH)_2$ (**10**)

UV/Vis (1-chloronaphthalene): λ (in nm) = 750, 674, 365.
IR (KBr): ν (in cm^{-1}) = 3408 (O-H), 1746, 1634, 1538, 1492, 1426, 1373, 1293, 1254, 1178, 1138, 1062, 1022, 967, 943, 856, 783 (C-Cl), 765 (C-Cl), 735, 516.

DCI-MS (negative ion mode, NH_3) *m/z* = 1181[M + H^+ - 2OH^-]$^-$, 1217[M + H^+]$^-$, 1252[M + 2Cl^- - 2OH^-]$^-$.

DCI-MS (positive ion mode, NH_3) *m/z* = 1181[M + H^+ - 2OH^-]$^+$, 1217[M + H^+]$^+$.

6.4.9 Synthesis of dihydroxygermanium(IV) hexadecachlorophthalocyanine (11)

Dihydroxygermanium(IV) hexadecachlorophthalocyanine (**11**) was prepared by modified version of hydrolisys of dichlorogermanium phthalocyanine described by Joyner and Kenney [1]. A 1.5 g of sample dichlorogermanium(IV) hexadecachlorophthalocyanine (**9**) (1.25 mmol) was mixed with 20 ml of pyridine and 20 ml of water solution of 25% ammonia hydroxide. The mixture was brought to reflux, and heating was carried on for 15 hours. After being cooled, the dark green suspension was filtered off and washed sequentially with pyridine, methanol, and acetone. The solid was further Soxhlet treated with methanol (8 h) and then with acetone (8 h). Drying in vacuum at 70 °C for 8 hours gave 0.9 g (63%) of a dark bluish-green powder.

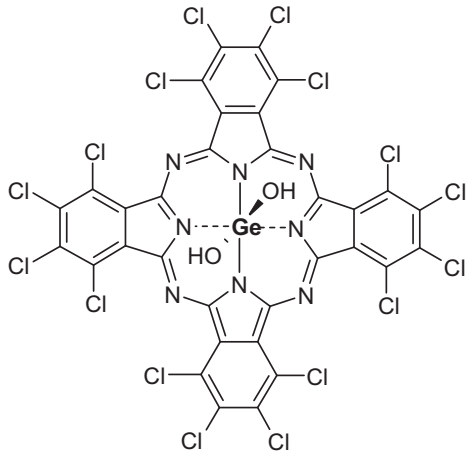

M = 1164 g mol^{-1}
$Cl_{16}PcGe(OH)_2$ (**11**)

UV/Vis (1-chloronaphthalene): λ (in nm) = 748, 672, 368.

IR (KBr): ν (in cm^{-1}) = 3400 (O-H), 1748, 1633, 1518, 1492, 1425, 1282, 1252, 1358, 1060, 963, 934, 798 (C-Cl), 746 (C-Cl), 712, 551, 498, 453.

DCI-MS (negative ion mode, NH_3) *m/z* = 1171.8[M]$^-$, 1206.8[M + 2Cl$^-$- 2OH$^-$]$^-$.

DCI-MS (positive ion mode, NH_3) *m/z* = 1170.8[M]$^+$, 1206.8[M + 2Cl$^-$ - 2OH$^-$]$^+$.

ESI-MS (negative ion mode) *m/z* = 1169.4[M$^-$], 1152.4[M - OH$^-$]$^-$.

6.4.10 Synthesis of difluorotin(IV) hexadecachlorophthalocyanine (12)

A 0.24 g sample of dihydroxytin(IV) hexadecachlorophthalocyanine (**10**) (0.2 mmol) was placed in a Teflon flask and treated with 10 ml of 40% HF for approximately 10 minutes. The mixture immediately assumed a bright red reflex with a pronounced green tinge. This mixture was evaporated to dryness on a steam bath; the resultant solid was placed in the thimble of a Soxhlet extractor and treated sequentially with pyridine (6 h), methanol (10 h) and acetone (8 h). After being dried in vacuum (70 °C, 8 h), 0.2 g (83%) of a blue powder was obtained.

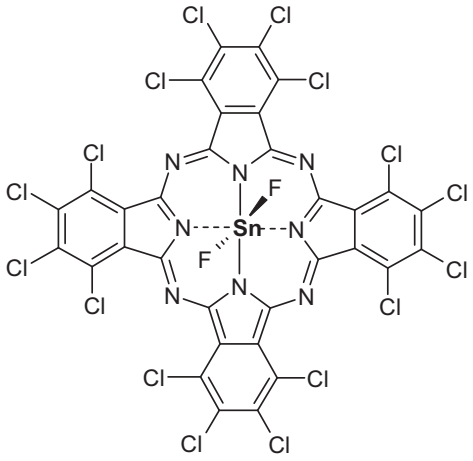

M = 1214 g mol^{-1}
$Cl_{16}PcSnF_2$ (**12**)

UV/Vis (1-chloronaphthalene): λ (in nm) = 746, 712, 671, 364.

IR (KBr): ν (in cm^{-1}) = 3013, 1749, 1633, 1519, 1492, 1426, 1366, 1325, 1292, 1254, 1178, 1139, 1106, 1062, 1023, 995, 968, 923, 881, 747 (C-Cl).

ESI-MS (negative ion mode) *m/z* = 1219.3[M^-], 1200.4[$M - F^-]^-$, 1181.4[$M – 2F^-]^-$.

6.4.11 Synthesis of difluorogermanium(IV) hexadecachlorophthalocyanine (13)

A 0.15 g sample of dihydroxygermanium(IV) hexadecachlorophthalocyanine (**11**) (0.13 mmol) was placed in a Teflon flask and treated with 8 ml of 40% HF for approximately 10 minutes. The mixture was evaporated to dryness on a steam bath; the resultant solid was placed in the thimble of a Soxhlet extractor and treated sequentially with methanol (12 h) and acetone (24 h). The product was dried in vacuum (70 °C, 6 h) yielding 0.14 g (93%) of a blue powder.

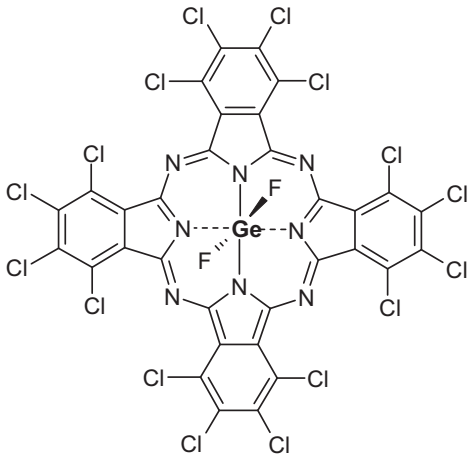

M = 1168 g mol^{-1}
$Cl_{16}PcGeF_2$ (**13**)

UV/Vis (1-chloronaphthalene): λ (in nm) = 739, 667, 359.

IR (KBr): ν (in cm^{-1}) = 3011, 1748, 1633, 1538, 1492, 1427, 1365, 1303, 1254, 1178, 1147, 1106, 1062, 1022, 992, 966, 920, 881, 746 (C-Cl).

ESI-MS (negative ion mode) *m/z* = 1173.4[M^-], 1156.4[$M – F^- + H^+]^-$.

6.4.12 Synthesis of bis(3,5-di-*tert*-butylphenoxy)tin(IV) hexadecachlorophthalocyanine (14)

Under argon atmosphere, a mixture of dichlorotin(IV) hexadecachlorophthalocyanine (**8**) (1.6 g, 1.3 mmol), 3,5-di-*tert*-butylphenol (1.1 g, 5.3 mmol), dry, powdered K_2CO_3 (0.74 g, 5.3 mmol) and 1,4,7,10,13,16-hexaoxacyclooctadecane (18-crown-6) (1.4 g, 5.3 mmol) was suspended in 15 ml of dry 1,2,4-trimethylbenzene. The resulting suspension was heated at 140 °C with stirring. The reaction was monitored by TLC (silica gel/toluene) and stopped when all of the dichlorotin(IV) hexadecachlorophthalocyanine (**8**) has been consumed (approximately 1.5 h). After cooling, the dark greenish-blue solution was poured into 60 ml of hexane; the precipitate formed was collected by centrifugation and washed five times with hexane. The crude product was chromatographed on silica gel using toluene as an eluent. Removal of the solvent and drying in vacuum at 60 °C (12 h) gave 0.45 g (22%) of dark green solid.

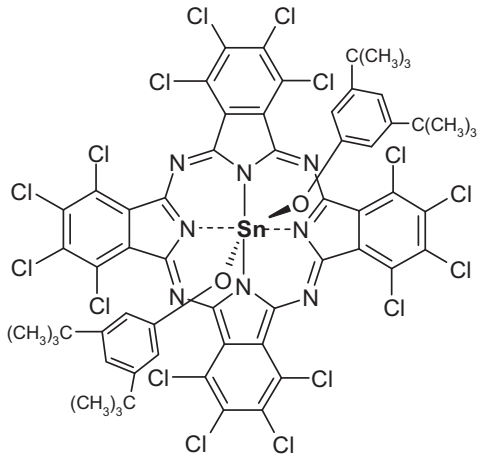

M = 1586 g mol^{-1}
$Cl_{16}PcSn(tBu_2P)_2$ (**14**)

UV/Vis (CH_2Cl_2): **λ** (in nm) = 733, 699, 661, 380.

IR (KBr): **ν** (in cm^{-1}) = 3124, 2965 (CH_3), 2867 (CH_3), 2902, 2839, 1749, 1637, 1542, 1492, 1419, 1351 ($C(CH_3)_3$), 1291, 1254, 1179, 1141, 1106, 1062, 1024, 999, 965, 939, 902, 862, 791 (C-Cl), 746 (C-Cl), 704 (C-Cl).

ESI-MS (negative ion mode) *m/z* = 1591.6[M]$^-$, 1533.1[M - C $(CH_3)_3^+$]$^-$, 1383.1[M –$OC_{14}H_{21}^-$]$^-$.

6.4.13 Synthesis of bis(3,5-di-*tert*-butylphenoxy)germanium(IV) hexadecachlorophthalocyanine (15)

A mixture of dichlorogermanium(IV) hexadecachlorophthalocyanine (**9**) (1 g, 0.83 mmol), 3,5-di-*tert*-butylphenol (0.34 g, 1.7 mmol), dry, powdered K_2CO_3 (0.23 g, 1.7 mmol) and 18-crown-6 (0.44 g, 1.7 mmol) was suspended in 12 ml of dry 1,2,4-trimethylbenzene under argon atmosphere. The suspension was heated at 140 °C with stirring, and the reaction was monitored by TLC (silica gel/CH_2Cl_2) and UV/Vis spectroscopy. The reaction was stopped

when all of the dichlorogermanium(IV) hexadecachlorophthalocyanine (**9**) has been consumed (approximately 50 minutes). After being cooled, 50 ml of hexane was added; the precipitate was centrifuged and washed five times with hexane. The crude product was purified on silica gel using CH_2Cl_2 as an eluent. The solid was evaporated to dryness and dry in vacuum at 60 °C for 6 h yielded 0.32 g (25%) of dark green solid.

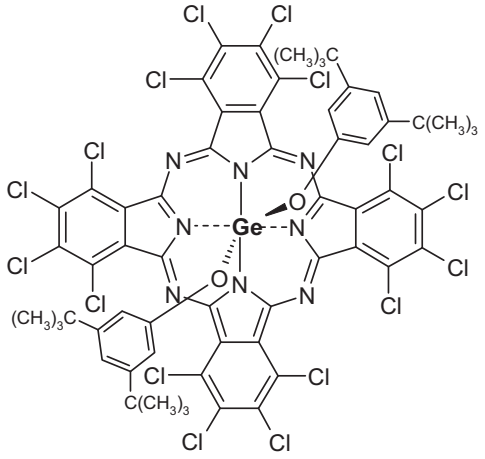

M = 1540 g mol^{-1}
$Cl_{16}PcGe(tBu_2P)_2$ (**15**)

UV/Vis (CH_2Cl_2): λ (in nm) = 731, 695, 659, 367.

IR (KBr): ν (in cm^{-1}) = 3013, 2966 (CH_3), 2902, 2867 (CH_3), 2839, 1749, 1633, 1538, 1492, 1421, 1362 ($C(CH_3)_3$), 1291, 1254, 1179, 1145, 1106, 1062, 1024, 992, 965, 922, 902, 880, 864, 747 (C-Cl), 704 (C-Cl), 596.

ESI-MS (negative ion mode) *m/z* = 1545.7[M]$^-$.

6.4.14 Synthesis of dichlorotin(IV) hexadecafluorophthalocyanine (16)

Dichlorotin(IV) hexadecafluorophthalocyanine (**16**) was prepared by a modified version of the synthesis described by Birchall [2]. Tetrafluorophthalonitrile (**IX**) (0.6 g, 3 mmol) and anhydrous $SnCl_2$ (0.29 g, 1.5 mmol) were dissolved in 10 ml of dry 1-chloronaphthalene under nitrogen atmosphere. The mixture was brought to reflux, and heating was continued for 2 hours. After being cooled, 50 ml of hexane was added; the precipitate was filtered off and then repetitively washed with diethyl ether in order to remove 1-chloronaphthalene. The crude product was placed in a sublimation apparatus, and the yellow-white impurities were sublimed at 10^{-2} Torr (1.33 Pa) at a bath temperature of 150 °C. Then the solid was placed in the thimble of a Soxhlet extractor and treated 48 hours with petroleum ether (b.p. 80–90 °C) in order to remove all unreacted tetrafluorophthalonitrile. The residue was dissolved in THF, filtered off, and the filtrate was concentrated on a rotary evaporator. The solid was redissolved in 5 ml of THF, precipitated with hexane, centrifuged, and the greenish supernatant was removed. This procedure was repeated until the supernatant was colorless. The same operation was performed with methanol as precipitating agent. The product was vacuum dried

(60 °C, 8 h) leading to 0.3 g (42%) of a dark blue powder. Any attempt to purify the product by column chromatography was not successful.

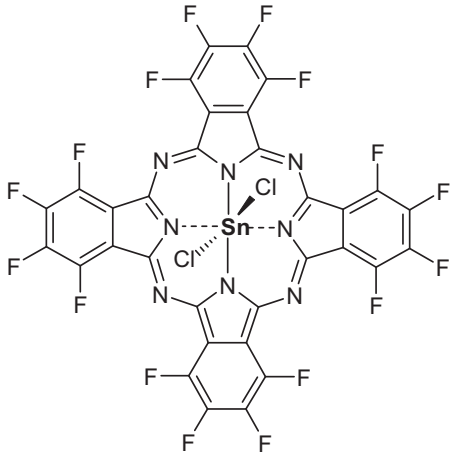

M = 990 g mol^{-1}
F_{16}PcSnCl_2 (16)

UV/Vis ($CHCl_3$): λ (in nm) = 708, 678, 637, 368.

IR (KBr): ν (in cm^{-1}) = 1743, 1634, 1524, 1489, 1455, 1427, 1352, 1302 (C-F), 1255 (C-F), 1178, 1140, 1062, 1023, 973, 925, 882, 830, 795, 753, 610.

ESI-MS (negative ion mode) *m/z* = 989.7[M^-], 954.8[M – Cl^-]$^-$, 919.8[M – 2Cl^-]$^-$.

6.4.15 Synthesis of dichlorogermanium(IV) hexadecafluorophthalocyanine (17)

A dry powder of tetrafluorophthalonitrile (**IX**) (0.3 g, 1.5 mmol) was placed into an ampoule. The vial was repeatedly flushing with argon, and then 0.06 ml of $GeCl_4$ (0.1 g, 0.5 mmol) was transferred into the ampoule via syringe. The tube was sealed under vacuum (10^{-2} Torr = 1.33 Pa) and heated at 250 °C for 18 hours. The solid product was crushed, dissolved in a minimum volume of chloroform and purified by column chromatography on silica gel using chloroform as the eluent. The blue band was collected and concentrated, affording 0.1 g (28%) of a blue microcrystals.

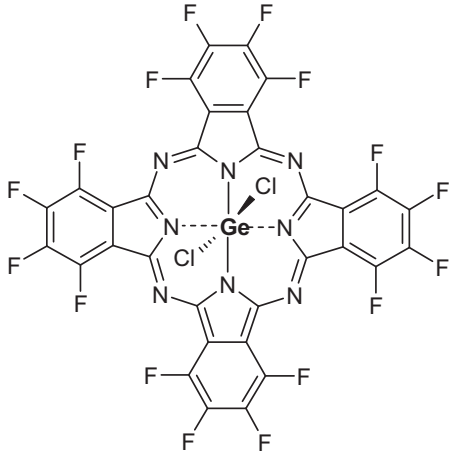

M = 944 g mol-1
F_{16}PcGeCl_2 (17)

UV/Vis ($CHCl_3$): λ (in nm) = 697, 666, 627, 357.

IR (KBr): ν (in cm^{-1}) = 1739, 1633, 1523, 1488, 1455, 1427, 1351, 1314, 1301, 1255 (C-F), 1177, 1140, 1062, 1022, 971, 884, 793, 751, 609.

ESI-MS (negative ion mode) *m/z* = 943.6[M^-].

6.4.16 Synthesis of dichlorotin(IV) 2,9,16,23-tetranitrophthalocyanine (18)

4-Nitrophthalic anhydride (**IV**) (2.5 g, 13 mmol), urea (3.14 g, 52 mmol), ammonium molybdate (0.03 g) and $SnCl_2$ were suspended in 20 ml of dry nitrobenzene The suspension was magnetically stirred and heated at 200 °C for 1 hours and then kept at 190 °C for additional 5 hours. The brownish green suspension was cooled to 90 °C, diluted with 70 ml of ethanol, filtered hot, and washed with ethanol, methanol, and acetone. The residue was placed in the thimble of a Soxhlet extractor and treated consecutively with petroleum ether (8 h), methanol (16 h) and acetone (16). The product was dried in vacuum at 80 °C (12 h) gave 2.2 g (76%) of a dark blue powder.

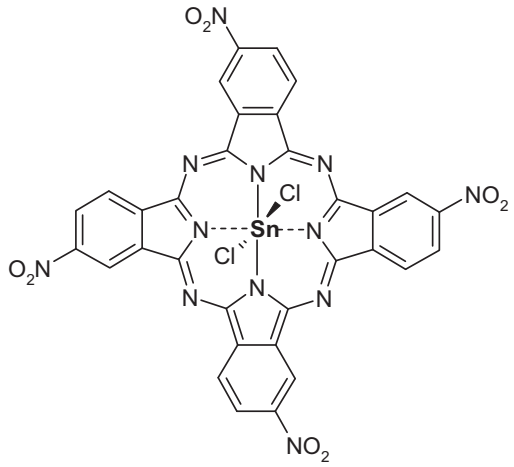

M = 882 g mol^{-1}
(βNO$_2$)$_4$PcSnCl$_2$ (18)

UV/Vis (DMF): λ (in nm) = 701, 348.

IR (KBr): ν (in cm^{-1}) = 3013 (=C-H), 2900, 1748, 1633, 1527 (NO_2), 1492, 1458, 1426, 1352 (NO_2), 1325, 1290, 1254, 1178, 1140, 1105, 1063, 1022, 994, 969, 919, 855, 754.

ESI-MS (negative ion mode) *m/z* = 881.8[M^-], 846.9[$M - Cl^-]^-$, 812[$M - 2Cl^-]^-$.

MS (MALDI-MS, Matrix:DCTD) *m/z* = 882.92[M^+], 845.94[$M - Cl^-]^+$, 812.99[$M - 2Cl^-]^+$.

6.4.17 Synthesis of dichlorotin(IV) 1,8,15,22-tetranitrophthalocyanine (19)

3-Nitrophthalic anhydride (**V**) (1.6 g, 8.5 mmol), urea (2 g, 32.5 mmol), and ammonium molybdate (0.015 g) were placed in a two-necked round-bottomed flask. 15 ml of dry 1-chloronaphthalene was added and the suspension was stirred for 5 minutes under nitrogen. Then 0.32 ml of $SnCl_4$ (0.73 g, 2.5 mmol) was added directly into the flask via syringe, and the mixture was heated at 200 °C for 2 hours. After being cooled, 50 ml of hexane was added, precipitate filtered off and washed with petroleum ether. The crude product was placed in the thimble of a Soxhlet extractor and treated consecutively with petroleum ether (8 h), diethyl ether (8 h) and ethyl acetate (8 h) to remove first brown and yellow impurities. Then the solid was dissolved in THF, filtered off, and the filtrate was concentrated. The product was further

redissolved in 10 ml of THF, precipitated with 70 ml of methanol, centrifuged, and the supernatant was removed. This operation was repeated until the supernatant was colorless. Finally the product was dried in vacuum at 60 °C (12 h) led to 0.4 g (23%) of a dark blue powder.

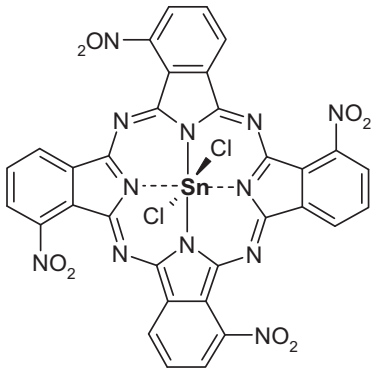

M = 882 g mol^{-1}
(αNO$_2$)$_4$PcSnCl$_2$ (19)

UV/Vis (THF): λ (in nm) = 685, 632, 339.

IR (KBr): ν (in cm^{-1}) = 3131 (=C-H), 2974, 1738, 1633, 1537 (NO_2), 1492, 1426, 1359 (NO_2), 1290, 1254, 1178, 1139, 1106, 1062, 1023, 996, 881, 803, 753.

ESI-MS (negative ion mode) *m/z* = 881.8[M$^-$].

6.4.18 Synthesis of dichlorogermanium(IV) 2,9,16,23-tetranitrophthalocyanine (20)

4-Nitrophthalic anhydride (**IV**) (1 g, 5 mmol), urea (1.3 g, 20 mmol), and ammonium molybdate (0.01 g) were placed in a two-necked round-bottomed flask. 15 ml of dry nitrobenzene was added, and the suspension was stirred for 5 minutes under nitrogen. Then 0.23 ml of $GeCl_4$ (0.43 g, 2 mmol) was injected directly into the flask with a hypodermic needle, and the mixture was heated at 195 °C within 2 hours and then kept at 180 °C for additional 4 hours. The olive-brown suspension was cooled to 90 °C, diluted with 50 ml of ethanol, filtered hot, and washed with ethanol, methanol and acetone. The residue was placed in the thimble of a Soxhlet extractor and treated consecutively with petroleum ether (8 h), methanol (16 h) and acetone (16 h). Finally the product was dried in vacuum at 80 °C (12 h) yielded 0.6 g (58%) of a blue powder.

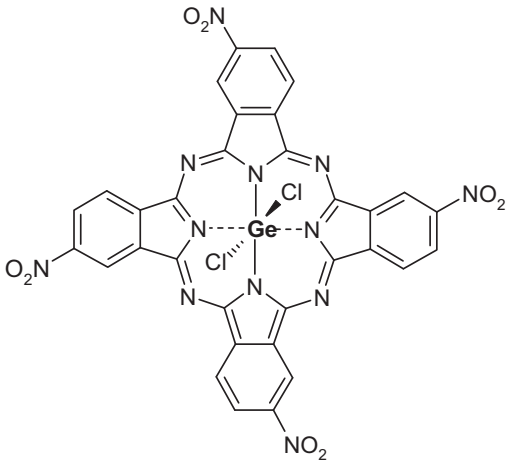

M = 836 g mol^{-1}
(βNO$_2$)$_4$PcGeCl$_2$ (20)

UV/Vis (DMF): λ (in nm) = 680, 344.

IR (KBr): ν (in cm^{-1}) = 3095 (=C-H), 2929, 1747, 1632, 1528 (NO_2), 1492, 1426, 1350 (NO_2), 1334, 1254, 1176, 1142, 1105, 1064, 1023, 968, 852 (C-H), 760, 728.

ESI-MS (negative ion mode) *m/z* = 835.9[M$^-$].

6.4.19 Synthesis of dihydroxygermanium(IV) 2,9,16,23-tetranitrophthalocyanine (21)

Dichlorogermanium(IV) 2,9,16,23-tetranitrophthalocyanine (**20**) (0.3 g, 0.36 mmol) was dissolved in 15 ml of pyridine. The flask was placed in an ice bath, and then 15 ml of 25% ammonium hydroxide was slowly added under magnetic stirring. The resulting mixture was heated at reflux for 17 hours. After being cooled to room temperature, the solution formed was evaporated to a solid with rotary evaporator under reduced pressure. The solid was placed in a thimble of a Soxhlet extractor and treated with methanol for 6 hours in order to remove yellow impurities and then with acetone (5 h). The solid was dried in vacuum (70 °C, 10 h) yielded 0.21 g (75%) of a dark blue powder.

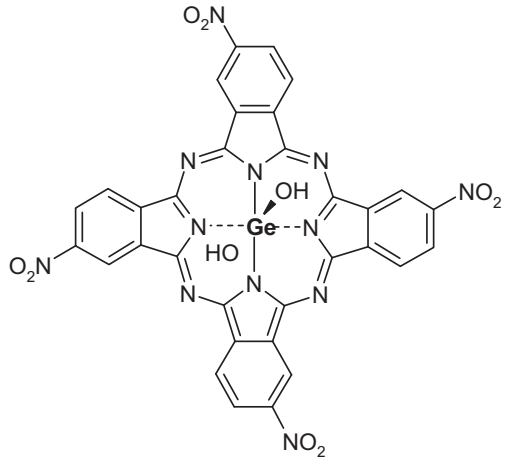

M = 800 g mol^{-1}
(βNO$_2$)$_4$PcGe(OH)$_2$ (21)

UV/Vis (pyridine): λ (in nm) = 682, 656, 358.

IR (KBr): ν (in cm^{-1}) = 3383 (OH), 3094 (=C-H), 2858, 2202, 1734, 1615, 1526 (NO_2), 1454, 1409, 1346 (NO_2), 1256, 1179, 1142, 1102, 1076, 1025, 997, 937, 887 , 851, 818 (C-H), 809, 760, 729, 682, 653, 485.

ESI-MS (positive ion mode) *m/z* = 783.1[M – OH$^-$]$^+$.

ESI-MS (negativeion mode) *m/z* = 799.9[M$^-$].

6.4.20 Synthesis of dichlorogermanium(IV) 1,8,15,22-tetranitrophthalocyanine (22)

A mixture containing 1.45 g of 3-nitrophthalic anhydride (**V**) (7.5 mmol), urea (1.8 g, 30 mmol), and ammonium molybdate (0.013 g) was magnetically stirred under nitrogen atmosphere. 15 ml of dry nitrobenzene was added, and the flask was placed in a metal bath at 180 °C. Then, 0.28 ml of $GeCl_4$ (0.53 g, 2.5 mmol) was added directly into the flask via syringe, the mixture was heated at 200 °C within 1 hour and then kept at 180 – 190 °C for additional 3 hours. After cooling, the mixture was poured into 60 ml of hexane. The precipitate was filtered, extracted with diethyl ether (8 h) and then with ethyl acetate (8 h) to remove brown and yellow impurities. Then the solid was dissolved in THF, filtered off, and the filtrate was concentrated. The product was further redissolved in 10 ml of THF, precipitated with 70 ml of methanol, centrifuged, and the supernatant was removed. This operation was repeated several times until the supernatant was colorless. After being dried in vacuum at 60 °C for 8 hours, 0.2 g (14%) of a dark blue powder was obtained.

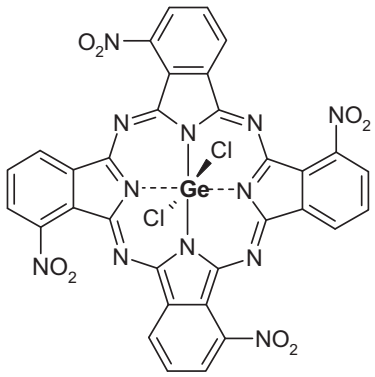

M = 836 g mol^{-1}
(αNO$_2$)$_4$PcGeCl$_2$ (22)

UV/Vis (DMF): λ (in nm) = 671, 338.

IR (KBr): ν (in cm^{-1}) = 3021, 1750, 1633, 1537 (NO_2), 1491, 1425, 1361 (NO_2), 1290, 1254, 1178, 1139, 1106, 1061, 1022, 994, 968, 920, 881, 746, 534.

ESI-MS (negative ion mode) *m/z* = 835.9[M$^-$].

6.4.21 Synthesis of bis(3,5-di-*tert*-butylphenoxy)germanium(IV) 2,9,16,23-tetranitrophthalocyanine (23)

A mixture of dichlorogermanium(IV) 2,9,16,23-tetranitrophthalocyanine (**20**) (0.6 g, 0.72 mmol), 3,5-di-*tert*-butylphenol (0.3 g, 1.4 mmol), dry, fine powdered potassium carbonate (K_2CO_3) (0.2 g, 1.4 mmol) and 18-crown-6 (0.38 g, 1.4 mmol) was suspended in 6 ml of dry 1,2,4-trimethylbenzene under argon atmosphere. The flask was placed in a metal bath at 120

°C. The reaction was allowed to proceed at 120 °C with magnetic stirring. The reaction was monitored by TLC (silica gel/$CHCl_3$) and stopped when all of dichlorogermanium(IV) tetra-2,9,16,23-nitrophthalocyanine had been consumed. The black – blue mixture was cooled, and the solvent was removed by distillation under reduced pressure. The resulting dark blue residue was purified on silica gel using THF as the eluent in order to remove large amounts of the impurities. After removal of the solvent, the solid was redissolved in a minimum volume of CH_2Cl_2 and loaded onto short silica column. Elution with CH_2Cl_2 afforded desired blue band. The solvent was removed, and the product was dried in vacuum at 60 °C for 6 hours.
Yield: 0.21 g (25%) of blue microcrystals.

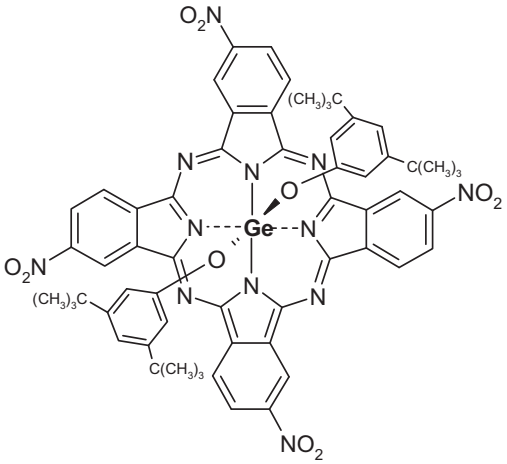

M = 1176 g mol^{-1}
(βNO$_2$)$_4$PcGe(*t*Bu$_2$P)$_2$ (23)

UV/Vis ($CHCl_3$): λ (in nm) = 687, 622, 354.

IR (KBr): ν (in cm^{-1}) = 3095, 2965 (CH_3), 2905, 2866 (CH_3), 1738, 1633, 1532 (NO_2), 1492, 1427, 1351 (NO_2), 1332, 1292, 1254, 1178, 1142, 1105, 1063, 1023, 998, 968, 905, 856, 800 (C-H), 760, 727.

ESI-MS (negativeion mode) *m/z* = 1176.3[M^-], 971.1[$M - C_{14}H_{21}O^-]^-$.

6.4.22 Synthesis of dichlorotin(IV) 2,3,9,10,16,17,23,24-octacyanophthalocyanine (24)

A dry powder of tetracyanobenzene (**X**) (0.15 g, 0.85 mmol) was mixed with 0.6 g of anhydrous $SnCl_2$ (3.1 mmol). The mixture was transferred into a glass ampoule. After evacuating and flushing with argon the tube was sealed under vacuum (10^{-2} Torr = 1.33 Pa) and heated at 200 °C for 2 hours. The solid product was crushed, placed in the thimble of a Soxhlet extractor, and treated with acetone (12 h), and then with methanol (12 h). The product was air-dried.
Yield: 0.12 g (63%) of a dark blue powder.

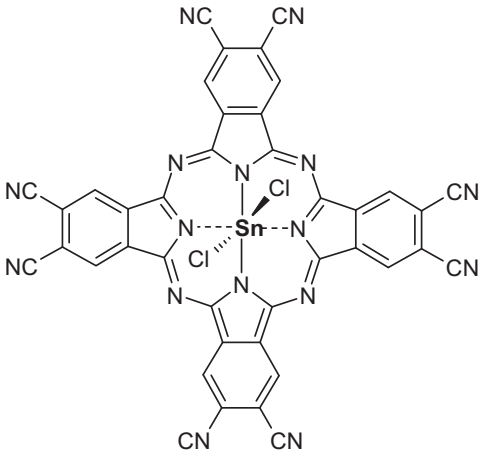

M = 902 g mol^{-1}
(CN)$_8$PcSnCl$_2$ (24)

UV/Vis (THF): λ (in nm) = 703, 632, 600, 372.

IR (KBr): ν (in cm^{-1}) = 2233 (C≡N), 1771, 1697, 1520, 1491, 1408, 1377, 1305, 1254, 1176, 1146, 1106, 1062, 1023, 995, 921, 881, 755, 126.

ESI-MS (negative ion mode) *m/z* = 901.7[M$^-$]; 866.8[M - Cl$^-$]$^-$, 831.9[M –2Cl$^-$]$^-$.

6.4.23 Synthesis of chloroindium(III) 2,9,16,23-tetrakis(*tert*-butyl)phthalocyanine (25)

This compound was prepared according to method described by Hanack [3]. A reaction mixture consisting of $InCl_3$ (0.3 g, 1.36 mmol), of 4-*tert*-butylphthalonitrile (**VI**) (1 g, 5.43 mmol), and of DBU (0.2 ml) in 5 ml of freshly distilled quinoline was stirred at 180 °C for 5 hours. The solvent was removed by distillation under reduced pressure. A dark green residue was chromatographed on silica gel using chloroform as the eluent in order to get rid of large amounts of the impurities. The crude product was then recrystallized from mixture of CH_2Cl_2/MeOH (4:3) by slowly evaporating the more volatile CH_2Cl_2 in a rotary evaporator at 40 °C under slightly reduced pressure. To complete crystallization, the mixture was kept in a refrigerator overnight. Phthalocyanine was collected by filtration, washed three times with methanol and dried in vacuum at 80 °C for 13 hours.

Yield: 0.56 g (47%) of a blue microcrystals.

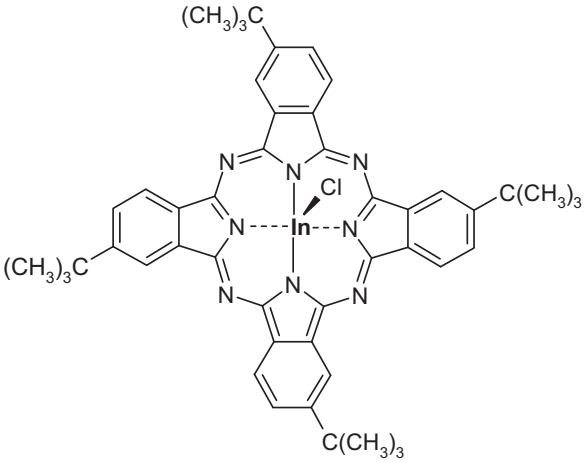

M = 886 g mol^{-1}
(***t*-Bu)$_4$PcInCl** (**25**)

UV/Vis ($CHCl_3$): λ (in nm) = 698, 668, 629, 340.

IR (KBr): ν (in cm^{-1}) = 2964 (CH_3), 2865 (CH_3), 1749, 1633, 1519, 1490, 1426, 1364 ($C(CH_3)_3$), 1328, 1255, 1178, 1145, 1105, 1064, 1022, 995, 968, 922, 882, 778, 746, 692, 671, 525.

ESI-MS (negative ion mode) *m/z* = 886.3[M$^-$].

6.5 References

[1] R. D. Joyner, M. E. Kenney, *J. Am.Chem. Soc.*, **1960**, 82, 5790.

[2] J. M. Birchall, R. N. Haszeldine, J. O. Morley, *J. Chem. Soc. (C),* **1970**, 2667.

[3] M. Hanack, H. Heckmann, *Eur. J. Inorg. Chem.*, **1998**, 367.

7. Preparation of films of phthalocyanines embedded in different polymers

The aim of this research was to prepare solid-state thin films of various phthalocyanine (Pc) compounds embedded in different polymers on glass or sapphire via spin casting and drop casting techniques. By UV/Vis spectra the distribution of the phthalocyanines in the polymer solid-state samples was probed, and thicknesses of the films were measured using a Dektak instrument.

7.1 Materials

The following tetra-substituted **(nPhO)$_4$PcSnCl$_2$** (**5**), **(fPhO)$_4$PcSnCl$_2$** (**6**), **(fPhO)$_4$PcGeCl$_2$** (**7**), **(*β*NO$_2$)$_4$PcGe(*t*Bu$_2$P)$_2$** (**23**), **(*t*-Bu)$_4$PcInCl** (**25**), **(PhO)$_4$PcH$_2$** (**26**) [1], **(*t*-BuPhO)$_4$PcH$_2$** (**27**) [1], **(Sul)$_4$PcGa** (**28**) [2], octa-substituted **(BuO)$_8$PcZn** (**29**) [1, 3], **(BuO)$_8$PcPb** (**30**) [1, 3], **(BuO)$_8$PcCu** (**31**) [1, 3], and hexadeca-substituted **Cl$_{16}$PcSn(*t*Bu$_2$P)$_2$** (**14**), **Cl$_{16}$PcGe(*t*Bu$_2$P)$_2$** (**15**), **F$_{16}$PcSnCl$_2$** (**16**) [4] phthalocyanines were chosen for the preparation of thin films in polymers.

The synthesis and structural characterizations of **(nPhO)$_4$PcSnCl$_2$** (**5**), **(fPhO)$_4$PcSnCl$_2$** (**6**), **(fPhO)$_4$PcGeCl$_2$** (**7**), **(*β*NO$_2$)$_4$PcGe(*t*Bu$_2$P)$_2$** (**23**), **Cl$_{16}$PcSn(*t*Bu$_2$P)$_2$** (**14**), **Cl$_{16}$PcGe(*t*Bu$_2$P)$_2$** (**15**) and **F$_{16}$PcSnCl$_2$** (**16**) were carried out as described in Chapter 6.4. The phthalocyanine compounds, **(PhO)$_4$PcH$_2$** (**26**) [1], **(*t*-BuPhO)$_4$PcH$_2$** (**27**) [1], **(Sul)$_4$PcGa** (**28**) [3], **(BuO)$_8$PcZn** (**29**) [1, 2], **(BuO)$_8$PcPb** (**30**) [1, 2] and **(BuO)$_8$PcCu** (**31**) [1, 2] shown in **Figure 7.1** were previously synthesized and characterized.

Solvents were purified by distillation. Methylcyclohexanone was used as a mixture of isomers (Merck-Schuchardt). All other chemicals were commercially available and used without further purification. The following commercially available organic polymers were used: poly(styrene) (PS) (BASF), poly(methylmethacrylate) (PMMA) (Acros Organics) $\overline{M}_w$ = 350000 and $\overline{M}_n$ = 60000, poly(vinylchloride) (PVC) (Aldrich) $\overline{M}_w$ = 106000 and $\overline{M}_n$ = 60000. As carriers for thin films commercial glass slides size 20 x 20 mm and thickness 1 mm from Menzel-Glaser and circular sapphire plates with a diameter 25 mm, thickness 1.00 mm from RODITI were used.

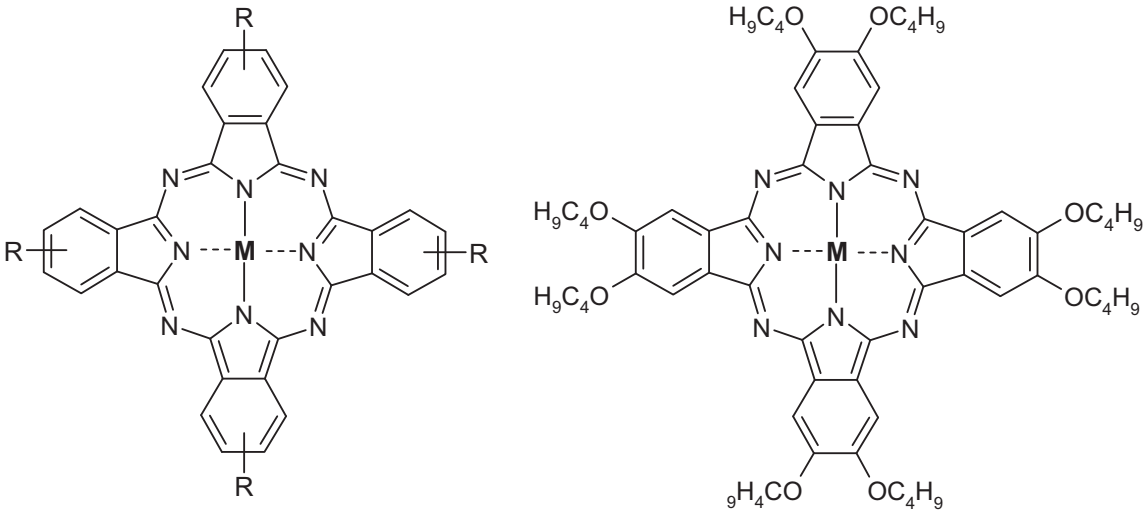

26 M = 2H, R = $-OC_6H_5$
27 M = 2H, R = $-OC_6H_5$-$C(CH_3)_3$
28 M = Ga(OH), R = $-SO_3H$

29 M = Zn
30 M = Pb
31 M = Cu

Figure 7.1 Structure of phthalocyanine complexes **26** - **31**.

7.2 Instrumental methods

A spin coater CONVAC 1001S was used for solid-state films preparation. UV/Vis spectra were recorded on a Perkin Elmer Lambda 2 to probe the linear optical properties of films. The resulting film thicknesses were measured using a Dektak 3030 TS instrument.

7.3 Preparation of phthalocyanine films

7.3.1 Films prepared by spin casting technique

For the preparation of the polymer solutions 3 g PS or 1.3 g PVC was dissolved in 10 mL methylcyclohexanone under stirring for 24 h. In the case of PMMA 1.5 g of this polymer was dissolved in 10 mL methylcyclohexanone by treatment in an ultra sonic bath approximately for 30 h to form a clear viscous solution. Solutions of phthalocyanines were prepared by dissolving 1.5×10^{-3} mol of each phthalocyanine in 0.5 mL appropriate solvent in order to obtain concentrations of 3×10^{-3} mol L^{-1}. Composite solutions for coating were prepared by mixing 0.5 mL of phthalocyanine solution with 2.5 mL of a polymer solution to obtain phthalocyanine concentrations of 1×10^{-3} mol L^{-1} (**Table 7.1**). In case of compounds, **27** and **29,** 7.5×10^{-3} and 3×10^{-3} mol of Pcs were taken to prepare final concentration of phthalocyanines in polymer solution determined to be 5×10^{-3} and 2×10^{-3} mol L^{-1}, respectively.

Table 7.1 Solvent for dissolving the phthalocyanines and concentration of Pc in polymer solution.

Compound	Solvent	Concentration of Pc in polymer solution [mol L^{-1}]
$(nPhO)_4PcSnCl_2$ (5)	$CHCl_3$	1×10^{-3}
$(fPhO)_4PcSnCl_2$ (6)	toluene	1×10^{-3}
$(fPhO)_4PcGeCl_2$ (7)	toluene	1×10^{-3}
$Cl_{16}PcSn(tBu_2P)_2$ (14)	toluene	1×10^{-3}
$Cl_{16}PcGe(tBu_2P)_2$ (15)	toluene	1×10^{-3}
$F_{16}PcSnCl_2$ (16)	THF	1×10^{-3}
$(\beta NO_2)_4PcGe(tBu_2P)_2$ (23)	$CHCl_3$	1×10^{-3}
$(t\text{-}Bu)_4PcInCl$ (25)	$CHCl_3$	1×10^{-3}
$(PhO)_4PcH_2$ (26)	toluene	1×10^{-3}
$(t\text{-}BuPhO)_4PcH_2$ (27)	toluene	5×10^{-3}
$(Sul)_4PcGa$ (28)	water	1×10^{-3}
$(BuO)_8PcZn$ (29)	$CHCl_3$	1×10^{-3} [a] and 2×10^{-3} [b]
$(BuO)_8PcPb$ (30)	toluene	1×10^{-3}
$(BuO)_8PcCu$ (31)	toluene	1×10^{-3}

[a] for drop coating method
[b] for spin coating method

The solutions were gently stirred for ~ 20 min in order to get homogeneous solution and to minimise bubbles formation. The undertaking effort to make films was preparation of multi-layer polymeric films on glass substrates.

Mono-layer films were prepared by dropping approximately 0.3 mL of a solution containing 1×10^{-3} mol L^{-1} of a Pc and 0.038 g PVC or 0.044 g PMMA onto a glass or sapphire plate rotating with speed of 3000 rpm for 5 min. Afterwards the layer was dried at 100 ^{o}C for 1 h. Multi-layer films were obtained by a sequential deposition and spin casting process. As carrier for multi-layer films, glass slides were used. The films were treated at 100 ^{o}C for 1 h between successive layer preparations. Optically homogenous films possessing deep glassy

blue or green appearance were obtained. Films with 3 to 7 layers were prepared possessing thicknesses between 0.8 and 2.3 μm. The abbreviation system for Pc films in different polymers is same as described in Chapter 5th. Number of layers, their thicknesses and UV/Vis data of phthalocyanine films are collected in **Table 7.2**.

Table 7.2 Thickness (*d*), number of layers and UV/Vis data of phthalocyanine films in polymers.

Compound	Polymer	Solid-state sample	No of layers	Absorbance at 532 [nm]	*d* [μm]	Q-band [nm]
$(nPhO)_4PcSnCl_2$ (5)	PMMA	**5PMMA3**	3	0.1054	0.9	704
		5PMMA6	6	0.1331	1.8	704
$(fPhO)_4PcSnCl_2$ (6)	PMMA	**6PMMA3**	3	0.0793	1.0	708
		6PMMA6	6	0.0851	2.3	708
$(fPhO)_4PcGeCl_2$ (7)	PMMA	**7PMMA3**	3	0.0824	1.0	700
		7PMMA6	6	0.0940	1.9	699
$Cl_{16}PcSn(tBu_2P)_2$ (14)	PMMA	**14PMMA3**	3	0.1010	0.9	737
		14PMMA6	6	0.1393	2.0	737
$Cl_{16}PcGe(tBu_2P)_2$ (15)	PMMA	**15PMMA3**	3	0.1049	0.9	728
		15PMMA6	6	0.1617	1.9	728
$F_{16}PcSnCl_2$ (16)	PMMA	**16PMMA3**	3	0.0820	0.8	707
		16PMMA6	6	0.1362	1.8	707
$(\beta NO_2)_4PcGe(tBu_2P)_2$ (23)	PMMA	**23PMMA3**	3	0.1043	0.8	708
		23PMMA6	6	0.1863	1.5	707
$(t\text{-}Bu)_4PcInCl$ (25)	PMMA	**25PMMA3**	3	0.0797	0.9	693
		25PMMA6	6	0.1167	1.9	694
$(nPhO)_4PcSnCl_2$ (5)	PVC	**5PVC4**	4	0.0711	0.9	707
		5PVC7	7	0.1067	1.8	707

$(fPhO)_4PcSnCl_2$ (6)	PVC	**6PVC4**	4	0.0574	1.0	709
		6PVC7	7	0.0688	2.3	709
$(fPhO)_4PcGeCl_2$ (7)	PVC	**7PVC4**	4	0.0800	1.0	703
		7PVC7	7	0.0814	1.9	702
$Cl_{16}PcSn(tBu_2P)_2$ (14)	PVC	**14PVC4**	4	0.0933	0.9	738
		14PVC7	7	0.1581	1.6	738
$Cl_{16}PcGe(tBu_2P)_2$ (15)	PVC	**15PVC4**	4	0.0906	0.8	731
		15PVC7	7	0.1315	1.5	731
$F_{16}PcSnCl_2$ (16)	PVC	**16PVC4**	4	0.1128	0.9	712
		16PVC7	7	0.1802	1.9	713
$(\beta NO_2)_4PcGe(tBu_2P)_2$ (23)	PVC	**23PVC4**	4	0.1360	0.8	695
		23PVC7	7	0.2096	1.5	693
$(t\text{-}Bu)_4PcInCl$ (25)	PVC	**25PVC4**	4	0.0762	0.8	701
		25PVC7	7	0.0847	1.4	701

Also two-side films (double layer) were fabricated. For two-side films a mono-layer of polymer-phthalocyanine composite was deposited in addition on the reverse side under the same condition as described above. As carrier for a double layer phthalocyanine films sapphire substrates were used. Number of layers, thickness of one and other side of films and overall thicknesses as well as UV/Vis data of double layer phthalocyanine films are presented in **Table 7.3**.

Table 7.3 Thickness (*d*), number of layers and UV/Vis data of two-side phthalocyanine films in polymers.

Compound	Polymer	Solid-state sample	No of layers	Absorbance at 532 [nm]	*d* [μm]			Q-band [nm]
					one side	other side	total	
$(PhO)_4PcH_2$ (26)	PVC	**26PVC3**	1+2	0.346	0.1	0.4	0.5	626
(*t*-$BuPhO)_4PcH_2$ (27)	PS	**27PS3**	2+1	0.193	0.3	0.2	0.5	604
$(BuO)_8PcZn$ (29)	PS	**29PS3**	2+1	0.180	0.3	0.3	0.6	676
$(BuO)_8PcZn$ (29)	PVC	**29PVC4**	2+2	0.176	0.3	0.2	0.5	677
$(BuO)_8PcPb$ (30)	PVC	**30PVC5**	3+2	0.402	0.3	0.2	0.5	717
$(BuO)_8PcCu$ (31)	PMMA	**31PMMA7**	5+2	0.305	0.6	0.3	0.9	615

7.3.2 Sol gel solution for drop coating

At first solution by mixing 2 g tetraethoxysilane (TEOS), 1 g phenyltriethoxysilane (PhTriEOS), 10 mL ethanol and 0.33 mL 1N HCl was prepared. A solution of 1.58×10^{-5} mol of compound **$(Sul)_4PcGa$** (**28**) in 2 mL of water was added. The mixture was stirred for 2 hours at 60 ^{0}C. After this time 0.2 mL of poly(ethylene glycol) (PEG) was added, and the mixture was stirred at 60 ^{0}C for additional 1hour.

7.3.3 Films prepared by drop casting technique

A glass ring with a diameter of 25 mm and a height of 10 mm was placed onto a sapphire substrate. 3 mL of the polymer-phthalocyanine solution containing 1×10^{-3} mol L^{-1} of a Pc was poured onto a sapphire substrate using a syringe. The solution thickness inside the glass ring was ~ 5-6 mm. The majority of the organic solvent was slowly evaporated at room temperature for 48 h. The film was additionally dried at 100 ^{0}C for 5 hours. Concentrations, thicknesses and some UV/Vis data of drop coated phthalocyanine films are collected in **Table 7.4**.

Table 7.4 Thickness (*d*) and UV/Vis data of drop coated phthalocyanine films in polymers.

Compound	Polymer	Abbreviation for Pc film	Concentration Pc in film [mol L^{-1}]	Ab at 532[nm]	*d* [µm]	Q-band [nm]
(Sul)$_4$PcGa (28)	-	**28GaPcGel**	0.436	0.317	109.0	672
(BuO)$_8$PcZn (29)	PMMA	**29PMMA1**	0.430	1.450	244.0	642
(BuO)$_8$PcPb (30)	PS	**30PS1**	0.435	1.083	205.0	631
(BuO)$_8$PcCu (31)	PMMA	**31PMMA1**	0.432	1.316	117.0	662

7.4 References

[1] D. Wöhrle, G. Schnurpfeil, G. Knothe, *Dyes and Pigments*, **1992**, 18, 91.

[2] G. Schneider, D. Wöhrle, W.Spiller, J. Stark, G. Schulz-Ekloff, *Photochem. Photobiol.*, **1994**, 60, 333.

[3] D. Wöhrle, V. Schmidt, *J.Chem.Soc., Dalton Trans.,* **1988**, 549.

[4] J. M. Birchall, R. N. Haszeldine, J. O. Morley, *J. Chem. Soc. (C),* **1970**, 2667.

8. Optical limiting properties of phthalocyanine complexes in solutions and in films

8.1 Introduction

The domain of the nonlinear optics came into view in 1960 when Maiman [1] presented the first operating ruby laser. Soon frequency doubling in a quartz crystal illuminated by such a laser was demonstrated [2]. Lasers are devices which generate a visible or invisible light, based on stimulated emission of light. There exist common types of lasers: solid state, gas, fiber and semiconductor lasers. Solid-state lasers include the ruby laser that is the first invented laser [1], the Nd:glass, the Nd:YAG laser and the others. The Nd:YAG laser consist of Nd^{+3} dopants in an yttrium aluminium garnet ($Y_3Al_5O_{12}$) host. The Nd:YAG laser has an emission at 1064 nm, this laser light is transformed into light of second harmonic of frequency 2ν to produce green light at 532 nm.

The inorganic materials were initially made use of construction of nonlinear optic [3]. Early in the eighties was also growing interest in the use of organic materials for nonlinear optical (NLO) application, for instance molecules like azobenzene, benzene, and stilbene [4]. These molecules possess more benefits than inorganic materials such as large nonlinearities, small dielectric constants, low losses, sub-picoseconds response time, and moreover low cost of fabrication. One important class of organic NLO materials is phthalocyanines due to their exceptionally high thermal stability, processability, tremendous architectural flexibility, and highly conjugated π-system. Phthalocyanines have been shown to be the most promising materials for optical limiting available.

Optical limiting (OL) is a nonlinear effect depending on a decrease in the transmittance of the NLO material under high-intensity illumination. The theoretical background of phenomenon of optical limiting and reverse saturable absorption (RSA) and for a five-level system is presented in Chapter 3.1. Under a steady state approximation, Hercher [5] conducted a broad analysis of saturable absorbers using a three-level energy scheme, where the populations remain constant for the duration of the incoming pulse. He derived a general expression for the absorption coefficient in terms of a parameter called the saturation intensity, I_{sat}. Laser rate equations were used to stimulate the excitation and subsequent relaxation of the system. The vibrational levels of the electronic states are assumed negligible and for the sake of simplicity the laser pulse width is assumed to be longer than any of the lifetimes associated with the

levels. To further simplify matters it can be assumed that relaxation out of states S_2 and T_2 (**Figure 3.2**, Chapter 3.1) is so rapid that the population of these two levels may be neglected. Optical limiting with phthalocyanines was first reported by Coulter *et al.* [6] in 1989 for chloroaluminium(III) phthalocyanine (**CAP**) solution (**Figure. 8.1**).

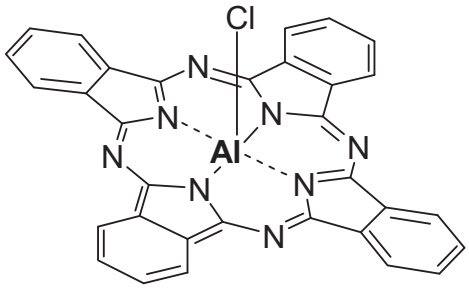

Figure 8.1 Chloroaluminium(III) phthalocyanine (**CAP**) reported as first for optical limiting.

The limiting measurements were carried out at 532 nm using 5 nanosecond pulses. It turned out that **CAP** exhibited reverse saturation absorption (RSA) and it is a promising candidate for good optical limiter. In the aftermath of this discovery many other phthalocyanines have been investigated in order to improve their optical limiting capabilities.

Phthalocyanines are very promising materials for optical limiting in the visible and NIR spectral range, because of their appropriate photophysical properties. In general, tendencies to improve OL effect in phthalocyanines are as follows:

- heavy metal ions in the ligand (increase of intersystem crossing rate from $S_1 \rightarrow T_1$),
- axial substituents (reduce aggregation and enhance of perpendicular moment),
- peripheral substituents with strong especially electron-withdrawing effect (alteration of the electronic properties, variation of transition dipole moment).

A number of various parameters have been determined and cited in literature to estimate the effectiveness of optical limiting materials (Chapter 3.1). In this work that investigate optical limiting properties of phthalocyanines in solution and in solid-state, there will be given different parameters for each compound that was measured. The following parameters will be presented for the prepared phthalocyanines as well as for their polymeric films:

- concentration of Pcs in solution,

- κ value *i.e.* the ratio σ_{ex}/σ_0 of the excited triplet state and ground state absorption cross section (κ <1 saturable linear absorption occurs, κ >1 reverse saturable absorption occurs which is necessary for OL),
- the effective imaginary third-order susceptibility ($\mathrm{Im}\{\chi^{(3)}\}$),
- linear absorption coefficient (α_0),
- the energy density at which the material saturates (F_{Sat});
- the intensity-dependent nonlinear absorption coefficient (β_I),
- the thickness (d) of Pc films.

8.2 Equipment and conditions of optical limiting measurement

Optical limiting measurements described in this thesis were conducted using the open-aperture z-scan [7]. They were performed using 6 ns Gaussian pulses from a Q switched Nd:YAG laser. The beam was spatially filtered to remove the higher order modes and tightly focused with a 9 cm focal length lens. The laser was operated at its second harmonic, *i.e.* 532 nm, with a pulse repetition rate of 10 Hz. The irradiation at 532 nm is then a near-resonant excitation.

This measures the total transmittance through the sample as a function of incident laser intensity while the sample is gradually moved through the focus of a lens (along the z-axis) with a stepper-motor-driven translation stage. The set-up is shown schematically in **Figure 8.2**.

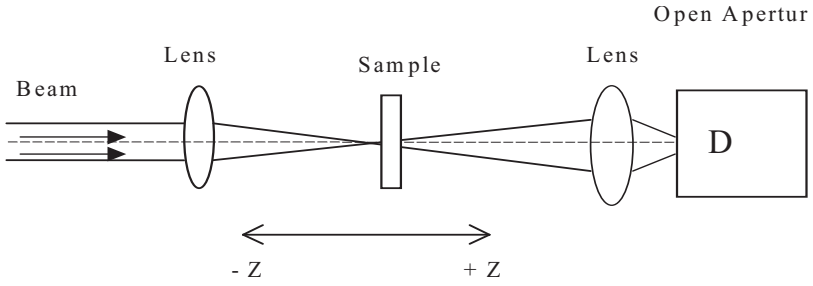

Figure 8.2 Open-aperture z-scans.

The normalized transmittance as a function of position z, $T_{\mathrm{Norm}}(z)$, is given by the following **Equation 8.1** [8]

$$T_{Norm}(z) = \frac{Log_e[1+q_0(z)]}{q_0(z)} \qquad (\mathbf{8.1})$$

where $q_0(z)$ is given by **Equation 8.2.**

$$q_0(z) = \frac{q_{00}}{1 + \left(z / z_0 \right)^2} \tag{8.2}$$

z_0 is the diffraction length of the beam, and q_{00} is given by **Equation 8.3** where $L_{eff} = \left[1 - \exp(-\alpha_0 L)\right] / \alpha_0 \beta_{eff}$.

$$q_{00} = \beta_{eff} I_0 L_{eff} \tag{8.3}$$

β_{eff} is the effective intensity dependent nonlinear absorption coefficient; I_0 is the intensity of the light at focus. L_{eff} is known as the effective length of the sample defined in terms of the linear absorption coefficient α_0, and the true optical path length through the sample, L. These equations were incorporated into a computer code and a least squares regression algorithm was used to fit this to the experimental data. All calculations were performed by James Doyle and Sean O'Flaherty from Department of Physics, Trinity College in Dublin.

The imaginary third-order optical susceptibility $\text{Im}(\chi^{(3)})$ which is directly related to the intensity dependent absorption coefficient β_{I} is expressed in **Equation 8.4**, where n_{o} is the linear refractive index, ε_{o} is the permittivity of free space, c is the speed of light and λ is the wavelength of the incident light.

$$\text{Im}\left(\chi^{(3)}\right) = \frac{n_0^2 \varepsilon_0 c \lambda \beta_I}{2\pi} \tag{8.4}$$

All solution experiments were undertaken using a 1 mm path length quartz cuvette. All samples were dissolved in appropriate organic solvent *i.e.* chloroform tetrahydrofuran (THF), dimethylformamide (DMF) and 1-chloronaphthalene. The phthalocyanine solutions were put into a low-power (60 W) sonic bath for about 1 hour in order to obtain homogenous and complete dissolution. Each solution was freshly prepared in Department of Physics, Trinity College in Dublin before experiment. The solid-state films of various phthalocyanine compounds embedded in different polymers prepared via spin casting and drop casting methods were characterised using the z-scan technique.

All open-aperture z-scan data sets were fitted using the method of least-squares regression with **Equation 8.1**, **8.2** and **8.3**. A typical open-aperture z-scan spectrum, for instance, for a 0.5 g L^{-1} solution of **(fPhO)$_4$PcGeCl$_2$** (**7**) in THF under incident focal intensity of 1.15 GW cm^{-2} is presented in **Figure 8.3**.

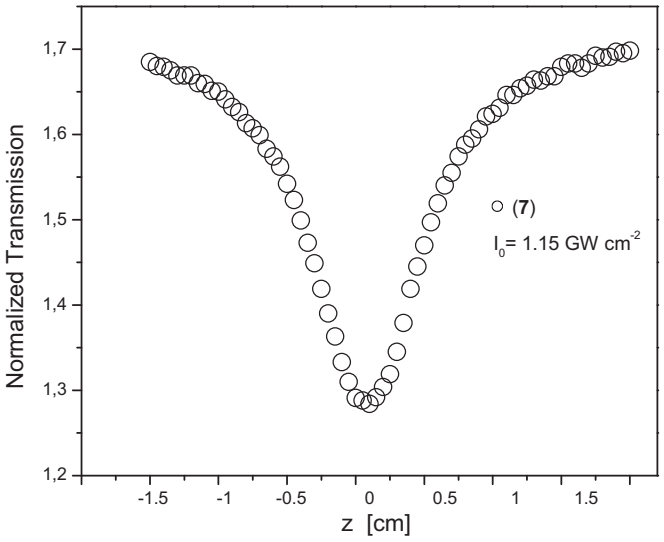

Figure 8.3 Normalized transmission of 0.5 g L^{-1} THF solution of **(fPhO)$_4$PcGeCl$_2$** (**7**) as a function of sample position z.

In **Figure 8.3** the normalized transmission of **(fPhO)$_4$PcGeCl$_2$** (**7**) solution varies with the distance from the focus of a Gaussian beam whose intensity I vary with z as follows [7] where E is the pulse energy in J, τ is the pulse duration in s, and $w(z)$ is the beam radius in m as a function of the distance from the focus z.

$$I(z) = E \Big/ \tau\, w^2(z)\pi \qquad (\mathbf{8.5})$$

The radius w of a Gaussian beam depends on the distance z from the focus given by **Equation 8.6** where w_0 is the beam-waist radius at the focus and z_0 is the diffraction length of the beam.

$$w^2(z) = w_0^2 \left(1 + z^2 \Big/ z_0^2\right) \qquad (\mathbf{8.6})$$

It was found that the nonlinear absorption coefficient β_I was not constant for all on-focus intensities. An example of plots of effective nonlinear absorption coefficient β_I against the on-focus beam intensity I_0 of 0.5 g L^{-1} solutions of **(fPhO)$_4$PcGeCl$_2$** (**7**) and **F$_{16}$PcGeCl$_2$** (**17**) in THF are shown in **Figure 8.4**. Each data point on the plots depicts an independent open-aperture z-scan of mentioned above compounds; the solid lines are drawn just as guides to the eye.

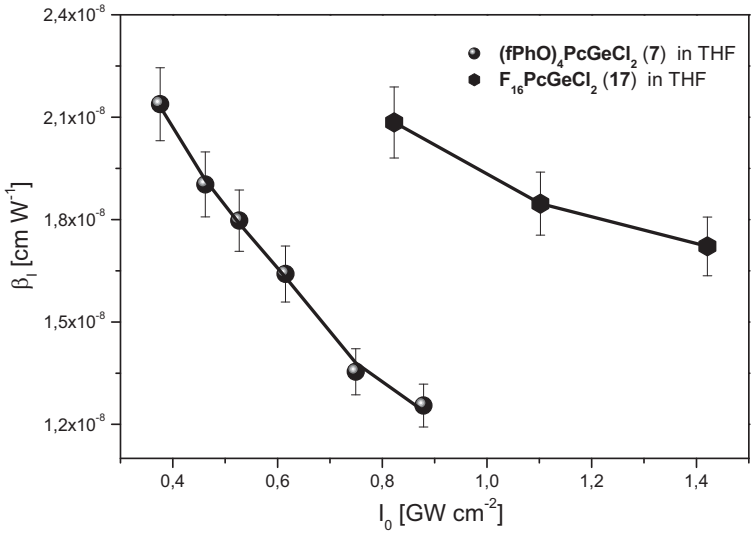

Figure 8.4 Effective nonlinear absorption coefficient β_I against the on-focus beam intensity I_0 of 0.5 g L^{-1} THF solutions of **(fPhO)$_4$PcGeCl$_2$** (**7**) and **F$_{16}$PcGeCl$_2$** (**17**).

Figure 8.4 shows that the effective nonlinear absorption coefficient β_I decreases with increasing focal intensity. Although, for the reverse saturable absorber exhibiting $\kappa > 1$ in the unsaturated regime where $I << I_{Sat}$, it could be expected that the nonlinear absorption coefficient should increase with I_0. This is in contrast to β_I measured in this study, which implies that the absorption effects were a combination of third- and higher odd-order nonlinear absorptions.

To investigate further optical limiting, the open-aperture spectra were manipulated, and the normalized transmission was plotted versus the incident energy density.

8.3 Optical limiting properties of phthalocyanine complexes in solution

8.3.1 Optical limiting properties of metal-free, dichloro-substituted germanium(IV) and tin (IV) 2,9,16,23-tetrakis(4-formylphenoxy)phthalocyanines

For the first time optical limiting properties of metal-free, tin(IV) and germanium(IV) 2,9,16,23-tetrakis(4-formylphenoxy)phthalocyanines were investigated. The z-scan measurements for a 0.5 g L^{-1} solution of each phthalocyanine were performed. Tetrahydrofuran (THF) was used as solvent. The NLO data obtained for **(fPhO)$_4$PcH$_2$** (**3**), **(fPhO)$_4$PcSnCl$_2$** (**6**) and **(fPhO)$_4$PcGeCl$_2$** (**7**) in solution are summarized in **Table 8.1**.

Table 8.1 The NLO data of **(fPhO)$_4$PcH$_2$** (**3**), **(fPhO)$_4$PcSnCl$_2$** (**6**) and **(fPhO)$_4$PcGeCl$_2$** (**7**) in solution.

Compound	c [g L^{-1}]	α_0 [cm^{-1}]	I_0 [GW cm^{-2}]	β_I [cm W^{-1}]	Im$\{\chi^{(3)}\}$ [esu]	F_{Sat} [J cm^{-2}]	κ [σ_{ex}/σ_0]
(fPhO)$_4$PcH$_2$ (**3**)	0.5 [a)]	3.65	0.7	1.3e-8	4.4e-12	30.7±3.9	5.7±0.5
(fPhO)$_4$PcSnCl$_2$ (**6**)	0.5 [a)]	1.02	0.5	3.3e-8	1.1e-11	13.6±0.8	16.9±0.7
(fPhO)$_4$PcGeCl$_2$ (**7**)	0.5 [a)]	1.02	0.4	2.1e-8	7.2e-12	14.2±0.8	13.0±0.5

[a)] Tetrahydrofuran (THF) used as solvent

All z-scans performed on solutions of **(fPhO)$_4$PcH$_2$** (**3**), **(fPhO)$_4$PcSnCl$_2$** (**6**) and **(fPhO)$_4$PcGeCl$_2$** (**7**) exhibited a decrease of transmittance about the focus typical of an induced positive nonlinear absorption of incident light. The nonlinear absorption coefficient β_I was found to be not constant for on-focus beam intensity I_0 for all discussed tetrakis(*p*-formylphenoxy)-substituted phthalocyanines. In **Figure 8.5** is shown the nonlinear absorption coefficient β_I as a function of the on-focus intensity for 0.5 g L^{-1} **(fPhO)$_4$PcGeCl$_2$** (**7**) in THF solution. It can obviously be seen that the β_I decreases with increasing magnitude of I_0. A similar effect was observed for solutions of **(fPhO)$_4$PcH$_2$** (**3**) and **(fPhO)$_4$PcSnCl$_2$** (**6**).

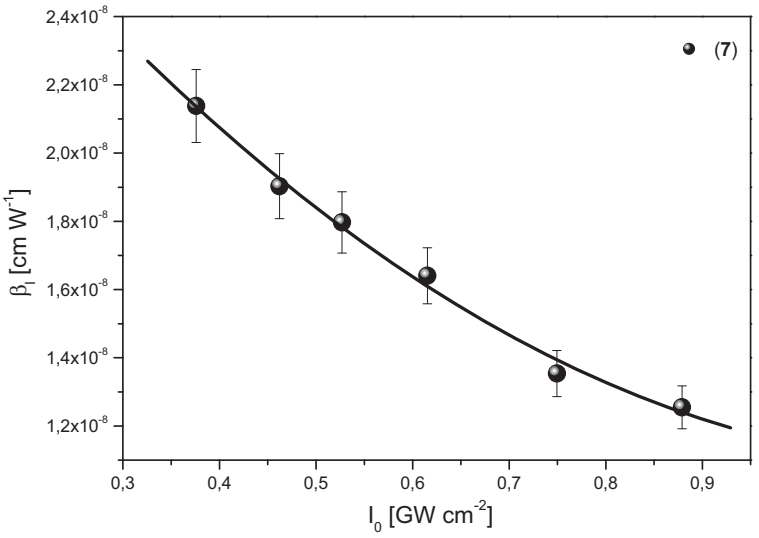

Figure 8.5 Plot of effective nonlinear absorption coefficient β_I against the on-focus beam intensity I_0 for compound **7** in THF. The data points represent an independent open-aperture z-scan and the solid line is drawn as guide to the eye.

The value of β_I increases in the succession $\beta_I(\mathbf{3}) < \beta_I(\mathbf{7}) < \beta_I(\mathbf{6})$ with **(fPhO)$_4$PcSnCl$_2$** (**6**) showing the highest value of $\beta_I(\mathbf{6}) = 3.3\times10^{-8}$ cm W^{-1} under 0.5 GW cm^{-2} laser irradiation. This indicates that the magnitude of the imaginary nonlinear responses at presented intensities considerably increases with increase in the size of the central metal as follows: 2H < Ge(IV) < Sn(IV). The same trend is observed in the magnitude of the third-order optical nonlinearities $\chi^{(3)}$, the value of $\chi^{(3)}$ of **(fPhO)$_4$PcH$_2$** (**3**) is significantly smaller than those of metallated phthalocyanines **(fPhO)$_4$PcGeCl$_2$** (**7**) and **(fPhO)$_4$PcSnCl$_2$** (**6**). The difference in magnitude of $\chi^{(3)}$ of metal-free compound **3** and its metal substituted counterparts, **(fPhO)$_4$PcGeCl$_2$** (**7**) and **(fPhO)$_4$PcSnCl$_2$** (**6**), can be explained by the fact that metal-to-ligand and/or ligand-to-metal charge transfer introduced by metal substitution contribute to the enhancement of third-order susceptibility [9].

The optical limiting data plotted as normalized transmission as a function of incident energy per pulse for **(fPhO)$_4$PcH$_2$** (**3**), **(fPhO)$_4$PcSnCl$_2$** (**6**) and **(fPhO)$_4$PcGeCl$_2$** (**7**) are depicted in **Figure 8.6**. **Figure 8.6** shows that **(fPhO)$_4$PcSnCl$_2$** (**6**) exhibits the best nonlinear response in terms of transmission versus pulse-energy density while **(fPhO)$_4$PcH$_2$** (**3**) possesses the weakest.

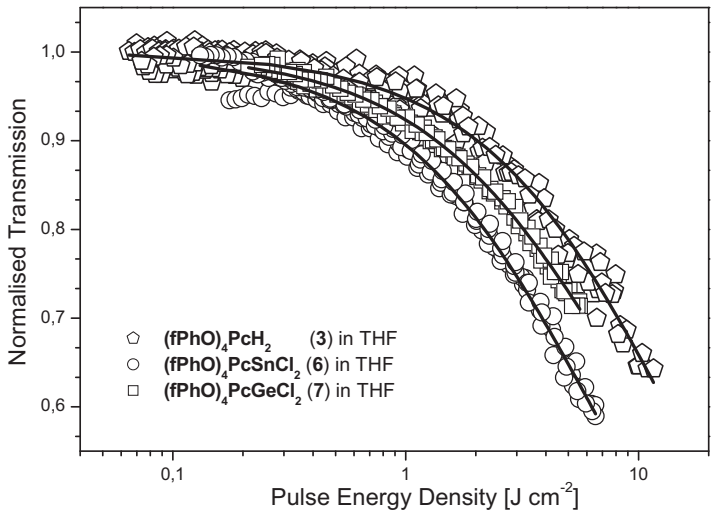

Figure 8.6 Plots of normalized transmission against incident pulse energy density for compounds **3**, **6** and **7** in THF solution. The solid lines are the theoretical curve fits.

The ratio of the excited to the ground state absorption cross section $\kappa = \sigma_{ex}/\sigma_0$ is dominated by the linear absorption coefficient α_0 [8]. The κ value is the largest for compound **6** and the smallest for metal-free phthalocyanine **3**. The κ coefficient of **(fPhO)$_4$PcSnCl$_2$** (**6**) is ~ 3 times larger than that of **(fPhO)$_4$PcH$_2$** (**3**), and, similarly, 1.3 times larger than that of **(fPhO)$_4$PcGeCl$_2$** (**7**).

The linear absorption coefficients α_0 for compound **6** is as large as for **7** (α_0(**6**), α_0(**7**) = 1.02) whereas for compound **3** is approximately 3.6 times larger. Thus, the much lower κ value of **3** can be explained by large value of its linear absorption coefficient (α_0(**3**) = 3.65).

The other apparent trend in nonlinear response of a series of tetrakis(*p*-formylphenoxy)-substituted phthalocyanines is in the saturation energy density F_{Sat}. The F_{Sat} value decreases from **(fPhO)$_4$PcH$_2$** (**3**) through **(fPhO)$_4$PcGeCl$_2$** (**7**) to **(fPhO)$_4$PcSnCl$_2$** (**6**), where F_{Sat} of **3**, **6** and **7** was determined to be 30.7, 14.2 and 13.6 J cm^{-2}, respectively. The considerable difference in the F_{Sat} value for metal-free phthalocyanine **3** in comparison with its metal substituted counterparts **6** and **7** by a factor of ~ 2.2 implies that the metallated phthalocyanines, in addition, contain two axial ligands, attenuate laser pulses of much lower energies than the metal-free Pc **3** does.

High value of the ratio of the excited to ground state absorption cross sections κ, the low energy saturation F_{Sat}, and large magnitude of the third-order optical nonlinearities $\chi^{(3)}$ make

tin and germanium phthalocyanines **6** and **7** with *p*-formylphenoxy peripheral groups, appealing candidates for practical limiters.

8.3.2 Optical limiting properties of metal-free and dichlorotin(IV) 2,9,16,23-tetrakis(4-nitrophenoxy)phthalocyanines in comparison with OL effect in dichlorotin(IV) 2,3,9,10,16,17,23,24-octacyanophthalocyanine

The OL performance of metal-free and tin(IV) 2,9,16,23-tetrakis(4-nitrophenoxy)phthalocyanines, and dichlorotin(IV) 2,3,9,10,16,17,23,24-octacyanophthalocyanine in THF at 532 nm with a pulse repetition rate of 10 Hz was investigated for the first time. The nonlinear optical responses of **(nPhO)$_4$PcH$_2$** (**4**), **(nPhO)$_4$PcSnCl$_2$** (**5**) and **(CN)$_8$PcSnCl$_2$** (**24**) in THF solution are presented in **Table 8.2**. Compound **5** shows a slightly larger β_I value, found to be 3.0 $\times 10^{-8}$ cm W^{-1} at 0.4 GW cm^{-2} laser irradiation, than compounds **4** and **24**, while compounds **4** and **24** exhibit comparable β_I value.

Table 8.2 The NLO data of **4**, **5** and **24** in solution.

Compound	c [g L^{-1}]	α_0 [cm^{-1}]	I_0 [GW cm^{-2}]	β_I [cm W^{-1}]	Im$\{\chi^{(3)}\}$ [esu]	F_{Sat} [J cm^{-2}]	κ [σ_{ex}/σ_0]
(nPhO)$_4$PcH$_2$ (4)	0.5 [a)]	5.02	1.7	2.3e-8	7.8e-12	19.6±2.3	4.3±0.3
(nPhO)$_4$PcSnCl$_2$ (5)	0.5 [a)]	1.30	0.4	3.0e-8	1.0e-11	7.7±0.4	10.2±0.3
(CN)$_8$PcSnCl$_2$ (24)	0.5 [a)]	4.78	1.3	2.5e-8	8.2e-12	17.8±2.0	4.2±0.3

[a)] tetrahydrofuran (THF) used as solvent

In a series of the three phthalocyanine complexes **4**, **5** and **24,** the $\chi^{(3)}$ grows as follows: $\chi^{(3)}$(**4**) < $\chi^{(3)}$(**24**) < $\chi^{(3)}$(**5**). Third-order optical nonlinearities $\chi^{(3)}$ values of 7.8×10^{-12}, 8.2×10^{-12} and 1.0×10^{-11} esu were obtained for **4**, **24** and **5**, respectively. The highest value of $\chi^{(3)}$ obtained for compound **5** shows that the influence of bulky electron-withdrawing peripheral substituents contributes to more efficient NLO effect than that of small cyano groups. Furthermore, the measured $\chi^{(3)}$ and β_I for **5** were slightly lower than the $\chi^{(3)}$ and β_I observed for **(*t*-Bu)$_4$PcInCl** (**25**) [8], ($\chi^{(3)}$(**25**) = 1.6×10^{-11} esu and β_I = 4.4×10^{-8} cm W^{-1}), and comparable with that of **(*t*-Bu)$_4$PcGaCl(*p*-TMP)** with bulky axial substituent *p*-trifluorophenyl (*p*-TMP) [8], ($\chi^{(3)}$(**(*t*-Bu)$_4$PcGa(*p*-TMP)**) = 1.1×10^{-11} esu and β_I = 2.9×10^{-8} cm W^{-1}) for the same concentrated solutions. It implies that compound **(nPhO)$_4$PcSnCl$_2$** (**5**)

possessing four electron-withdrawing *p*-nitrophenoxy groups in peripheral positions of the macrocycle and two chlorine in axial positions contributes to as large $\chi^{(3)}$ and β_I as **(*t*-Bu)$_4$PcInCl** (**25**) and **(*t*-Bu)$_4$PcGaCl(*p*-TMP)** do.

The open-aperture z-scan for a 0.5 g L^{-1} solution of **5** in THF is shown in **Figure 8.7 A**. This indicates that the compound **5** has a positive nonlinear absorption *i.e.* it is a reverse saturable absorber over this range of fluence. In the **Figure 8.7 B** is presented the minimum transmission T_{min} versus incident energy per pulse for compound **(nPhO)$_4$PcSnCl$_2$** (**5**). The minimum values of transmission T_{min} for compound **5**, which are accomplished in correspondence of the highest level of irradiation *i.e.* at the focus (z = 0), prove good OL performance with the lowest value of T_{min} = 0.64 at 0.16 mJ incident energy. The values of T_{min} of **5** vary from 0.64 to 0.72 under different incident energy.

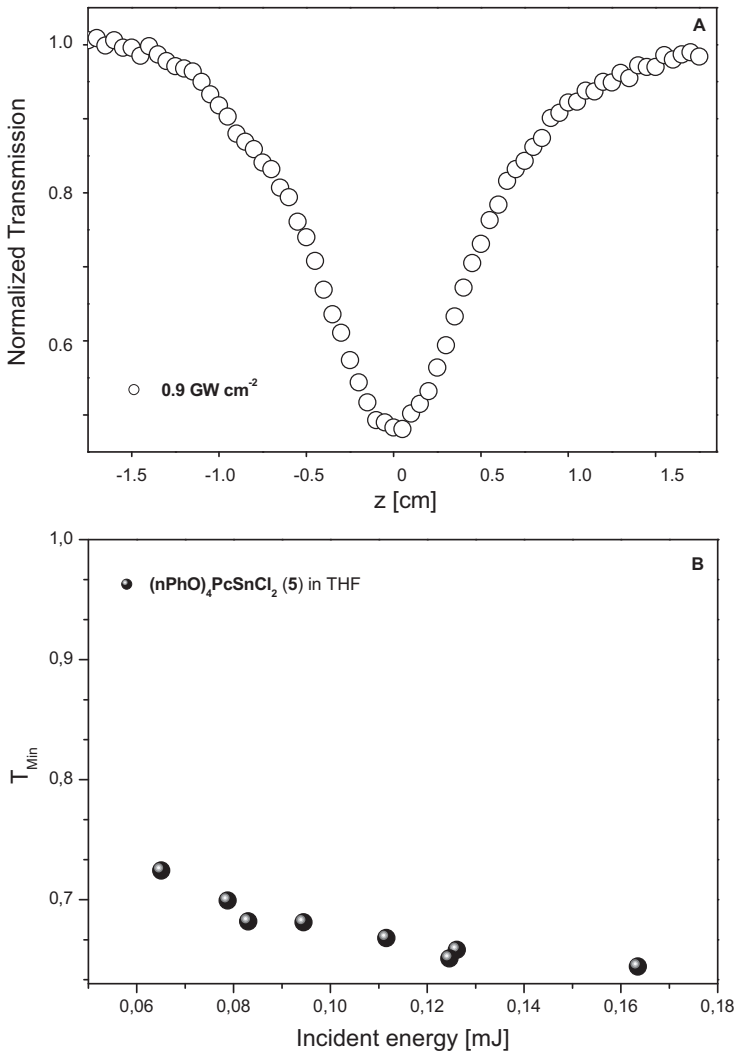

Figure 8.7 Normalized transmission at 532 nm of **5** in THF solution as a function of a sample position *z* (**A**, top), and plot of the minimum transmission T_{min} versus incident energy (**B**, bottom).

The optical limiting plotted as normalized transmission as a function of energy density, for compounds **4**, **5** and **24** is depicted in **Figure 8.8**. As shown in **Figure 8.8**, compound **5** exhibits better nonlinear response than compounds **4** and **24** while complexes **4** and **24** display almost the same nonlinear response.

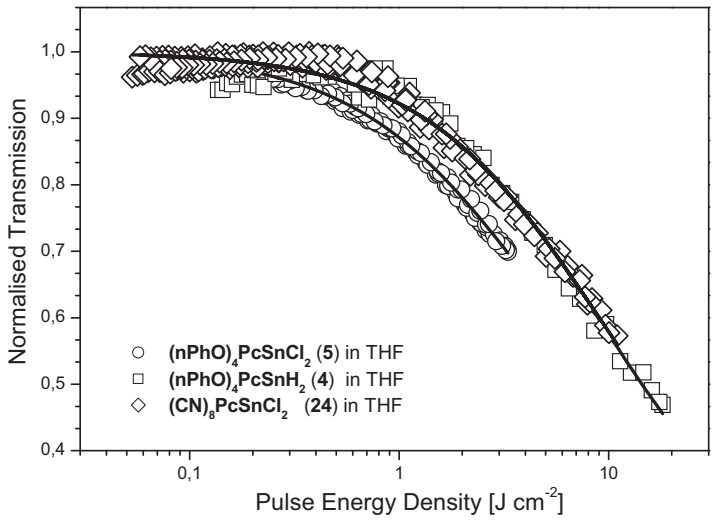

Figure 8.8 Plots of normalized transmission against incident pulse energy density for compounds **4**, **5** and **24**. The solid lines are the theoretical curve fits.

Comparing the κ values of **(nPhO)$_4$PcH$_2$** (**4**) and **(CN)$_8$PcSnCl$_2$** (**24**) with **(nPhO)$_4$PcSnCl$_2$** (**5**), the κ value of **5** is larger than those of the other two compounds, **4** and **24**, by a factor of ~ 2.4. However, the α_0 values for **(nPhO)$_4$PcH$_2$** (**4**) and **(CN)$_8$PcSnCl$_2$** (**24**) are almost equal whereas **(nPhO)$_4$PcSnCl$_2$** (**5**) shows the linear absorption coefficient α_0 approximately 3 times lower than **4** and **24**. The difference in α_0 values of **4**, **5** and **24** compares very well with the difference in their κ value that is different by a factor of ~ 3. The magnitude of the measured F_{Sat} is roughly the same for **(nPhO)$_4$PcH$_2$** (**4**) and **(CN)$_8$PcSnCl$_2$** (**24**) while **(nPhO)$_4$PcSnCl$_2$** (**5**) exhibit much lower F_{Sat} value, by a factor of ~ 2.5, than the other two compounds.

The **(nPhO)$_4$PcSnCl$_2$** (**5**) displays the largest β_I and the κ values, and the lowest energy saturation F_{Sat} of the three phthalocyanines discussed here, showing its good suitability as optical limiter.

8.3.3 Optical limiting properties of tin(IV) and germanium(IV) tetranitro-substituted phthalocyanines

For a series of tin(IV) and germanium(IV) tetranitro at α- and β-positions substituted phthalocyanines with different axial groups (**Figure 8.9**) the OL performance was investigated.

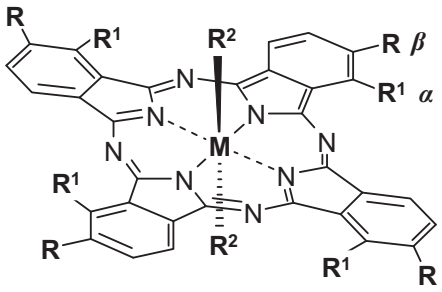

	R	R¹	R²	M
19	H	NO_2	Cl	Sn
22	H	NO_2	Cl	Ge
18	NO_2	H	Cl	Sn
20	NO_2	H	Cl	Ge
21	NO_2	H	OH	Ge
23	NO_2	H	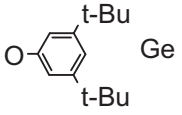	Ge

Figure 8.9 Tin(IV) and germanium(IV) tetranitro-substituted phthalocyanines.

Nanosecond measurements were performed for a 0.5 g L^{-1} solution of **(*β*NO_2)$_4$PcSnCl_2** (**18**), **(*α*NO_2)$_4$PcSnCl_2** (**19**), **(*β*NO_2)$_4$PcGeCl_2** (**20**) and **(*β*NO_2)$_4$PcGe(OH)$_2$** (**21**) in DMF, and for the same concentrated solution of **(*α*NO_2)$_4$PcGeCl_2** (**22**) and **(*β*NO_2)$_4$PcGe(*t*Bu$_2$P)$_2$** (**23**) in THF. All data concerning optical limiting performance on presented materials are collected in **Table 8.3**. The magnitude of nonlinear absorption coefficient β_I was found to be significantly similar for **(*β*NO_2)$_4$PcSnCl_2** (**18**), **(*β*NO_2)$_4$PcGeCl_2** (**20**) and **(*β*NO_2)$_4$PcGe(OH)$_2$** (**21**) while for **(*α*NO_2)$_4$PcSnCl_2** (**19**) and **(*β*NO_2)$_4$PcGe(*t*Bu$_2$P)$_2$** (**23**) the values of β_I were lower than for the others. The values of third-order optical nonlinearity $\chi^{(3)}$ for various axially substituted tin and germanium phthalocyanines having nitro peripheral groups diminish in a series: $\chi^{(3)}$(**21**) < $\chi^{(3)}$(**19**) < $\chi^{(3)}$(**23**) < $\chi^{(3)}$(**22**) < $\chi^{(3)}$(**18**) < $\chi^{(3)}$(**20**) where the **(*β*NO_2)$_4$PcGe(OH)$_2$** (**21**) exhibits the highest value of $\chi^{(3)}$(**21**) determined to be 1.6×10^{-11} esu.

Comparison of tetra-β-nitro-substituted phthalocyanines **18** and **20** with tetra-α-nitro-substituted phthalocyanines **19** and **22** shows that the β_I and $\chi^{(3)}$ values are lower for compounds **19** and **22**, implying that the peripheral substitution positions on the phthalocyanine ring can slightly influence the magnitude of the imaginary nonlinear response.

Table 8.3 The NLO data of **18**, **19**, **20**, **21**, **22** and **23** in solution.

Compound	c [g L^{-1}]	α_0 [cm^{-1}]	I_0 [GW cm^{-2}]	β_I [cm W^{-1}]	Im$\{\chi^{(3)}\}$ [esu]	F_{Sat} [J cm^{-2}]	κ [σ_{ex}/σ_0]
(βNO$_2$)$_4$PcSnCl$_2$ (18)	0.5 [b]	4.77	2.1	2.2e-8	7.7e-12	21.9±1.0	4.5±0.1
(αNO$_2$)$_4$PcSnCl$_2$ (19)	0.5 [b]	3.07	2.5	5.4e-9	1.8e-12	47.5±7.6	4.5±0.4
(βNO$_2$)$_4$PcGeCl$_2$ (20)	0.5 [b]	6.0	2.6	2.6e-8	8.8e-12	11.1±0.5	3.3±0.1
(βNO$_2$)$_4$PcGe(OH)$_2$ (21)	0.5 [b]	5.79	0.4	4.8e-8	1.6e-11	8.7±1.7	3.5±0.4
(αNO$_2$)$_4$PcGeCl$_2$ (22)	0.5 [a]	4.17	0.8	1.1e-8	3.7e-12	0.8±0.1	3.0±0.1
(βNO$_2$)$_4$PcGe(tBu$_2$P)$_2$ (23)	0.5 [a]	4.05	2.9	9.0e-9	3.0e-12		

[a] tetrahydrofuran (THF) used as solvent
[b] dimethylformamide (DMF) used as solvent

The nonlinear responses in terms of transmission versus pulse energy density for tin and germanium tetranitro-substituted phthalocyanines are presented in **Figure 8.10**.

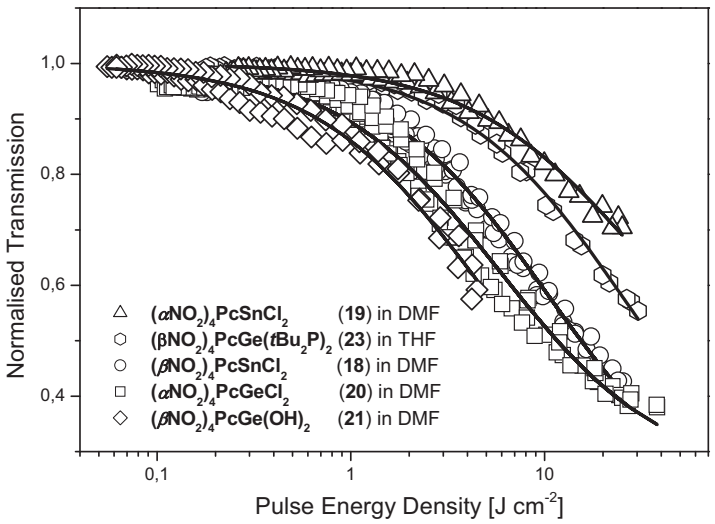

Figure 8.10 Plots of normalized transmission against incident pulse energy density for **18**, **19**, **20**, **21** and **23**. The solid lines are the theoretical curve fits to the experimental data.

Compounds **18** and **20** with peripheral groups at β-positions show similar magnitude of the nonlinear absorption, while **19** with peripheral groups at α-positions exhibit the lowest nonlinear responses.

The ratio of the excited to ground state absorption cross sections κ was found to vary from 3.0 to 6.4 in a series: **(αNO$_2$)$_4$PcGeCl$_2$** (**22**) ≤ **(βNO$_2$)$_4$PcGeCl$_2$** (**20**) < **(βNO$_2$)$_4$PcGe(OH)$_2$** (**21**) < **(βNO$_2$)$_4$PcSnCl$_2$** (**18**) = **(αNO$_2$)$_4$PcSnCl$_2$** (**19**). The tin complexes **18** and **19** display the same value of κ determined to be 4.5, likewise the germanium complexes **20**, **21** and **22** with the κ value of 3.0 to 3.5. The α_0 values followed the same trend as the β_I and $\chi^{(3)}$ values, being higher for β-nitro-substituted phthalocyanines than for phthalocyanines with peripheral substituents at α-positions. Moreover, tin complexes display higher κ factor than germanium compounds do.

The inverse situation in case of the magnitude of the saturation density F_{Sat} for compounds **18 - 23** takes place. Compound **18** and **20** saturate at relatively high energy density, while germanium phthalocyanines **20**, **21**, and **22** saturate at much lower energy density.

This study on NLO properties of various tin and germanium tetranitro-substituted phthalocyanines showed that the peripheral substitution positions on the phthalocyanine ring has a little effect on the measured optical limiting. It was found that the tin phthalocyanine complexes exhibited better NLO properties than germanium compounds.

8.3.4 Optical limiting properties of tin and germanium hexadeca-substituted phthalocyanines

In case of **Cl$_{16}$PcSnCl$_2$** (**8**) and **Cl$_{16}$PcGeCl$_2$** (**9**), it was impossible to gain any information from the scans of their solutions. This might be due to induced thermal effects in these samples from laser irradiation, which could be caused by the presence of impurities. The optical limiting of di(3,5-*tert*-butyl)phenoxy-substituted tin(IV) and germanium(IV) perchlorophthalocyanines was investigated in chloroform solution. For **Cl$_{16}$PcSn(*t*Bu$_2$P)$_2$** (**14**) and **Cl$_{16}$PcGe(*t*Bu$_2$P)$_2$** (**15**) solutions it was impossible to fit a theoretical curve to produce the NLO parameters of F_{Sat} and κ. The optical limiting of tin(IV) and germanium(IV) hexadecafluorophthalocyanines was investigated in THF solution while hexadecachloro-substituted phthalocyanines were dissolved in 1-chloronaphtalene. Both solvents did not show any NLO behaviour at the used level of irradiation. NLO parameters for **Cl$_{16}$PcSnF$_2$** (**12**), **Cl$_{16}$PcGeF$_2$** (**13**), **Cl$_{16}$PcSn(*t*Bu$_2$P)$_2$** (**14**), **Cl$_{16}$PcGe(*t*Bu$_2$P)$_2$** (**15**), **F$_{16}$PcSnCl$_2$** (**16**) and **F$_{16}$PcGeCl$_2$** (**17**) complexes are listed in **Table 8.4**. Comparison of tin hexadeca-substituted phthalocyanines: **12**, **14**, **16** with germanium hexadeca-substituted phthalocyanines: **13**, **15**, **17** shows that larger values of nonlinear absorption coefficient β_I were obtained for tin phthalocyanines (β_I(**12**) = 1.5×10^{-8}, β_I(**14**) = 2.7×10^{-9} and β_I(**16**) = 3.9×10^{-8} cm W^{-1}) than for

the corresponding germanium compounds (β_I(**13**) = 1.2×10^{-8}, β_I(**15**) = 2.3×10^{-9} and β_I(**17**) = 1.8×10^{-8} cm W^{-1}). It indicates that increase in the size of the central metal lead to larger value of β_I. The same trend was observed for the third-order optical nonlinearities $\chi^{(3)}$ where tin complexes display higher $\chi^{(3)}$ values than germanium substituted counterparts. There are not significant differences in the $\chi^{(3)}$ values among compounds **12**, **13**, **14**, **15** and **17** while **16** exhibits value of $\chi^{(3)}$ an order of magnitude higher of the others. The highest magnitude of $\chi^{(3)}$ of **16** can be explained by the fact that the presence of the electron-withdrawing fluorine groups at the peripheral positions of the macrocycle and additionally the large size of the central metal contribute to the enhancement of the third-order susceptibility.

Table 8.4 The NLO data for **Cl$_{16}$PcSnF$_2$ (12)**, **Cl$_{16}$PcGeF$_2$ (13)**, **Cl$_{16}$PcSn(*t*Bu$_2$P)$_2$ (14)**, **Cl$_{16}$PcGe(*t*Bu$_2$P)$_2$ (15)**, **F$_{16}$PcSnCl$_2$ (16)** and **F$_{16}$PcGeCl$_2$ (17)** in solution.

Compound	c [g L^{-1}]	α_0 [cm^{-1}]	I_0 [GW cm^{-2}]	β_I [cm W^{-1}]	Im$\{\chi^{(3)}\}$ [esu]	F_{Sat} [J cm^{-2}]	κ [σ_{ex}/σ_0]	T_{Min}
12	0.5 [c]	2.57	0.4	1.5e-8	6.6e-12	23.2±4.8	6.0±0.9	0.82
13	0.5 [c]	0.38	0.3	1.2e-8	5.2e-12	27.7±18.0	4.6±2.1	0.88
14	0.5 [d]		2.6	3.2e-9	1.1e-12			0.75
15	0.5 [d]		2.8	2.3e-9	8.7e-13			0.78
16	0.5 [a]	2.73	1.2	3.9e-8	1.3e-11	12.9±0.28	7.3±0.1	0.40
17	0.5 [a]	3.8	1.1	1.8e-8	6.2e-12	16.3±1.0	4.4±0.1	0.50

[a] Tetrahydrofuran (THF),
[c] 1-chloronaphthalene (Cln),
[d] chloroform ($CHCl_3$) used as solvents

Furthermore, the minimum value of normalized transmission T_{min} of **F$_{16}$PcSnCl$_2$ (16)**, **F$_{16}$PcGeCl$_2$ (17)**, **Cl$_{16}$PcSnF$_2$ (12)** and **Cl$_{16}$PcGeF$_2$ (13)** complexes are lower than that of the corresponding hexadecafluoro- and hexadechloro-substituted phthalocyanines, **F$_{16}$PcTiO** and **Cl$_{16}$PcTiO**, disclosed by D. Dini [10]. The observed T_{min} values follow the order **F$_{16}$PcSnCl$_2$ (16)** (T_{min} = 0.4) < **F$_{16}$PcGeCl$_2$ (17)** (T_{min} = 0.50) < **F$_{16}$PcTiO** (T_{min} = 0.52) [10] for phthalocyanines with the fluorine at the periphery of the macrocycle, and **Cl$_{16}$PcSn(*t*Bu$_2$P)$_2$ (14)** (T_{min} = 0.75) < **Cl$_{16}$PcGe(*t*Bu$_2$P)$_2$ (15)** (T_{min} = 0.78) < **Cl$_{16}$PcSnF$_2$ (12)** (T_{min} = 0.82) < **Cl$_{16}$PcGeF$_2$ (13)** (T_{min} = 0.88) < **Cl$_{16}$PcTiO** (T_{min} = 0.90) [10] for phthalocyanines possessing the chlorine peripheral substituents. This shows that the heavy metal effect and the fluorine

peripheral substituents with stronger electron-withdrawing effect than chlorine groups have remarkable influence on NLO effects of phthalocyanines.

The ratio of the absorption cross sections κ for tin phthalocyanines, **12** and **16**, is larger than that of germanium substituted counterparts **13** and **17**, by a factor of ~ 1.5, whereas the κ value of **13** and **17** are almost equal. The measured values of the linear absorption coefficient α_0 for tin compounds **12** and **16** are comparable, determined to be 2.73 cm^{-1} for **16** and 2.57 cm^{-1} for **12**, but lower by a factor of ~ 1.5 than for $\mathbf{F_{16}PcGeCl_2}$ (**17**). The lowest value of α_0 was found for compound $\mathbf{Cl_{16}PcGeF_2}$ (**13**).

In terms of the magnitude of the reduction in normalized transmission relative to incident pulse energy density (**Figure 8.11**), compound $\mathbf{F_{16}PcSnCl_2}$ (**16**) shows the best nonlinear optical response of the others, whereas compounds **12**, **13** and **17** exhibit close similarities in their nonlinear optical responses.

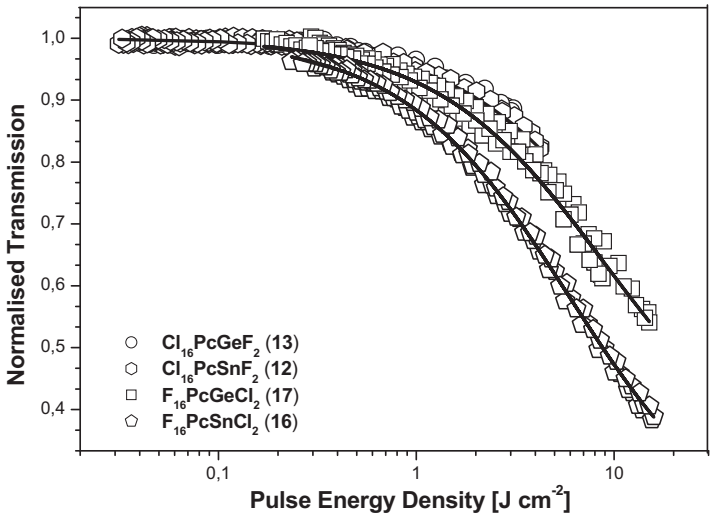

Figure 8.11 Plots of normalized transmission against incident pulse energy density for **12**, **13**, **16** and **17**. The solid lines are the theoretical curve fits to the experimental data.

The F_{Sat} values for tin and germanium hexadecafluoro-substituted phthalocyanines, **16** and **17**, are similar, determined to be 12.9 and 16.3 J cm^{-2}, respectively, and considerably lower than compared to complexes with chlorine groups at the periphery of the macrocycle, **12** and **13**. The F_{Sat} values calculated for **12** and **13** were 23.2 and 27.7 J cm^{-2}, respectively. This shows that tin and germanium perfluoro-substituted phthalocyanines **16** and **17** decrease the

energy saturation by a factor of ~ 1.7 than their peripherally perchloro-substituted counterparts.

Generally, this study disclosed that more electron-withdrawing groups at the peripheral positions of the macrocycle produce better optical limiting performance.

8.4 Optical limiting properties of phthalocyanine complexes embedded in polymer films

8.4.1 Optical limiting effect in tin and germanium tetrakis(*p*-formylphenoxy)-substituted phthalocyanines in PMMA and PVC films

Optical limiting of solid-state (films) of tin(IV) and germanium(IV) tetra(*p*-formylphenoxy)-substituted phthalocyanines embedded in PMMA and PVC and with various numbers of layers was measured first time. The NLO parameters of solid samples are summarized in **Table 8.5**. The films of phthalocyanines in PMMA and PVC are designated as described in Chapter 5th, *e.g.*, **6PMMA3** designates 3-layer film of phthalocyanine **6** in PMMA polymer. The magnitude of the nonlinear absorption coefficient β_I for solid-state samples **6PMMA3**, **7PMMA3**, **6PVC4** and **7PVC4** is slightly higher or comparable in comparison with the corresponding 6-layer and 7-layer films. The measured β_I and $\chi^{(3)}$ for **6PPMA3** film were found to be an order of magnitude higher than these of the corresponding film with 6 layers *i.e.* **6PMMA6**. The lower β_I and $\chi^{(3)}$ values for **6PMMA6** than for **6PMMA3** can be influenced by a polar environment of a host polymer. However, 4- and 7-layer films of **(fPhO)$_4$PcSnCl$_2$** (**6**) and **(fPhO)$_4$PcGeCl$_2$** (**7**) in PVC display comparable β_I and $\chi^{(3)}$ values, where for 7-layer films the β_I and $\chi^{(3)}$ values are slightly higher than that of 4-layer films. The lack of increase in the magnitude of β_I and $\chi^{(3}$ for 3-layer films in comparison with and 4-layer films of **6** and **7** in PMMA can be caused by interactions between phthalocyanines or/and even with the polymer host. However, the β_I and $\chi^{(3)}$ are much higher for multi-layer **(fPhO)$_4$PcSnCl$_2$** (**6**) and **(fPhO)$_4$PcGeCl$_2$** (**7**) films in various polymers than for the corresponding phthalocyanine investigated in solutions, by two orders of magnitude in case of β_I and four orders of magnitude in case of $\chi^{(3)}$. Moreover, the linear absorption coefficient α_0 of compounds **6** and **7** in solutions is substantially smaller than for multi-layer films of those compounds.

Table 8.5 The NLO parameters of **(fPhO)$_4$PcSnCl$_2$** (**6**) and **(fPhO)$_4$PcGeCl$_2$** (**7**) in PMMA and PVC films.

Solid state sample	d [μm]	α_0 [cm^{-1}]	I_0 [GW cm^{-2}]	β_I [cm W^{-1}]	Im$\{\chi^{(3)}\}$ [esu]	F_{Sat} [J cm^{-2}]	κ [σ_{ex}/σ_0]
6PMMA3	1	1844	0.2	3.7e-5	1.4e-8	6.1±1.8	6.7±1.3
6PMMA6	2.3	851.1	0.4	9.3e-6	3.5e-9	15.3±3.4	8.0±1.3
7PMMA3	1	1914.5	0.6	5.4e-5	2.0e-8	11.6±1.1	12.0±0.8
7PMMA6	1.9	1110.3	0.7	4.0e-5	1.5e-8	6.6±0.5	9.0±0.4
6PVC4	1	1334.7	0.3	1.5e-5	6.0e-9	20.2±7.2	10.9±3.1
6PVC7	2.3	688.04	0.4	1.6e-5	6.6e-9	10.2±1.4	10.7±1.1
7PVC4	1	1900.7	0.7	6.0e-5	2.4e-8	5.91±0.7	10.8±0.7
7PVC7	1.9	961.5	0.6	5.1e-5	2.0e-8	5.28±0.4	10.4±0.5

Optical limiting plotted as normalized transmission against pulse energy density for multi-layer films of **6** embedded in PMMA and PVC with respect to **(fPhO)$_4$PcSnCl$_2$** (**6**) in THF solution is shown in **Figure 8.12**. **Figure 8.12** shows that the magnitude of nonlinear absorption is not considerably different for the various solid-state samples of **6** and for solution of **(fPhO)$_4$PcSnCl$_2$** (**6**). The **6PVC7** shows slightly better reduction of transmission with increasing pulse energy in comparison with **6** in THF solution but the magnitude of nonlinear absorption of **6PMMA3**, **6PMMA6** and **6PVC4** films is comparable or faintly worse than for **6** in solution. However, the thicker films, **6PMMA6** and **6PVC7**, due to higher Pc concentration led to a lower normalized transmission relative to the pulse energy than thinner films, **6PMMA3** and **6PVC4**.

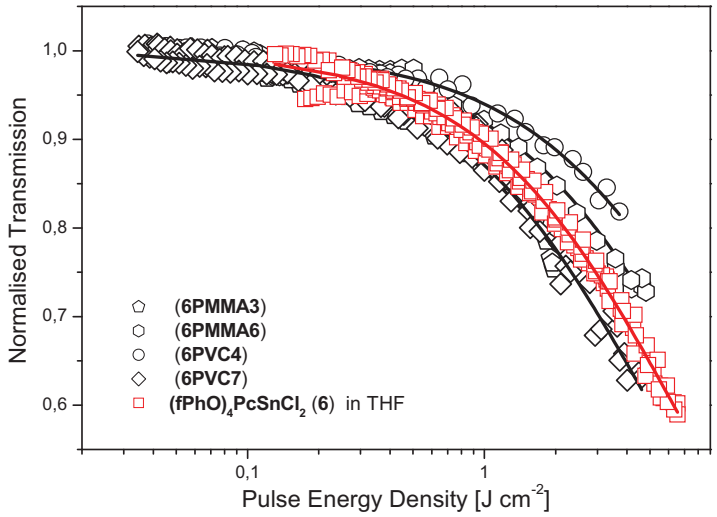

Figure 8.12 Optical limiting, plotted as normalized transmission against incident pulse energy, for solid-state samples: **6PMMA3**, **6PMMA6**, **6PVC4** and **6PVC7** in comparison with **6** in THF. The solid lines are the theoretical curve fits to the experimental data.

Figure 8.13 shows optical limiting plotted in terms of the reduction in normalized transmission relative to pulse energy density for multi-layer films of compound **7** in PMMA and PVC with respect to **(fPhO)$_4$PcGeCl$_2$** (**7**) in solution. The multi-layer films of **7** noticeably outperform compound **7** in solution (**Figure 8.13**). The magnitude of nonlinear absorption of films of compound **7** in PMMA and PVC increases as follows: **7PMMA3** < **7PVC4** < **7PMMA6** < **7PVC7**, implying that thicker films with a higher content of phthalocyanine show better optical limiting than thinner films.

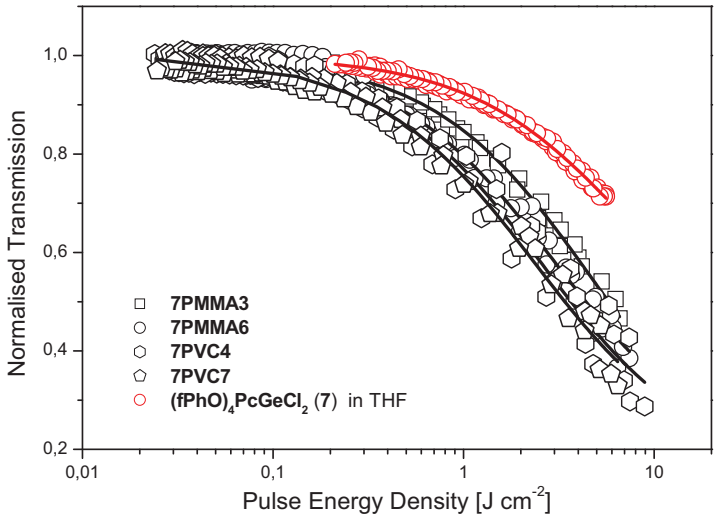

Figure 8.13 Optical limiting, plotted as normalized transmission against incident pulse energy, for samples **7PMMA3**, **7PMMA6**, **7PVC4** and **7PVC7** in comparison with **7** in THF. The solid lines are the theoretical curve fits to the experimental data.

The κ values are comparable for 3- and 6-layer films in PMMA, and for 4- and 7-layer films in PVC of **(fPhO)$_4$PcSnCl$_2$** (**6**) and **(fPhO)$_4$PcGeCl$_2$** (**7**). This indicates that the *p*-formylphenoxy peripheral groups effectively suppress molecular aggregation. The saturation density F_{Sat} of **7PMMA3** and **6PVC4** is ~ 2 times bigger than that of **7PMMA6** and **6PVC7**, while in the case of **7PVC4** and **7PVC7** is very similar. The comparison of the magnitude of F_{Sat} for compound **7** in PMMA and PVC with **7** in solution shows that films of **7** in PMMA as well as in PVC saturate at an energy density lower by a factor of ~ 2.5 than **7** in solution.

Figure 8.14 A and **B** shows the absorption spectra of films of **6** and **7** in various polymers and, for comparison, the spectra of compounds **6** and **7** in $CHCl_3$ solution. Qualitatively, this spectral evidence shows that compounds **6** and **7** in polymeric films do not exhibit tendency to aggregate even in films with 6 or 7 layers. Although, the absorption spectra of PMMA films of compounds **6** and **7** are slightly broader than those of PVC films.

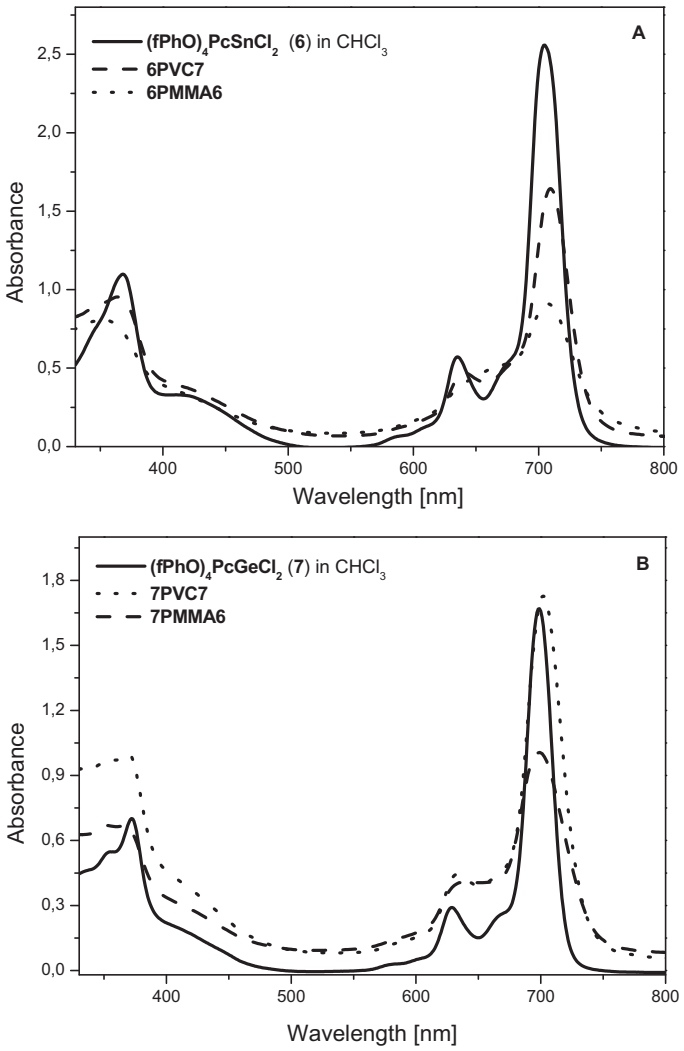

Figure 8.14 Absorption spectra of multi-layer **(fPhO)$_4$PcSnCl$_2$** (**6**) (**A**, top) and **(fPhO)$_4$PcGeCl$_2$** (**7**) (**B**, bottom) films in PVC and PMMA, compared to that of **(fPhO)$_4$PcSnCl$_2$** (**6**) and **(fPhO)$_4$PcGeCl$_2$** (**7**) in $CHCl_3$ solution.

The absence of molecular aggregation in multi-layer films of tin and germanium tetra(*p*-formylphenoxy)phthalocyanines, **6** and **7**, in various polymer matrices reflects large magnitudes of the third-order optical nonlinearities $\chi^{(3)}$ and the nonlinear absorption coefficient β_I. Moreover, thicker films give rise to a significant reduction in the saturation energy density.

High value of the nonlinear absorption coefficient β_I, the significantly low energy saturation F_{Sat} and large magnitude of the third-order optical nonlinearities $\chi^{(3)}$ of multi-layer polymeric

films of **(fPhO)$_4$PcSnCl$_2$** (**6**) and **(fPhO)$_4$PcGeCl$_2$** (**7**) in comparison with **6** and **7** in solutions make them an interesting candidates as practical optical limiters.

8.4.2 Optical limiting effect in dichlorotin(IV) 2,9,16,23-tetrakis(4-nitrophenoxy)phthalocyanine and in bis(3,5-di-*tert*-butylphenoxy)germanium 2,9,16,23-tetranitrophthalocyanine in PMMA and PVC films

Optical properties of multi-layer **(nPhO)$_4$PcSnCl$_2$** (**5**) films in various polymer matrices were determined, and compared with multi-layer **(*β*NO$_2$)$_4$PcGe(*t*Bu$_2$P)$_2$** (**23**) films in the same polymer matrices. The NLO data are listed in **Table 8.6**.

Table 8.6 The NLO data of **(nPhO)$_4$PcSnCl$_2$** (**5**) and **(*α*NO$_2$)$_4$PcGe(*t*Bu$_2$P)$_2$** (**23**) in PMMA and PVC films.

Solid state sample	d [μm]	α_0 [cm^{-1}]	I_0 [GW cm^{-2}]	β_I [cm W^{-1}]	Im$\{\chi^{(3)}\}$ [esu]	F_{Sat} [J cm^{-2}]	κ [σ_{ex}/σ_0]
5PMMA3	0.9	2782.4	1.1	1.8e-4	6.7e-8	3.7±0.3	9.1±0.4
5PMMA6	1.8	1659.9	1.25	1.7e-4	6.2e-8	2.5±0.2	8.0±0.3
5PVC4	0.9	1876.4	0.7	1.6e-4	6.4e-8	2.89±0.2	13.7±0.7
5PVC7	1.8	1330.7	0.7	1.2e-4	4.7e-8	2.85±0.2	9.0±0.4
23PMMA3	0.8	2980	0.3	8.7e-5	3.2e-8	5.3±0.7	7.2±0.6
23PMMA6	1.5	2928	0.6	1.9e-4	7.3e-8	2.3±0.2	5.6±0.2
23PVC4	0.8	3885.7	0.7	2.3e-4	9.1e-8	4.3±0.5	7.8±0.5
23PVC7	1.5	3294.4	0.5	6.1e-5	2.4e-8	5.4±0.7	4.5±0.3

The magnitude of the third-order nonlinearity $\chi^{(3)}$ of **5PMMA3**, **23PMMA3**, **5PVC4** and **23PVC4** films does not differ from the corresponding films with higher number of layers, **5PMMA6**, **23PMMA6**, **5PVC7**, and **23PVC7**, respectively. The same trend is observed in case of the nonlinear absorption coefficient β_I for **5PMMA3** and **5PVC4** films, having similar values of β_I as their thicker analogues, **5PMMA6** and **5PVC7**. The different situation takes place in case of films of **23** in PMMA, the β_I value is an order of magnitude higher for thicker **23PMMA6** than for thinner **23PMMA3** film. This is in contrast to the PVC films of **23**, where **23PVC7** exhibits lower β_I value than thinner **23PVC4** film. It indicates that **23** in PMMA films give better the magnitude of the imaginary nonlinear response than in PVC

films. Compounds **5** and **23** in multi-layer PMMA and PVC films show considerably higher values of β_I and $\chi^{(3)}$, approximately four orders of magnitude, than **5** and **23** in solution.

Plots of the normalized transmission against the pulse energy density for multi-layer films of compound **5** in PMMA and PVC and multi-layer films of compound **23** in PMMA and PVC are compared to the corresponding phthalocyanines in solution, **5** and **26** (**Figure 8.15** and **8.16**). Comparison of 3- and 4-layer films with 6- and 7-layer films in PVC and PMMA of **5** and **23** in terms of the magnitude of the reduction in normalized transmission relative to incident energy density shows that thicker films (**5PMMA6**, **5PVC7**, **23PMMA6**, **23PVC7**) lead to a lower normalized transmission than thinner films (**5PMMA3**, **5PVC4**, **23PMMA3**, **23PVC4**). The magnitude of nonlinear absorption of films of **5** (**Figure 8.15**) and **23** (**Figure 8.16**) in PMMA and PVC vary with number of layers, being larger for **5PMMA6** and **23PMMA6**, implying that increase of thickness of films contribute to a better magnitude of nonlinear response and make them an attractive for practical application.

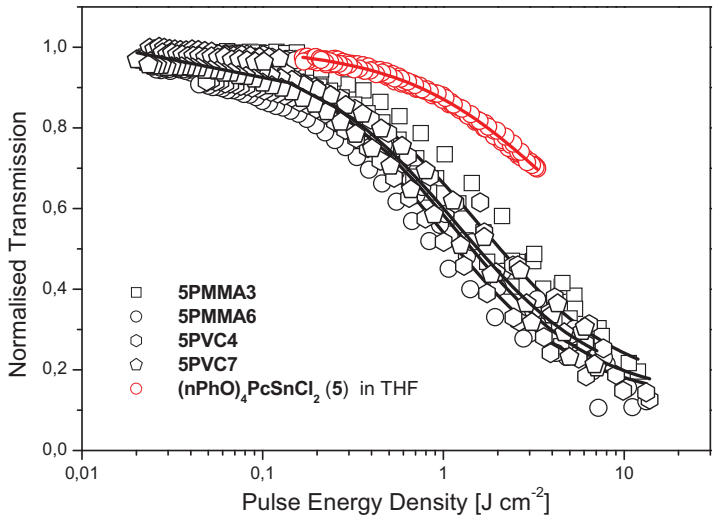

Figure 8.15 Optical limiting, plotted as normalized transmission against incident pulse energy, for samples **5PMMA3**, **5PMMA6**, **5PVC4** and **5PVC7** in comparison with **5** in THF solution. The solid lines are the theoretical curve fits to the experimental data.

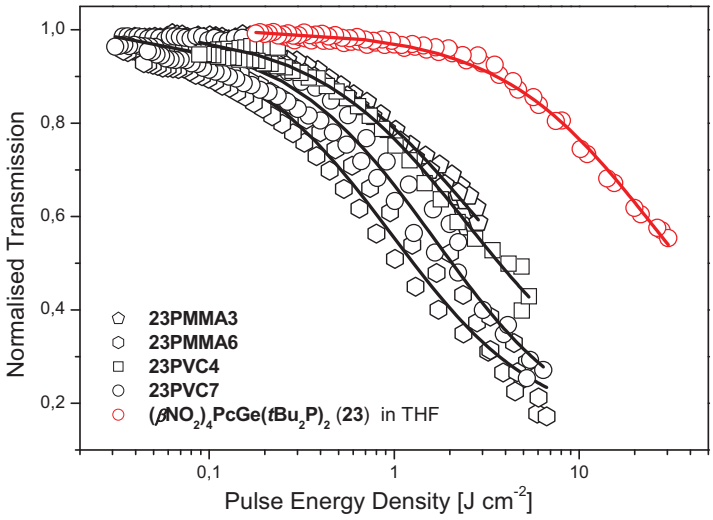

Figure 8.16 Optical limiting, plotted as normalized transmission against incident pulse energy, for samples **23PMMA3**, **23PMMA6**, **23PVC4** and **23PVC7** in comparison with **23** in THF solution. The solid lines are the theoretical curve fits to the experimental data.

Moreover, multi-layer films of **5** exhibit outstanding optical limiting in relation to compound **5** in solution. It can be seen in **Figure 8.15** that only ~ 10% transmission occurs for **5PMMA3**, **5PMMA6**, **5PVC4** and **5PVC7** at a high energy density 10 Jcm^{-2}. In addition, films of compound **23** clearly show better optical limiting properties (**Figure 8.16**) than **23** in solution.

Comparison of optical limiting between multi-layer films of **$(nPhO)_4PcSnCl_2$** (**5**) and multi-layer **$(\beta NO_2)_4PcGe(tBu_2P)_2$** (**23**), taking into account the same polymer matrix, shows that not so much differences can be seen in their nonlinear responses in terms of transmission versus pulse energy density (**Figure 8.17**). However, the nonlinear optical response for films in PMMA was better for 6-layer than 3-layer films (**23PMMA3** < **5PMMA3** < **23PMMA6** < **5PMMA6**) and in case of films in PVC, the nonlinear optical response of films of **5** is better than those of **23** (**23PVC4** < **23PVC7** < **5PVC4** < **5PVC7**). This again shows that thicker films exhibit better optical limiting. In addition, compound **5** in films displays better optical limiting than **23** (**Figure 8.17**).

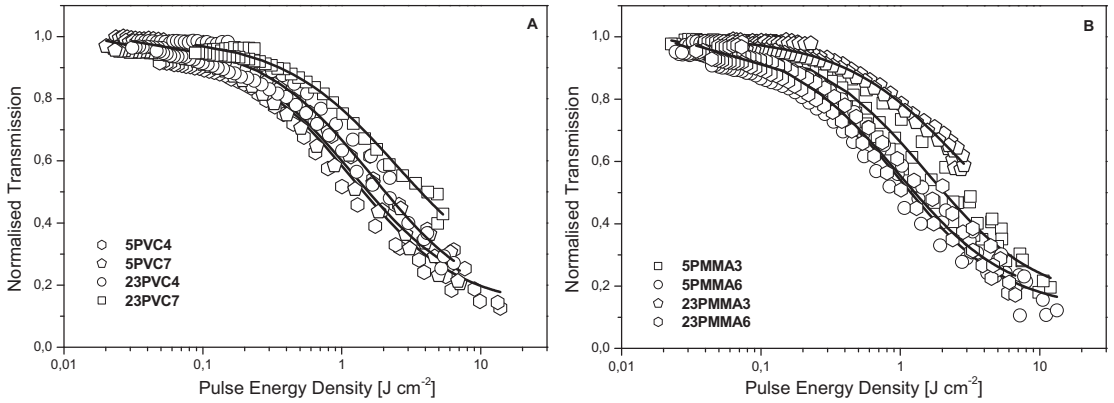

Figure 8.17 Comparison of optical limiting, plotted as normalized transmission against incident pulse energy between multilayer **(nPhO)$_4$PcSnCl$_2$** (**5**) films and multi-layer **(βNO$_2$)$_4$PcGe(tBu$_2$P)$_2$** (**23**) films in PMMA (**A**), and in PVC (**B**).

The differences between multi-layer films of **5** and **23** are observed in their κ values. The multi-layer **(nPhO)$_4$PcSnCl$_2$** (**5**) films in PMMA as well as in PVC has greater magnitude of κ than the multi-layer **(βNO$_2$)$_4$PcGe(tBu$_2$P)$_2$** (**23**) films in same polymers, by a factor of ~ 1.5. The decrease of κ value with increasing the number of layers is observed. This evidence can be seen much pronounced for multi-layer **(βNO$_2$)$_4$PcGe(tBu$_2$P)$_2$** (**23**) films. This is attributed to a greater tendency to aggregate for **(βNO$_2$)$_4$PcGe(tBu$_2$P)$_2$** (**23**) than for **(nPhO)$_4$PcSnCl$_2$** (**5**). The influence of the host lattice and intermolecular interactions caused by aggregation in case of **(βNO$_2$)$_4$PcGe(tBu$_2$P)$_2$** (**23**) can provoke the decay of the upper triplet state [11].

The κ coefficient for **5** in PMMA films, determined to be κ = 9.1 and 8.0 for **5PMMA3** and **5PMMA6**, respectively, is almost same as for **5** in solution (κ(**5**) = 10.2) even though for **5PVC4** κ value is higher *i.e.* κ = 13.7 than for solution of **5**. The higher number of layers in films reflects a significantly low magnitude of the saturation energy density F_{Sat} for presented films. The saturation density decreases with increasing thickness of films (**Table 8.6**). Films of **5** in PMMA and PVC, contrary to **5** in solution, exhibit significantly low F_{Sat} values, ranging from 3.7 to 2.5 J cm^{-2} and being ~ 3 times lower than F_{Sat} of **5** in solution.

The extraordinarily high values of β_I and $\chi^{(3)}$, high value of the ratio of the excited to ground state absorption cross-section κ, and extremely low saturation energy density for **5** and **23** in PMMA and PVC films estimate that those materials are interesting for practical optical limiting devices.

8.4.3 Optical limiting effect in dichlorotin(IV) hexadecafluorophthalocyanine and in bis(3,5-di-*tert*-butylphenoxy)-substituted tin(IV) and germanium(IV) perchlorophthalocyanines in PMMA and PVC films

NLO properties of multi-layer spin coated films of dichlorotin(IV) hexadecafluorophthalocyanine (**16**) and di(3,5-*tert*-butylphenoxy)-substituted tin(IV) and germanium(IV) perchlorophthalocyanines, **14** and **15**, in various polymers were investigated. The nonlinear parameters are listed in **Table 8.7**.

Table 8.7 The NLO data of $\mathbf{Cl_{16}PcSn(}t\mathbf{Bu_2P)_2}$ (**14**), $\mathbf{Cl_{16}PcGe(}t\mathbf{Bu_2P)_2}$ (**15**) and $\mathbf{F_{16}PcSnCl_2}$ (**16**) in PMMA and PVC films.

Solid-state sample	d [μm]	α_0 [cm^{-1}]	I_0 [GW cm^{-2}]	β_I [cm W^{-1}]	Im$\{\chi^{(3)}\}$ [esu]	F_{Sat} [J cm^{-2}]	κ [σ_{ex}/σ_0]
14PMMA3	0.9	2503.5	0.3	7.0e-5	2.6e-8	5.6±0.9	7.4±0.7
14PMMA6	2.1	1540.2	1.0	5.5e-5	2.1e-8	5.5±0.8	6.6±0.5
15PMMA3	0.9	2566.3	0.3	7.4e-6	3.0e-9	40.1±55.0	6.2±6.7
15PMMA6	1.9	1959.3	1.4	3.5e-5	1.3e-8	9.9±0.8	5.7±0.3
14PVC4	1	2245.4	0.5	7.4e-5	2.9e-8	6.0±0.6	8.8±0.5
14PVC7	1.6	2258.3	1.0	5.8e-5	2.3e-8	1.3±0.1	4.9±0.1
15PVC4	0.8	2673.2	0.5	8.6e-5	3.4e-8	5.9±0.9	8.8±0.8
15PVC7	1.5	1990	0.55	1.2e-4	4.7e-8	2.9±0.2	7.4±0.2
16PMMA3	0.8	2304.9	0.4	9.9e-5	3.7e-8	6.3±0.9	10.4±1.0
16PMMA6	1.8	1718.2	0.45	5.0e-5	1.9e-8	7.1±1.5	6.9±0.9
16PVC4	0.9	2932.4	0.6	1.5e-4	5.9e-8	3.6±0.5	8.1±0.6
16PVC7	1.9	2155.3	0.9	1.3e-4	5.2e-8	2.7±0.2	6.0±0.2

The magnitude of the measured third-order nonlinearity $\chi^{(3)}$ is approximately same for multi-layer films of **14**, **15** and **16** in PVC and PMMA. It can be seen that 3- and 6-layer films in PMMA and 4-and 7-layer films in PVC do not exhibit noticeable differences of the $\chi^{(3)}$ values with increase in layers of films. The observed β_I values of solid-state samples **16PMMA3**, **16PMMA6**, **16PVC4**, **16PVC7** vary with polymer matrix. Multi-layer films of **16** in PVC have the β_I an order of magnitude higher than multi-layer films of **16** in PMMA matrix. The

difference in magnitude of β_I for films in PVC and in PMMA of **16** is well compared with the difference in their $\chi^{(3)}$ values, which are also larger for films in PVC than for the latter. The β_I for compound **15** in PMMA and PVC films follows the same trend as for **16**, being an order of magnitude larger for PVC films than for PMMA films. In addition, **15PMMA6** and **15PVC7** films have an order of magnitude higher β_I value than their analogues possessing lower number of layers, **15PMMA63** and **15PVC4**, implying that bulky axial substituents and 16 electron-withdrawing substituents in the peripheral positions of the macrocycle effectively suppress the molecular aggregation and increase the magnitude of the imaginary nonlinear response. The β_I values for films of **14** are similar for films in PMMA and for multi-layer films in PVC and again higher for films in PVC than in PMMA. Compounds **14**, **15** and **16** in multi-layer films of PMMA and PVC exhibit the β_I and $\chi^{(3)}$ values approximately five orders of magnitude larger than in solutions.

Comparison between optical limiting in terms of transmission versus pulse energy density for solution of **16** and for its multi-layer films in various polymers, shows that better nonlinear response is observed for films in PVC and PMMA of **$F_{16}PcSnCl_2$** (**16**) than for solution of **16** (**Figure 8.18**).

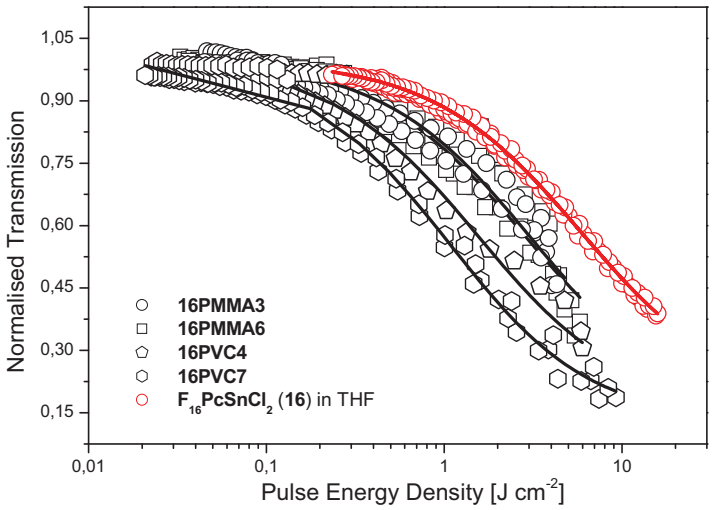

Figure 8.18 Optical limiting, plotted as normalized transmission against incident pulse energy, for multi-layer **$F_{16}PcSnCl_2$** films in PVC and PMMA in respect with **16** in THF. The solid lines are the theoretical curve fits to the experimental data.

The magnitude of nonlinear absorption of films of **16** shows that the nonlinear optical response of **16** in PVC is better than in PMMA films, and that thicker films exhibit better optical limiting than thinner films.

Comparison of multi-layer films of **$Cl_{16}PcSn(tBu_2P)_2$** (**14**), **$Cl_{16}PcGe(tBu_2P)_2$** (**15**) and **$F_{16}PcSnCl_2$** (**16**), considering the substituents in the peripheral positions of macrocycle and the central metal of phthalocyanines, shows that the largest magnitude of nonlinear response displays films of compound **14** (**Figure 8.19 A** and **B**).

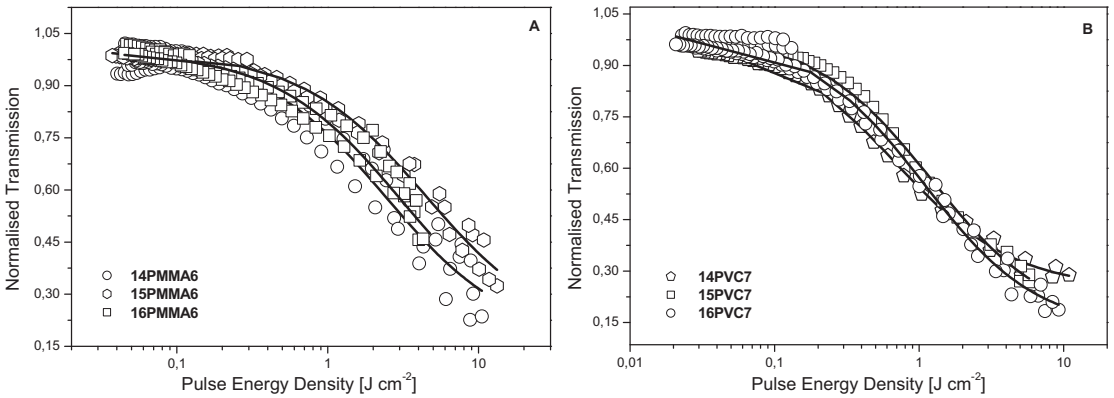

Figure 8.19 Comparison of optical limiting, plotted as normalized transmission against incident pulse energy between multi-layer **$Cl_{16}PcSn(tBu_2P)_2$** (**14**), **$Cl_{16}PcGe(tBu_2P)_2$** (**15**) and **$F_{16}PcSnCl_2$** (**16**) films in PMMA (**A**), and in PVC (**B**).

Moreover, taking into account the same polymer matrix, compound **14** in PMMA and in PVC exhibits the best optical limiting, while **16PMMA6** and **16PVC7** show better nonlinear response than **15PMMA6** and **15PVC7** (**Figure 8.19 A** and **B**). This indicates that the heavy atom effect of tin and more electron-withdrawing fluorine peripheral substituents give rise to a better optical limiting. It can be seen that nonlinear response for **14** in PMMA is better than for **15** (**Figure 8.20 A**), furthermore **14PMMA3** shows slightly better optical limiting than **15PMMA6**, even though **15PMMA6** is ~ 2 times thicker (**Table 8.7**) than **14PMMA3**. **Figure 8.20 A** shows that it is noticeable difference in the magnitude of nonlinear absorption for 4- and 7-layer films of **14** and **15** in PVC, being the largest for **14PVC7** with thickness of 1.6 μm and the lowest for **15PVC4** with thickness of 0.8 μm. This confirms again that the size of the central metal, taking into account the same axial and peripheral substituents of phthalocyanines, has considerable influence on optical limiting.

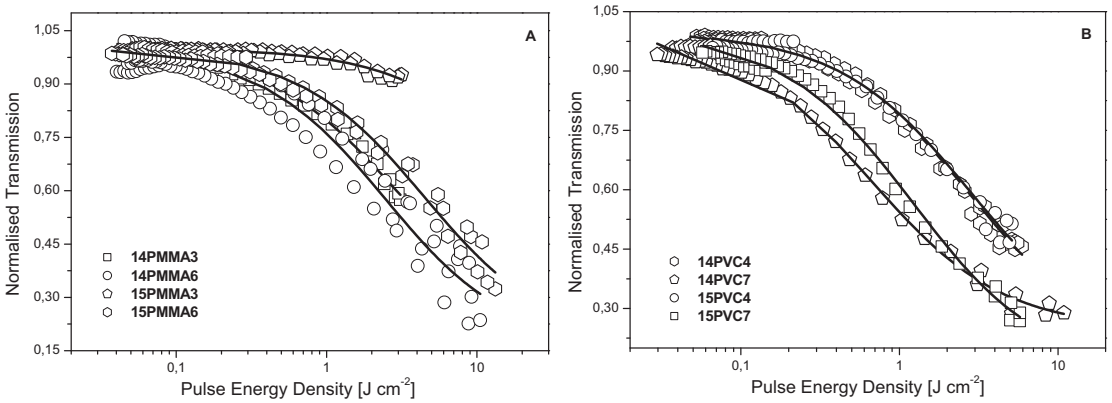

Figure 8.20 Comparison of optical limiting, plotted as normalized transmission against incident pulse energy between multi-layer **$Cl_{16}PcSn(tBu_2P)_2$** (**14**) films and multi-layer **$Cl_{16}PcSn(tBu_2P)_2$** (**15**) films in PMMA (**A**), and in PVC (**B**).

The ratios of the absorption cross section κ were found to decrease insignificantly with increase of thickness of films in both polymers for three compounds presented here. The κ value ranges from 4.9 to 10.4, being the highest for **16PMMA3** and the lowest for **14PVC7**. Multi-layer films of **16** in PMMA and PVC have slightly lower κ values than 1**6** in solution. The lower κ coefficients for 6-layer PMMA and 7-layer PVC films compared to 3-layer PMMA and 4-layer PVC films of **14**, **15** and **16** can be caused by interactions between phthalocyanines or polymer host. The absorption spectra of 6-layer PMMA and 7-layer PVC films of **14**, **15** and **16** compared to the corresponding solutions presented in **Figure 8.21 A**, **B** and **C** show that the absorption spectra of films are slightly broader than that of solutions, and shoulders on the shorter wavelength side of the Q-bands appear, suggesting that some part of compounds **14**, **15** and **16** in films exist in aggregated state. Nevertheless, the Q-band position of films does not change with the growth of their thickness. Besides, no meaningful changes of the shape of Q-bands can be seen from the comparison of mono-layer with 6-layer films in PMMA, and 4-layer with 7-layer films in PVC, respectively.

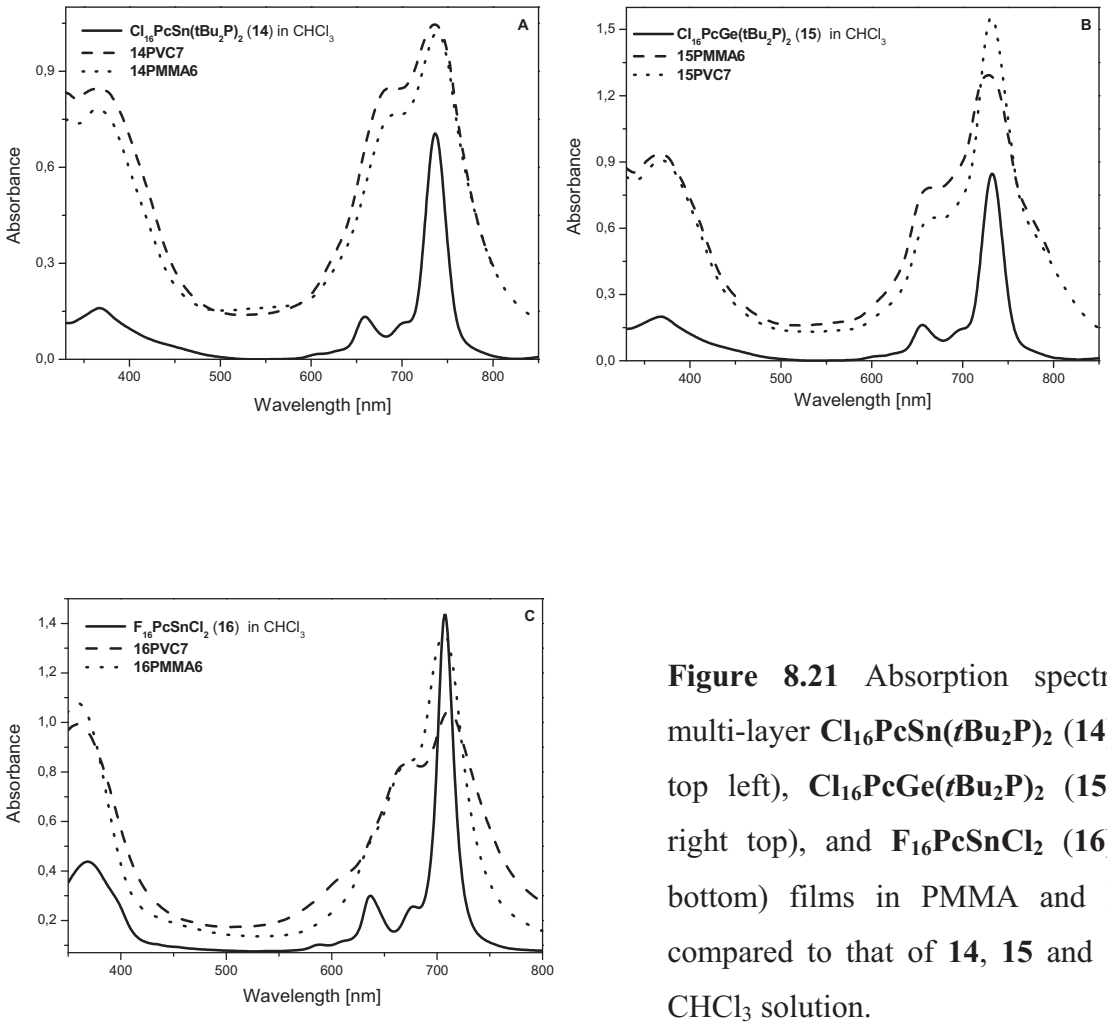

Figure 8.21 Absorption spectra of multi-layer **$Cl_{16}PcSn(tBu_2P)_2$** (**14**), (**A**, top left), **$Cl_{16}PcGe(tBu_2P)_2$** (**15**) (**B**, right top), and **$F_{16}PcSnCl_2$** (**16**) (**C**, bottom) films in PMMA and PVC, compared to that of **14**, **15** and **16** in $CHCl_3$ solution.

On the other hand, the magnitude of the saturation density F_{Sat} for films of **14**, **15** and **16** compounds decreases with the increasing layers of films. The difference in value of F_{Sat} for 4-layer and 7-layer films in PVC is much bigger than for 3-layer and 6-layer PMMA films of compounds **14**, **15** and **16**. The F_{Sat} value of **16PVC4** was determined to be 3.6 J m^{-2}, lower than that of **14PVC4** and **15PVC4**, by a factor of ~ 1.6, while **16PVC7** and **15PVC7** have comparable F_{Sat} values *i.e.* 2.7 and 2.9 J m^{-2} and ~ 2 times greater than the F_{Sat} observed for **14PVC7**. This suggests that thickness of the resulting films having the reflection in the Pc concentration in solid-state can effectively influence on the reduction of the magnitude of energy density. In addition, the magnitude of the saturation density F_{Sat} for multi-layer **$F_{16}PcSnCl_2$** (**16**) films in various polymers is substantially lower than that of **16** in solution.

The multi-layer films of axially substituted tin and germanium perchloro- and perfluoro-substituted phthalocyanines in various polymers presented here, possess high β_I, $\chi^{(3)}$, and α_0

values, and additionally saturate at substantially low energy density. The films presented here can be interesting for practical application.

8.4.4 Optical limiting effect in chloroindium tetrakis(2,9,16,23-*tert*-butyl)phthalocyanine in PMMA and PVC films and for comparison in solution

Two of many compounds with the best-described optical limiting properties [8] are highlighted in **Table 8.8**: chloroindium tetrakis(*tert*-butyl)phthalocyanine **(*t*-Bu)$_4$PcInCl** (**25**) [8] and palladium octahexylphthalocyanine (**(C$_6$H$_{13}$)$_8$PcPd**) [8]. Compound **(*t*-Bu)$_4$PcInCl** (**25**) exhibit very high reported κ and $\chi^{(3)}$ values but dramatically high F_{Sat} and average β_I values. In contrast, the Pd compound shows higher β_I and lower F_{Sat} values, but a low κ value. It is not easy to estimate which phthalocyanine will be better optical limiter, and it is important that those compounds were not investigated in polymer films by now.

Table 8.8 The NLO data of **tBu$_4$PcInCl** (**25**) and **PdPc(C$_6$H$_{13}$)$_8$** in solution.

Compound	c [g L^{-1}]	α_0 [cm^{-1}]	I_0 [GW cm^{-2}]	β_I [cm W^{-1}]	Im$\{\chi^{(3)}\}$ [esu]	F_{Sat} [J cm^{-2}]	κ [σ_{ex}/σ_0]
(*t*-Bu)$_4$PcInCl (25) [e]	0.5 [f]	0.53	0.5	4.4e-8	1.3e-11	24.2±0.8	27.4±0.6
(C$_6$H$_{13}$)$_8$PcPd [e]	1.0 [f]	2.60	0.5	9.6e-8	3.6e-11	2.1±0.1	5.9±0.1

[e] Reference [8]
[f] toluene (T) used as solvent

Multi-layer films of chloroaluminium tetrakis(*tert*-butyl)phthalocyanine (**25**) were prepared in various polymers (PVC and PMMA) and their NLO properties were investigated. The nonlinear parameters of **25** in PMMA and PVC films with different number of layers are presented in **Table 8.8**. The measured third-order nonlinearity $\chi^{(3)}$ and effective nonlinear absorption coefficient β_I for **(*t*-Bu)$_4$PcInCl** (**25**) in PMMA and PVC films are found to be two or three orders of magnitude higher than those of the corresponding to **25** as well as of **(C$_6$H$_{13}$)$_8$PcPd** in toluene solutions. This shows that **(*t*-Bu)$_4$PcInCl** (**25**) in polymers increases the magnitude of the imaginary nonlinear response at appropriate intensities.

The observed β_I and $\chi^{(3)}$ values of **25PMMA6** (β_I = 5.0e-5 esu and $\chi^{(3)}$ = 1.9e-8 esu) are higher than those of **25PMMA3** (β_I = 1.2e-5 esu and $\chi^{(3)}$ = 4.5e-9 esu), indicating that increase of thickness of film increase the magnitude of the imaginary nonlinear response. This is in contrast to the PVC films of **25**, the β_I and $\chi^{(3)}$ values are comparable for 3- and 7-layer PVC films.

Table 8.9 The NLO data of (***t*-Bu)$_4$PcInCl** (**25**) in PMMA and PVC films.

Solid-state sample	d [μm]	α_0 [cm^{-1}]	β_I [cm W^{-1}]	Im$\{\chi^{(3)}\}$ [esu]	F_{Sat} [J cm^{-2}]	κ [σ_{ex}/σ_0]
25PMMA3	1	1895.7	1.2e-5	4.5e-9	19.7±21.5	6.5±5.4
25PMMA6	2	1370	5.0e-5	1.9e-8	16.4±25.3	5.7±6.8
25PVC4	0.8	2290.7	1.2e-5	4.7e-9	21.8±27.2	8.1±5.8
25PVC7	1.4	1351.1	1.0e-5	4.1e-9	19.7±30.8	7.4±9.4

The values of the ratio of absorption cross section κ of **25** in polymer films are smaller approximately 4 times than the κ coefficient of **25** in solution what can be caused by relatively high linear absorption coefficient α_0 of films. On the other hand, the κ value for films of **(*t*-Bu)$_4$PcInCl** (**25**) is comparable or even higher than that for palladium octahexylphthalocyanine (**(C$_6$H$_{13}$)$_8$PcPd**) in toluene solution. The magnitude of nonlinear absorption (**Figure 8.22**) of films of compound **25** in PMMA and PVC varies with their thickness, increasing in the series: **25PVC4**, **25PMMA3**, **25PVC7**, **25PMMA6**, where **25PMMA6** is the thickest (d = 2.0 μm) and **25PVC4** the thinnest film (d = 0.8 μm), showing that increase of thickness of film contributes to a better magnitude of nonlinear response.

Comparison of the optical limiting, plotted as normalized transmission as a function of incident pulse energy, of multi-layer **(*t*-Bu)$_4$PcInCl** (**25**) films in PVC and PMMA with films of **(fPhO)$_4$PcSnCl$_2$** (**6**) and **(fPhO)$_4$PcGeCl$_2$** (**7**) is shown in **Figure 8.23**. It can be evidently seen that **(fPhO)$_4$PcGeCl$_2$** (**7**) in PMMA as well as in PVC films demonstrate better nonlinear absorption than films of **6** and **25**. Furthermore, solid-state samples, **25PMM6** and **6PMMA6**, and, **25PVC7** and **6PVC7**, show comparable nonlinear response, even though **6PVC7** demonstrates slightly better nonlinear response than **25PVC7** (**Figure 8.23 B**).

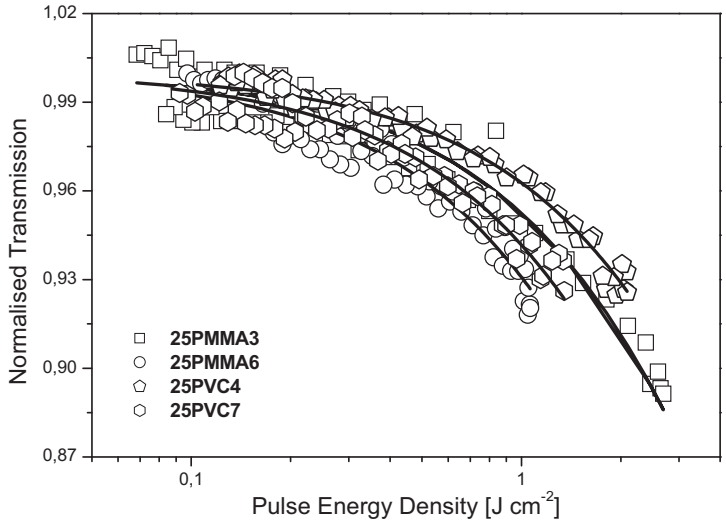

Figure 8.22 Optical limiting, plotted as normalized transmission against incident pulse energy, for multi-layer **(*t*-Bu)$_4$PcInCl** (**25**) films in PVC and PMMA. The solid lines are the theoretical curve fits to the experimental data.

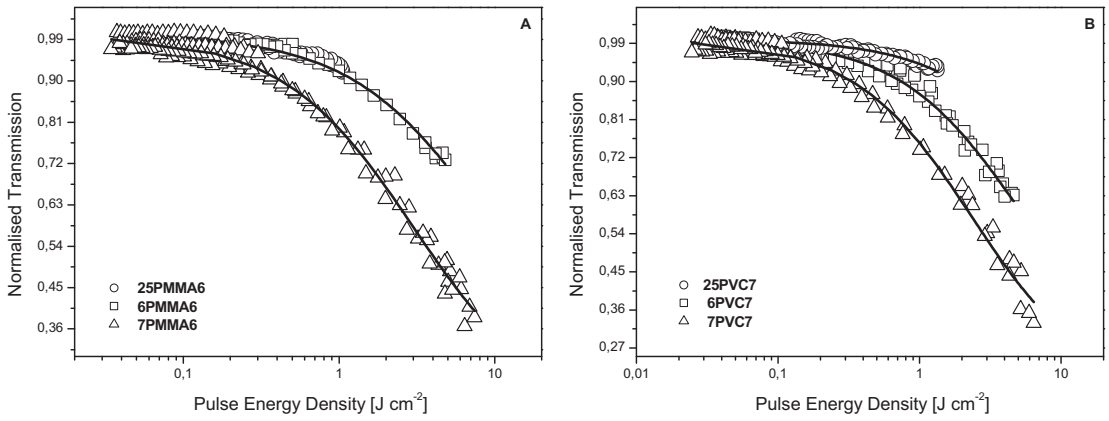

Figure 8.23 Optical limiting, plotted as normalized transmission against incident pulse energy, for 6-layer film in PMMA of **(*t*-Bu)$_4$PcInCl** (**25**) compared 6-layer PMMA films of **(fPhO)$_4$PcSnCl$_2$** (**6**) and **(fPhO)$_4$PcGeCl$_2$** (**7**) (**A**), and for 7-layer film in PVC of **(*t*-Bu)$_4$PcInCl** (**25**) compared 7-layer PVC films of **6** and **7** (**B**).

The magnitude of F_{Sat} is changed from **25PMM3** to **25PMMA6**, and from **25PVC4** to **25PVC7**, being lower for more multi-layer films. These points out that thicker film attenuate laser pulses at lower energies than thinner films do.

The optical limiting properties of **25** in multi-layer films of PMMA and PVC seem to be much better compared to its properties in solution. The high $\chi^{(3)}$ and β_I values, the low energy density F_{Sat} and high linear absorption coefficients α_0 for films of **25** confirm its good suitability as optical limiter.

8.4.5 Optical limiting effect in phthalocyanines in drop coated films

Optical limiting of drop coated films of metallated octabutoxyphthalocyanines **(BuO)$_8$PcZn** (**29**), **(BuO)$_8$PcPb** (**30**) and **(BuO)$_8$PcCu** (**31**) in poly(styrene) (PS) and PMMA were investigated. In addition, NLO properties of the hydrophilic tetraanionic tetrasulfophthalocyanine **(Sul)$_4$PcGa** (**28**) incorporated into sol gel film were determined. The NLO data of drop coated films are listed in **Table 8.10**. Unfortunately, the optical limiting of above-mentioned phthalocyanines was not investigated in solution.

The magnitude of third-order nonlinearity $\chi^{(3)}$ is of the same order for each film, being the highest for **31PMMA1** and the lowest for **30PS1**. The measured β_I was found to be comparable for **29PMMA1** (β_I(**29**) = 8.5×10^{-6} cm W^{-1}) and **30PS1** (β_I(**30**) = 6.0×10^{-6} cm W^{-1}) whereas for **31PMMA1** the β_I value was almost double than for both **29PMMA1** and **30PS1** but for sol gel, **28GaPcGel**, ~ 3 times smaller than for **29PMMA1** and **30PS1** films. Comparison of drop coated with spin coated films discussed previously (Chapters 8.4.1 to 8.4.4) points out that the measured $\chi^{(3)}$ and β_I are approximately an order higher for spin coated films in PMMA and PVC. In addition, the κ coefficients are found to be very low for all drop coated films.

Table 8.10 The NLO data of **(Sul)$_4$PcGa** (**28**), **(BuO)$_8$PcZn** (**29**), **(BuO)$_8$PcPb** (**30**) and **(BuO)$_8$PcCu** (**31**) in drop coated films.

Solid-state sample	d [μm]	α_0 [cm^{-1}]	β_I [cm W^{-1}]	Im{$\chi^{(3)}$} [esu]	F_{Sat} [J cm^{-2}]	κ [σ_{ex}/σ_0]	Transmitted Energy [mJ]	T_{min}
28GaPcGel	109	67.0	2.4e-6	-	2.2±0.07	3.4±0.05	7.8e-3	0.41
29PMMA1	244	136.9	8.5e-6	3.2e-9	0.9±0.08	1.8±0.05	9.53e-5	0.057
30PS1	205	121.7	6.0e-6	2.5e-9	1.5±0.06	1.9±0.02	5.48e-4	0.074
31PMMA1	117	258.9	1.4e-5	5.1e-9	2.5±0.17	1.8±0.04	1.65e-4	0.051

Very low κ, rather low $\chi^{(3)}$ and β_I values (compared to Pc films prepared by spin coating method) of drop coated films can be caused by strong molecular interactions and big packing

of phthalocyanines during their preparation. In case of all drop coated films, their absorption spectra are dominated by aggregation. The absorption spectra of all films: **28GaPcGel**, **29PMMA1**, **30PS1** and **31PMMA7** are significantly broader than those of the corresponding phthalocyanines **28**, **30** and **31** in solutions, and the Q-band of each film is widely batochromic shifted against Q-band in the corresponding phthalocyanine in solution.

The optical limiting plotted as normalized transmission as a function of energy density for drop coated films of **(Sul)$_4$PcGa** (**28**), **(BuO)$_8$PcZn** (**29**), **(BuO)$_8$PcPb** (**30**) and **(BuO)$_8$PcCu** (**31**) is presented in **Figure 8.24**.

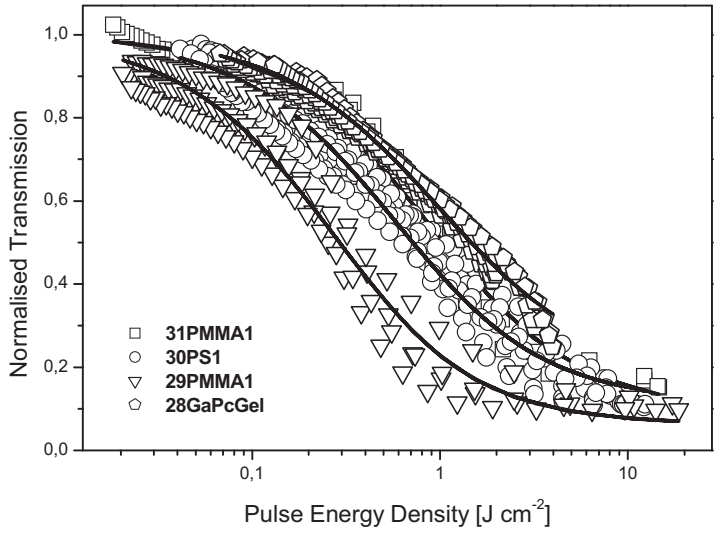

Figure 8.24 Optical limiting, plotted as normalized transmission against incident pulse energy, for drop films: **28GaPcGel**, **29PMMA1**, **30PS1** and **31PMMA1**. The solid lines are the theoretical curve fits to the experimental data.

With regard to the magnitude of the reduction in normalized transmission relative to incident energy density, the drop coated film of **(BuO)$_8$PcZn** (**29**) exhibits the best nonlinear response among the four drop coated films while films of **(Sul)$_4$PcGa** (**28**) and **(BuO)$_8$PcCu** (**31**) show comparable nonlinear responses.

The sol gel film of **(Sul)$_4$PcGa** (**28**) has a κ value ~ 2 times larger than the other three drop coated films of octa-substituted phthalocyanines, **(BuO)$_8$PcZn** (**29**), **(BuO)$_8$PcPb** (**30**) and **(BuO)$_8$PcCu** (**31**). Compounds **29**, **30** and **31** possess almost the same magnitude of κ ranging from 1.8 to 1.9. The difference in the magnitude of κ values for these compounds is dominated by the difference in their linear absorption coefficients α_0, being ~ 2 times greater

for **29PMMA1** and **30PS1** than for **28GaPcGel** and ~ 4 times greater for **29PMMA1** than for **28GaPcGel**.

Furthermore, the energy saturation F_{Sat} is extremely low for all investigated drop coated films. The value of F_{Sat} calculated for **29PMMA1** is the lowest, determined to be 0.9 J cm^{-2}. For the other three films the energy density F_{Sat} is comparable, ranging from 1.5 to .2.5 J cm^{-2} (**Table 8.10**). The energy saturation F_{Sat} increases in a series: **29PMMA1** < **30PS1** < **28GaPcGel** < **31PMMA1**, and with the same order, the thicknesses of films decrease. This nicely shows that the increase of thickness considerably decreases the energy saturation and drop coated films attenuate laser pulses at very low energies.

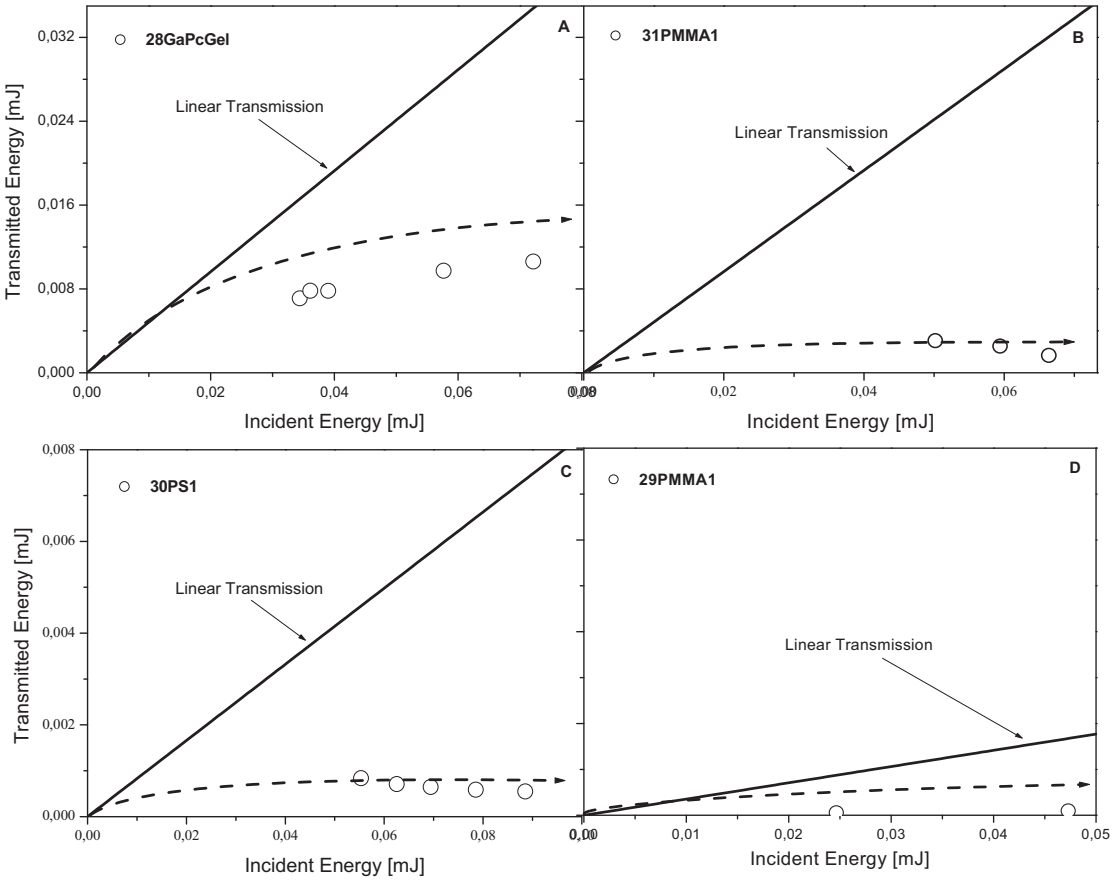

Figure 8.25 Alternative few of optical limiting for drop coated films: **28GaPcGel** (**A**), **29PMMA1** (**D**), **30PS1** (**C**) and **31PMMA1** (**B**) presents incident versus transmitted energy per pulse for the device at the optimal limiting location relative to the focal plane of the lens in the apparatus. The solid lines represent the linear optical response and the dashed line is a sketch through the data representing the nonlinear optical limiting response.

Moreover, the drop coated film of **29** exhibits the lowest magnitude of the transmitted energy presented in **Figure 8.25 D** (**Table 8.10**). The observed transmitted energy versus incident energy for **28GaPcGel**, **30PS1** and **31PMMA1** was almost similar but being an order of magnitude higher than for **29PMMA1**. The minimum values of transmission T_{min} which are accomplished in correspondence of the highest level of irradiation, *i.e.* at the focus (z = 0), is the highest for **28GaPcGel**, T_{min} = 0.41 at 0.04 mJ incident energy, and considerably lower for **29PMMA1**, **30PS1** and **31PMMA1**, being 0.057, 0.074 and 0.051, respectively. It suggests that a better OL performance with the lowest value of T_{min} exhibit metallated octabutoxy-substituted phthalocyanines compared to sol gel of **(Sul)$_4$PcGa** (**28**).

8.4.6 Optical limiting effect in tetra- and octa-substituted phthalocyanines in double layer films

The optical limiting of the double layer films of octabutoxy-substituted phthalocyanines **(BuO)$_8$PcZn** (**29**), **(BuO)$_8$PcPb** (**30**), **(BuO)$_8$PcCu (31)**, and of metal-free tetra-substituted phthalocyanines **(PhO)$_4$PcH$_2$** (**26**) and **(*t*-BuPhO)$_4$PcH$_2$** (**27**) were investigated.

The theoretical study of optical limiting devices built from reverse saturable absorbers published in details Miles in 1994 [12]. He demonstrated that for a tandem device (two layers separated) that there will exist some point where the transmission for a given focused laser pulse would be a minimum for the particular device. If this is considered in terms of the open aperture z-scan technique this optimal device position will correspond to the minimum transmission T_{min} point in the z-scan. For the double layer films, it will be presented such curves using the minimum transmission only. It will be presented incident versus transmitted energy per pulse for the device at the optimal limiting location relative to the focal plane of the lens in the apparatus. In these plots, the solid lines represent the linear optical response and the dashed line is a sketch through the data representing the nonlinear optical limiting response.

The double layer films were prepared by spin coating method on both sides of sapphire substrate. The minimum transmission T_{min} at appropriate incident energy of double layer films is presented in **Table 8.11**.

Table 8.11 The T_{min} of **$(PhO)_4PcH_2$** (**26**), **$(t\text{-}BuPhO)_4PcH_2$** (**27**), **$(BuO)_8PcZn$** (**29**), **$(BuO)_8PcPb$** (**30**) and **$(BuO)_8PcCu$ (31)** in double layer films.

Compound	d [μm]	Incident Energy [mJ]	T_{Min}
26PVC3	0.5	0,041	0,488
		0,098	0,234
27PS3	0.5	0,047	0,332
		0,080	0,187
		0,116	0,146
		0,134	0,169
29PS3	0.6	0,042	0,355
		0,090	0,231
29PVC4	0.5	0,042	0,352
		0,092	0,207
30PVC5	0.5	0,034	0,391
		0,040	0,442
31PMMA7	0.9	0,047	0,139
		0,090	0,060

The alternative few of optical limiting for **26PVC3** and **27PS3** are presented in **Figure 8.26** and **8.27**. The minimum transmission versus incident energy presented for **26PVC3** and **27PS3** in **Figure 8.26 A** and **Figure 8.27 A** decreases with increasing incident energy. The minimum transmission T_{min} for **26PVC3** is slightly bigger than for **27PS3** at comparable incident energy. The transmitted energy grows with the incident energy until the threshold is achieved. When the threshold value is reached, the transmitted energy becomes a constant value for any larger input light energy (**Figure 8.27 B** and **8.28 B**). For double layer films, **26PVC3** and **27PS3**, the limiting threshold is ~ 0.07 and ~ 0.08 mJ, respectively.

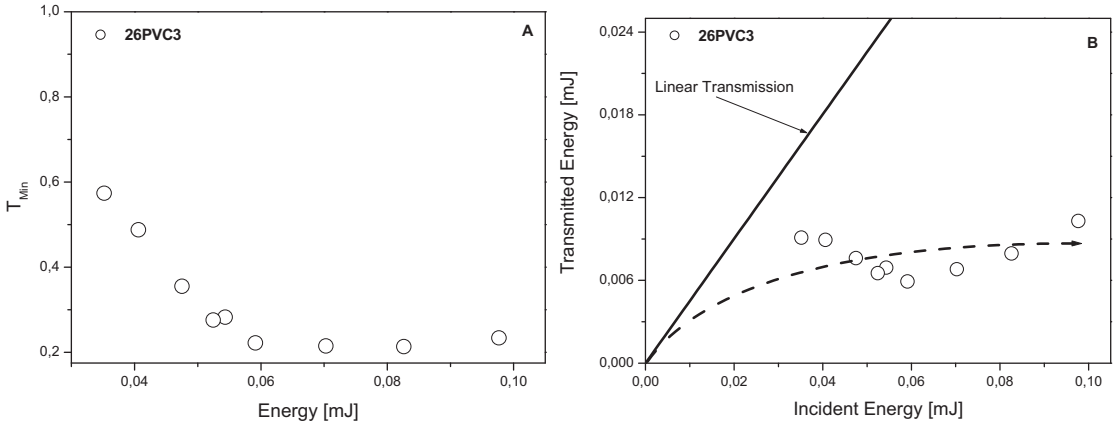

Figure 8.26 Alternative few of optical limiting of **26PVC3**. The minimum transmission versus incident energy (**A**) and incident versus transmitted energy per pulse for the device at the optimal limiting location relative to the focal plane of the lens in the apparatus (**B**). The solid lines represent the linear optical response and the dashed line is a sketch through the data representing the nonlinear optical limiting response.

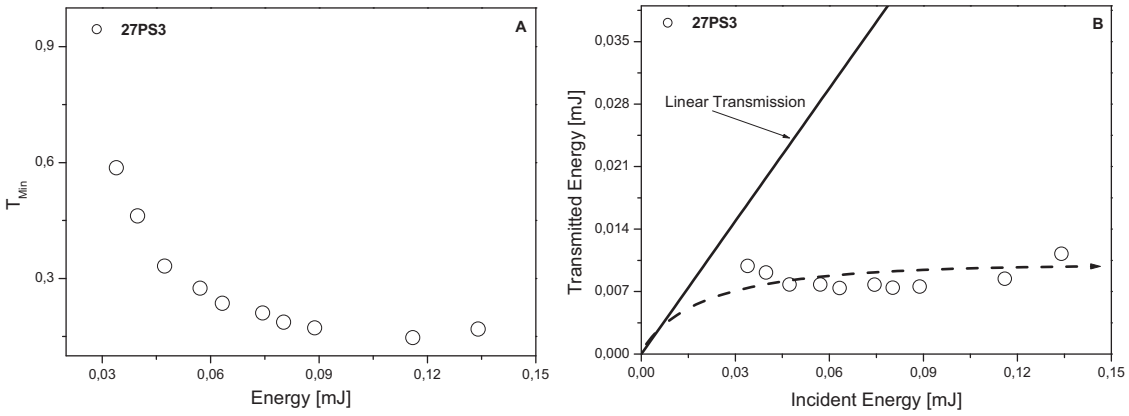

Figure 8.27 Alternative few of optical limiting of **27PS3**. The minimum transmission versus incident energy (**A**) and incident vs. transmitted energy per pulse for the device at the optimal limiting location relative to the focal plane of the lens in the apparatus (**B**).

The films of metal-free phthalocyanines, **26** and **27**, even in different polymers, exhibit similar optical limiting response. The thickness for the double layer films of metal-free complexes is equal for both films, determined to be 0.5 μm. In addition, the absorption spectra of **26** in PVC and **27** in PS show broad Q-band, which is widely blue-shifted in comparison to Q-band in chloroform solutions.

Comparison of optical limiting of compound **29** in PS and PVC (**Figure 8.28 A** and **B**) shows slightly better nonlinear optical limiting response of **29PVC4**. However, double layer films, **29PS3** and **29PVC4** possess comparable the minimum transmission (T_{min}) at same incident energy.

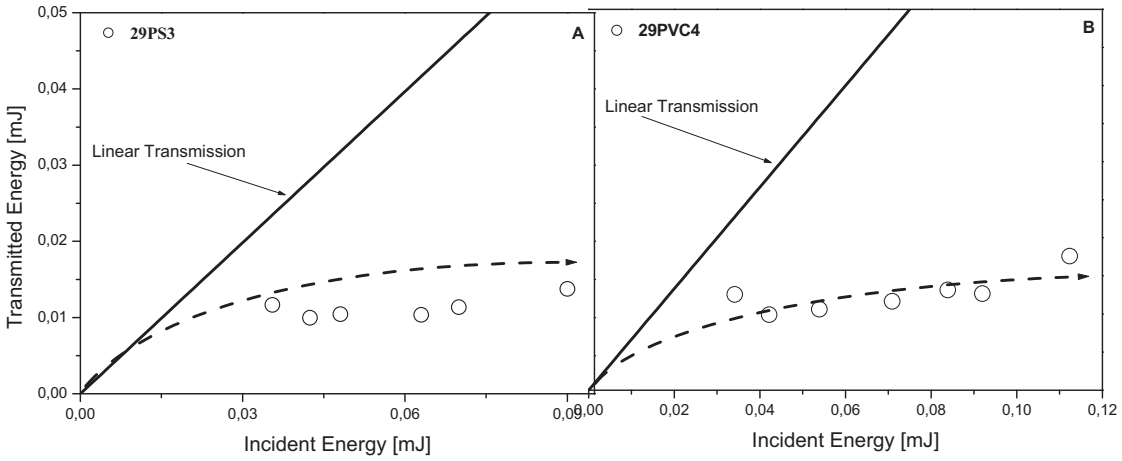

Figure 8.28 Alternative few of optical limiting of **29PS3** (**A**) and **29PVC4** (**B**) present incident versus transmitted energy per pulse for the device at the optimal limiting location relative to the focal plane of the lens in the apparatus.

The limiting threshold value of the transmitted energy for films, **29PS3** and **29PVC4** is same, determined to be ~ 0.01 mJ. The lowest value of minimum transmission was found for **31PMMA7** T_{min} = 0.06 at 0.09 mJ incident energy. The film of **31** in PMMA possess the highest thickness among double layer films presented here, determined to be 0.9 μm. The film **31PMMA7** exhibits the best nonlinear optical response (**Figure 8.29 B**) and limited the transmitted energy to between 0.0027 and 0.0035 mJ. However, **30PVC5** shows the worst optical limiting (**Figure 8.29 A**). The highest value of the minimum transmission T_{min} that is, maximum absorption at the focus of the lens I_0 as the scan is done, shows **30PVC5** among the double layer films of octabutoxy-substituted phthalocyanines, what confirms its poor suitability as optical limiter.

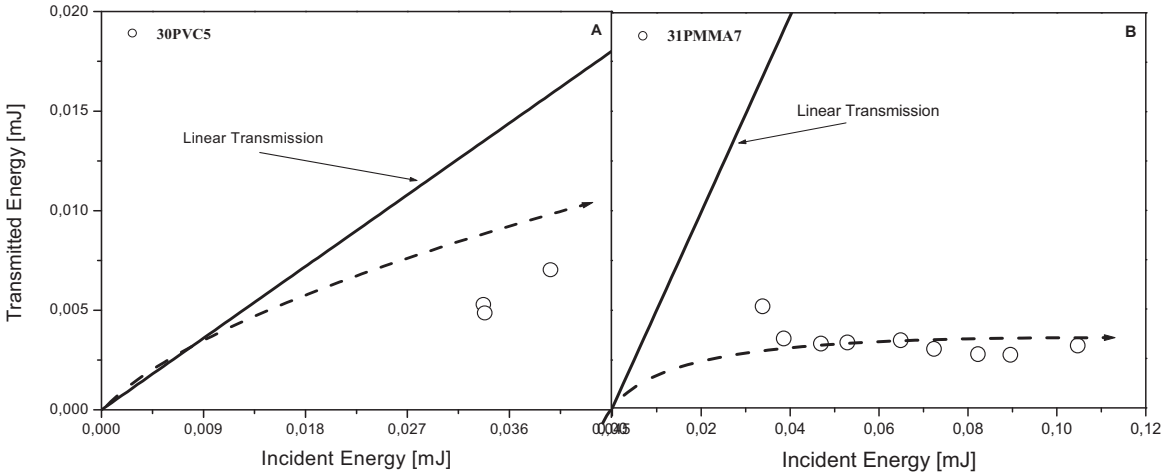

Figure 8.29 Alternative few of optical limiting of **30PVC5** (**A**) and **31PMMA7** (**B**) present incident versus transmitted energy per pulse for the device at the optimal limiting location relative to the focal plane of the lens in the apparatus.

Taking into account the minimum transmission T_{min} and plots of alternative optical limiting, a good candidate for optical limiter seems to be **31PMMA7** film with the highest thickness and the best T_{min}. On the other hand, it is rather difficult to estimate the NLO properties of the double layer films discussed here without NLO parameters such as the effective intensity dependent nonlinear absorption coefficient β_I, $\chi^{(3)}$, the energy density F_{Sat}, the linear absorption coefficients α_0, or the value of κ, and in addition, without possibility to compare OL in films with their NLO properties in solutions.

8.5 Conclusion

The purpose of this study was to determine the optical limiting properties of a series of germanium, tin and metal free phthalocyanines with various electron-withdrawing peripheral substituents and to compare them with polymeric films of those phthalocyanines. Multi-layer films of PVC and PMMA containing the phthalocyanines were obtained by spin coating on glass substrates. Absorption spectra were used to measure the linear optical properties. In polymer films, most phthalocyanines were totally monomeric and not aggregated. The optical limiting of double layer films of **(BuO)$_8$PcZn** (**29**), **(BuO)$_8$PcPb** (**30**), **(BuO)$_8$PcCu** (**31**), **(PhO)$_4$PcH$_2$** (**26**) and **(*t*-BuPhO)$_4$PcH$_2$** (**27**) in PS, PVC and PMMA were also investigated. In addition, the drop coated films of Zn, Pb, Cu octabutoxy-substituted phthalocyanines were prepared and their NLO properties were determined. The optical limiting properties of the

phthalocyanines in solution and in polymer films were measured by the open-aperture z-scan technique. All measurements were performed using 6 ns pulses from a Q-switched Nd:YAG laser. The laser was operated at its second harmonic, 532 nm, with pulse repletion of 10 Hz. The compounds were characterized by the effective imaginary third-order susceptibility $\chi^{(3)}$, the effective intensity dependent nonlinear absorption coefficient β_I, the energy density at which the material saturates F_{Sat} and the value of κ (ratio σ_{ex}/σ_o of the excited triplet state and ground state absorption cross section).

The optical limiting properties of the tin and germanium phthalocyanines in multi-layer films of PMMA and PVC were mostly better compared to OL properties of Pcs in solution. The multi-layer films of tin and germanium phthalocyanines in various polymers exhibit lower value of energy density, much higher magnitude of third-order nonlinearity and of nonlinear absorption coefficient in comparison with phthalocyanines in solution. It was found that tin phthalocyanines in most cases act as better optical limiters than germanium phthalocyanines. Some devices exhibit excellent combination of $\chi^{(3)}$, β_I, F_{Sat} and κ values. Especially the phthalocyanines: **(nPhO)$_4$PcSnCl$_2$** (**5**), **(fPhO)$_4$PcSnCl$_2$** (**6**), **(fPhO)$_4$PcGeCl$_2$** (**7**), **Cl$_{16}$PcSn(*t*Bu$_2$P)$_2$** (**14**), **Cl$_{16}$PcGe(*t*Bu$_2$P)$_2$** (**15**) and **F$_{16}$PcSnCl$_2$** (**16**) in PVC and PMMA films have good combination of NLO factors what makes them interesting for practical application. In addition, **(nPhO)$_4$PcSnCl$_2$** (**5**) in polymeric films exhibits better OL performance than **(*t*-Bu)$_4$PcInCl** (**25**). Moreover, the plots of normalized transmission against pulse energy density show that some films seem to be a suitable as practical optical limiters.

The examined drop coated films exhibit extremely low energy density what is important for practical application. On the other hand, the κ values for all drop coated films were found to be very low, implying that the intermolecular interactions caused by aggregation provoke the decay of the upper triplet state.

8.6 References

[1] T. H. Maiman, *Nature*, **1960**, 187, 493.

[2] P. A. Franken, A. E. Hills, C. W. Peters, G. Weinreich, *Phys. Rev. Lett.,* **1961**, 7, 118.

[3] N. Bloembergen, *Nonlinear Optics, Benjamin,* New York, **1965**.

[4] H. S. Nalwa, S. Miyata, Eds., *Nonlinear Optics of Organic Molecular and Polymeric Materials,* CRC Press, Boca Raton, Florida, **1996**.

[5] M. A. O. Hercher, *Appl. Opt.*, **1967**, 6, 947.

[6] D. R. Coulter, V. M. Miskowski, J. W. Perry, T. H. Wei, E. W. Van Stryland, D. J. Hagan, *Proc. SPIE,* **1989**, 1105, 42.

[7] M. Sheik-Bahae, A. A. Said, T. H. Wei, D. J. Hagan, E. W. Van Stryland, *IEEE. J. Quantum Electron.*, **1990**, 26, 760.

[8] S. M. O'Flaherty, S. V. Hold, M. J. Cook, T. Torres, Y. Chen, M. Hanack, W. J. Blau, *Adv. Mater.*, **2003**, 15, 19.

[9] J. S. Shirk, J. R. Lindle, F. J. Bartoli, C. A. Hoffman, Z. H. Kafafi, A. W. Snow, *Appl. Phys. Lett*., **1989**, 13, 1287.

[10] D. Dini, *Int. J. Mol. Sci.,* **2003**, 4, 291.

[11] J. S. Shirk, R. G. S. Pong, S. R. Flom, H. Heckmann, M. Hanack, *J. Phzs. Chem A*, **2000**, 104, 1438.

[12] P. A. Miles, *Applied Optics*, **1994**, 33, 6965.

9. Summary and future work

9.1 Summary

A series of metal-free, tin and germanium tetra-, hexadeca- and one octa-substituted phthalocyanines were synthesized, characterized and studied with regard to their nonlinear optical (NLO) properties. The phthalocyanines were characterized by IR, UV/Vis and mass spectroscopy. In order to check the practical application of the prepared compounds as optical limiters some of them were used for preparation multilayer films in different polymers by the spin coating method on glass substrates. Additionally, spin and drop coated films of previously synthesized metallated octa- and tetra-substituted phthalocyanines [1-3] were prepared. The synthesized phthalocyanine complexes and all fabricated films were examined with regard to optical limiting by the z-scan measurements.

Tin and germanium phthalocyanines substituted with the variety of electron-withdrawing peripheral (CN, Cl, F, NO_2, *p*-formylphenoxy, *p*-nitrophenoxy) and axial substituents (Cl, F, OH, di(*tert*-butyl)phenoxy) were synthesized. Compounds **5**, **6** and **7** were obtained by a three step synthesis (Chapter 4.2) in good yields. Firstly, starting materials **1** and **2** were prepared then the metal-free phthalocyanines **3** and **4** were synthesized and finally the insertion of metal into metal-free complexes gave the desired compounds **5**, **6** and **7**. The phthalocyanine complexes **5**, **6** and **7** were purified and analytically characterized (Chapter 6.4), exhibiting good solubility in common organic solvents and no tendency to aggregation. On account of this, these complexes were used for the preparation of films (Chapter 7.3.1). A series of tin and germanium tetranitro-substituted at α and β positions phthalocyanines were prepared in order to check the influence of position of peripheral substituents on optical (Chapter 4.2) and nonlinear optical properties (Chapter 8.3.3). The results demonstrate that compounds **19** and **22** tetranitro-substituted at α-positions display a 10 cm^{-1} red shift of the NO_2 vibration in comparison with **18** and **20** complexes substituted at β-position. Absorption spectra show that the Q-band is ~10 nm blue-shifted in complexes **19** and **22** in relation to the Q-band in **18** and **20** complexes caused by the influence of the electron-withdrawing nitro groups which cause a hypsochromic shift of the Q-band depending on their positions of the macrocycle. Additionally, dichlorotin(IV) octacyano-substituted phthalocyanine and a known compound **23** [4] were prepared (Chapter 4.2 and 6.4). The synthesis of tin and germanium hexadecachloro- and hexadecafluoro-substituted phthalocyanines were also performed. Various types of axial ligands were introduced into the macrocycle in order to check their

influence on NLO properties. The synthesis of compounds **8** and **9** were performed by two methods, in bulk and in solution (Chapter 4.3). UV/Vis absorption spectra of all perchloro-substituted phthalocyanines **8** - **13** show Q-bands situated at longer wavelength ~ 750 nm. The halogenation on the peripheral positions of the phthalocyanines generally causes a bathochromic shift of the absorption bands [5]. The enhancement of solubility of tin and germanium hexadecachloro- and tetranitro-substituted phthalocyanines *i.e.* **8**, **9** and **20** was attained by the introduction of a bulky substituent such as 3,5-di-*tert*-butylphenol in the axial positions (Chapter 4.3). As expected, the di(*tert*-butyl)phenoxy axial substituents enhance considerably the solubility and reduce the tendency to form aggregates in solution. In addition, di(*tert*-butyl)phenoxy group as axial ligand introduce a dipole moment perpendicular to the macrocycle, which alters the electronic structure of the macrocycle and furthermore give rise to better optical limiting effect in the phthalocyanines. In contrast to perchloro-substituted complexes **8** and **9** the synthesized perfluoro-substituted phthalocyanines **16** and **17** exhibit great solubility in common organic solvents. Compound **16** was prepared by a modified version of the synthesis described by Birchall [6] (Chapter 4.3). However, synthesis of **17** was only achieved by bulk reaction (Chapter 6.415). Any attempts of preparation of compound **17** in solution failed (Chapter 4.3).

During synthesis of **14**, **15**, **16** and **17** some side reactions occurred that led to replacement of some peripheral groups by others. During synthesis of compound **16** the nucleophilic substitution of fluoride by chloride ions took place indicated by mass spectra (Chapter 4.3). The displacement of fluoride by chloride ion during synthesis of **16** was not reported before. Interestingly, the extension of the duration of the synthesis of compounds **14** and **15** and big excess of 3,5-di-*tert*-butylphenol and catalyst gave peaks in the mass spectra with a difference by 170 units, suggesting substitution of peripheral chlorine groups by di(*tert*-butyl)phenoxy ($C_{14}H_{21}0$) groups. The side products detected in above-mentioned syntheses were not separated and remained as impurities.

The phthalocyanines were characterized by IR, UV/Vis and mass spectroscopy (Chapter 6.4). The absorption spectra of the synthesized Pcs mainly show the red-shift of the Q- and B-bands which is usually associated with the presence of electron-withdrawing groups at the periphery of the macrocycle. Additionally, the Q-band of germanium complexes is ~ 10 nm red–shifted than that of tin complexes, caused by decreasing electronegativity of central the metal Ge → Sn which shifts charge into the ring and raises the energy of the $a_{2u}(\pi)$ HOMO [7, 8].

For practical NLO application of phthalocyanines the construction of solid devices is required. Thus, the multi-layer films based on compounds **5**, **6**, **7**, **14**, **15**, **16**, **23** and **25** in PMMA and PVC polymers were fabricated by spin coating technique (Chapter 7.3). Additionally, two-side and drop coated films of compounds **26**, **27**, **29**, **30**, **31** and one sol gel of **28** was prepared (Chapter 7.3.1, 7.3.2 and 7.3.3). The films were in detailed characterized with regard to their thickness, concentration, electronic data (Chapter 5.2 and 7.3) and optical limiting properties which will be summarized later. Compounds: **5**, **6**, **7**, **14**, **15**, **16** and **25** either in PVC or PMMA films do not exhibit tendency to form aggregates. The bulky peripheral substituents, *p*-nitrophenoxy and *p*-formylphenoxy, and axial groups effectively diminish cofacial aggregation. The Q-band position of phthalocyanines **5**, **6**, **7**, **14**, **15**, **16** and **25** in spin coated films is similar or slightly blue- or red-shifted compared to spectra in solutions. The shape and position of Q-band of the multi-layer films do not differ in particular from mono-layer films. Compounds **26**, **27**, **23** and **31** exhibit a clear tendency to form cofacial aggregates in spin coated films. Each of drop coated film of **29**, **30**, **31** and **28** show domination of aggregation. The Q-band in drop coated films is significantly broader and blue-shifted relative compared to solution spectra. This is caused by strong molecular interactions and big packing of phthalocyanines during long time of their drying. Generally, phthalocyanines in films prepared by drop casting method tend to aggregate whereas in spin coated films most phthalocyanines are totally monomeric and not aggregated.

This study determined comprehensive insight on the optical limiting properties of a series of synthesized germanium, tin and metal-free phthalocyanines with various electron-withdrawing peripheral substituents, and polymeric films of some phthalocyanines. The optical limiting of double layer films of **26**, **27**, **29**, **30** and **31** in PS, PVC and PMMA were also investigated (Chapter 8.4.6). In addition, the drop coated films of Zn, Pb, Cu octabutoxy-substituted phthalocyanines were prepared and their NLO properties were determined (Chapter 8.4.5). The optical limiting properties of the phthalocyanines in solution and in polymer films were measured by the open-aperture z-scan technique. The compounds were characterized by the effective imaginary third-order susceptibility $\chi^{(3)}$, the effective intensity dependent nonlinear absorption coefficient β_I, the energy density at which the material saturates F_{Sat} and the value of κ.

In a series of tin, germanium and metal-free tetrakis(*p*-formylphenoxy)- and tetrakis(*p*-nitrophenoxy)-subbstituted phthalocyanines **3** - **7**, it was found that the $\chi^{(3)}$, β_I, and κ values raise with increase in the size of the central metal as follows: 2H < Ge(IV) < Sn(IV) (Chapter

8.3.1 and 8.3.2). This is due to the heavy atom effect that the tin phthalocyanines present the best OL properties. Moreover, compound **5** with more electron-withdrawing *p*-nitrophenoxy peripheral substituents saturates at double lower F_{Sat} than **6** with *p*-formylphenoxy groups as substituents, indicating the influence of electron-withdrawing peripheral substitution on OL effect.

For a variety of tin and germanium tetranitro at α- and β-positions substituted phthalocyanines **18** - **23** with different axial groups the OL performance were investigated in solutions (Chapter 8.3.3). It was found that the compound **18** and **20** with nitro groups substituted at β-positions show slightly better optical limiting performance in relation to compounds **19** and **22** with nitro groups at α-positions of the macrocycle.

The OL effect of tin and germanium phthalocyanines with perchloro and perfluoro peripheral substitution were investigated in solutions (Chapter 8.3.4). The results show that the strong electron-withdrawing effect of fluorine groups at the peripheral positions of the macrocycle produce better optical limiting performance.

The optical limiting properties of the tin and germanium phthalocyanines in multi-layer films of PMMA and PVC are in most cases better compared to OL properties in solutions (Chapter 8.4). The multi-layer films of tin and germanium phthalocyanines in various polymers exhibit lower value of energy density, much higher magnitude of third-order nonlinearity and of nonlinear absorption coefficient in comparison with phthalocyanines solution. It was found that tin phthalocyanines in most cases act as better optical limiters than germanium phthalocyanines. Some devices exhibit excellent combination of $\chi^{(3)}$, β_I, F_{Sat} and κ values. Especially the phthalocyanines: **5**, **6**, **7**, **14**, **15** and **16** in PVC and PMMA have good combination of NLO factors which makes them interesting for practical application. In addition, it was found that polymeric films based on compound **5** exhibit better OL performance than films of **25**. Moreover, the plots of normalized transmission against pulse energy density show that some films seem to be a suitable as practical optical limiters.

The examined drop coated films exhibit extremely low energy density which is important for practical application (Chapter 8.4.5). On the other hand, the κ values for all drop coated films were found to be very low, implying that the intermolecular interactions caused by aggregation provoke the decay of the upper triplet state.

9.2 Future work

In the beginning of this work films previously synthesized and characterized tetra and octa-substituted phthalocyanines by Prof. Wöhrle group were prepared and further investigated with regard to their OL properties. The extended study of this series of complexes in relation to their OL properties can be done in the following ways:

- To determine the OL properties of compounds **26** – **31** in solution and than compare them with OL properties of previously prepared films
- The preparation of multi-layer films till for instance 10 layers
- In case of drop coated films to shorten the time of evaporation of the solvents by dropping smaller but highly concentrated amounts of polymeric phthalocyanine solutions on the substrate.

In this study the optical limiting effect of many new and described in literature phthalocyanines were investigated in solutions and films. It was shown that bulky electron-withdrawing peripheral substituents in case of compounds **5**, **6** and **7** influence the optical limiting effect of those compounds by altering the spatial relationship between neighbouring molecules. Considering that the presence of bulky axial molecules of perchloro-substituted compounds **14** and **15** considerably enhance the solubility and alter the OL properties, a series of tin(IV) and germanium(IV) perchloro-substituted phthalocyanines axially substituted by **A** – **F** (**Figure 9.1**) molecules is worth preparing. The influence of axial substituents **A** – **C** (**Figure 9.1**) on OL effect should be compared with previously synthesized by Shirk and Hanack [9-12] (*t*-Bu)$_4$PcInX with X = **A** – **C**. The next step would be the introduction of other bulky axial substituents like **E** and **F** (**Figure 9.1**) to compounds **8** and **9** in order to compare the OL properties of compound **14** and **15** with bulky di(*tert*-butyl)phenoxy (**Figure 9.1 D**) substituents in solution and in solid state.

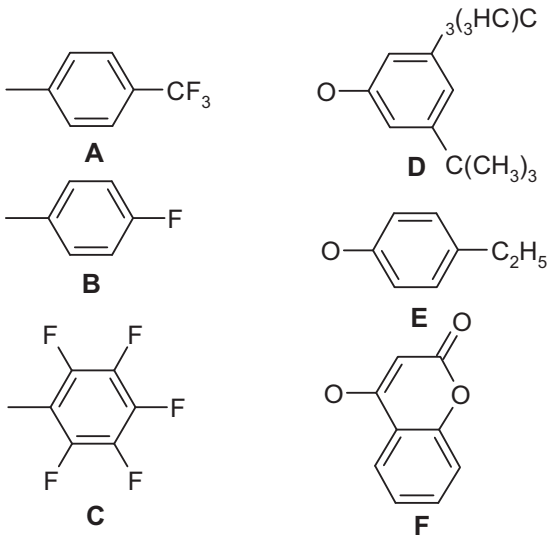

Figure 9.1 Proposed axial substituents.

The wide-ranging insight of NLO properties of Pcs in solutions and in films presented in this study show that the peripheral and axial substituents, central ion and tendency to aggregation play important role on optical limiting effect. Moreover, the optical limiting properties of phthalocyanines in multi-layer films are influenced by a polar environment of a host lattice.

According to a NLO results presented in this study the proposed concept of various ways for preparation films of tin and germanium phthalocyanines could be further investigated:

- multi-layer films including layer of compound **6** possessing a relatively high absorption cross section κ and followed by a layer of compound **5** exhibiting the low energy dependent saturation F_{Sat} in PVC or PMMA prepare by spin coating method,
- multi-layer films of **16** peripherally substituted by strong electron-withdrawing fluorine groups and complex **14** peripherally substituted by chlorine groups and with bulky axial ligands prepare in the same manner as above-mentioned,
- multi-layer films of compound **5**, **6** and **7** possessing excellent combination of $\chi^{(3)}$, β_I, F_{Sat} and κ values,
- drop coated films of compound **5**, **6**, **7**, **14**, **15**, **16**, and **23** in PVC and PMMA in order to compare their optical and nonlinear optical properties in relation to previously prepared spin coated films.

9.3 References

[1] D. Wöhrle, G. Schnurpfeil, G. Knothe, *Dyes and Pigments*, **1992**, 18, 91.

[2] G. Schneider, D. Wöhrle, W.Spiller, J. Stark, G. Schulz-Ekloff, *Photochem. Photobiol.*, **1994**, 60, 333.

[3] D. Wöhrle, V. Schmidt, *J.Chem.Soc., Dalton Trans.,* **1988**, 549.

[4] M. Hanack, H. Heckmann, *Eur. J. Inorg. Chem.*, **1998**, 367.

[5] T. Takeuchi, H. B. Gray, W. A. Goddard, *J. Am. Chem. Soc.*, **1994**, 9730, 116.

[6] J. M. Birchall, R. N. Haszeldine, J. O. Morley, *J. Chem. Soc. (C),* **1970**, 2667.

[7] M. Gouterman, *J. Chem. Phys.*, **1959**, 30, 1139.

[8] M. Gouterman, F. P. Schwarz, P. D. Smith, D. Dolphin, *J. Chem. Phys.*, **1973**, 59, 676.

[9] J. S. Shirk, R. G. S. Pong, S. R. Flom, H. Heckmann, M. Hanack, *J. Phys. Chem. A.*, **2000**, 104, 1438.

[10] M. Hanack, T. Schneider, M. Barthel, J. S. Shirk, S. R. Flom, R. G. S. Pong, *Coord. Chem. Rev.*, **2001**, 219, 235.

[11] M. Hanack, D. Dini, M. Barthel, S. Vagin, *Chem. Rec.*, **2002**, 2, 129.

[12] D. Dini, M. Hanack, M. Barthel, *Eur. J. Org. Chem.*, **2001**, 3759.